A Lipid Fusion Based Method for the Single Molecule Study of ATP Synthase

Aidan Niall Russell

University College

Trinity Term 2014

A thesis submitted in partial fulfilment of the requirements for the degree of Doctor of Philosophy at the University of Oxford

Abstract

A Lipid Fusion Based Method for the Single Molecule Study of ATP Synthase

Aidan Niall Russell
University College
Department of Physics
Trinity Term 2014

A thesis submitted in partial fulfilment of the requirements for the degree of Doctor of Philosophy at the University of Oxford

ATP synthase is a ubiquitous transmembrane protein that utilises the free energy available from ion gradients across lipid membranes to synthesise adenosine triphosphate (ATP). It may be separated into two parts – the membrane-embedded (i.e. hydrophobic) F_O and the hydrophilic F_1. Each undergoes a rotary motion. Single-molecule studies on the rotation of the isolated hydrophilic F_1 have been performed for many years; attempts to construct an experiment in which to view the rotation of the membrane-embedded F_1F_O complex under high space- and time- resolution (such as by attachment of a rotational probe) have not yet seen a satisfactory method emerge in the literature. Most particularly, a clear ability to generate and control a proton-motive force across the membrane in which the F_1F_O is sited is needed to probe ATP synthesis.

This thesis presents the development of a candidate method for such single-molecule studies.

By the use of a water-in-oil emulsion, giant unilamellar lipid vesicles are formed which entrap arbitrary components – including functionalised gold nanospheres of 60-100 nm diameter, which move freely in the internal space. A charge-based lipid fusion is developed, using mixtures of natural lipid extracts with anionic and cationic lipids. It is demonstrated that anionic giant vesicles fuse with cationic small vesicles with full content mixing and transfer of bilayer leaflets. It is shown that F_1F_O is functional in the cationic lipid mixture. Methods are shown to bind such a cationic proteoliposome to a surface and for it to fuse with an anionic giant vesicle containing functionalised gold nanospheres. Backscatter laser darkfield is used to search for rotation of the gold nanospheres under ATP hydrolysis conditions of the F_1F_O; unidirectional rotation is seen in one instance and other suggestive traces are shown with speculative analysis. Further work is proposed.

Acknowledgements

Although the pursuit of a DPhil can at times seem solitary, I have received support from many people. I would most particularly like to thank my supervisor, Dr Richard Berry, who has been – and I see as I review the acknowledgements in DPhil theses of past students that I am not alone in this thought – an inspiration. I have learned a great deal.

Many particular thanks also to Berry group member Dr Robert Ishmukhametov, whose expertise has often been key and who has always been ready with new suggestions for improvement as the project has developed.

My thanks also to the other members of the Berry group, including Dr Ashley Nord, Mr Ren Lim, Mr Samuel Tusk, Ms Dewei Jia, Mr Bastiaan Leerkotte, Ms Diana Di Paolo, Dr Irwin Zaid, and Dr James Flewellen for both insightful discussions on the project and friendship. My thanks also to past lab members Dr Bradley Steel, for the Matlab code used in single-molecule analysis, and Dr Wei Meng Ho, who worked on a previous attempt to show single-molecule rotation of ATP synthase.

I would like to thank those in the Armitage group who welcomed me during my time in the Department of Biochemistry for the initial two years of my DPhil, in which I worked on a different project.

I would like to thank everyone at the Doctoral Training Centre, whose innovative and flexible funding model has benefited me greatly. My thanks also to the research councils for funding me in various capacities over my graduate studies. I am privileged to be paid to do this.

University College has been a beautiful environment and a great source of friendship – many thanks to all those who make it such a great place to be.

Finally I would like to thank my parents – and my whole extended family – for providing me with such inspirational role models and for being such wonderful people.

Contents

Chapter 1 Introduction

The functions of life are mediated, in general, by proteins which are encoded in DNA. Two ubiquitous forms of energy storage and conversion in the cell are ion gradients across a membrane and the molecule adenosine triphosphate (ATP); the protein complex that stands between the two is ATP synthase. ATP in the cell is a molecule far from equilibrium; with concentrations in the cell typically 1-3 orders of magnitude higher than its counterpart adenosine diphosphate (ADP), chemical equilibrium between the two lies 8-10 orders of magnitude in the other direction [1]. The synthesis of an ADP and free phosphate to ATP in this pool hence requires a free energy input and conversely the hydrolysis of ATP to ADP and free phosphate releases free energy – like an elastic band under tension, pulled further out or relaxed inwards.

Although ATP can also be generated from ADP and phosphate via a substrate-level phosphorylation, the majority of ATP in life forms from bacteria to mammals is produced by ATP synthases. Upstream other processes generate the transmembrane proton gradient by which the ATP synthase then operates; ATP synthase is thus the final part of a long chain to synthesise ATP, which is in turn used by many downstream cellular processes as an energy storage mechanism –

energy that is released by cleavage of phosphate to reform ADP under the same far-from-equilibrium conditions.

Remarkably, this ATP synthesis operation is achieved by a conformational change that results in rotary motion of the protein. However to describe the ATP synthase as extraordinary might perhaps be misleading, since it is the very ordinariness of it – in the sense of its ubiquity amongst so many living organisms – that is one of its most notable features. The central position of ATP synthase in essentially all life forms is certainly of interest to evolutionary studies; the structurally and functionally similar F-, V-, and A-type ATP synthases and ATPases (meaning performing hydrolysis only, with no synthesis) have been hypothesised to have evolved from a single ancestor RNA-translocating protein possibly sitting in an early semi-permeable membrane [2], [3].

Single-molecule studies can reveal information about the physical changes in proteins that underlie their function, can reveal small scale steps in between the initiation of a process and its outcome, and can elucidate variations in individual molecules; such as variability in the rate of a process that might otherwise be seen only as a constant average. This paradigm of the physical study of biological systems continues to reveal fine details of those mechanisms and it is my hope that the work described in this thesis can contribute to the techniques in use for such studies of ATP synthase and other proteins.

1.1 Proton-Motive Force and ATP Synthase Function

Lipid bilayer membranes are in principle impermeable to ions (though measurable levels of permeability will always be present [4]). When forming an enclosed space, these membranes can hence define proton gradients which may be used by ATP synthase and other transmembrane protein complexes (such as the bacterial flagellar motor [5]) as an energy source; the traversal of protons through a transmembrane protein channel down the proton gradient releases free energy and allows work to be performed. Note that some life-forms operate by a sodium-motive force; the principle is the same.

For such proton gradients to act as an energy store naturally in turn requires the input of free energy for the ongoing formation of these gradients as they are depleted, which is undertaken by several other upstream protein complexes that are somewhat more species-dependent than the ATP synthase (which is highly conserved). In plants and some bacteria, this originates in the photosynthetic complexes which transduce energy from incoming photons. In other bacteria (including *E. Coli*) and mitochondria a set of protein complexes release free energy from an electron transport chain using nutrient inputs.

In gram-negative bacteria such as *E. Coli* these systems are arranged such that the cytoplasm (main interior space of the cell) is depleted of protons compared to the outside environment; the cytoplasm is hence referred to as the N-phase (negative). The region outside the energy-transducing membrane of the cell is thus in relative excess of protons and referred to as the P-phase (positive). Such definitions can similarly be made in the cases of mitochondria and chloroplasts.

In all these species, the ATP synthase and other proton-pumping complexes are sited across the energy-transducing membrane between these two phases.

It will be instructive to consider two components of proton-motive force; one is related to the concentration of protons on either side of the membrane, and one is related to the number of charge carriers. The component to describe proton concentration step changes across the membrane (or chemical potential) is generally referred to as ΔpH and the component to describe charge step changes across the membrane (or electrical potential) is Δψ. A definition of the proton-motive force (pmf) as an electrochemical potential is instructive in understanding this relationship:

$$\mathrm{pmf} = \Delta\psi - \frac{2.303\mathrm{k_B T}}{\mathrm{e}}\Delta\mathrm{pH}$$

k_B is the Boltzmann constant, e is the charge on the electron, and T is the temperature. The reader can readily convince themselves that these units are consistent and pmf will be expressed in V. Hence 1 pH unit is equivalent to around 60 mV. In terms of direction, the pmf is by convention defined as the condition in the P-phase minus the condition in the N-phase. This is a formulation of the Nernst equation, which describes the potential across a membrane due to an ion concentration difference (expressed here as ΔpH and hence involving a factor of 2.303 to account for the use of log base 10 in pH rather than base e used in the Nernst equation).

From this definition we readily perceive that if a pmf exists across a bilayer, this potential can be used to perform work. To synthesise ATP from ADP and

phosphate under far-from-equilibrium conditions of around 10^1-10^3 ATP for each ADP (such as generally exists in the cell) requires 0.7-1.0 × 10^{-19} J Gibbs free energy per molecule (i.e. 40-60 kJ per 1 mol ATP [1]). Generally pmf in the cell generated from the upstream primary proton pumps is of the order 100-200 mV; this is equivalent to around 2-3 pH units. Induced pmf conditions of this order have been used to observe ATP synthesis from F_1F_O of varying origins in an ADP and phosphate environment [6]–[9]. In few organisms does such a large ΔpH occur; since the capacitance of the lipid bilayer (around 1 μFcm^{-2}; see discussion in section 5.5.1) is such that for a given number of protons transmitted across the bilayer a significant Δψ is developed before an equivalently significant ΔpH has the opportunity to do so (given buffering capacity of the interior space), and so Δψ will be dominant over ΔpH (however chloroplasts are one example where ΔpH dominates).

Although we have discussed ΔpH and Δψ as equivalent, several research groups have reported results suggesting that one or other of the two components is essential, or at least more important, in the free energy release that accompanies the passage of a proton down the electrochemical gradient and so results in ATP synthesis [10]–[14]. For research groups seeking to contribute to the current understanding of pmf and its operation in F_1F_O using single-molecule techniques, it is important that the bilayer across which the F_1F_O is sited can form a pmf with control over both ΔpH and Δψ. This is an energisable bilayer. The challenge of coupling this with a microscopy system that allows single-molecule visualisation

with high space- and time-resolution is the central aim towards which the methodology pursued in this thesis seeks to contribute.

1.2 The ATP Synthase – Structure and Function

ATP synthase describes a variety of rotary transmembrane protein complexes that synthesise the molecule adenosine triphosphate (ATP) from adenosine diphosphate (ADP) and phosphate. In general the ATP synthases operate by means of a proton-motive force across an energy-transducing lipid bilayer in which the protein complex is embedded; by the passage of protons through the complex down the proton gradient, conformational changes are initiated in the protein which allow an ADP molecule and a phosphate bound separately on the complex to be brought together and provide conditions for them to bind and form ATP. In some species, including the *E. Coli* species studied here, it is possible for this operation to be reversed; the cleavage of ATP to ADP and phosphate then allows the transfer of protons against the prevailing gradient. Note that the ATP hydrolysis/synthesis reaction can be summarised as:

$$\mathrm{ATP}^{4-} \cdot \mathrm{Mg}^{2+} + \mathrm{H_2O} \rightleftharpoons \mathrm{ADP}^{3-} \cdot \mathrm{Mg}^{2+} + \mathrm{HPO_4^{2-}} + \mathrm{H}^{+}$$

Where Mg^{2+} is required to be complexed with ATP/ADP for coordination at the catalytic site [15], [16].

There are two different types of ATP synthase of which the F-type is one group that is found in the mitochondria of eukaryotic cells, in bacteria, and in plant chloroplasts. The other known type is the A-type found in archaea; though, there are also other structures which operate purely by hydrolysis of ATP in order to

generate a proton gradient; the V-type ATPase found in the vacuoles of eukaryotic cells is one that is similar in structure to both the F- and A-type synthases. The F-type only will be discussed here. F-ATP synthases across different species certainly have differences in the subunits, but are largely conserved and operate in essentially the same manner. Some of these differences will be highlighted where they are of interest; the most studied in structural and biochemical studies is the bovine-heart mitochondria, whereas the most studied for single-molecule assays has been bacterial.

1.2.1 Structure

F-type ATP synthase is a transmembrane protein complex consisting of two separable parts – the membrane-bound F_O and the non-membrane F_1. Both are rotary. This remarkable separability, which is even reversible, has certainly aided in its study. Crystallographic studies have revealed most of the structure and we can present the majority of the solved structure here using different sources. I will not go into great detail of the chemical structures involved, however, giving only outlines where they will aid in understanding function.

The convention has arisen to refer to the $ab_2\delta\alpha_3\beta_3$ components as the stator and the $\gamma\varepsilon c_n$ as the rotor. The main recognisable head of F_1 consists of an alternating set of three α-subunits and three β-subunits, with the functional binding sites for ADP and phosphate/ATP lying between them and mostly on the β-subunit. The γ-subunit protrudes from the centre of this hexameric arrangement, whose overall diameter is some 11.5 nm [17]. The α- and β-subunits are highly similar in their structures; differing conformational states of each of the three pairs of

subunits were revealed in the structures which underlie their function and demonstrate differing states of ATP or ADP and phosphate binding [18]–[21]. The γ-subunit is an asymmetric structure which fits between these subunits depending on this conformational arrangement.

The $b_2\delta$ structure forms a rigid outer stalk which ensures coupling between the movements of the headpiece and the γ- and ε-subunits. When comparing mitochondrial and bacterial F-ATP synthases, the δ presented here for the bacterial case is replaced by its homologue oligomycin-sensitivity conferral protein (OSCP) in the mitochondrial case [22]. The ε- in the bacterial case is then referred to as δ- in the mitochondrial case and there is a further ε-subunit in the mitochondrial case which has no homologue in the bacterial protein. There are further differences in the b-stalk. To avoid confusion, only the bacterial case is presented in Figure 1.2 (since this thesis will describe a study of *E. Coli* F_1F_O).

The c-ring consists of between 8-15 copies of the c-subunit arranged symmetrically, with the number depending on the organism; this and the a-subunit are membrane-embedded. The number of c-ring subunits in F_O varies across species; the smallest number observed is 8 in bovine mitochondria [23], the largest is up to 15 in some cyanobacteria [24], and in the *E. Coli* studied here the number has been shown to be 10 [25]–[27]. The a-subunit lies between the membrane embedded portion of the b_2-stalk and the c-ring; its structure is not yet known to high resolution.

The myriad number of c-subunits observed across species is a far cry from the early expectation that this number would necessarily be a multiple of the three

ATP molecules synthesised per full rotation [28] and obviously indicates a flexibility in the coupling between the F_O rotation and that of the F_1. This is understood to be due to flexibility in the rotor, particularly the ε- subunit as well as the γ- subunit, with the stalk of b- and a-subunits being stiff – thus allowing rotational energy to be elastically stored and negating the need for stiff coupling between the two motors – a result concluded with cross-linking single-molecule experiments in the groups of Wolfgang Junge [29], [30] and Hiroyuki Noji [31], and further probed in Förster resonance energy transfer (FRET) studies in the group of Michael Börsch [32].

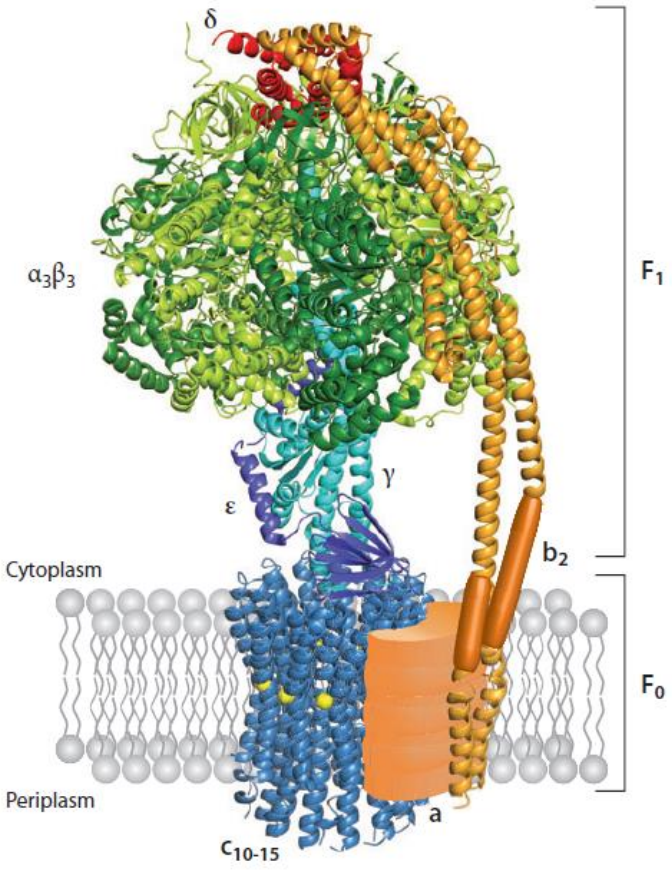

Figure 1.1
F_1F_O-ATP Synthase mosaic model showing available structures. Image reproduced from [193] and has been formed through available structures on the Protein Data Bank using the c-ring of *Ilyobacter Tartaricus*, the F1, δ-subunit, and membranous part of b from *E. Coli*, and the remainder of the b_2 subunit from bovine mitochondria. More recent results have shown that the b2-dimer interfaces with the a- and c-subunits simultaneously [194]–[196].

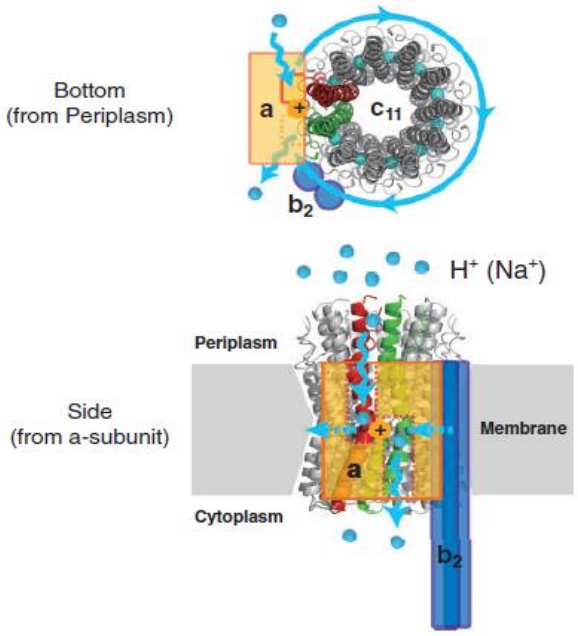

Figure 1.2
The structure of the c-ring and hypothesised function of the a-subunit. This shows an 11-c-subunit structure from *Ilyobacter Tartaricus*. Two of the 11 are highlighted red and green as they interface with the a-subunit. Blue represents protons (or sodium in the case of this species). As one proton is brought in and reaches the binding site on the exposed c-subunit, another leaves for the other side of the membrane. Image reproduced from [197].

1.2.2 Function

On the F_1, each of the three β-subunit binding sites will at any one time exhibit a different conformation depending on the extent to which it has bound ADP and phosphate loosely, tightly (i.e. formed ATP), or whether it is empty and ready to receive new substrates for synthesis (or equivalently hydrolysis). Under widely-accepted models, the binding of ATP under hydrolysis mode is accompanied by a gradual formation of hydrogen bonds with the binding sites that induces these conformational changes in a manner that provides a constant torque that is consistent with single-molecule observations [33], [16]. This initial power stroke is accompanied by a second that is driven by elastically-stored energy in the β-subunit as the phosphate and ADP are released from the binding site.

To describe the sequence of movements of the ϒ-subunit due to binding and release of substrates at the β-subunit, we must bear in mind that all three binding

sites act cooperatively. The complete sequence of events under hydrolysis was recently most clearly described by Noji's group for the case of thermophilic F_1 in an elegant series of experiments, after some years in which the order of release of ADP and phosphate was uncertain [34]–[36]. If we consider the ϒ-subunit to be at position 0° upon the binding of ATP to one β-subunit, the first power stroke is induced by this binding to move the ϒ-subunit to 80°. Binding and release at other sites induces movement to 200°. At this point ATP is hydrolysed to ADP and phosphate, but this is energetically neutral and no movement is induced. Movement to 240° is induced at another site, which also induces the release of ADP. Movement to 320° is induced at another site, and finally the release of phosphate induces the second stroke at this site to 360°. Hence free energy has been released at one site for two movements: 0-80° and 320-360°. With the three β-subunit binding sites acting together, the full movement can be seen to be due to the cooperative action of the three sites; each of which induces a total 120° of movement in the rotational cycle of 360° at different moments.

Movement is transmitted through both the γ- and ε-subunits; the γ-subunit fits in position dependent on the movements of the $\alpha_3\beta_3$ headpiece and these movements hence induce the characteristic rotation of the γ-subunit. The ε-

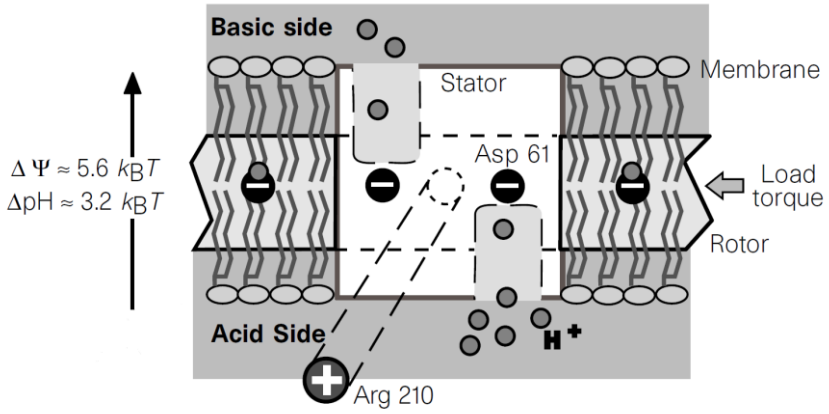

Figure 1.3 Model of c-ring torque generation combined with a-subunit half-channels. Figure reproduced from [38].

subunit (bacterial) has been found to play a role in coupling the movement of the $\alpha_3\beta_3$ headpiece to the rotation of the c-ring and also has been found to play a selective inhibitory role which is thought to be dependent on its conformational state [37].

The a-subunit is involved in proton translocation along with the c-subunits; in synthesis mode torque is generated by this proton translocation and transmitted through γ and ε to the headpiece, or the opposite operation for hydrolysis. The ion-binding mechanism at the c-ring is conserved across species despite the variation in the number of c-subunits (meaning different numbers of protons – or equivalently Na^+ in some species – translocated per ATP, since the number of ATP per full cycle is always three). This H^+ binding site is located at the recess between each two adjacent c-subunits and provides a tight binding of the proton whilst the subunits rotate through the membrane; the binding is then thought to be loosened only when the site is exposed to the a-subunit, at which point the proton leaves to one side of the membrane and another takes its place from the other side [38]. The rotor will only move to one side once a proton has been bound, as a bare binding site will not enter the membrane region. The proton will also not be released into the hydrophobic interior of the membrane; proton half-channels and a conserved positive reside in the a-subunit are thought to prevent back-slipping of the rotor and ensure its movement in one direction is favourable and goes with the gradient of protons (in synthesis mode). Molecular dynamics models have demonstrated the plausibility of such an arrangement but it will take a crystal structure of the a-subunit to more fully understand the mechanisms

involved [39], [40]. Hence free energy is released by the rotation, since it is biased in one direction, and this is transferred to the stator and performs work on the opening and closing of binding sites and release of synthesised ATP. In hydrolysis mode (for species that are capable of both) the free energy released from ATP hydrolysis is higher than that of proton translocation and this leads to the enforced rotation of the c-ring in the opposite direction, driving the transfer of protons against the prevailing gradient.

1.3 Historical Context of the Study of F-ATP Synthase

1.3.1 Bulk Studies

The history of ATP synthase research can perhaps best be traced to the first isolation of the water-soluble F_1 portion of bovine-heart F_1F_O by the group of Efraim Racker in 1960 [41], [42]. In 1966 the membrane-embedded F_O portion was also isolated [43]. Although the observation of oxidative phosphorylation was established, the mechanism responsible for the final stage (ATP synthesis from ADP and phosphate) had not before been isolated. It was in 1961 that Peter Mitchell had first proposed that the phosphorylation was coupled to the translocation of protons across the membrane in which the ATP synthase was known to be sited [44]. This was later confirmed when in 1971 Yasuo Kagawa, in the lab of Efraim Racker, established the method of reconstitution of the protein into liposomes [45]; though earlier experiments involving ATP generation due to rapid pH transitions had also been pivotal in convincing the community of the hypothesis [46]. Later in 1977 in Kagawa's own lab ATP synthesis with

reconstituted protein from bacteria was demonstrated [47]. Shortly afterwards a particularly elegant demonstration by Racker's lab reconstituted the protein together with the transmembrane protein complex bacteriorhodopsin; the proton gradient required for the ATP synthase was generated by the bacteriorhodopsin in a light-dependent manner [48].

In 1977 Paul Boyer made a proposal for the mechanism by which ATP synthase couples the translocation of protons to ATP synthesis which came to be known as the binding change mechanism; stating that it is primarily the difference in the energy of binding of the ATP or ADP/P that is coupled to proton translocation rather than the hydrolysis/synthesis itself and later, in 1982, updated to crucially include an overall rotation of the protein structure due to subunit movement through three different states as ATP or ADP/P is bound and released [49], [50]. In 1994 it was the group of John Walker whose crystallographic work on the structure of bovine mitochondrial F_1 showed that this rotary mechanism was possible [19] and in 1997 this rotation was directly observed in a single-molecule experiment on isolated bacterial F_1 by the group of Kazuhiko Kinosita [51]. Earlier cross-linking experiments having laid the ground for the acceptance of this result [52], and Wolfgang Junge's group having shown rotation in bulk polarisation anisotropy measurements in 1996 [53].

1.3.2 Single-Molecule Studies of F_1 and Detergent-Solubilised F_1F_O

This 1997 paper by Noji, Yasuda, Yoshida, and Kinosita [51] essentially founds the field of single-molecule studies of the F_1 and F_1F_O to which this thesis aims to contribute. The use of the isolated non-membrane F_1 component rather than the

full F_1F_O demonstrates the relative simplicity of the study of this component, given its water-soluble nature. In this founding paper, a fluorescent actin filament was attached to the γ-subunit of the $\alpha_3\beta_3\gamma$ subcomplex which forms the minimal F_1. The protein was attached to a glass coverslip by a non-specific binding of horseradish peroxidase modified with an NTA molecule to bind Ni^{2+} ions, which in turn held the deca-histidine-tags incorporated into the three β-subunits by genetic manipulation. Three binding sites provides stability against counter-rotation and prevents rocking on the surface. The actin filament was attached via a cysteine on the γ-subunit, introduced also by mutagenesis, which had been labelled with biotin. The biotin-binding protein streptavidin was used as an intermediary to bind to the γ-subunit site; biotin on the actin then completes the sandwich-bonding. The actin filament was observed under the microscope to rotate unidirectionally in the presence of ATP and ceased upon addition of the inhibitor sodium azide. This was performed with a strain derived from a thermophilic (stable at high temperatures) *Bacillus* bacteria and expressed in *E. Coli*; later it was performed directly in an *E. Coli* derived strain [54] and in an extended F_1 subcomplex $\alpha_3\beta_3\gamma\varepsilon$ including the ε-subunit [55]. The same methodology was then used with a full F_1F_O complex to show directly that the c-ring rotates [56], [57] by stabilising the membrane-bound F_O components with detergent. Critically this demonstrated that the rotation of γ and ε is then coupled to the rotation of the c-ring, upon hydrolysis of ATP. Clearly, such an approach cannot be used to study ATP synthesis as there is no possibility to create a proton-motive force without an enclosed bilayer system.

Although the fluorescent actin filament provides a striking demonstration of rotation, its bulkiness leads to significant viscous drag – which limits the extent to which studies using this technique can claim to elucidate the properties of the rotation mechanism as it operates in vivo. To address this, a technique previously innovated for the study of the rotary bacterial flagellar motor was imported; laser dark-field microscopy [58]. By discarding unscattered light and observing only that which leaves the sample at high angles, scattering objects appear bright on a dark background. By the conjugation of differing loads, Yasuda et al. [59] showed that the rotation rate of the F_1 motor was independent of load with beads of 100 nm diameter or less (i.e. the load was effectively zero below this level). Hence they were able to observe the rotation of the F_1 with high-speed measurements that elucidated their previous observation of three steps at 120° separations [60] by the observation of sub-steps. As well as the three ATP molecules hydrolysed per turn (120°) they observed a substep around 90° presumed to be driven by ATP binding, and a further 30° step to 120° presumed to be driven by release of a hydrolysis product; later studies corrected this observation to 80° and 40° [61], [62].

The use of gold nanospheres as a marker perhaps naturally led to the innovation of magnetic beads as a manipulator; by applying a rotationally-varying magnetic field then in 2004 Kinosita's group was able to induce the minimal-F_1 $\alpha_3\beta_3\gamma$ subcomplex – which had only been observed to be capable of ATP hydrolysis – to actually synthesise ATP from ADP and phosphate in a fixed reaction volume when rotation of the γ-subunit-attached bead was forced in the opposite

direction to that observed under hydrolysis [63]. When the magnets were turned off, ATP-hydrolysis driven rotation resumed until the ATP that had been synthesised by this mechanically-induced rotation was expended. Even more remarkably, in 2005 Hiroyuki Noji's group was able to perform this experiment with femtolitre-sized sealed containers holding a single F_1 molecule each and demonstrate directly the long-inferred result that three ATP molecules are synthesised per full rotation of the molecule; as expected it was also shown that when the magnets are switched off, three ATP molecules are also hydrolysed per rotation. Additionally it was found that subunit ε was required for the synthesis direction result, as chemomechanical coupling was significantly less efficient when using the minimal subcomplex $\alpha_3\beta_3\gamma$ than when using the $\alpha_3\beta_3\gamma\varepsilon$.

1.3.3 Single Molecule Studies of F_1F_O in a Bilayer

Detergent-based systems continued to be of interest for their relative simplicity and given the number of unanswered questions to probe under hydrolysis, however in 2005 Yoshida's demonstration of a decoupling between the a-subunit and c-ring in a detergent-solubilised system [64] made it clear that there was a real need to approach the problem of F_1F_O rotation with more native-like membrane-embedded systems. Interestingly Noji's group recently (September 2013) demonstrated that it is possible to maintain proper structure of the protein under detergent-based conditions as measured by sensitivity to the inhibitor DCCD (1,3-dicyclohexylcarbodiimide), if the proper conditions are used [65]. Nevertheless the goal of energisation of the bilayer for the study of ATP synthesis-driven rotation – and hence the function of the protein in vivo – is clear and several research groups besides our own have pursued it.

In an early study in 2002 Masamitsu Futai's lab embedded F_1F_O in a membrane fragment in which an actin filament was attached to the β- or a-subunits; the F_1F_O was attached to the glass coverslip via his-tags on the c-ring – this meant that the c-ring was immobilised, but it was found that the a-subunit then rotated around the c-ring so this was not functionally a problem [66]. Although rotation due to ATP hydrolysis could be observed, the system fundamentally did not allow a proton-motive force as the bilayer consisted of a fragment that was not controlled or sealed; hence ATP synthesis was not possible.

Concurrently to these developments, in 2002 FRET labelling of subunits by Michael Börsch et al. in the group of Peter Gräber allowed observation of rotation by the varying level of resonance transfer that occurs when the distance between a donor and acceptor fluorophore located at different sites on the protein varies [67]. Crucially, this approach is compatible with an enclosed liposome-embedded system to allow full coupling of the protein and the observation of synthesis (along with confirmation that this occurs by a rotation in the opposite direction to hydrolysis). Later in Börsch's own group this technique has been used to show c-ring rotation with 10 steps for the 10 c-ring subunits in *E. Coli* in 2009 [26], twisting of subunits during rotation [32], [68], and further insights on subunit movements during hydrolysis and synthesis modes have been elucidated [69]–[71]. However the time resolution from fluorescent approaches is less than that available from darkfield by gold scattering, which is limited only by the speed of the camera itself (given sufficient scattered photons defined by the laser input, since there are no bleaching effects).

In the meantime Ishmukhametov et al., in the group of Wayne Frasch, in 2010 utilised lipid nanodiscs to embed F_1F_O in a small ring of lipids and thus achieve a more native state; steps in the rotation of the c-ring were probed under hydrolysis conditions. This study also used gold nanorods rather than nanospheres. Since the nanodisc is open, there is no pmf.

In 2009, Kinosita's group published a 'giant liposome'-based approach in which proteoliposomes containing F_1F_O were dried out on a surface and then rehydrated to form liposomes with diameters around 100 μm [72]. By using such a large structure they found they could insert a pipette for the injection of functionalised 0.7 μm microspheres, for attachment to the F_1F_O and observation of rotation. The F_1F_O was bound via his-tags on the β-subunits to the coverslip surface, with biotin-labelling on the 10 c-ring subunits via a cysteine-modification; rotation of the c-ring under ATP hydrolysis was observed due to binding of the microspheres to the c-ring internal to the giant liposome (via biotin-streptavidin). The advantage of such a large probe was immediate identification of rotation without the need for advanced microscopy or data analysis. Although rotation under hydrolysis conditions was reported, it was stated that it had not been possible to develop the proton gradient required for synthesis as the membrane had proven too permeable. In its novel use of an enclosed lipid structure, this approach has some broad similarities to that described in this thesis.

Finally in 2013, well into the research presented in this thesis, Noji's group demonstrated a system based on the controlled release of 'caged protons' embedded in an agarose layer on one side of a bilayer. With ATP synthase

embedded in the bilayer, it was then possible to generate a proton gradient and so a proton-motive force [73]. The c-ring was held to the surface by his-tags and the rotation of the β-subunit was observed with an 80 nm gold nanosphere attached via biotin-streptavidin. Although rotation in the ATP synthesis direction was observed upon activation of the ΔpH, the rotation rate was slow (2.7 Hz) and the proton-motive force, due to the nature of the bilayer used, cannot be expected to maintain a Δψ, consisting essentially only of a local ΔpH. The possibility to study the interaction of these two components in proton-motive force is therefore not present in this system.

The observation of 'slow' rotation rates in this most recent paper brings us to a discussion regarding the speed of rotation we might expect to observe. Single-molecule studies on F_1 have shown that, since the rotation rates observed can be up to some 10-fold higher (up to 700 Hz) than expected based on bulk measurements of ATP hydrolysis under the same conditions, up to 90% of isolated F_1 is expected to be inactive at any one time due to Mg-ADP inhibition [74]. Detergent-stabilised studies of F_1F_O rotation under hydrolysis have seen maximum rates around 350 Hz (though at 37 °C) [75]. FRET studies, which are capable of probing the native operation of F_1F_O across a properly energised bilayer (typically being sited in a freely-moving liposome; see discussion in 1.4.1), have observed slower hydrolysis rates that correlate with those expected from bulk measurements of activity (similarly for synthesis rates) [70]. Similar results were obtained for hydrolysis with lipid nanodisc insertion [27]. Certainly we can say that bulk rates can form a lower bound on our expectations and single-

molecule F_1 studies give us an upper bound within which to design our experimental arrangement. Single-molecule F_1 rotation rates under the zero-load condition have been measured to depend on ATP concentration in a similar manner to bulk rates of hydrolysis activity (Michaelis-Menten kinetics) [50], [59]. Typically hydrolysis rotation would be measured at saturating ATP levels, which corresponds to about 1 mM or above (meaning rate is maximum).

1.4 The Lipid Membrane, Liposomes, and Lipid Fusion

1.4.1 Lipid Membranes and Liposomes

Phospholipids are amphipathic molecules, consisting of a hydrophilic region (the 'head') and a hydrophobic region (the 'tail'). Hydrophilic regions will readily form hydrogen bonds with water (owing to charge distributions) whilst hydrophobic regions will not. When placed in water, these molecules will tend to self-assemble into structures with the hydrophilic region exposed and hydrogen-bonded to water and the hydrophobic region hidden. Many structures can emerge from such interactions, which will also be affected by the shape of the lipid molecules. With two elongated hydrophobic hydrocarbon chains, the structures phospholipids form in solution will be affected by the width of the hydrophobic chain region relative to the hydrophilic head: structures include micelles, in which all hydrophobic tails point inwards, and inverted micelles, in which all hydrophobic tails point outwards. In bilayers elongated sheets are formed in which hydrophobic tails are hidden and only the hydrophilic region is exposed.

Such bilayers can form large sheets with essentially arbitrary overall shape, though a sphere ensures the end hydrophobic regions are also hidden. By its nature this spherical structural format creates an enclosed aqueous space, separate from the exterior - defining arguably the most essential feature of a cell. Indeed, cells from bacteria to human use phospholipids to form their boundary in this manner, though generally through complex arrangements of the structures with multiple bilayer structures, high densities of embedded transmembrane proteins, and in many cases the use of scaffolds to define the cell shape.

In membranes in cells, there are many additional protein components which will affect the permeability of the lipid membrane to various ions. In order to simplify the study of these systems, they can be purified and reconstituted into purified lipid bilayers – in this way, one may study the isolated behaviour of a single transmembrane protein. Ionophores can be used to introduce selective permeability of the membrane to separate ΔpH and $\Delta\psi$, to gain insights into the role of each [76]. Such phospholipid bilayers have been studied in a variety of approaches from planar formats [77], [78], and lipid vesicles (liposomes) [79], [80], as well as emulsion formats based on the contact of monolayers [81]–[83] and other self-assembling structures [84] both for insights into the properties of the lipids themselves as well as properties of isolated biological components. Lipid structures, particularly liposomes, are of interest as delivery vehicles for nanotechnological research; as enclosed reaction volumes [85] or, in particular, as drug delivery systems [86]. There has been interest in the study of liposomes and

their behaviour, including fusion, as model systems of the behaviour of lipid membranes in cells [87].

Typically a range of sizes of the unilamellar vesicles (meaning consisting of one single bilayer, rather than multilamellar – or even multivesicular – structures that can form spontaneously without controlled conditions) that are of most interest for such studies can be defined; small (or SUV; often defined up to 100 nm diameter but I will here use the term up to 200 nm), large (or LUV, up to 1 μm diameter), and giant (or GUV, up to 100 μm diameter) [88] . However, for clarity throughout this thesis I will adopt the term GUV for all vesicles formed by the emulsion method here developed irrespective of their actual size – which can be below 1 μm.

1.4.2 Giant Vesicles and Transmembrane Proteins

Giant vesicles as cell models is one paradigm of synthetic biology that offers promise for the study of cellular mechanisms through the creation of a minimally viable system. In this way we can remove the extraneous influences that can make the construction of tractable experiments, as well as the interpretation of results, highly challenging in studies on single whole-cells. Indeed, it is the simplicity of such models that then becomes their strength for probing these mechanisms [89], [90]. Their relatively large size compared to single molecules makes optical microscopy more practical than with SUV or LUV systems. However for the study of transmembrane proteins, GUVs offer challenges since the well-established insertion of purified transmembrane proteins into SUVs or smaller LUVs by the use of detergents to disrupt the membrane and allow

insertion, followed by removal of detergent, would be expected to disrupt the giant vesicle to the extent that it would collapse and reform as smaller structures. Whereas some transmembrane proteins, particularly pore-forming structures such as the well-studied toxin α-hemolysin, are able to self-insert into bilayers spontaneously and without the addition of a detergent [91], [92] (and see also the supplementary information of Christensen et al [93]) such behaviour is not observed for F_1F_O, necessitating more complex strategies. The use of detergent, and subsequent disruption of liposome structures, is not a problem with an SUV (which will reform at a similar size) – but the larger size of a GUV is its very advantage. However it is worth noting that Daniel Levy's group in April 2013 demonstrated that the inclusion of detergents for the insertion of transmembrane proteins was not completely incompatible with the retention of larger giant vesicles structures, but that in fact the use of carefully-tuned levels of detergent could allow a GUV to remain stable and for the highly robust transmembrane proteins utilised to very slowly (up to 16 hrs) incorporate into the membrane and remain functional [94].

Successful incorporation of functional transmembrane proteins into GUVs has been reported by several groups using dehydration of proteoliposomes (SUVs) onto a surface followed by rehydration to reform new, giant vesicles [95]–[97]. Again this requires the use of highly robust proteins; though, this technique was reported with an ATP synthase that retained functionality by using a uniquely hardy thermophilic *Bacillus* strain that has not been made widely available [98].

Other techniques that have been developed in response to the need for less harsh treatments for the insertion of more fragile membrane proteins include multiple fusion-based approaches such as peptide-induced fusion [99], in which a short amino acid sequence coupled to the lipid bilayer of a proteoliposome induces fusion with a GUV and subsequent functional delivery of bacteriorhodopsin. In a lipid-cosolvent method [100], proteoliposomes formed conventionally are mixed with a lipid-containing oil phase over a 12+ hr period to induce mutual fusion and result in protein-containing GUVs upon separation of the two phases. In a slow spontanteous-fusion based method [101], proteoliposomes and GUVs are mixed in a concentrated form and incubated for 12+ hrs in which proteins are found to incorporate into GUVs in a mechanism that is not totally clear but perhaps related to lipid composition, concentration of objects, and temperature. In oligonucleotide-induced fusion [102], complementary single strands of DNA are conjugated to lipids and induce fusion of the attached liposomes upon meeting (as well as being useful for tethering liposomes to the surface). In liposome fusion, separate liposomal vesicles merge together to form a new single object. Ca^{2+}-induced fusion of mutually anionic proteoliposomes with either each other [103], or with planar bilayers [104], [105], have a substantial history in the literature (Ion Channel Reconstitution, edited by Christopher Miller, offers a review on this field [106]). A recent publication (July 2014) on protein-mediated fusion using the isolated SNARE proteins that typically mediate lipid fusion in cells, combining an F_1F_O proteoliposome with a primary proton pump to generate ATP synthesis, offers an exciting approach that has been demonstrated to be compatible with F_1F_O [107].

1.4.3 F_1F_O Delivery to a Giant Vesicle System by Charge-Based Lipid Fusion

Since *E. Coli* F_1F_O is a particularly non-robust protein, requiring careful handling during its purification, then reconstituting the protein into a lipid environment before attempting approaches to incorporate into a larger structure should offer the best method for ensuring retention of function of the protein. Hence this lends itself to a fusion-based method; some fusion methods that have been established have already been discussed and, whilst those that had been published by the earlier stages of this research were generally considered possible research avenues, they were not pursued based on their complexity or the practical availability of required components. Charge-based fusion, however, has often been studied for its relative simplicity, requiring few if any components beyond charged lipids readily available.

Whilst charge-based fusion studies in the literature have most often focussed on mutually anionic lipid pairs induced to fuse by the addition of divalent cations (particularly Ca^{2+} [87], [108], [109]), there is also long-standing precedent for the use of complementary cationic and anionic lipid pairs [93], [110], [111]. Such oppositely-charged lipid mixtures fuse essentially immediately upon encountering each other. This fusion is not expected to be controllable in the same way that Ca^{2+}-induced fusion of mutually anionic lipid pairs can be stopped by the removal of the calcium ion; however the significant advantage it does offer is that by its nature there are two clearly distinct sets of objects that will not fuse within their own set. This allows us to define our giant vesicle as one set and our proteoliposome as another. Cationic lipids have a long history of use in medical

research for transfection; by wrapping DNA with such cationic lipids then a cell (this method is particularly used for eukaryotic cells) can fuse with the charged lipid-DNA complex and absorb the DNA contents [112].

The nature and timing of charge-based fusion events has been studied using high-speed cameras [113], generally proceeding rapidly via an initial hemifusion – in which the bilayer partially fuses but content mixing does not occur – to full fusion with full content mixing and the formation of a new structure with a mixed lipid bilayer (the rates and final outcomes of which depend on lipid composition and hence the strength of mutual attraction). Hemifusion can also be a stable end-state, depending on lipid compositions.

1.5 The Current State of F_1F_O Models to be Tested

There remain many questions regarding the operation of ATP synthase (both in general and regarding variation across species) that can hope to be addressed by a single-molecule darkfield assay with proper bilayer energisation. Some of the most pressing at least in broad terms would be:

- What is the mechanism behind fully coupled rotation of the F_1F_O complex; what are the steps of rotation and their relation to the 10-fold c-ring and the 3-fold αβ complex, the dwell times for synthesis, hydrolysis, or ion transport; in particular, are synthesis and hydrolysis mechanisms simply the reverse of each other, or do they differ in their mechanistic behaviour
- What is the level of proton-motive force required for synthesis and what is the relationship between the components ΔpH and Δψ (and also how does

this vary across different species; see for example the work of Peter Gräber's group on this in bulk studies [114], [115])

- Under what conditions does the motor switch between hydrolysis and synthesis modes (in species that are capable of both)
- What is the coupling between the c-ring and the a-subunit (and other subunits) and how does it vary with proton-motive force
- What is the relationship between proton-motive force and the load the F_O motor is capable of driving
- How do synthesis- and hydrolysis-driven rotation respond to varying levels of ATP, ADP, inhibitors, and proton-motive force (and across different species)

1.6 Overview of the Methodology Developed in this Thesis

This thesis will describe the development of a lipid-fusion-based approach that allows the modular development of components for a single-molecule study of membrane-embedded F_1F_O to be formed individually and brought together at the coverslip surface for viewing under a microscope. This methodology would immediately be applicable to extensions of the technology to include further components – such as active proton-pumping systems like proteorhodopsin, or passive ionophores such as valinomycin for the separation of ΔpH and $\Delta\psi$ (and development of diffusion potentials). Most particularly this approach, by defining

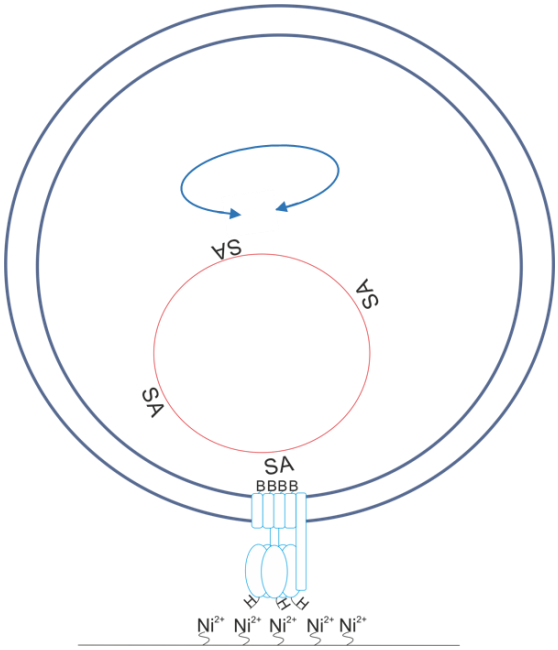

Figure 1.4
Overall schematic view of the final experimental aim. The F_1F_O (light blue) is embedded in a giant unilamellar vesicle (dark blue) which contains a gold nanosphere (red) functionalised with streptavidin (or neutravidin etc). The mutant F_1F_O has biotin-labelling ('B') on each of its c-subunits introduced via an engineered cysteine at that site. There are three hexa-histidine tags ('H') on the F_1 - one on each β-subunit. These can be bound to a Ni^{2+}-functionalised coverslip. The firm grip of three hexa-histidine tags means the rotation of the c-ring is expected to be transmitted directly to the gold bead. The motion of the gold bead can be observed though darkfield microscopy with high time- and space-resolution. pmf is clearly defined between the interior and exterior of the giant vesicle.

a clearly enclosed vesicle volume, is intended to allow formation of proton-motive force and hence the study of ATP synthesis-driven rotation. It is only by defining such a fully enclosed space, as occurs in a cell, that this becomes tractable.

This approach has been developed for use with a functionalised gold nanosphere of 40 nm-100 nm diameter, given the microscopy intended is an already-developed laser backscatter darkfield microscope with high space- and time-resolution, but other probes such as gold nanorods would likely be compatible. The addition of fluorophores – either internal to the giant vesicle or within the bilayer for the study of pH or membrane potential – has been assumed to be of interest from the start and has been explored. Optical devices innovated for the simultaneous study of a gold probe by backscatter darkfield with fluorescent probes are described.

By the use of lipid-in-oil emulsion, I have developed a giant vesicle system which can incorporate arbitrary objects. I have demonstrated that it is possible to form such giant vesicles incorporating a functionalised gold nanosphere of appropriate size for rotational studies present internally and freely moving in the interior space. This allows for the attachment of such a functionalised gold nanosphere to the displayed c-subunits of the F_1F_O (which will face the interior of the vesicle). To my knowledge the inclusion of freely-moving gold nanospheres of this size within the interior space of lipid vesicles has no precedent.

I have developed a methodology for the insertion of the F_1F_O into a separate small unilamellar vesicle (SUV) by standard detergent-based methods followed by the fusion of the SUV and GUV together to form a new post-fusion product GUV. This prevents the contact of detergent with the giant vesicle and thus allows the retention of its interior contents. A charge-based fusion based on mixtures of anionic and cationic lipids with natural (zwitterionic) lipid extracts has been developed; content mixing and mixing of lipid leaflets have both been demonstrated. Hence transfer of transmembrane proteins would also be expected and evidence is provided of functional F_1F_O in a post-fusion product by the quenching of a ΔpH-sensitive fluorescent probe. To my knowledge this approach has no precedent for the transfer of functional transmembrane proteins from one liposomal object to another (though some other fusion methods have been used to transfer functional transmembrane proteins, such as by the use of SNARE proteins [107], and SUVs and GUVs have previously been shown to undergo complementary charge-based fusion [116]).

In order to view rotation the F_1F_O requires an anchoring on the exterior of the giant vesicle to a coverslip surface; then viewing through the microscope a laser backscatter darkfield microscope allows high-contrast viewing of a gold nanosphere without interference from the giant vesicle structure, which is minimally scattering. The mutant F_1F_O is attached via his-tags on the three β-subunits to the coverslip and the gold nanosphere is attached internally via biotin-avidin linkage to the c-ring subunits (by the use of cysteine modifications on mutant F_1F_O functionalised with biotin). Since the β-subunits are firmly held with three anchoring points, the c-ring should rotate in hydrolysis and synthesis modes in opposite directions. The choice to orient the F_1F_O in this manner is driven by its more favourable insertion into proteoliposomes in an F_1-outward orientation; it has been assumed that upon fusion it will retain this orientation in the post-fusion giant vesicle.

The aim of the project as presented in this thesis has been to develop a method for viewing the single-molecule hydrolysis-mode rotation of the c-ring subunit; though the approach has been designed with the study of synthesis-mode rotation as its eventual end-goal, this is not within the scope of the thesis. There were many steps to overcome in the development of the methodology; the only steps that had previously been established within the research group were the purification of the mutant F_1F_O and the approaches to single-molecule study by darkfield (on isolated F_1).

I see the current work as sitting within the paradigm of the giant unilamellar vesicle as a cell model and would hope that using the methods developed within

this research it would be possible to expand upon the study of ATP synthase into the inclusion of other transmembrane proteins such as bacteriorhodopsin for controllable energisation of the giant vesicle structure and beyond into the study of other mechanisms incorporable into a giant vesicle via lipid fusion-based transfer and subsequent single-molecule study under the microscope.

Chapter 2 Methods, Equipment, and Materials

2.1 Introduction

This thesis describes the development of a new methodology; to that end 'methods' in some sense describes the bulk of the work performed, in that much was developed and refined with no starting base of experience within the research group. As each step in the development of the methodology outlined in Chapter 1 was overcome, the next step had to be developed before the proposed system outlined in section 1.6 could be arrived upon. Gradual optimisation inevitably results from the development of new protocols; I have presented methods in their currently-finalised form in this chapter and in some cases discussion of the development of these protocols and earlier approaches are presented in the results chapters that follow where it has seemed of interest. I have also in this chapter given description of the more standard biochemical assays used; results of these assays are then also presented in the results chapters that follow. It is my intention that by providing full descriptions of all methods used, the results that follow in the next chapters will be most immediately straightforward to understand. Also presented in this chapter are descriptions of the microscopy utilised and also, in some cases, developed during the project.

2.2 Microscopy and Related Equipment

The bulk of development of the protocols utilised a relatively simple Nikon Eclipse TE2000-U inverted microscope, with fluorescent illumination provided by a Nikon HB-10104AF mercury arclamp providing a wide-spectrum illumination with a high intensity that was typically attenuated with neutral-density filters (the extent of blocking is noted on images where relevant) and utilising a filter cube for selection of appropriate wavelengths. A Nikon Plan-Fluor 100x oil objective was used for all microscopy images shown, with a numerical aperture of 1.30. Several cameras were used throughout the project, with most results presented here using a Toupcam UCMOS05100KPA for colour image-capture and a Thorlabs 340M-GE for higher-sensitivity black and white recording (note that this camera includes an artifact at high gain which leads to a segmentation where the left half of the image is brighter than the right, and images presented in the thesis have been adjusted to remove this; there remains an artifact of some black lines running vertically). Also used were a Watec WAT-902H Ultimate and a WAT-2215 for the highest-sensitivity responses in black and white and in colour, respectively.

In order to develop darkfield capability alongside fluorescent illumination, an insert device was designed and built during the course of this research jointly by Dr Robert Ishmukhametov, myself, and Dr Richard Berry to be compatible with this Nikon inverted microscope and currently has patent-pending status. Its description follows in section 2.2.1.

For single-molecule rotation studies, a backscatter laser darkfield microscope designed and built by Dr Richard Berry, Dr Yoshi Sowa, Dr Bradley Steel, Dr Ashley Nord, and Dr Richard Branch was available. This utilised a Photron Fastcam 1024PCI camera capable of recording up to 109 500 frames per second (hence around 20 μs time resolution). The arrangement sits on an air table, with sub-nanometre noise. Since backscattering darkfield aims to monitor the movement of a single bead, we can locate its centre with an arbitrary accuracy – it is hence the noise of the stage which becomes critical in ensuring we can track this motion accurately. An earlier iteration of this design was previously described [117], though some alterations have been made to the light paths in the current arrangement. Single-molecule studies presented in Chapters 5 (on F_1) and 6 (on F_1F_O) have made use of this microscope. This utilises a 633 nm laser (Melles Griot LHX1, 10 mW), as well as an LED for brightfield viewing (Thorlabs M617L2).

In the interest of developing the use of a supercontinuum broad-spectrum (or 'white-light') laser acquired by the research group (NKT Photonics SuperK Extreme EXW), a wavelength-selection system to allow particular narrow or broad wavelengths to be isolated from this source was designed and built by Dr Richard Berry, the author Aidan Russell, Dr Ashley Nord, and Dr Bradley Steel and currently has patent-pending status. This system was combined with the laser darkfield microscope for some proof-of-principle tests and it is hoped its use will be expanded in future work; it can be used both to replace the current 633 nm input for backscattering darkfield (either at this or a different wavelength)

and can also be used to provide fluorescent illumination for combination of this technique with darkfield. It is described further in section 2.2.2.

2.2.1 Backscatter Darkfield Insert Device

Although the simple Nikon microscope used was readily capable of forward-scatter darkfield illumination by means of a specially-adapted condenser and a variable numerical-aperture objective, this required swapping around of components and was difficult to combine with epifluorescence in the same field of view owing to the numerical aperture required for forward-scatter darkfield. In order to simplify this arrangement, and build upon the research group's earlier work with backscatter darkfield, the concept of the backscatter insert was arrived at due to the design of the inverted microscope; this included a sizeable gap directly beneath the objective typically used for the insertion of a Wollaston prism for differential interference contrast (DIC). 4 mm high, 20 mm wide, and 45 mm deep, this gap allowed just enough room for the careful insertion of a secondary light-path by the direction of an optical fibre coupled to a strong LED light-source and the placement of a 45° rod-mirror in the centre of the optical axis of the objective. This mirror both directs the incoming light vertically upwards onto the sample (from its incoming horizontal axis) and also removes from the imaging optics further down the microscope that light which is directly reflected back. Since most of the light passes straight through the sample, then all that is collected on the imaging path is the light which has been scattered backwards by the sample at some angle high enough that it is not directed back onto to the rod-mirror itself (but not too high that it fails to be collected by the objective). This design follows from previous work for backscatter darkfield

microscopy with 45° mirrors partially occupying the back-focal plane including by the Berry group in the laser darkfield microscope previously outlined (section 2.2), as well as similar systems such as that by Ueno et al [118]. The novelty of the device lies in its ready ability to immediately and reversibly modify an existing commercial microscope to backscatter darkfield capability without any requirement for additional adjustments or alignments.

This device currently has patent pending status and it is hoped that it may be developed for commercialisation. Furthermore its applications to interference reflection microscopy and epifluorescence have been documented by Dr Ishmukhametov; its expansion to include a TIRF capability, by the movement of the rod-mirror slightly out of the centre of the objective axis, has been suggested but not yet tested (such as in the system by Mashanov et al [119]). Overall aspects of the design were suggested by Dr Berry. My contribution to this device has been to design and build the current prototype's main body; including particularly aspects related to the placement and alignment of the rod-mirror that have improved its image quality compared to the first prototype built by Dr Ishmukhametov. Several images taken with this device are presented in Chapter 4 (Figure 4.2), which make clear its robust benefit to this project in ease of imaging and assessment of giant vesicle objects and the movement of entrapped gold nanospheres. When using the device to combine both the darkfield lightpath with the fluorescent lightpath of the microscope, as presented in Figure 4.2, some light from the fluorescent lighpath is lost due to the presence of the mirror near the back focal plane – the proportion of light lost has not been

characterised but naturally is observed to negatively impact image quality to some extent (however this is not problematic for the immediate purpose of the observation of gold nanospheres within GUVs as demonstrated in Figure 4.2).

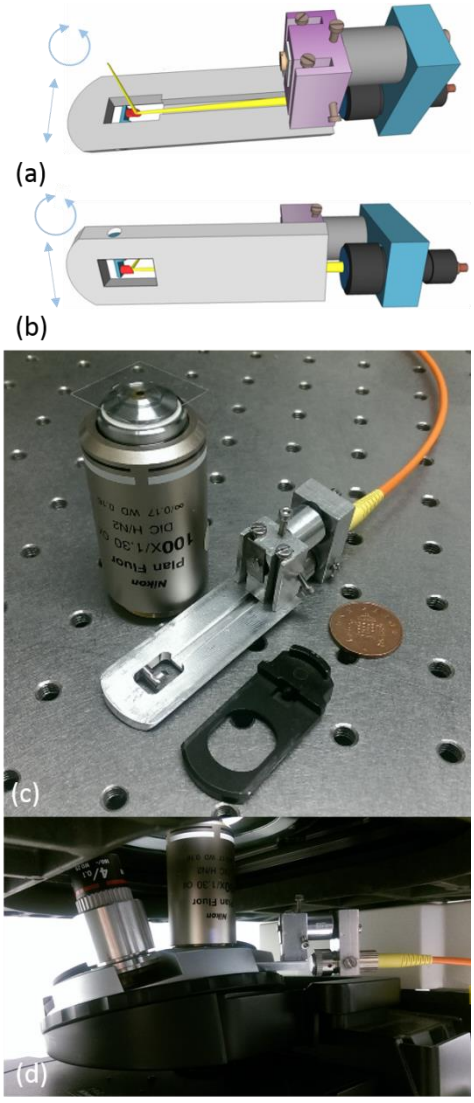

Figure 2.1
The most recent prototype of the backscatter darkfield insert device. (a) and (b) show schematics of the device including an illustration of the light path from the LED. (c) shows the device next to a 100x objective and the Wollaston prism whose shape the device was constructed to mimic in order to fit within the microscope design, as well as a current one-pence coin for size comparison. (d) shows the device in action fitted under the microscope objective in the Wollaston prism slot. The rod-mirror in the device (highlighted red in (a) and (b)) is designed to be moveable in the two modes indicated; further into or out of the central light-space, or rotated in position to direct the beam at a particular angle up through the objective. The arrangement at the back of the device (colour purple, blue, black, and grey in (a) and (b)) is designed to allow the incoming light beam from the optical fibre to be precisely directed onto the rod-mirror and directed upwards through the objective. It is hoped that further iterations will improve the prototype. The schematic images (a) and (b) were produced by Dr Ishmukhametov and the photographs (c) and (d) by the author. Currently the design is pending patent approval.

2.2.2 Supercontinuum Laser Wavelength Selection Device

The supercontinuum laser outputs a coherent beam from 400 nm – 2400 nm. The essential design feature of the wavelength selector is to split the light with a prism, creating a spectrum of light with predictable spatial separation of

wavelengths in one dimension. This spectrum can then be physically obstructed by black-coated metal, to absorb some portions of the spectrum, while the desired portions are allowed to pass through gaps machined in the metal blocking components and then allowed to reform back through the prism into a beam of now arbitrarily-limited wavelengths. This beam is then coupled to a fibre and output to a microscope. Essentially this forms a completely arbitrary selection of any of: a single wavelength of a desired laser input, a broad spectrum of wavelengths, several independent wavelengths, or several broad wavelength regions as desired.

The device currently has patent pending status and it is hoped that it may be developed for commercialisation. So far its use has been limited; I present one image in Chapter 5 (Figure 5.8) that was taken as a proof-of-principle. Dr Berry and Dr Steel designed the overall arrangement and built the first prototypes. My contribution has been to design and build the current prototype of the physical wavelength selector, which operates by use of an aluminium mask with variable width and horizontal position of a gap to allow particular wavelengths in the spectrum through whilst blocking the majority. I also built the initial lightpath arrangement, though this has since been iterated by Dr Nord into the current prototype.

Owing to the design resulting in no physical impedance of the selected wavelength regions, there is little significant distortion or signal loss that commonly accompanies other commercially-available wavelength selection systems based on acousto-optical tuneable filters (AOTFs), spectral filters, or

diffraction gratings. Further to this, the system is economical in cost and has only one moving part - the blocking component (which should maximise its lifetime and minimise maintenance expense). The use of a prism allows higher laser power without damage to the components than a diffraction grating, which was found to be damaged during operation when tested. Furthermore AOTFs would only allow narrow bands, which would also be limited when using spectral filters, while this system is in principle fully adjustable as and when required for any bandwidth or wavelength region of interest.

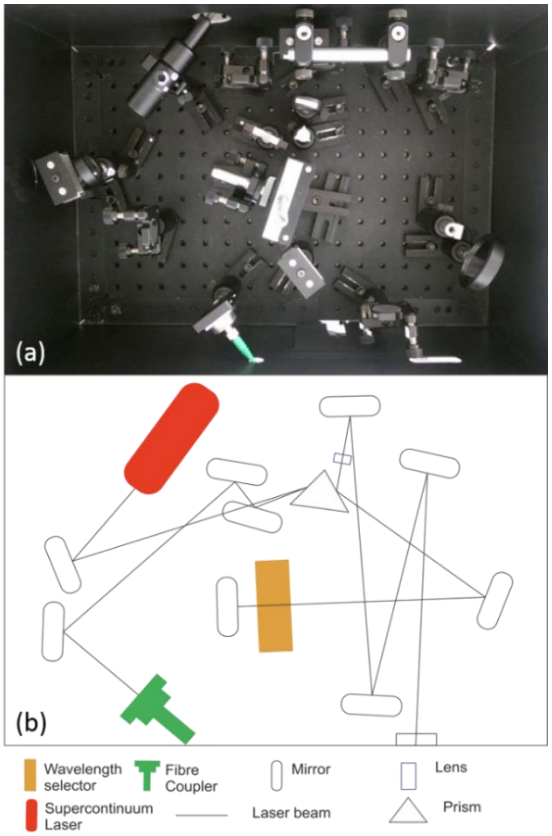

Figure 2.2
The most recent prototype of the supercontinuum wavelength selector device. (a) photograph and (b) schematic. The laser beam is split by a prism and sent to the physical wavelength selection device where it is spatially filtered, then reflected back along the same path and recombined. The beam here is sent down a slightly different path to the incoming light, meaning it can be picked up by a mirror at this point and sent down to the fibre coupler and on to the attached microscope or other end point. A fraction of the beam after spatial filtering is reflected at the prism and this is picked off down a separate path to form the reference beam at low intensity which can be read off by the user (by projecting onto paper).

2.3 Notes on Protocols

2.3.1 Lipids Used in this Thesis

There are seven different lipids that appear in this study. First of all I must make clear a distinction between two types of phosphatidylcholine I have used; for

purification of protein, I have used a Sigma-supplied "L-α-phosphatidylcholine Type II-S" from soybean, which gave four bands on thin-layer chromatography (Chapter 4, Figure 3.8). For liposome and proteoliposome formation (section 2.6.1), I have consistently used a distinct extract which I have referred to generally in the text as 'Soybean PC'; supplied by Avanti Polar Lipids, it is stated to consist of 40% L-α-phosphatidylcholine, along with 16% phosphatidylethanolamine, 11% phosphatidylinositol, and 33% 'unknown' components; though, I have presented results that give a single band on thin-layer chromatography for this mixture (again, see Figure 3.8). Its use is owing to its having been established by others in the research group to give stable proteoliposomes; this is also demonstrated by findings presented in section 3.3.2, as well as its low economic cost. For future work the refinement of the lipid mixture to a pure format rather than a natural extract will be important to ensure total reproducibility of the work. Secondly the charged lipids 1-palmitoyl-2-oleoyl-*sn*-glycero-3-phosphate ("POPA"), which is anionic, and 1,2-dioleoyl-3-trimethylammonium-propane ("DOTAP"), which is cationic, are used for charge-based fusion studies. These are both supplied in a pure form by Avanti. Finally two lipid-conjugated fluorophores were also used; these are *N*-(7-nitrobenz-2-oxa-1,3-diazol-4-yl)-1,2-dihexadecanoyl-*sn*-glycero-3-phosphoethanolamine (NBD-PE, Life Technologies), where NBD fluorophore exists on the head group, and cholesteryl 4,4-difluoro-5,7-dimethyl-4-bora-3a,4a-diaza-s-indacene-3-dodecanoate (BODIPY-cholesteryl, Life Technologies), a derivative of cholesterol also with a fluorophore conjugated.

Since Soybean PC is a natural lipid mixture (including some "unknown" components), but we know that purer forms of Soybean PC have a dominant species with a molecular mass of 775, and since DOTAP as a pure species has a molecular mass of 698 while POPA has a mass of 696 (hence broadly similar), I have adopted the simple convention of stating the composition of mixtures as a percentage by mass only and not by molar ratios (which would not be meaningful for the "Soybean PC" mixture used; these molecular mass numbers are sourced from the supplier).

2.3.2 Chemicals used in this Thesis

All chemicals were supplied by Sigma unless otherwise stated.

2.4 Protein Purification

2.4.1 F_1F_0 Expression and Purification from *E. Coli*

The protocol is based on one originally established by Dr Ishmukhametov et al. [120]. The main innovation introduced into the purification compared to the cited version has been the addition of reducing agents to biotin-labelling steps (the development of this step is described in Chapter 3). There are many alternative purification protocols in the literature such as those established in the group of Masamitsu Futai [121], the group of Alan Senior [122], and the group of Robert Fillingame [123]; the procedure used here is rapid, saving both experimental time and typically yielding higher activity than alternative methods (as reported by Ishmukhametov et al.).

Strains

Escherichia coli F_1F_O-ATP Synthase used in this study was expressed in the DK-8 *E. Coli* strain [124], which lacks the ATP synthase operon in its chromosome. This is complemented by derivatives of the pVF2 plasmid – which contains a cysteine-free ATP synthase base with hexa-histidine tags on each of the three β-subunits, inserted four amino acids from the N-terminus. From this cysteine-free base three mutants were available: a single cysteine on each of the three α-subunits, a single cysteine on each of the ten c-subunits, and a third with both of these modifications. In each case the cysteine has been inserted two amino acids from the N-terminus on the respective subunit. Tetracycline resistance is present in the DK-8 chromosome and ampicillin resistance is present in the pVF2 plasmid. These plasmids were constructed previously and the c-subunit mutant has been used in single-molecule studies [27]. Full sequences are listed in the appendix.

Buffers

French press buffer: 200 mM Tris (tris(hydroxymethyl)aminomethane), 100 mM KCl, 5 mM $MgCl_2$, 100 µM EDTA (ethylenediaminetetraacetic acid), 2.5% glycerol, pH 7.8 (typically 200 ml used per purification; this buffer can be made in bulk and stored at 4 °C). **Membrane extraction buffer**: 50 mM Tricine (*N*-[tris(hydroxymethyl)methyl]glycine), 100 mM KCl, 40 mM 6-aminocaprioc acid, 15 mM *p*-aminobenzadimine, 0.8% L-α-phospatidylcholine (Sigma; from soybean, type II-S), 1.5% octyl glucopyranoside, 0.5% sodium deoxycholate, 0.5% sodium cholate, 2.5% glycerol, 30 mM imidazole, 2 mM $MgCl_2$, 0.1 mM EDTA, pH 7.5 (typically 80 ml used per purification; this buffer is made only on the day of purification). **Ni-NTA column elution buffer**: as membrane extraction buffer

with 180 mM imidazole final concentration (typically 3 ml made per purification, with 2 ml used and the rest stored at -20 °C for use in BCA or other assays to follow). **Biotin-labelling buffer**: as membrane extraction buffer with 60 μM biotin-maleimide, or around 40x the expected F_1F_O concentration (Thermo Scientific, EZ-Link Maleimide-PEG_2-Biotin). **Reducing buffer**: as membrane extraction buffer with 250 mM β-mercaptoethanol (2 ml per purification; only required for c-subunit cysteine modification).

Protocol

Taking a frozen stock of the desired mutant (stored at -80 °C), a sterile loop is inserted and then directly placed into 60 ml Luria Broth (LB) including 200 mg/L ampicillin and 12.5 mg/L tetracycline. This is incubated at 37 °C overnight at 200 rpm shaking; meanwhile 4-6 L of LB are prepared and autoclaved ready for the next day. Each 10 ml of the stationary cell culture is diluted into 1 L of LB (including ampicillin, but not tetracycline) for 4-6 L total (note ribbed flasks give a better yield of cells). This is incubated for 5-7 hrs at 37 °C with 200 rpm shaking. Cells are subject to centrifugation at 5000 g 23 mins 4 °C (in a JLA 8.1000 Beckman rotor). The supernatant is discarded and the cell pellets resuspended into two 40 ml JA-20 centrifuge tubes (using some LB medium). This is subject to centrifugation 12 000 g 15 mins 4 °C (in a Sigma 3K30 centrifuge), the supernatant discarded and the cell pellet stored in -80 °C to be left overnight for a break in the protocol.

The pellet is thawed from cold storage into lukewarm French press buffer to 40 ml, and kept on ice. A glass homogeniser (Fisher Scientific, 30 ml) is used to

resuspend the pellet, and DNase 1 (Thermo Scientific) 5-10 µl is added. The suspension is French pressed twice; a pressure of typically 1000-1200psi is used (in an SLM Aminco FA-078 French press). The solution is placed into one JA-20 centrifuge tube and subjected to a 7000 g 15 mins 4 °C spin (in a Sigma 3K30 centrifuge), upon which the supernatant (containing F_1F_O within sub-bacterial particles) is collected and the pellet (containing cell debris) is discarded.

All steps from this point must be performed strictly in a cold room or on ice. The supernatant is subjected to ultracentrifuge at 200 000 g (average; this corresponds to 50 000 rpm in a 70Ti Beckman rotor) for 1 hr at 4 °C. The pellet (containing F_1F_O within sub-bacterial particles) is resuspended in 20 ml of membrane extraction buffer; the supernatant (containing cytoplasmic contents) is discarded. A small glass homogeniser is used (Fisher Scientific, 3 ml) for resuspension; the homogenised sample (containing F_1F_O) is left on rollers in a cold room for 90 mins. This is then subject to ultracentrifugation under the same conditions of 200 000 g 1 hr 4 °C. The supernatant (containing F_1F_O) is kept on ice and the pellet (containing membrane fragments) is discarded.

In the meantime a gravity Ni-NTA column (Bio-Rad, Poly-Prep Chromatography Column) is arranged and 1.5 ml of Ni-NTA bead solution (Qiagen) placed and allowed to settle. This occupies 0.75 ml once excess water and solvents have passed out of the column. The column is washed with 10 ml of water. For purification of c-subunit cysteine mutants requiring biotin-labelling, the column must also be washed with 2 ml of 500 mM imidazole pH 7.5 to prepare it for the reducing step (this is not required for cysteine-free samples or for α-subunit

cysteine modification). 5-10 ml of membrane extraction buffer is run through the column to equilibrate. The sample supernatant, which occupies around 20 ml, can then be added stepwise. As it comes through the base of the column it is collected and once the sample has completely run through it is passed through the column a second time. The column is then washed with extraction buffer; the full 10 ml capacity of the column is filled twice (the F_1F_O is now bound to the Ni-NTA column via its his-tag).

For c-subunit cysteine mutants requiring biotin-labelling: 2 ml reducing buffer is added to the column and allowed to sit for 10 mins (by placing a cap on the end of the tube). The column is then washed with membrane extraction buffer in four steps; 2 ml, 3 ml, 5 ml, 10 ml. The steps help to ensure that any reducing buffer left on the sidewalls of the column is washed fully away (for other strains: reducing buffer and associated wash are not required). 2 ml of biotin-labelling buffer are added and allowed to sit for 10 mins (for the cysteine-free strain this step is also not required). The column is then washed with membrane extraction buffer 2 ml, 5 ml. Finally the sample is eluted from the column with 1-2 ml of Ni-NTA column elution buffer. The first 0.5 ml eluted is discarded and the next 1 ml is retained. This is the sample volume and contains the purified F_1F_O.

The protein samples may be tested immediately for ATP hydrolysis activity and/or protein concentration or placed into storage in liquid nitrogen for testing later; this is performed by dropping 10 µl at a time directly into liquid nitrogen. These frozen droplets are collected in cryotubes and stored in liquid nitrogen

until required. ATP synthesis activity could also be tested however this was not performed in this study.

2.4.2 F_1 Purification

F_1 was also purified occasionally. This is utilised in Chapter 5. This utilised a separate strain with cysteine on the γ-subunit and hexa-histidine tags at the α-subunits. Purification was performed by myself and by Dr Ishmukhametov. The protocol followed that published previously [125]. The initial stages are the same as above (including antibiotic resistance) until after the first ultracentrifugation step.

After ultracentrifugation, the supernatant is discarded and the pellet resuspended in stripping buffer (5.0 mM TES, pH 7, 40 mM 6-aminocaproic acid, 1 mM EDTA, 1 mM DTT (dithiothretol), 5% (v/v) glycerol) to 45 ml in 70Ti tube. This is subjected to 50 000 rpm 60 min 4C (70Ti rotor). The supernatant is mixed with 10x buffer (0.5 M Tricine, pH 8.0, 1 M KCl, 300 mM imidazole, 50 mM $MgCl_2$) in a 10:1 (v/v) ratio. Glycerol is added to 15% (v/v) final concentration. This is loaded onto a Ni-NTA column (0.75 ml of resin, prepared as described previously with no imidazole step) equilibrated in 1x buffer (50 mM Tricine, pH 8.0, 100 mM KCl, 30 mM imidazole, 5 mM $MgCl_2$, 15% glycerol). The column is washed with 1x buffer two times. To biotin-label the F_1, biotin-maleimide (Pierce) is added to the column in an equimolar (approximate) concentration in 1x buffer. Then, the column is washed twice more with 1x buffer. To elute F_1, 2 ml F_1 elution buffer (50 mM Tricine, pH 8.0, 100 mM KCl, 180 mM imidazole, 5 mM $MgCl_2$, 15% glycerol)

is added to the column. The first 0.5 ml eluted is discarded and the next 1 ml retained. F_1 is stored in droplets in liquid nitrogen.

2.5 Characterising Solubilised Protein

2.5.1 BCA Protein Concentration Assay

Bicinchoninic acid (BCA) assay is used to determine final protein concentration as eluted from the Ni-NTA column. Other equivalent assays include the Lowry method or the Bradford method [126], [127]. This concentration measurement gives both an immediate assessment of the success of the purification and allows for calibration on the protein activity assays to follow. A kit (Pierce) was used and the fast protocol followed. Since imidazole in the elution buffer is known to interact with the BCA reagent, an equal volume of elution buffer to the protein sample volume is added to the BSA calibration samples to correct for this offset. A Varian Cary 50 WinUV spectrophotometer was used to measure changes in absorbance at 562 nm; plastic 1 ml cuvettes offer sufficient transparency at this wavelength.

2.5.2 Protein Gels: Tricine-SDS-PAGE

Sodium dodecyl sulfate polyacrylamide gel electrophoresis (SDS-PAGE) unfolds protein and displays individual subunits separated by mass. Schägger's protocol for Tricine-SDS-PAGE [128] was followed with very little modification. Ruby-sypro was from Bio-rad and their fast staining protocol was observed.

Buffers

Separate cathode and anode buffers are used; for the gel tank system used this corresponded to the internal and external parts of the tank respectively. **Cathode**

buffer: 100 mM Tris, 100 mM Tricine, 0.1% SDS (Sodium Dodecyl Sulfate, Acros Organics), pH uncorrected. **Anode buffer**: 100 mM Tris, 22.5 mM HCl, pH 8.9. 5x loading buffer: 300 mM Tris, 50% glycerol, 0.001% bromophenol blue pH 7.0.

Protocol

Samples are prepared with a variable amount of protein depending on the later processing planned, but typically 1-10 µg is loaded per well (2.5 µg gives good results in Ruby Sypro staining); in an eppendorf the required volume of protein is added along with 2 µl of 5x loading buffer and SDS (Agros Organics) to a final concentration of 3% (typically SDS was prepared as a 20% solution in water). Water is added to a final volume of 10 µl per sample. Samples are heated to 90 °C for 2 mins to unfold protein. Typically a gradient gel of 4-20% polyacrylamide (Expedeon) gave best results across all F_1F_O subunits, however a 10-20% gradient gel (Bio-Rad) was also used occasionally for better viewing of the lower subunits (particularly the c-subunit). Samples are loaded to each lane of the gel, with an additional lane used for 3-5 µl of protein ladder (Benchmark, Life Technologies) for size calibration (or a pre-stained ladder for Western transfer procedures; ColorPlus, New England Biolabs). The gel tank is connected to a power supply and run at 140 V until the blue marker of the ladder is seen to reach the bottom of the gel (around 45 mins). The power supply is removed, the gel separated from its plastic container and rinsed in distilled water. The gel may then be stained or taken for further processing. Note that attempts to run the gel at a lower voltage of 30 V for the initial stages (until the sample has entered the stacking gel, as advised in Schägger's protocol paper [128]) were not observed to improve results.

For reducing conditions, up to 250 mM beta-mercaptoethanol may be included with each sample (perform on a separate gel to non-reducing conditions).

2.5.3 Protein Activity by NADH Absorption

This assay has been used since the earliest studies of ATPases [129] to measure ATP hydrolysis rates. Note that this assay can also be performed on protein embedded in proteoliposomes and this is described in Chapter 3; the protocol is the same. PEP is phosphoenolpyruvate, PK is pyruvate kinase, LDH is lactate dehydrogenase, NADH is nicotinamide adenine dinucleotide (reduced form); PK and PEP form the ATP regenerating system and LDH and NADH are secondary components that allow this regeneration to be monitored in the spectrophotometer. EDTA is ethylenediaminetetraacetic acid and is often used in small amounts to chelate any stray metal ions (this is not essential). As ATP is hydrolysed to ADP and phosphate, the reaction of ADP and PEP is catalysed by PK to form ATP and pyruvate. In turn, the reaction of pyruvate and NADH is catalysed by LDH to form lactate and NAD^+. Since NADH absorbs at 340 nm, and NAD^+ does not, the reaction can be monitored by changes in absorbance at this wavelength.

Protocol

100 µl of the desired functional buffer (such as 100 mM KCl, 25 mM Tris, 25 mM Bis-Tris, 2 mM $MgCl_2$, 0.1 mM EDTA, pH 8.0) is loaded into a quartz cuvette. Added to this is 2 mM PEP, 1 mM ATP, and approximately 10 units each of PK and LDH; these compounds are made in low-buffering capacity solutions at: PEP 90 mM, ATP 100 mM, PK and LDH approximately 1200 units/ml each with 100 mM

KCl, 2 mM TES, 10% glycerol pH 7.5. The amount of PK and LDH to add should be calibrated against a known quantity of ADP; it should be sufficient PK and LDH (along with 2 mM PEP and 200 µM NADH) that the quantity (which should be selected by taking a maximum expected rate of ATP hydrolysis per second for the quantity of protein to be added and then including a comfortable margin of 20-50x that amount) of ADP added is 90% converted to ATP within 1-2 seconds based on the NADH response. This ensures that the PK/LDH response will never be rate-limiting and true ATPase activity will be measured. Typically this corresponded to around 5-10 µl of the described concentrations of each.

The absorption at 340 nm is set to zero in the spectrophotometer against the sample and then NADH 200 µM is added (note absorbance is expected to be around 1.2; much lower than this could indicate degradation of the NADH stock, typically stored at 100 mM). Once a stable signal has been observed for 1-2 mins, roughly 0.1 µg of protein is added and mixed (protein must be thawed from liquid nitrogen and immediately kept on ice, being withdrawn only just prior to addition to the sample volume). If the signal continues to be observed for 3-10 mins, the plunging absorbance signal will cease once all the NADH has been exhausted. This provides a useful calibration to the addition of an F_1-inhibition compound such as 50 mM sodium azide on a later repeat; if such a compound is added long before NADH is exhausted, then the subsequent halting of NADH oxidation on addition of sodium azide affirms that the reaction observed is due to the upstream action of F_1F_O. Typically three measurements would be made at each condition in order to provide a reliable average. Room temperature should

be noted since this will affect activity rates (no temperature control on the spectrophotometer used was available).

Post-Measurement Calculation

In order to convert the measured gradient of activity into a rate, we must bear in mind the units used to describe activity: μmoles of substrate converted per minute per mg of protein (generally referred to as units/mg). The stoichiometry of NADH turnover to ATP is 1:1 so we must simply calculate the number of μmoles of NADH converted per minute using the extinction coefficient 6.22 $mM^{-1}cm^{-1}$. The later, linear part of the trace is taken when measuring the gradient. To then convert to ATP per second, we multiply by 500 (assume a molecular mass of F_1F_O of 500 kDa) to now obtain units of μmoles ATP per μmole F_1F_O per min; dividing by 60 we obtain ATP converted per F_1F_O per second.

2.5.4 Western Blot and Specific Labelling of Biotinylated Subunits

Western blotting displays protein subunits separated by SDS-PAGE to probes for testing of binding sites; it was first described in 1979 [130] and the protocol described varies only slightly from there, after guidance from colleagues and also reference to a helpful guide from GE Healthcare (particularly for the specific labelling steps) [131].

Buffers

Transfer buffer is 25 mM Tris, 192 mM glycine, 20% methanol, pH is uncorrected; it should be kept chilled prior to use (4 °C). **TBS** is Tris-Buffered Saline 50 mM Tris, 150 mM NaCl, pH 7.5.

Protocol

First, a Tricine-SDS-PAGE gel is performed as previously described with 10 μg of protein per well and using a pre-stained protein ladder as a reference. No further processing or staining should be performed on the gel prior to the Western blot and the transfer should start soon after the gel is finished to reduce the effect of any diffusion of bands that may occur in the gel over time.

Four pieces of cellulose blotting paper (Whatman) are cut to the same size as the gel to be transferred, along with one piece of polyvinylidene fluoride (PVDF) membrane with 200 nm pore size (Bio-Rad). Blotting paper is soaked in transfer buffer and laid onto a blotting cassette over a sponge pad. The gel is carefully and smoothly placed on top of the damp paper. The PVDF membrane is first soaked in pure methanol for 5 mins, then transfer buffer. The membrane is then placed carefully and smoothly on top of the gel (the membrane should not be touched with bare hands) followed by the other two pieces of blotting paper and a sponge pad. The cassette is closed and placed in the appropriate orientation into the tank alongside an enclosed ice pack to keep the tank cooled (the protein will migrate towards the anode; note the anode is typically coloured red and the cathode black). The power supply is arranged to provide a constant 100 V over 1 hr; the pre-stained ladder allows assessment of the efficiency of transfer. The transfer buffer will be warmed during the procedure. Note that the use of higher electrical potential settings gave poor results owing to overheating, leading to a smearing of bands on the transfer.

The membrane is then removed and placed in a 5% solution of milk powder in TBS for 1 hr, in order to block non-specific binding. The membrane is then washed in TBS and submerged in 20 ml TBS complemented with streptavidin-Alexa 647 fluorescent probe (Life Technologies) at a concentration of 0.25 µg/ml for 1 hr. It is then washed in TBS and either placed directly into a fluorescence-capable gel scanning system (Bio-Rad Pharos FX-Plus) to view bands in the expected wavelength, or allowed to dry and scanned within a few hours (no significant difference in image quality was observed between these two approaches tested). Note that despite the use of a pre-stained ladder it may not be immediately obvious which side of the membrane gives the clearer fluorescence image; therefore it is best to image both.

2.6 Proteoliposomes: formation and characterisation

2.6.1 Reconstitution of solubilised F_1F_O into liposomes using detergent

The protocol is based on the one published accompanying the F_1F_O purification protocol used [120], with some modifications based on the experience of colleagues. First, liposomes must be formed and then insertion performed – this was always done on the same day since the stability of liposomes themselves was not particularly well-characterised.

Formation of Liposomes

Lipids were generally stored in chloroform at -20 °C at concentrations around 25 – 100 mg/ml. DOTAP and POPA were purchased in this format as pure extracts. Soybean PC, which is a natural lipid mixture, was purchased as a solid and also

suspended in chloroform at 100 mg/ml. Bodipy-cholesteryl was purchased as a solid and suspended in chloroform at 1 mg/ml. Generally, 10 mg of chloroform-dissolved lipid is added to a glass vial and evaporated using nitrogen flow (around 2-3 mins) and then using a vacuum (around 30-60 mins). 1 ml of the desired buffer is then added to the vial and the sample left for 30 mins incubation to allow the lipid to enter suspension. The standard buffer used was 100 mM KCl, 50 mM MOPS, 2 mM $MgCl_2$, 10% glycerol, pH 8.0 (buffer 1). This results in 10 mg/ml of lipid, which was typically used – though 5 mg/ml has also been used successfully.

Liposome formation is performed by extrusion with a 100 nm pore size (Whatman Nucleopore Track Etch Membrane); with the sample passed between a filter 21 times using an extrusion system with two 1 ml syringes (Avanti mini-extruder). Such liposomes are expected to be unilamellar.

Insertion of F_1F_0 into Liposomes to Form Proteoliposomes

To 300 µl of liposomes is added 200 µl of buffer 1 and the sample cooled on ice. After 5-10 mins, 100 µl of purified solubilised protein is added (thawed from liquid nitrogen storage and kept on ice to retain function) along with 30 µl of 10% sodium cholate (0.5% final concentration; stock is made in buffer 1 and stored -20 °C). This sample is immediately placed into 4 °C for exactly 15 mins with gentle agitation. In the meantime a sephadex column has been set up at room temperature (Bio-Rad Poly-Prep); Sephadex G-50 bead solution (Sigma; previously hydrated with water from the supplied dried form for a 50% solution stored at 4 °C) is placed and allowed to settle to 2 ml (once excess water has

passed out of the column). Beads are washed with 10 ml of water and then 5-10 ml of buffer 1 to equilibrate. After the 15 min incubation of protein and liposomes the sample is placed onto the equilibrated sephadex column, which removes the detergent (having been equilibrated with the buffer containing no detergent). The first 0.7 ml eluted is discarded and the next 1 ml is collected to form the proteoliposome sample volume.

Since the formation of proteoliposomes is time-consuming and results in larger volumes of proteoliposomes than are generally used in a day of experiments, then proteoliposomes were generally stored in liquid nitrogen after formation – for which glycerol is intended as an aid to stability. In cases where a lower quantity of protein was desired to be used (for example, to create single-F_1F_O proteoliposomes) then it is expected that 100 µl of solubilised protein could be replaced simply with the desired reduced amount (perhaps 10 µl of solubilised protein) diluted with elution buffer from the purification to make 100 µl. These suggested numbers are based on previous studies which have suggested that around this reduced ratio of lipid-to-protein (400/1), with 100 nm liposomes size, single F_1F_O proteoliposomes can be expected [132]; this has not actually been tested here to verify single F_1F_O insertion under these conditions.

2.6.2 Testing Proton Pumping with ACMA

This method is longstanding for the measurement of ΔpH across energisable bilayers by transmembrane proteins and is described also in the paper from which the F_1F_O purification protocol has been derived [120]. ACMA is 9-Amino-6-

Chloro-2-Methoxyacridine and FCCP is carbonyl cyanide p-trifluoromethoxy-phenylhydrazone.

Protocol

First, proteoliposomes are prepared as previously described; they can be tested immediately or after storage in liquid nitrogen. Anything from 5-50 µl of proteoliposomes might be required for a clear trace on the test, out of a usual 1 ml prepared (assuming 100 µl of solubilised protein at 2 mg/ml used; readjust for smaller protein volumes).

Typically a large quartz cuvette (Hellma) is used, to accommodate a magnetic stirring bar, and so a 2 ml volume is required (use of quartz is not actually critical at this wavelength). The fluorimeter (Photon Technology International) is set to excite at 410 nm and to read the emission at 475 nm. After proteoliposomes are added to the 2 ml buffer volume (typically 100 mM KCl, 50 mM MOPS, 2 mM $MgCl_2$, pH 8.0) and magnetic stirring initiated, 0.5 µM ACMA (stored in ethanol as a 1 mM solution from the supplied solid at -20 °C) is added to the reaction volume. ACMA will rapidly enter the proteoliposome bilayers and hence proteoliposomes should be added first – before the ACMA – but the signal takes around 3-10 mins to stabilise. Once a stable level has been observed for 1 min, 250 µM ATP is added (higher concentrations than this have been observed to lead to fluorescent artifacts and should be avoided) and quenching observed over 1-5 mins. Once the quenching signal is no longer decreasing, addition of 0.5 µM FCCP (stored in ethanol as a 1 mM solution from the supplied solid at -20 °C)

allows protons to traverse the bilayer and quenching should rapidly return to around its original level as the pmf is dissipated.

Note on DCCD Incubation

1,3-dicyclohexylcarbodiimide (DCCD) can be used to completely inhibit proton pumping. By taking the solid (stored at -80 °C) into ethanol, a concentration (around 2.5 mM typically) is taken such that by adding a small volume (0.5 µl) to a proteoliposome volume (25 µl) then the final concentration is 50 µM DCCD. The volumes should be such that ethanol does not make up more than about 2% of the final volume, since this could damage lipid structures. An equal volume of ethanol can be added to a control for comparison. Incubation is 30-60 mins.

2.6.3 Thin-Layer Chromatography (TLC)

This method separates lipids based on characteristic progression up a silica plate. The protocol below was adapted largely from Timothy Schuh's helpful guide [133], with additional insight from some reviews on the subject [134], [135], and represents normal-phase TLC. The two steps allow greater separation of multiple compounds, though is not really necessary for an analysis of purified lipids.

Protocol

Two sealable chambers are prepared, with a height and width sufficient to hold a TLC plate (Machery-Nagel, Alugram SIL G/UV 818160, 0.2 mm thick silica layer on aluminium backing 5 cm x 10 cm). Two solvent mixtures are prepared with 50 ml volume and placed in one of each of the chambers; to chamber 1: chloroform 27.5 ml, methanol 16.5 ml, acetic acid 4.5 ml, water 1.5 ml, to chamber 2: heptane 34.5 ml, diethylester 14.5 ml, acetic acid 1 ml. The dimensions of the chamber

should be such that the height of the liquid above the base is less than 2 cm. A large piece of cellulose paper is placed in the chamber; this will absorb some of the solvent to reduce concentration gradient effects present in the air in the chamber. The chambers must always be kept sealed, except to quickly move samples in or out.

A pencil line is placed across the width of a TLC plate, 2cm from the base. 5 evenly spaced circles along this line mark sample positions. Samples are placed onto these circles with a small volume at a time (around 1-10 µl) and the solvent allowed to evaporate before further sample is added; total lipid added should be in the range 10-100 µg.

To run the sample it is placed into chamber 1, from which the solvent mixture will contact the plate at its base and diffuse upwards – this process is readily apparent from the change in colour of the plate. When the solvent has reached around halfway up (which takes around 10 mins), it is removed from the chamber and allowed to air-dry (which takes around 30 sec). It is then placed into chamber 2 with the same orientation and left until the solvent reaches within around 1cm from the top of the plate (around 10 mins). It is then removed from the chamber and allowed to air dry for around 5 mins. The plate is then submerged in 0.2% amido black in 1 M NaCl for 5-10 mins, until clear bands appear, and then washed in 1 M NaCl and left to air-dry.

2.7 Characterisation of Lipid Fusion

2.7.1 Calcein Method for the Determination of Content Mixing

This method assesses whether fusion of lipid vesicles with content mixing has taken place by the formulation of two sets of liposome objects containing compounds that exhibit fluorescence when mixed. Cobalt interacts with calcein and inhibits its fluorescence, but EDTA chelates the cobalt and leaves calcein free to fluoresce strongly. The protocol is based on that developed in Robert MacDonald's group [136], [137]. Calcein is 2',7'-{[bis(carboxymethyl)amino]methyl} fluorescein (MP Biomedicals).

Protocol

Buffer 1 is 100 mM NaCl 10 mM Tris pH 7.5. Liposomes are prepared similarly to the standard protocol given previously, but the dried cationic lipid film (i.e. 50% DOTAP 50% Soybean PC) is resuspended in 1 mM calcein, 1 mM cobalt chloride, 85 mM NaCl, 10 mM Tris, pH 7.5 at 5 mg/ml of lipid; anionic lipid (variable compositions of POPA and Soybean PC) is resuspended in 100 mM NaCl 10 mM EDTA pH 7.5 also at 5 mg/ml of lipid. Both are extruded with 200 nm filter size. Anionic liposomes are then passed through a Sephadex G-50 column (2 ml bead volume) to remove external EDTA (column pre-equilibrated with buffer 1), which provides a dilution from a starting volume of 630 µl to 1 ml. 150 µl Cationic liposomes are diluted with 1 ml of buffer 1 and subjected to ultracentrifugation at 50 000 rpm 2 hrs 4 °C in a Beckman TLA-100.1 rotor (88 000 g average) and resuspended in 150 µl of buffer 1. This removes a substantial level of external calcein and although this allows for a clear positive signal of fusion to be seen, calculations of total liposomes fused are not performed due to the less than

complete removal of external calcein offered by this procedure [137]. To a 2 ml sample volume of buffer 1, 10 µl of cationic liposomes and 10 µl of buffer 2: 20 mM $CoCl_2$ 100 mM NaCl 10 mM Tris pH 7.5 (to a final concentration of 100 µM $CoCl_2$) are added and left to equilibrate for 30-60 mins. This level of external cobalt will equilibrate with calcein over this time to give a steady signal of calcein fluorescence (if the sample is viewed immediately, a gradually decreasing fluorescent signal is seen). The pre-equilibrated sample is then placed into a fluorimeter with magnetic stirring, and after observation of a stable signal for around 100 seconds, 20 µl anionic liposomes are added. After the signal has been observed around 300 sec (or until it settles to a constant level) then 10 µl further buffer 2 is added. After observation of the signal for around 100 seconds, 200 µl of 10% Triton X-100 (Fisher Scientific, in buffer 1) is added and the response observed for around 100 seconds or until steady.

2.8 Giant Vesicles: Formation and Characterisation

2.8.1 Formation of Giant Vesicles with Internal Entrapment of Desired Components

The development of this protocol, along with its antecedents in the literature, is described in some detail in section 4.2.1 along with references.

Protocol

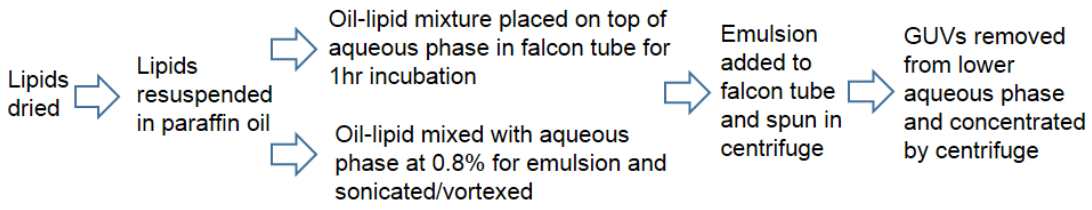

3 ml of 0.2 mg/ml lipid suspended in paraffin oil is required for each giant vesicle preparation (paraffin oil puriss from Sigma; density is 0.827-0.890 g/mL at 20 °C). Typically a 12x concentrated sample is prepared for storage at room temperature for up to one week; chloroform-dissolved lipids 2 mg Soybean PC lipid is mixed with 0.5 mg POPA and chloroform is then evaporated under nitrogen flow, leaving a thin dried film of lipid on the tube walls and 1 ml of paraffin oil is added to make a 2.5 mg/ml suspension. Glass 1 ml tubes were commonly used, though 1.7 ml low-bind plastic eppendorfs (Corning Axygen Maxymum Recovery) were found to give best resuspension of dried lipids into oil; however this could lead to interaction between the chloroform solvent and the plastic tube walls and would be disfavoured in future work. After at least 1 hr of incubation with oil (up to overnight), the oil-lipid suspension is subjected to vortex 5 mins, then bath sonication for 1 min, then a pipette tip is inserted and scratched against the tube walls and finally a further vortex treatment for 5 mins to ensure full lipid resuspension. The concentrated oil-lipid mixture is then left on gentle shaking until required. First, 3 ml of the desired external buffer (different buffers tested are described in Chapter 4; however typically 20 mM KCl 10 mM MOPS 0.1 mM $MgCl_2$ pH 8.0 has been used) is placed in a 50 ml cylindrical tube (Corning; 28 mm in diameter). 160 µl of 12x oil-lipid suspension is diluted to 2 ml (hence 0.2 mg/ml) and layered carefully on top of the buffer in the cylindrical tube. This is incubated for exactly 60 mins at room temperature. A flat interface between layers should form rapidly (less than 1 min); failure to do so can indicate poor resuspension of lipids in oil.

In the meantime, an emulsion is prepared with 80 µl of 12x oil-lipid suspension diluted to 1 ml in a 1.7 ml eppendorf tube. For the 'inner contents' of giant vesicles used to form the aqueous phase of the emulsion, 8 µl is typically used out of a larger volume prepared (typically 30 µl for ease of pipetting). Using concentrated components, the inner contents will contain the same buffer composition as the aqueous external buffer used (typically a 5x concentrated buffer is prepared), along with ficoll-400 to 17% as a density agent (w/v, typically prepared as a 50% solution in water weekly and stored at 4 °C), and any other components of interest (such as fluorophores – often pyranine is included at 300 µM, or functionalised gold nanospheres – preparation for this is described in a separate section below). 8 µl of this inner contents preparation is then added to the 1 ml prepared oil-lipid suspension (0.2 mg/ml). This mixture is then placed in a vigorous vortex for 20 mins, followed by a bath sonication for 1 min, followed by further vortexing for 5-10 mins. This is timed such that the end corresponds with 60 mins of incubation of the aqueous buffer and oil-lipid suspension interface in the 50 ml cylindrical tube earlier described. The 1 ml of emulsion is then carefully added to the 2 ml of oil-lipid (which is on top of 3 ml of buffer). The cylindrical tube is then carefully placed directly into a Beckman CS-6R swinging-bucket centrifuge and spun at 4250 rpm 30 mins 25 °C (corresponding to 3000 g average). Using a syringe with a long needle, around 30 µl of the same aqueous buffer used is first loaded into the syringe and the syringe is then carefully plunged through the oil phase into the aqueous phase below. The buffer is expelled, which creates flow and helps to remove any oil that may have passed into the syringe. A further careful loading and unloading of around 200 µl of the

syringe helps to resuspend any pelleted giant vesicles located at the base of the aqueous phase. 1 ml is then removed and the syringe wiped on tissue paper to remove any attached oil. This is performed twice more to extract the full 3 ml, which is placed in a 15 ml cylindrical tube to allow the sample to homogenise across the three extracted 1 ml volumes. This 3 ml volume can be used directly, or can be concentrated by subjecting to further centrifugation – typically a 2000 g 15 mins 4 °C condition is used with 1 ml of sample in a 1.7 ml plastic eppendorf (a higher speed of 22 000 g 10 mins 4 °C condition is used under some conditions – see discussion in Chapter 4). After pellet formation then the original 1 ml would typically be resuspended in around 50 µl of buffer for a concentrated sample of giant vesicles.

Notes on the Inclusion of Functionalised Gold Nanospheres

Functionalised gold nanospheres can be included in the 8 µl 'inner contents' step for emulsion formation; they will then form part of the interior of the formed GUVs, as will any other substance or compound (such as a fluorescent probe) included at this step. Both BBI Solutions and Nanopartz-supplied gold, at 60 nm and 100 nm diameters, have been used and corresponding functionalisations with streptavidin, neutravidin, and biotin have all been successfully incorporated into giant vesicles.

Nanospheres are prepared by first washing in 15 mM HEPES pH 8.0 (buffer 2); 5 µl typically of the gold suspension as supplied at 1.5×10^{12} nanospheres/ml (for Nanopartz 60 nm; volume can be adjusted as appropriate for different starting concentrations) typically provides a sensible amount for roughly 1-3 nanospheres

per larger giant vesicle (though note high amounts of heterogeneity; many vesicles will contain no gold, some will contain large numbers). This is diluted to 500 µl in buffer 2 and spun 10 000 g 3 mins, using a low-bind 500 µl eppendorf for best recovery (Eppendorf Protein LoBind; other conditions can lead to clumping of nanospheres on sidewalls). Removing the supernatant, the sample is washed in the same manner twice more and then a final spin with a smaller 50 µl volume under 10 000 g 30 sec is performed to allow removal of liquid with good retention of the pellet. Inner contents should be prepared such that concentrated solutions still allow for the addition of up to 2 µl more water to form final dilutions; this is required as it is essentially impossible to ensure total removal of all liquid from the gold nanosphere sample and this could hence cause a higher dilution of inner contents than intended (affecting both osmotic properties and density of final giant vesicles). Typically 10 µl total volume would be prepared from which 8 µl is then added to the oil-lipid suspension to form the emulsion as previously described. Note that bath sonication for up to 1 min along with pipetting is required for proper resuspension of gold after centrifugation (this can generally be assessed by the strength of the red colour seen in the final suspension).

Previous Protocol with Extruder System

For much of the earlier stages of the research, an extrusion system was used to form the stabilised emulsion rather than the vortex system presented above (this is how giant vesicles were first successfully prepared). Aside from this emulsion preparation, all other steps for formation were the same. An 800 nm extrusion filter (Whatman Nucleopore Track Etch Membrane) was used with the same mini-extruder system with two 1 ml syringes used for liposome formation

(Avanti). The system is first equilibrated with paraffin oil to remove any aqueous droplets internal to the system. The 1 ml of oil-lipid suspension with 8 µl of aqueous phase is then passed through the filter 11-21 times slowly (since the oil is viscous, this could take up to 45 mins). Since this protocol was rather labour-intensive, using the vortex significantly simplified development.

2.8.2 NBD-PE Incorporation for Assessment of Lamellarity of Giant Vesicles

The method was first developed in Richard Sleight's group [138] and this protocol has been developed from there and also with reference to the papers of Sophie Pautot et al. [139], [140].

Protocol

Giant vesicles are formed as described previously, but with a fraction of NBD-PE in the lipid mix conforming to 0.25% weight fraction. Hence, for a 12x concentrated stock: 2 mg Soybean PC, 0.5 mg POPA, 6 µg NBD-PE are evaporated and prepared with paraffin oil as described previously. Several aqueous buffers can be used, such as 20 mM KCl 10 mM MOPS pH 8.0, and internal contents are simply the same buffer with 17% ficoll (w/v) as described previously. To view under the microscope, only small volumes of giant vesicles are required and so this can be taken out of the remaining volume of intact giant vesicles untested in the fluorimeter. Since the resulting 3 ml solution is to be analysed in bulk, 1.4 ml (around half of one sample) may be added directly to a fluorimeter and augmented with 0.6 ml buffer. The quenching solution of sodium hydrosulfite is prepared at 1 M; 1.74 g sodium hydrosulfite and 1.21 g Tris and make up to 10.7 g total with water; pH is around 10 (prepared daily). 10% Triton X-100 reduced is

also made up in the same aqueous buffer (prepared daily; note that tests with several other detergents including standard Triton X-100, sodium cholate, and octyl glucopyranoside all yielded artifacts in controls for this assay). A fluorimeter is used with magnetic stirring bar. Excitation for the NBD fluorophore is at 470 nm and emission is read at 550 nm. To quench, 50 µl of the 1 M sodium hydrosulfite is added to the 2 ml solution of GUVs, making 2.5 mM final concentration. To open vesicles, 200 µl of 10% Triton X-100 reduced is added to the 2 ml volume (1% final).

2.9 Surface Approaches and Single Molecules

2.9.1 Modification of glass surface – PLL-PEG-NTA-Ni

The selection of this method and the development of the protocol is discussed in Chapter 5. These crafted-polymers were first described by Zhen et al. [141] and have since been commercialised by Susos; PLL is polylysine and PEG is polyethylene glycol.

Protocol

PLL (20kDa) grafted with PEG (2kDa) (supplied by Susos; hereafter called "plain-PEG") solid (stored at -20 °C under desiccation) is measured out into a 15 mM HEPES pH 5.0 buffer (buffer 1) at 1 mg/ml. To this non-functional base is added 0.05-0.1 mg/ml of PLL (20kDa) grafted with PEG(3.4kDa)-NTA ("PLL-PEG-NTA") solid, such that functionalised PLL-PEG-NTA might be expected to make up 5-10% of the surface and non-functionalised PLL-PEG the remainder. A flow slide is made up (Menzel-Gläser coverslip, 22×60 mm) using double-sided tape (Scotch; around 100 µm thickness); the mixture is then passed into the flow slide tunnel

(20-50 µl), where it is left to bind to the glass of the coverslip for 10-30 mins (no significant improvement was observed, in initial tests, beyond 10 mins). The tunnel is then washed with buffer 1 (200 µl for a thorough wash), before 10 mM $NiCl_2$ 15 mM HEPES pH 5.0 is flowed in and incubated for 1 min (50 µl). The tunnel is then washed with buffer 1 (200 µl), then further washed with whatever sample buffer is desired for measurements to follow (as long as this has a pH of below 10 the PLL-PEG should remain attached to the surface; this was verified with binding controls up to pH 9.0 presented in section 5.3). The surface is hence functionalised.

2.9.2 F_1 rotation assay

The central format of this rotation assay was well-established within the group and the DPhil thesis of Dr Thomas Bilyard proved a useful guide. The use of PLL-PEG-NTA-Ni was novel and based on the studies presented in Chapter 5, leading up to this assay as a rotation test of this system. Rotational data was analysed by a Matlab code previously written by Dr Bradley Steel (with small additions to this code contributed by Dr Ashley Nord and Mr Samuel Tusk).

Protocol

A flow slide is set up and the chamber modified with PLL-PEG-NTA and PLL-PEG as described previously, including incubation with $NiCl_2$ for 1 min. Biotinylated gold beads are prepared by first diluting 10 µl of the beads as supplied into 1 ml of 10 mM HEPES pH 8.0, then subjecting to centrifugation at 14 000 rpm 2 mins to pellet and resuspending in 1 ml for a second wash – finally the pellet is

resuspended in 100 µl of 100 mM KCl 50 mM MOPS 2 mM $MgCl_2$ 10 mg/ml BSA pH 7.0 buffer (buffer 1).

F_1 at 1 mg/ml is diluted 1000x into a buffer of buffer 1 and flowed into the chamber to incubate for 10 mins. A wash is performed by flowing 200 µl of buffer 1 through the chamber. Neutravidin at 0.1 mg/ml in buffer 1 is then flowed in to incubate for 1 min. A wash is performed and biotinylated gold nanospheres with 60 nm diameter are flowed in for a 15 min incubation. Finally the sample is washed and activity buffer (buffer 1 plus 3 mM ATP 2 mM PEP 20 units/ml PK) is flowed into the sample volume.

The sample is then viewed in the laser backscatter darkfield microscope. Typically a laser power at 633 nm of 1-4 mW is used; a lower power measurement than this (using a power meter Thorlabs PM100A) could indicate a misalignment of the laser input. For assessment of rotation, a speed of 2500 fps on the camera (Photron Fastcam 1024PCI) provides ample temporal resolution (though the assessment of the most subtle substeps would require more and the camera is capable of 109 500 fps). Judicious alteration of the shutter speed can help to ensure that no pixels are saturated; this would compromise the later fitting of Gaussian profiles by the Matlab analysis program utilised.

2.9.3 F_1F_0 Giant Vesicle Rotation Assay

Protocol

Giant vesicles are prepared including functionalised gold; 60 nm streptavidin-coated gold (Nanopartz) is used according to the protocol previously described under giant vesicle formation (section 2.8.1). When giant vesicles have been

prepared and concentrated by centrifugation into a 100 µl volume, FCCP is added (from an ethanol stock at 1 mM) to 50 nM (presumably up to 500 nM should be fine; this has not been totally optimised) and incubated with giant vesicles.

First the gravity flow slide described in Chapter 5 (section 5.2) is prepared and loaded with PLL-PEG-NTA, followed by $NiCl_2$ as described previously under the surface modification protocol.

Cationic proteoliposomes (inclusion of 0.5% Bodipy-cholesteryl allows for straightforward assessment of binding) are then loaded under the 250x dilution and buffer conditions described in section 5.3.1 (100 mM KCl 25 mM Tris 25 mM BisTris 0.1 mM $MgCl_2$ pH 7.0 for 5 mins); further additions of more concentrated proteoliposomes (100x, 50x) can increase the level of binding but these may be expected to include more non-specifically bound objects. After buffer exchange to that in which giant vesicles are formed (20 mM KCl 10 mM MOPS pH 8.0; inclusion of $MgCl_2$ could not be assessed with fusion tests so is omitted). Finally concentrated giant vesicles are slowly loaded into the sample volume (this can be viewed in brightfield). The slide is then taken to a swinging-bucket centrifuge and spun 100 g 10 mins to move giant vesicles towards the coverslip surface. This can be assessed under the fluorescence microscope before transferring the slide to the laser darkfield microscope. Brightfield viewing on the laser darkfield can be used to find the correct surface since giant vesicles are faintly visible.

Using the flow system, the buffer in the sample volume can now slowly be replaced with activity buffer (eg 20 mM KCl 10 mM MOPS 2 mM $MgCl_2$ 2 mM PEP 10 units/ml PK 1 mM ATP; or essentially whatever the giant vesicles were

formed in plus $MgCl_2$, ATP, PEP, and PK). The slide is viewed on the laser darkfield microscope (see section on F_1 rotation for insights on the use of the microscope).

Notes on removal of external functionalised gold nanospheres

It is noted that in a typical giant vesicle preparation including functionalised gold nanospheres internally, then after formation some gold nanospheres are observed externally to giant vesicles (see, for example, images presented in Figure 4.2).

Since this provides distraction for a single-molecule darkfield experiment, a condition was found in which to remove most of these particles – though in the event this was not utilised for the experiment presented in Chapter 6. A concentrated giant vesicle preparation may be subjected to a wash to remove any free streptavidin- (or neutravidin-) gold nanospheres by incubating the sample with around 5 µl of biotin-functionalised magnetic beads (Turbobeads, PEG-biotin) for 5 mins. Using a magnet these beads are then drawn off, taking functionalised gold that is external to giant vesicles with them. Biotin-magnetic beads must first be washed 3-5 times in 1 ml of the buffer used to form giant vesicles to remove any protectants in the solution which could interfere with later F_1F_O function. By viewing under the microscope then a clear reduction in the presence of external gold nanospheres is seen, without any apparent change to giant vesicles.

Chapter 3 Protein Purification and Function

3.1 Introduction

Towards the establishment of a reliable, repeatable single-molecule study of the rotation of ATP synthase, it is critical that the protein can be reliably and repeatedly purified with as high a yield and functionality as practical. *E. Coli* mutants that had previously been developed are used (see section 2.4.1).

In order to verify protein has been purified with good yield, without impurities, and with function intact, several assays are typically performed; protocols are described in Chapter 2 and results are here presented. Furthermore in order to investigate properties of the mutants used, several further assays were performed in order to probe the modifications and build on previously published results using these same strains. Although purifications were typically performed around every 3 months, results here are presented with detailed analysis of two of the lattermost purifications; context is then given in discussion of typical results.

The results presented in this chapter should then ensure that further development towards building a single molecule system as described in later chapters are built on solid ground. Furthermore characterisation regarding

insertion into a fusogenic lipid mixture is described; the context for the use of this lipid mixture is presented in Chapter 4.

F_1F_O was purified from mutant *E. Coli* on a regular basis as required and stored, as solubilised protein in detergent, with liquid nitrogen. The benefit of the described protocol to other published methods is precisely its simplicity and rapidity, with faster purifications tending to give higher yields of functional protein – particularly since F_1F_O, once separated from its native membrane environment into a detergent-solubilised state, will rapidly denature if warmed much above freezing. Protein purification itself was generally a joint effort between myself and Dr Robert Ishmukhametov; however, all characterisation results presented here are entirely my own work.

3.2 Characterising Purified ATP Synthase

Having purified the protein according to the protocol described in Chapter 2; starting with up to 6 L of *E. Coli* cells generally results in 1-2 ml of purified protein in a detergent-solubilised state (i.e. stabilised by detergent rather than in a lipid membrane) in the elution buffer, which includes a high level of imidazole used to separate the protein from the Ni-NTA column in the final stage of the purification. This purified protein can now be characterised. Typically the protein is immediately stored in liquid nitrogen upon completion of the purification and studies performed later on thawed protein kept on ice to inhibit damage at higher temperatures. The protein's function is expected to remain essentially constant under liquid nitrogen storage (but in practice is rarely stored longer than 6 months).

The mutant of most interest out of the four available included a cysteine modification on each of the ten c-subunits only, since this would allow for a specific biotin-labelling site (via the use of biotin-maleimide to chemically bond to the cysteine site during purification). This site is then expected to be exposed to the interior of the proposed giant vesicle system (see later chapters for further discussion of the system). The completely cysteine-free mutant is then also studied as a comparison for function and binding. Also included here is a mutant with cysteines on both the c-subunits and the α-subunits; this was used in earlier studies and so was generally available in storage for some of the non-functional characterisation studies described (see appendix for full sequences). This double mutant was of interest for potential utilisation of its α-cysteine site for surface-binding via biotin-avidin, but this was not utilised owing to his-tags proving a reliable approach; see Chapter 5 for discussion of this.

3.2.1 Protein Concentration by BCA Assay

This assay will allow calculation of the mass of protein in a given volume. Based on a calibration curve with known quantities of BSA (as a test protein), a straight-line fit gives an equivalence of absorbance measured at 562 nm to quantity of protein in the sample volume. Five test volumes of each protein sample are then averaged and the equivalent concentration per ml is calculated from the calibration. The standard deviation of the test results give an estimate of the error value on the measurement, which is expected to be driven largely by the potential for pipetting errors.

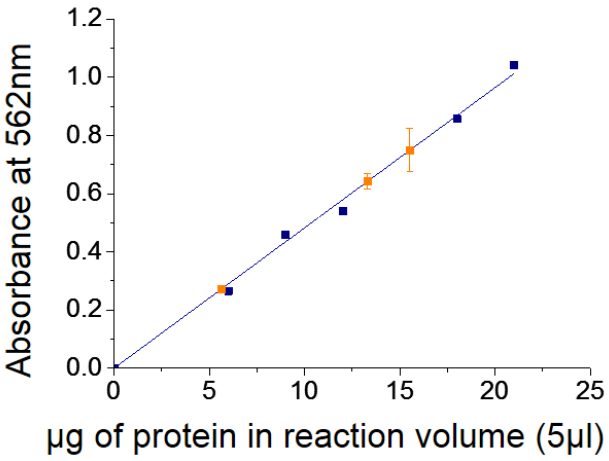

Figure 3.1
Graphical representation of BCA data. Calibration (blue points and fitted line) superimposed with the averages of test measurements of three protein samples, fitted to the line (orange), including one standard deviation as error in absorbance. Reaction volume is scaled to arrive at concentration in mg/ml

Based on this calculation, the concentration of the cysteine-free protein sample was measured to be **3.1 ± 0.3 mg/ml**. The concentration of the biotin-labelled c-ring cysteine sample was measured to be **2.7 ± 0.1 mg/ml**. The concentration of the biotin-labelled α- and c-ring cysteine sample, which was not typically used for activity studies but which was used on occasion for structural studies including some to follow on biotin-labelling, was measured to be **1.12 ± 0.04 mg/ml**.

These yields are very typical; generally 2-3 mg/ml is a good yield for cysteine-free and c-ring cysteine mutants and 1-2 mg/ml is a good yield for the dual α- and c-subunit cysteine mutant. Since the dual mutant generally has a lower yield, and since its extra biotin-labelling on the α-subunit was largely superfluous for this project, it was not much used. Use of 4-6 L of LB typically results in around 20-25 g of wet cell weight. Given the number of potential variables in the purification; from the starting mass of cells to the length of time of purification, or the exact conditions to yield sub-bacterial particles in the French press (a particularly variable component of the purification process) then variations in yields of some 30% between preparations were of no surprise.

3.2.2 Protein Gels and Identification of Subunits

Although we have verified the presence of protein of some kind by the BCA method, to verify our expected protein and the absence of other impurities or unwanted proteins then polyacrylamide gel electrophoresis allows identification of subunits based on size. Subunits are visualised through interaction with a dye such as silver [142] (which gave good results, but was labour-intensive and required 10 μg protein per lane), Coomassie blue (which was found to give poor resolution for the c-subunit), or Ruby Sypro (which was found to give the best results across subunits, with only 2.5 μg protein required per lane). Alternatively, further processing may be performed.

The denaturing gel procedure used most widely is glycine-SDS-PAGE, also known as the Laemmli procedure [143]. However, this procedure was found to give poor results for viewing of the c-subunit, which is of particular interest here due to the mutant strain containing modifications introducing cysteines. A modified procedure known as Tricine-SDS-PAGE, or the Schägger procedure, is established in the literature for the more optimal viewing of subunits with masses below 20 kDa [128], [144] and this procedure was found to allow all subunits to be well visualised. There are eight protein subunits in F_1F_O and all eight could be readily identified in Ruby Sypro staining with the Schägger procedure by comparison to the molecular weight ladder as seen in Figure 3.2. These are α (55 kDa), β (50 kDa), γ (31 kDa), a (30 kDa), δ (20 kDa), b (17 kDa), ε (15 kDa), and c (8.3 kDa) [145]. The additional bands seen and not identified are most likely impurities in the sample (of which there are few). Note that a- and b-subunits appear shifted on the gel compared to their actual mass (this is standard in the literature).

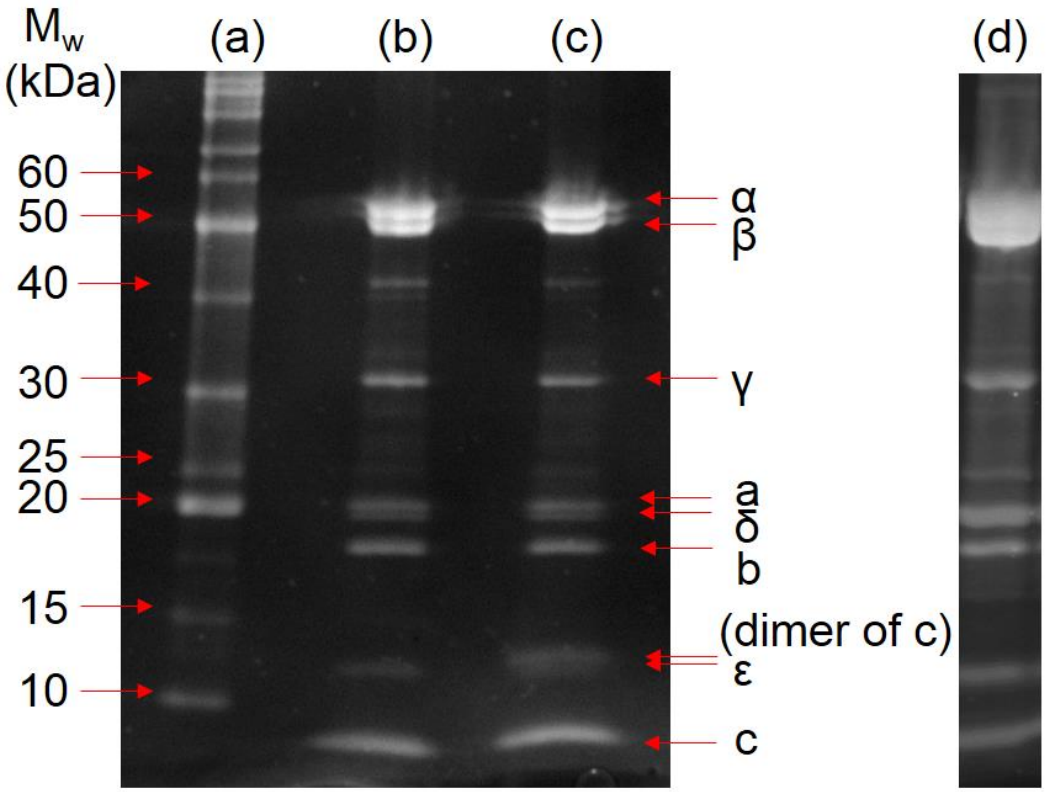

Figure 3.2
Fluorescent view of Ruby Sypro staining of purified F_1F_O. (a) shows molecular weight ladder. (b) 2.5 µg cysteine-free mutant and (c) 2.5 µg fully biotin-labelled c-ring cysteine mutant. Gel is performed under non-reducing Schägger conditions as described in section 2.5.2. Note the faint dimer of c-subunit is seen in (c), indicating less than 100% labelling with biotin; this is discussed in section 3.2.4. Use of reducing conditions on the gel itself eliminated this dimer seen in (c); this has been appended in lane (d) from a separate gel and scaled for comparison (note that this lane represents 10 µg protein, hence the greater difficulty separating α and β. Note the dimer of c is also not present in the cysteine-free mutant (b), which aligns with the hypothesis of disulfide bonds between the inserted cysteines. Gels used are 4-20% gradient polyacrylamide, which provided good separation of all subunits; however for better separation of ε- and the c-subunit dimer, a 10-20% gel was also used and this is presented in section 3.2.4 (Figure 3.5).

As identified in Figure 3.2, a dimer of the c-subunit is seen only in the case of mutant F_1F_O with cysteine on the c-subunits. This has implications for biotin labelling and an investigation into this is discussed in Section 3.2.4. When run under reducing conditions, this dimer is no longer seen and the monomer of c-subunit is seen as a thicker band. From the gels shown in Figure 3.2, we can conclude that all subunits are present and the protein has been well purified with good specificity and no loss of subunits. Gel conditions are outlined in section 2.5.2.

3.2.3 F_1F_O ATP Hydrolysis Activity by NADH assay

F_1F_O will hydrolyse ATP also in a solubilised state, in which the formation of a pmf is not possible. The ATP regenerating system can be used to reconvert ADP that has been hydrolysed by F_1F_O back to ATP and thus maintain a steady concentration of ATP. In order to measure the turnover of ATP by F_1F_O we utilise the absorption at 340 nm of NADH, which is absent in its oxidised form NAD^+, to which it is converted as part of the regenerating system. Hence upon the hydrolysis of ATP we see a reduction in the concentration of NADH and thus a diminishment in the level of absorption seen at this wavelength. The protocol is given in section 2.5.3.

Figure 3.3 is intended to be representative of each trace taken and shows a single test of the cysteine-free mutant and the biotin-labelled c-ring cysteine mutant protein. At the start of the experiment, ATP regenerating system with enzymes PK and LDH and substrate PEP as well as ATP and Mg^{2+} are present in the reaction volume in excess. Activity is initiated by the addition of around 0.1 μg of

protein; to understand the initial lag phase seen, we must appreciate that we are looking only indirectly at the activity of F_1F_O. Initially there is a low-ADP environment and so the rate of activity of PK/LDH will be below optimal; only once more ADP is produced by F_1F_O does the rate of PK/LDH reconversion back to ATP increase, and so in turn only then does the oxidation of NADH reach its optimal rate. Hence in this case the gradient data should be taken only from the latter, linear, part of the trace. The addition of sodium azide prior to terminating measurement verifies that the ADP is produced by the F_1 part of the F_1F_O, since this is an F_1-specific inhibitor.

The NADH assay was favoured over other, ostensibly simpler, techniques such as the Phenol Red assay; since the ATP regeneration ensures a constant concentration of ATP which should minimise Mg-ADP inhibition.

Three measurements of each mutant were taken at pH 8.0 at room temperature. By calculating activity from the gradient and then taking the average and making an estimate of the error from the standard deviation, we arrive at protein activity at pH 8.0 at **25.5 °C** (room temperature) over three measurements calculated in the cysteine-free mutant to be **19.3 ± 3.8 units/mg** and in the fully biotinylated c-subunit cysteine mutant to be **25.1 ± 2.1 units/mg**.

Such rates were at the mid- to higher end of what was typically obtained; varying from 15 – 25 units/mg depending on the purification and, as has been stated, this will also vary with room temperature. Based on these rates we can estimate the activity per molecule, if we assume all molecules are active; this would give us for

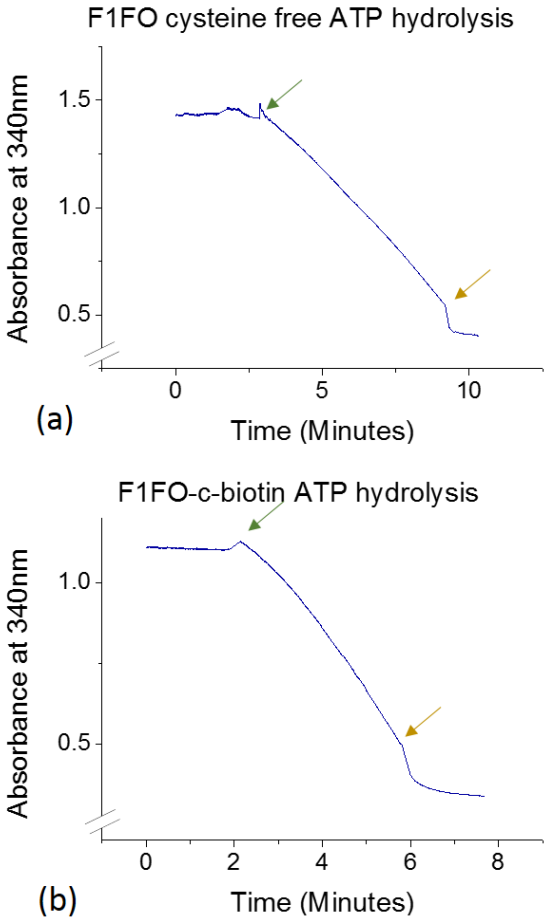

Figure 3.3
Representative traces of ATP hydrolysis activity. (a) purified cysteine-free mutant F_1F_O in a solubilised state and (b) purified biotin-labelled c-subunit mutant in a solubilised state, as measured by absorbance of NADH at 340 nm. ATP, PK, LDH, and PEP (ATP regenerating system) all present in reaction volume at the start of the experiment. Green arrow indicates the addition of approximately 0.1 µg of protein in each case. Gold arrow indicates the addition of 50 mM sodium azide in each case, at which activity immediately ceases. This inhibitor acts on the F_1 part of F_1F_O (5 µl of 1 M sodium azide added to 100 µl total volume). Note the initial curve of the downward slope in each case; the gradient of activity is calculated from the later, linear part of the trace.

the cysteine-free mutant a calculation of **160 ± 31 ATP per second** and for the fully biotinylated c-subunit cysteine mutant **210 ± 17 ATP per second**. By dividing these figures by three (for three ATP per revolution) we can arrive at an estimate (at least at the lower bound) of the rate of rotation we might expect to see in a single-molecule assay (i.e. 50-70 Hz; see discussion in section 1.3.3).

3.2.4 Biotin Modification of the c-Subunit

Following an SDS-PAGE gel, a method to further investigate chemical binding sites on subunits is Western blotting. We know that the electrophoresis procedure will unfold each subunit and place it at a characteristic vertical position on the gel based on its size; this unfolding will leave any chemical binding sites exposed. However the location of the subunit within a gel with

small pore diameters means that probes to these binding sites may be unable to reach them. This would certainly be expected to be the case for a probe of the biotin-binding protein streptavidin, which is a large complex of around 60kDa and which is used to complement the biotin site on the c-subunit mutant used in this study. Therefore a transfer directly from the gel to an appropriate membrane provides a way in which to ensure this biotin site becomes exposed and open to identification.

In initial experiments, no reducing step was used prior to addition of biotin-maleimide during the purification protocol for c-subunit mutants (see section 2.4.1) – hence I refer to this as the 'original' purification protocol. Later investigation revealed that this provided only a weak labelling and so the finalised protocol as presented in section 2.4.1 was developed based on results I present here.

It was hypothesised that the dimerisation of the c-subunits seen on the mutant strain, discussed in an earlier section, was due to disulfide bond formation between adjacent cysteines (which are in close proximity in the ring structure). Since each cysteine may only form one bond, it would thus become unavailable for modification with biotin-maleimide. However for the same reason by chance some subunits in the ring could dimerise in such a way that lone subunits would be left unbonded inbetween. With no unbonded neighbours with which to form a disulfide, these subunits remain monomeric and available for labelling and possibly represents the fraction that was initially observed to be labelled in the original non-reducing purification protocol (see Figure 3.4d); though this may

really have only been a background level of non-specific binding. It was hence concluded that reducing conditions would need to be applied to these disulfide bonds prior to labelling with biotin-maleimide for more complete binding.

Given that potentially only one F_1F_O would face an avidinated gold nanosphere in a giant vesicle in the methodology proposed here (and without proper characterisation, we could be left with a less than 1-in-10 labelling efficiency) it was important that all purified F_1F_O be as well-labelled as practically achievable with biotin on the c-ring to give maximum chances of success. This therefore became an investigation of some interest.

Initial studies of reducing conditions performed by Dr Ishmukhametov showed that varying concentrations of reducing agent dithiothreitol (DTT) up to 100 mM did not result in monomeric c-subunits when observed under SDS-PAGE (results not shown) and so finally the strong condition described in Chapter 2 was characterised to provide the results that are presented here: 250 mM beta-mercaptoethanol incubated with solubilised protein on the Ni-NTA column (at the final stages of the purification procedure) for around 10 mins, then washed thoroughly and labelled with biotin-maleimide. In order to make a Ni-NTA column compatible with such high reducing conditions, it was found to first be necessary to wash the column with 500 mM imidazole. Once cysteines have been labelled with biotin, they will no longer be available to dimerise.

The Western blot presented in Figure 3.4 demonstrates that the final level of specific biotin-labelling achieved is strong. The fully biotin-labelled c-subunit

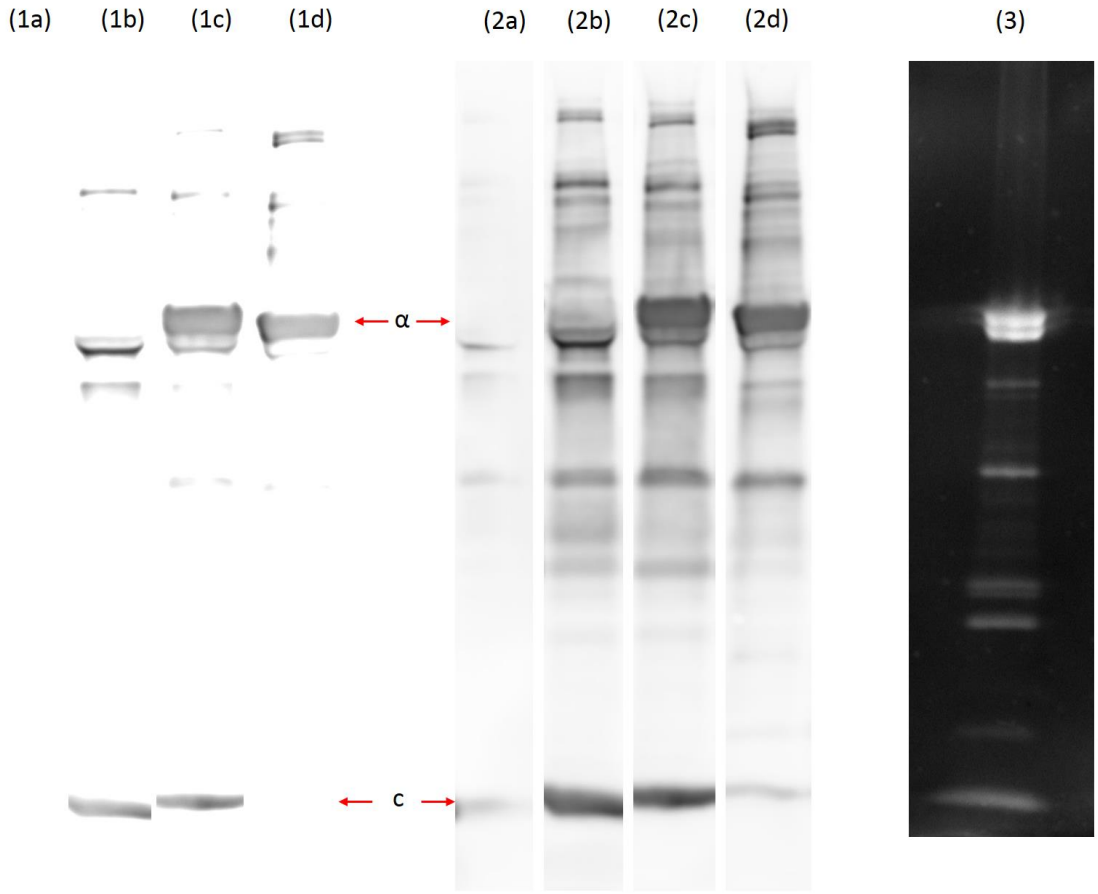

Figure 3.4
(1) and (2) show a fluorescent view of a single Western blot labelled with fluorescent streptavidin to indicate biotin sites on subunits. Black and white have been inverted to give a clearer contrast for the reader. In image (1) brightness is set such that only the very strongest bands are seen. In image (2) brightness is set so that weaker bands are also seen. Lane (a) is loaded with cysteine-free mutant; lane (b) with biotin-labelled c-subunit cysteine mutant; (c) with biotin-labelled α and c-subunit cysteine mutant; lane (d) is the original purification protocol of the biotin-labelled α and c-subunit cysteine mutant. It is apparent that biotin labelling is present in the expected sites of c-subunit on (b) and both α- and c-subunit in (c) in high amounts. There is also a non-specific binding which would seem to be at the β-subunit in both with a high strength. Other strongly labelled sites at higher molecular weights are most likely impurities in the sample. On (d) it is clear that whilst α- has been well-labelled, the labelling on the c-subunit is only at the background level (see lane 2d for this). Image (3) is a comparison taken from a separate SDS-PAGE (using the same 4-20% gel type) with Ruby-Sypro staining as previously seen in Figure 3.2, from which subunits identified in images (1) and (2) can be verified (refer back to Figure 3.2). As expected, biotin labelling on the cysteine-free mutant (a) is extremely low, indicating that non-specific levels seen in lanes 2b-d are largely due to biotin-maleimide having bound non-specifically rather than non-specific binding of the fluorescent streptavidin (cysteine-free mutant is not exposed to biotin-maleimide during purification). Western was performed after SDS-PAGE with 4-20% gradient polyacrylamide gel (compare to Figure 3.2) under reducing Schägger conditions as outlined in Chapter 2, with equal amounts of protein (10 µg) loaded into each well. Low molecular weight bands seen in lanes (1b,1c,1d) are presumably impurities present at a low level (since they are not seen in lane (3)) but with many free cysteines which subsequently become labelled with biotin-maleimide.

mutant gives a strongly labelled band at the c-subunit and the fully biotin-labelled α- and c-subunit mutant gives strong bands at both sites. This can be contrasted to the original labelling protocol without reducing conditions, where the c-subunit labelling is only seen at the background level (though the α-subunit labelling is strong, with no disulfide bridge formation possible here due to the relatively large distance between cysteines at this site; this corresponds with the hypothesised explanation). As can be seen, there is some background labelling particularly of the β-subunit. Since this labelling is not present in the cysteine-free sample, this is thought to indicate a non-specific binding of the maleimide-biotin added during purification rather than a non-specific attachment of the avidin probe to non-biotinylated sites (the cysteine-free protein is never exposed to maleimide-biotin during purification). The plasmids in question have previously been sequenced and are known not to contain extra cysteines beyond those stated (see appendix for sequences). Some effort towards completely eliminating any non-specific binding of maleimide-biotin to subunits not containing cysteines could be explored, but given that the protein function is not impaired then the outcome presented was considered very strong; particularly since the avidinated gold nanospheres to be used in the project will not be expected to be exposed to sites other than the c-subunits.

In order to further investigate how well-labelled the c-subunits are under this protocol, SDS-PAGE under non-reducing conditions gives an indication of the proportion of c-ring subunits that are dimerised under the final purification condition. This was first presented in Figure 3.2 using a 4-20% gradient

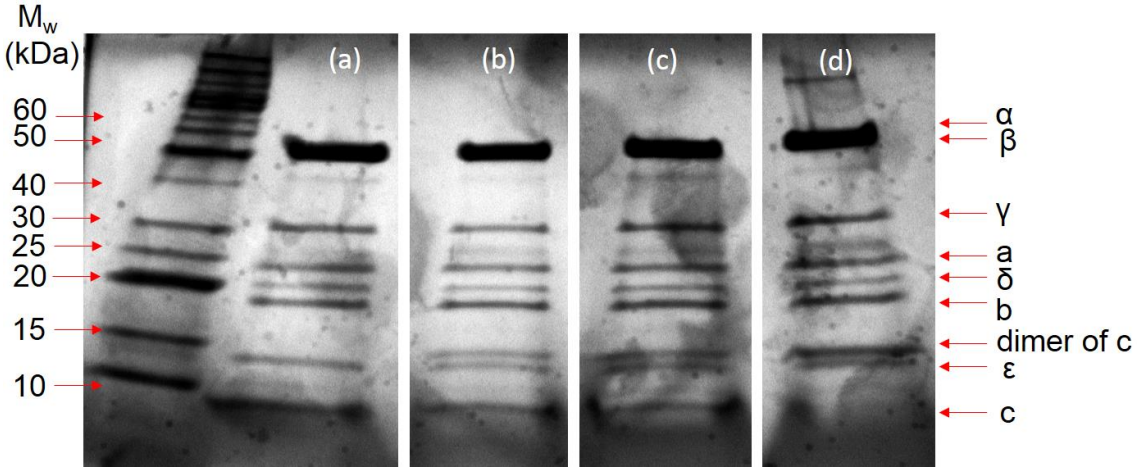

Figure 3.5

Fluorescent view of Ruby Sypro staining of purified F_1F_O, with black and white inverted in order to provide a clearer contrast (image quality problematic with these gels). (a) cysteine free, (b) fully biotin-labelled c-ring cysteine mutant, (c) fully biotin-labelled α- and c-ring cysteine labelled mutant, and (d) previous protocol weakly biotin-labelled c-ring cysteine mutant. The leftmost lane is a molecular weight ladder. SDS-PAGE is performed under non-reducing Schägger conditions as described in Chapter 2, with 2.5 µg protein loaded into each well. Note the much-improved resolution between ε- and the hypothesised c-ring dimer in this 10-20% polyacrylamide gel compared to the 4-20% gel presented in Figure 3.2.

polyacrylamide gel, however a 10-20% gradient gel can give better separation of these lower molecular-weight subunits (though it tends to give poorer images overall and so was less favoured in general). This is presented in Figure 3.5. Given the relatively poor image formed with these gels, a quantitative analysis was challenging as the background level is highly variable. Nevertheless a random sampling of intensities in bands performed in ImageJ indicates, as can be seen readily by eye, that the majority of the signal for the c-subunit is present in the monomer band in Figure 3.5(b), is roughly equally monomer and dimer in Figure 3.5(c), and is majority dimer in band Figure 3.5(d). To clarify, this gel is performed in non-reducing Schägger conditions and the analysis would assume that only properly biotin-labelled c-subunits are monomeric. Dimeric bands are assumed to have been unlabelled close-proximity subunit pairs. Based on this we

can suggest that more than half of the ten c-ring subunits have been labelled by the 250 mM beta-mercaptoethanol reducing condition, which is certainly not the case for the original purification protocol for labelling. Since only 1-2 biotin labels on the c-ring per protein are really required, this was considered a more than satisfactory outcome and should certainly give a stronger chance of success for the single-molecule experiment than the original purification protocol without this reducing step.

Although the cysteine modification on this mutant located at the c-ring has been established by sequencing, its modification with biotin via the biotin-maleimide reaction carried out as part of the purification process has not been well characterised in past studies. In particular such reducing treatment was not reported in a study with biotin-maleimide labelling of the same mutant [27].

3.3 Function of Purified F_1F_O in Proteoliposomes

The aims of the project necessitate that F_1F_O be inserted into a bilayer in order to study its native function and ability to move protons across the bilayer; so far only its ability to hydrolyse ATP has been characterised in the activity tests presented. Additional to this basic need of characterisation, the protein requires a temporary transit mechanism in order to be delivered into the final bilayer system. This is described in Chapter 1 as the logic for a lipid fusion-based approach. An initial detergent-mediated insertion into a transit vehicle, followed by the fusion of this object with the final bilayer construct, was the hypothetical basis from which the project started. To this end protein function in proteoliposomes is here described in both the natural lipid extract of a soy bean

mixture ("Soybean PC" – see discussion section 2.3.1 for clarification on lipids used) and the fusogenic lipid mixture of this same lipid extract combined with a synthetic positively-charged (or 'cationic') lipid DOTAP in a 50% mixture of each by mass. Results for fusion, including content mixing and protein delivery are shown in Chapter 4.

Three proteoliposome data sets are presented; a 100% Soybean PC proteoliposome sample of each of the cysteine-free mutant and the c-subunit cysteine mutant for comparison of the two mutants in a stable, neutral lipid environment and straightforward activity characterisation (particularly the assessment of any effect on activity of the biotin modification steps outlined). Finally a fusogenic lipid set is presented using the c-subunit cysteine mutant; this represents the actual format in which the functionalised protein is expected to be delivered. This can be compared to the same mutant in the neutral Soybean PC lipid format.

3.3.1 Proton Pumping by ACMA Quenching

The ACMA quenching assay will confirm proton transfer across the membrane bilayer; it demonstrates both full protein complex function and proper insertion into liposomes. The transfer of protons across the bilayer by F_O upon hydrolysis of ATP by F_1 leads to a reduction of pH internal to the proteoliposome relative to the exterior. Though several models exist for the mechanism of action, it is known that ACMA forms a dimer which binds to negatively charged lipids in the membrane (such as the phosphatidylethanolamine and phosphatidylserine present in Soybean PC – see section 2.3.1) under such conditions of pH difference

[146], [147]. The dimers are thought to form around the water-lipid interface internal to the liposome [148], and are known not to form in pure neutral (zwitterionic) lipid mixtures [146]. The spectral properties of the dimer are shifted such that they are effectively non-fluorescent in the experimental conditions used to excite the monomer [148], [149].

Hence the action of F_O to move protons internal to the liposome leads to a lowering of intensity of fluorescent emission as read at 475 nm (termed quenching) which can be detected with high sensitivity [150]. This consequent reduction in fluorescence intensity is measured in a bulk assay using a fluorimeter and is indicative of proton pumping activity. The amount of quenching is known to be affected by numerous conditions on the experiment and so quantitative analysis of ΔpH between experiments are not considered justifiable [151]. However the clear signal of quenching, and subsequent return of fluorescence upon addition of the uncoupling agent FCCP, can be taken as showing both a successful F_1F_O insertion and also the final evidence of a successful purification procedure as a whole.

FCCP operates by infiltrating the lipid bilayer and transporting protons back through the membrane, thus rapidly dissipating the proton concentration difference. ACMA will then be unquenched, so the return of the fluorescent signal to around its original strength will confirm that the observed diminishment of fluorescence was indeed due to proton transport and not any potential artifact.

Additionally, the inhibitor DCCD can be used to covalently modify the c-ring of F_O and render it unable to pump protons (and so unable to form an ACMA quenching signal) [152]–[154]. Inclusion of DCCD therefore forms a specific inhibition against F_O activity and demonstrates the ACMA quenching signal seen is due to ATP synthase and not any other proton-pumping mechanism. DCCD also can be used when measuring protein activity by NADH, as in this case it will not totally inhibit function as the F_1 part of F_1F_O is still able to hydrolyse ATP at a reduced rate with a characteristic reduction of around 70-90% [120], [154], [155]. Note that although DCCD can also inhibit the F_1 by a separate interaction, this requires an Mg^{2+}-free environment and so DCCD will be expected to inhibit the F_O part of F_1F_O only under the conditions used [156].

In the charts presented in Figure 3.6 and Figure 3.7, proteoliposomes and ACMA are present at the initiation of the experiment but ATP is not. ATP is added at the time indicated and quenching is initiated, indicating F_1F_O activity. To complete the experiment, the uncoupler FCCP is added to dissipate the proton gradient across the bilayer – fluorescence then returns to around its starting level.

The charts shown in Figure 3.6 are intended as clear controls for the finalised conditions of the single-molecule experiment as presented in Chapter 6 – F_1F_O is fully biotin-labelled (described section 3.2.4), is presented in the fusogenic cationic lipid mixture used (see Chapter 4), and is also tested in a 10 mM MOPS buffer plus 20 mM KCl – which is used in the current single-molecule protocol as presented in Chapter 6 (to promote lipid fusion; see section 4.3.1) – alongside the

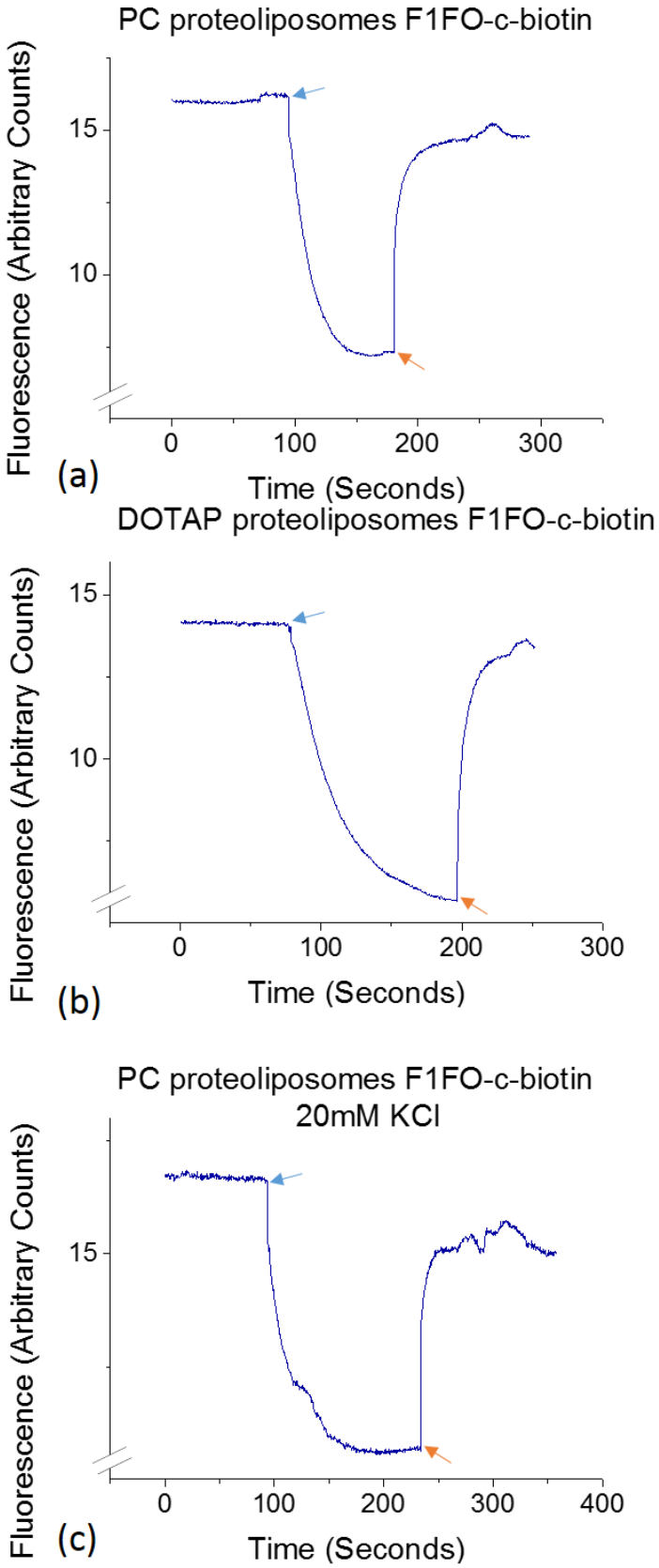

Figure 3.6
ACMA quenching traces for fully biotin-labelled c-subunit cysteine mutants purified according to the finalised protocol (with strongly reducing conditions). In each case proteoliposomes and 0.5 µM ACMA are present at the start of the experiment and allowed to equilibrate for several minutes. After observation of a steady signal, the blue arrow indicates addition of 250 µM ATP to the reaction volume (2 ml cuvette with magnetic stirring). Downward slope indicates pumping of protons across the proteoliposome membrane. After signal reaches around its deepest point, the addition of FCCP at 0.5 µM is indicated by the orange arrow. (a) shows the mutant inserted into 100% Soybean PC proteoliposomes, (b) shows the mutant inserted into 50% DOTAP 50% Soybean PC proteoliposomes, (c) shows the same proteoliposomes used in (a) but the buffer is now 20 mM KCl 10 mM MOPS 2 mM $MgCl_2$ pH 8.0, whereas (a) and (b) take place in 100 mM KCl 50 mM MOPS 2 mM $MgCl_2$ pH 8.0. Clear positive signals of ACMA quenching are seen in all cases (20 mM salt is of interest for single-molecule studies presented in Chapter 6). Note these cases do not represent equal volumes of proteoliposomes (a=4 µl, b=25 µl, c=4 µl).

more typical 50 mM MOPS buffer plus 100 mM KCl that was used to favour F_1F_O function.

Note that in Figure 3.6, the comparison of neutral (100% Soybean PC) proteoliposomes and cationic (50% DOTAP 50% Soybean PC) proteoliposomes involves higher volumes of the cationic proteoliposomes to obtain comparable quenching signals. This was typical; there could be many reasons for this and we note that ACMA is not properly quantitative in any case. The ACMA dye itself could be less effectively incorporated into this lipid mixture, or it could indicate fewer cationic proteoliposomes are present in a given volume, or it could indicate weaker protein activity, or perhaps reflect some effect of the efficiency of protein insertion into the cationic lipid mixture. Nevertheless it is significant that we have been able to see F_1F_O proton pumping in this cationic lipid mixture; the protein is clearly properly functional. Further study on comparative function is presented in Section 3.3.2. In order to demonstrate that proton-pumping seen is due to the action of F_O, a comparative DCCD study is presented in Figure 3.7; this study was performed on an earlier purification which had the less than optimal biotin-labelling presented in Figure 3.4(d). The three cases of c-subunit cysteine mutant in cationic and neutral lipid mixtures, as well as cysteine-free mutant in neutral lipid mixture are presented. 50 μM DCCD was incubated with the proteoliposomes for 30-60 mins prior to the readings and it is clear that proton pumping activity has ceased completely in all these cases. Since DCCD was dissolved in ethanol, then for Figure 3.7 to allow a direct comparison each

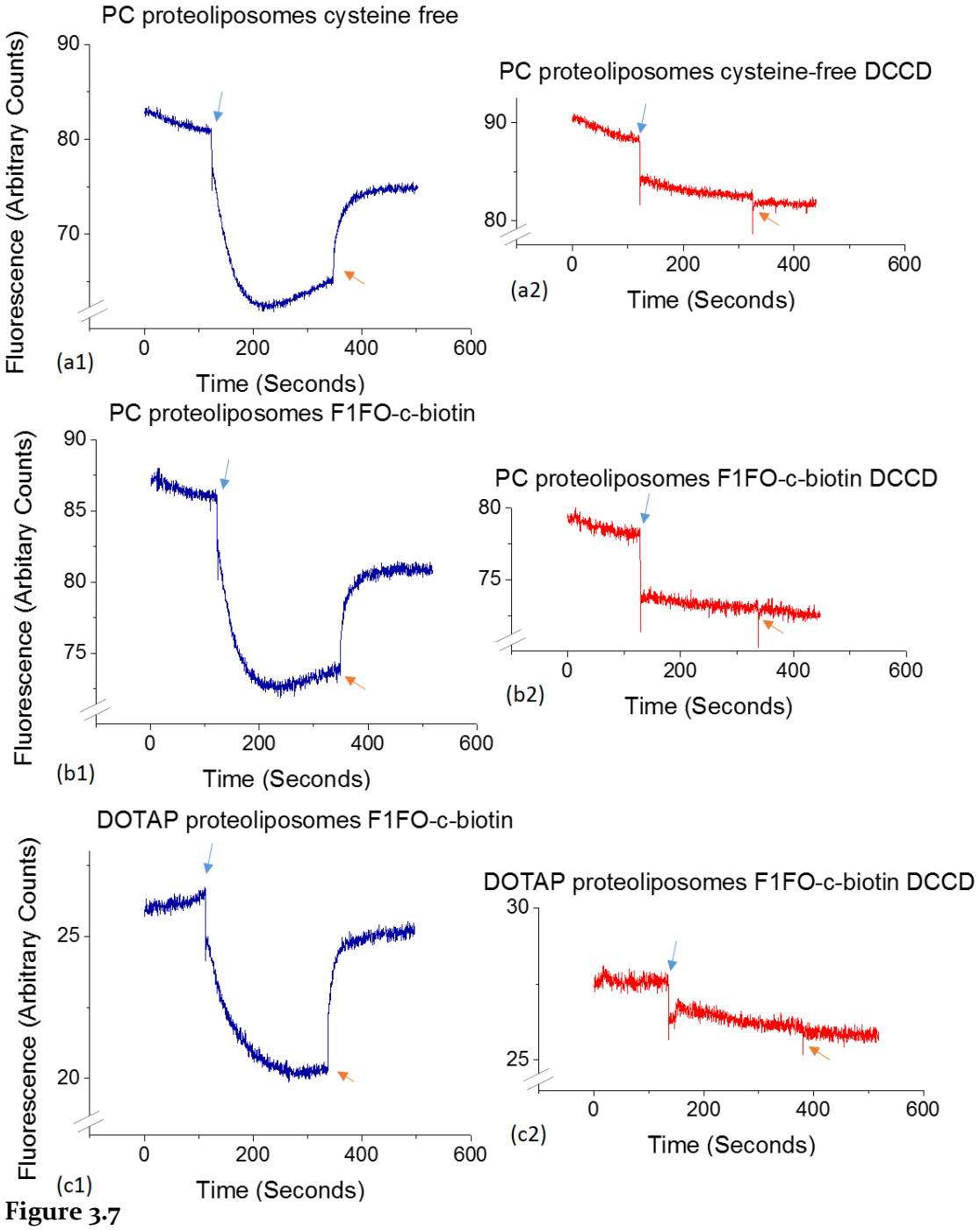

Figure 3.7

Comparative ACMA quenching including comparison on incubation with DCCD (shown at the same scale). In each case proteoliposomes and ACMA (at 0.5 µM) are present at the start of the experiment; the blue arrow indicates addition of 250 µM ATP, and the orange arrow the addition of 0.5 µM FCCP. Each a2-c2 shows proteoliposomes pre-incubated with 50 µM DCCD in ethanol for 30-60 mins, while each a1-c1 shows the same corresponding volume of proteoliposomes incubated with ethanol for the same period as a control (demonstrating cessation of proton-pumping seen in a2-c2 is due to DCCD, rather than ethanol). a1,a2 show cysteine-free mutant in 100% Soybean PC lipids. b1, b2 show c-subunit cysteine mutant in 100% Soybean PC lipids. c1, c2 show c-ring cysteine mutant in 50% DOTAP 50% Soybean PC lipids. Since DCCD is an F_O-specific inhibition, this confirms the proton pumping observed is performed by incorporated F_1F_O.

accompanying control trace had also been incubated with the same small volume of plain ethanol for an equal time.

3.3.2 Thin Layer Chromatography Analysis for Proteoliposomes

Since the purification protocol for F_1F_O includes appreciable levels of lipids in the elution buffer, it will be of interest to establish what the actual lipid composition is of proteoliposomes after reconstitution (this is relevant for the analysis of comparative response of the protein in different lipid compositions to follow in section 3.3.3). Thin-layer chromatography (TLC) was used; this method separates lipid samples into individual components based on their characteristic progression up a silica gel plate (see description in section 2.6.3) [135]. We may compare the behaviour of a known pure standard to a sample of liposomes/proteoliposomes to determine the lipid composition. This forms an initial and rapid method of analysis.

The 'Sigma PC' used in the purification process is present at 8 mg/ml in the protein sample and so might be expected to have a final concentration of 0.8 mg/ml in the proteoliposome sample; and the Avanti 'Soybean PC' (see section 2.3.1) used in the liposome preparation is present at 10 mg/ml in the liposome sample and so 3 mg/ml in the final proteoliposome sample. Hence the Sigma PC could potentially introduce a significant contamination to the expected lipid composition, which we test here.

Interestingly, only one band was observed for the 'Soybean PC' lipid mixture typically used for liposomes formation and reconstitution of protein, despite its advertisement by that company as a mixture (see section 2.3.1). By comparison of

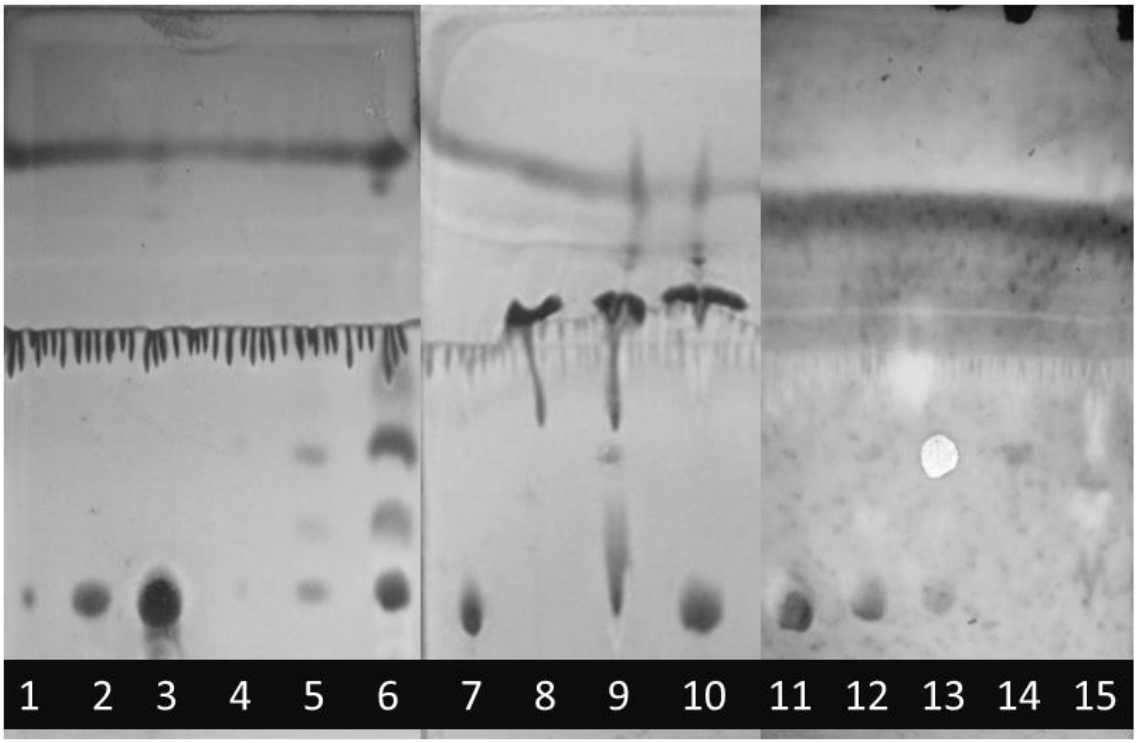

Figure 3.8
TLC plates showing the results of several analyses. Bands 1-3 Avanti Soybean PC 1 µg, 10 µg, 100 µg respectively. Bands 4-6 Sigma PC 1 µg, 10 µg, 100 µg respectively. It is clear that Avanti PC consists of one band and Sigma PC consists of four bands. Band 7 25 µg Soybean PC. Band 8 25 µg DOTAP. Band 9 cationic liposomes 50% DOTAP 50% Soybean PC (roughly 100 µg); band 10 cationic proteoliposomes 50% DOTAP 50% Soybean PC (roughly 100 µg). Band 11 neutral liposomes 100% Avanti Soybean PC (roughly 100 µg); band 12 neutral proteoliposomes 100% Avanti Soybean PC (roughly 30 µg); band 13 a further set of 100% Soybean PC proteoliposomes which have been tested for ACMA quenching (roughly 30 µg); band 14 80% PE and 20% POPA liposomes; band 15 solubilised F_1F_O (containing Sigma PC lipid). It is clear that the cationic proteoliposomes (lane 10) consist only of Avanti Soybean PC (7) and DOTAP (8) and not the Sigma PC used in the protein purification (5/6), at least to any significant level (since we can resolve down to around 10 µg judging by the controls in lanes 4-6 for Sigma PC, so could resolve down to around 10% of the total added to lanes 9 and 10). The solvent front line halfway up represents solvents of chamber 1, and the second higher up is the solvent front from chamber 2.

this Soybean PC and DOTAP bands to the 'Sigma PC' used in extraction buffer (which shows four bands, more in line with expectations from the company's stated composition), we see that 'Sigma PC' is not present in either proteoliposome set (fusogenic or non-fusogenic). It may be inferred that 'Sigma PC' is completely or largely removed from the final proteoliposome formulation during sephadex passage (section 2.6.1). This gives an initial indication in

agreement with the hypothesis that proteoliposomes are formed with the lipid composition only of the liposomes used to form them and none of the lipids used to solubilise the F_1F_O.

3.3.3 Comparative Stability of Activity by NADH Assay in Proteoliposomes

It has been suggested that the relative ACMA quenching as a proportion of the starting level of fluorescence intensity could hint at poorer function or stability in the cationic lipid mixture compared with 100% soybean PC (this could also be an artifact due to the interaction of ACMA with the different lipid mixture, or represent lower protein insertion in the cationic lipid mixture). This effect was seen over more than one preparation to worsen from the time of preparation; this observation prompted further investigation with a more quantitative and reliably consistent method than ACMA itself – the NADH measure of ATP hydrolysis.

We may hypothesise that initially protein function in the two cases is essentially very similar, but that over time the function degrades more rapidly in the cationic case than the neutral case. We may also suggest that freezing and thawing has a more substantial impact on the cationic proteoliposomes than the neutral. Although the use of a sephadex column during insertion of protein into liposomes is expected to remove most excess F_1F_O not inserted, nevertheless to first eliminate the contribution of any protein still potentially present in a non-reconstituted form then proteoliposomes were first pelleted in an ultracentrifuge after reconstitution. It was expected that protein concentration within proteoliposomes could be measured, however attempts at this yielded inconsistent results (possibly due to DOTAP having unexpected interactions with

the assay beyond that studied for phospholipids [157], [158]) and this was not pursued since it was still possible to compare equal volumes and thus compare relative changes in activity for equal volumes of proteoliposomes.

To clarify exact conditions used: proteoliposomes were first prepared in the general manner described in section 2.6.1, but in a buffer including 10% glycerol (100 mM KCl 50 mM MOPS 2 mM $MgCl_2$ 10% glycerol pH 8.0). These proteoliposomes were then diluted 4.5x into a buffer containing no glycerol and a reduced concentration of $MgCl_2$ (100 mM KCl 50 mM MOPS 0.1 mM $MgCl_2$ pH 8.0, since this was found to aid pellet formation of DOTAP liposomes) and subjected to 50 000 rpm 2 hrs 5 °C in a TL-100 Beckman tabletop ultracentrifuge (88 000 g average). The pellet was resuspended in the standard buffer 100 mM KCl 50 mM MOPS 2 mM $MgCl_2$ at a 3x concentrated form compared to the starting volume before dilution.

The proteoliposomes in this form were then tested for ATPase activity with NADH over three time periods – the first, around 12 hrs after their first formation (due to the preparation time involved). During this time proteoliposomes were subjected to the 2-hour long centrifugation process described, but otherwise kept at room temperature. Secondly they were tested again after a further 12 hrs at room temperature, and a third time after a further 24 hrs at room temperature. Finally a sample frozen in liquid nitrogen at the point of 12 hrs past the first formation was thawed and tested (this test was performed 48 hrs after first formation, but it was assumed that any damage done to the protein upon freezing is then largely unaffected by how long the protein is kept at liquid

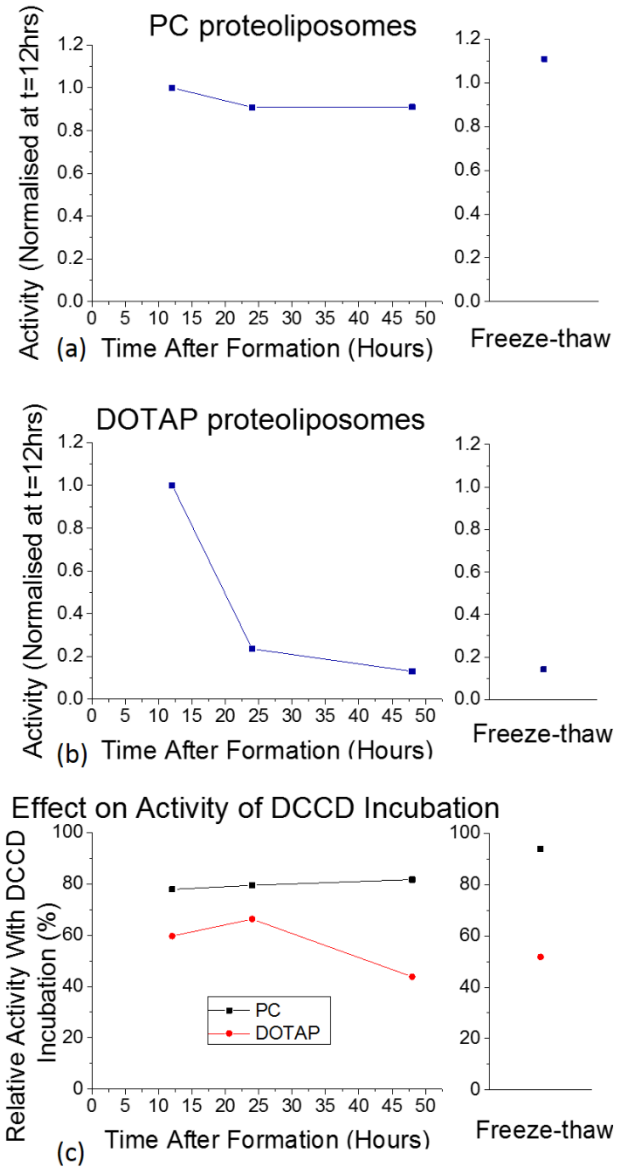

Figure 3.9
Summary of results for study of both relative ATP hydrolysis over time by NADH, and effect of DCCD incubation on ATP hydrolysis activity over time. In (a,b) equal volumes of proteoliposomes are tested over time, with the first measurement at 12 hours post-formation normalised to 1: (a) shows 100% Soybean PC proteoliposomes and (b) 50% DOTAP 50% Soybean PC proteoliposomes. In both (a) and (b) three measurements are made of activity over 48 hours, plus a final freeze-thaw measurement (sample frozen in liquid nitrogen 12 hours after formation, thawed 36 hours later and tested). Note that equal activity of PC vs DOTAP/PC proteoliposomes at 12 hours is not implied. In (c) for each measurement made of ATP hydrolysis activity over time for (a) and (b) then a second measurement of DCCD-incubated proteoliposomes is made and the inhibition level calculated. Hence in the 100% Soybean PC case, both activity (a) and DCCD inhibition (c) remain fairly constant over time. In the 50% DOTAP 50% Soybean PC case, activity falls and DCCD inhibition also falls implying structural damage to the protein over time in the cationic environment.

nitrogen temperatures since this is the established manner in which it is stored for many months at a time).

Additionally, in each case samples of proteoliposomes were also incubated with 50 μM DCCD for 30-60 mins prior to testing in order to compare activity with the non-DCCD treated case. From this we derive a DCCD-inhibition response at each time-point. This should help to reveal if instabilities in the bilayer might contribute to uncoupling of the c-ring to other subunits. If such uncoupling

occurs, we can hypothesise that the function can most likely not be recovered by delivery of the protein into a more stable lipid environment since it would presumably be permanently damaged. Sensitivity to DCCD therefore gives us further information regarding the nature of the expected reduction in activity over time.

As seen in Figure 3.9, ATP hydrolysis activity for equal volumes of cationic proteoliposomes yielded a clear reduction over the time of the experiment whilst neutral proteoliposomes were stable. Freezing cationic proteoliposomes in liquid nitrogen and then thawing yielded a similar reduction in activity as indicated. Furthermore DCCD inhibition levels were also reduced with time, as well as when frozen and thawed, as indicated, suggesting the reduction in activity was also accompanied by modification of the subunit interactions. Note that in each case the activity has been normalised to that seen on the first measurement and a comparison has not been made between absolute activity in the cationic and neutral cases since the amount of protein present in each was not measured.

These results suggested caution in the use of frozen cationic proteoliposomes. Many experiments required structural formats of the protein, such as surface binding, and in these cases proteoliposomes frozen and stored in liquid nitrogen were generally used in order to conserve protein and to save time. For activity assays, particularly when developing new methodologies, cationic proteoliposomes could be freshly prepared on the day so as to ensure maximal activity. In practice this is difficult owing to preparation time, so a compromise

must be struck between preparation time and potentially reduced protein function.

For the development of initial single-molecule rotation studies, it is significant we do still expect activity from such freeze-thawed cationic proteoliposomes and ACMA quenching can still be observed after freeze-thawing (I have not displayed this but it simply typically requires a higher volume to obtain the same signal as that seen in Figure 3.6 for a sample made on the same day). It is not clear to what extent the reduction in ATP hydrolysis activity might be caused by some F_1F_O completely ceasing hydrolysis activity, or all operating at a reduced rate, or some combination of the two. Nevertheless it still seems perfectly reasonable to expect such frozen-thawed samples to rotate under hydrolysis for single-molecule analysis, so it will be a question of the balance of available time whether such studies to initially demonstrate ATP hydrolysis-driven rotation be undertaken by frozen-thawed proteoliposoms or those freshly made for stronger activity. Optimisation of the lipid mixture with reduction in the percentage fraction of cationic lipids, or substitution for other lipids, seems likely to yield improved and more natural DCCD inhibition responses for frozen-thawed samples once such rotation studies have been clearly established and the time can be dedicated to such optimisation.

3.4 Summary and Conclusions

F_1F_O has been purified with good yield as measured by BCA protein concentration, with all subunits intact as measured by SDS-PAGE, and with proper function both of ATP hydrolysis, as measured by NADH absorption, and

of coupled proton transfer as measured by ACMA quenching. Through DCCD inhibition it was shown that ACMA quenching was due to F_1F_O, since this is an F_O-specific inhibitor, and through sodium azide it was shown that ATP hydrolysis observations by NADH were due to F_1F_O since this is an F_1-specific inhibitor. Such purifications have become routine and regularly give similar results to those presented, with high reliability. ATP synthesis activity has not been measured and would represent future work as single-molecule studies develop.

Regarding biotin-labelling of cysteine-modified subunits, an investigation has revealed that high levels of reducing agents are required to be introduced into the purification procedure for proper labelling to occur (250 mM beta-mercaptoethanol has been used with success). Even under the high reducing conditions used, some dimerisation of the c-subunit is still seen in SDS-PAGE gels – suggesting labelling is still less than 100%. Nevertheless a strong improvement on initial labelling conditions was seen and, with 10 c-subunits available, analysis of bands suggests that at least half have been labelled – more than sufficient for the stated aims. It is noted that although this mutant had previously been utilised for single-molecule studies with biotin-labelling of the c-subunits, reducing conditions were not described [27].

Regarding the use of a fusogenic lipid mixture 50% DOTAP 50% Soybean PC (expanded upon further in Chapter 4); it is found that purified F_1F_O is indeed functional in this mixture and ATP hydrolysis by NADH and protein transfer by ACMA are both observed. Further investigations suggest that this lipid mixture is not optimal as protein function is seen to degrade both over 24 hrs and also when

samples are frozen and thawed. It is suggested that samples be freshly prepared for optimal activity when using this lipid mixture (this is not required for purely Soybean PC lipid, which demonstrates more stable function over time and with freeze-thawing). It is expected that charged lipid concentration might be later reduced, or other charged lipids might be introduced – cationic derivatives of phosphatidylcholine (such as described by MacDonald et al. [137]) may perhaps be expected to have a more protein-compatible response than DOTAP – this is a matter of ongoing investigation in the research group. Nevertheless it should not be diminished that such a strongly-charged lipid composition (selected to give the best chance for observation of lipid fusion) has indeed been shown to be compatible with protein function; the damage inferred over time (and in freeze-thawing) from reduction in hydrolysis rate and DCCD inhibition would seem to still allow for initial single-molecule rotation studies to proceed for attempts to observe hydrolysis-driven rotation, before later optimisation.

Thin-layer chromatography has been used to give an initial positive indication that liposomes after protein insertion (referred to as proteoliposomes) contain the same lipid contents as the liposomes prior to protein insertion; meaning that the lipids used during protein solubilisation are not seen at detectable levels. This corresponds with the hypothesis that the lipid composition of proteoliposomes is unchanged after protein insertion, though further testing would be required for a definitive conclusion.

Chapter 4 Lipid Fusion and Giant Vesicles

4.1 Introduction

The methodology proposed in Chapter 1 calls for the incorporation of a rotational probe – a gold nanosphere – within an enclosed lipid vesicle. Several of the past approaches to the problem of darkfield studies of F_1F_O-ATP synthase rotation have attempted to form a planar bilayer across a surface (or use a droplet hydrogel bilayer based approach – research on the latter is ongoing within the Berry group). With open access to the protein in this case, a rotational probe could be added and allowed to bind to the protein once the assembly of the system has been performed; that is not so with the proposal here, in which gold must be present from the start (notwithstanding some kind of injection system).

Some references to the incorporation of gold nanospheres into the interior space of lipid vesicles can be found [159], [160], though the bulk of the literature is more geared towards the incorporation of hydrophobic gold into the bilayer or decoration of external leaflet of the bilayer – generally for nanomedicine applications [161]. Nanospheres in such publications, where they were found, are generally of the order of 10 nm and can be obtained in substantially higher concentrations that those of interest for dark field microscopy (which are of diameters 40-100 nm).

Initial experiments, not presented here, attempted to separate an assumed small fraction of liposomes containing gold nanospheres formed by extrusion. With 40-100 nm diameter gold nanospheres in the highest commercially obtainable concentrations, separation was attempted based on their change in relative density to empty liposomes via a gradient-centrifugation method. No apparent success was seen; it is clear that such an approach was impractical to readily repeat and optimise, not least for the economic cost of high concentrations of functionalised gold nanospheres. The downstream insertion of F_1F_O into such a hypothetical liposome whilst retaining the gold nanosphere internally poses its own difficulties, since detergent-mediated insertion is expected to equalise the internal and external conditions.

The methods that were developed to address these problems are twofold; both elements were based on antecedents in the literature but present distinct novelties in their approach and their combination. Lipid vesicle fusion allows the combination of vesicle objects formed in distinct manners to suit their particular purposes. Giant vesicles formed by an emulsion method allow totally independent formulation of the interior vesicle content compared to the exterior – relatively 'high value' components (such as gold nanospheres) can then be entrapped at high concentration with little loss to the exterior. This is by contrast to both extrusion and the detergent-mediated protein insertion methodology used for proteoliposomes, by which the interior and exterior buffer environments are equalised and hence in which the compounds to be internalised must be present in relative abundance and the non-internalised remainder later removed

by filtration or centrifugation washing. Hence by combining fusion and giant vesicles by emulsion, proteoliposomes can be formed on the order of 100 nm size; gold-containing giant vesicles will be of the order of 2-10 μm, and these objects can then be fused together to form a new post-fusion giant vesicle with gold internally and F_1F_O embedded in the membrane. Needless to say with a novel approach, none of these technologies existed in the research group at the start of the project.

4.2 Giant Vesicle Formation and Characterisation

Although several methods for the formation of giant vesicles exist in the literature, only formation by water-in-oil emulsion allows us to encapsulate contents in the interior space of the vesicles entirely separately from the exterior aqueous space; the method explored here was first developed in 2003 by Sophie Pautot et al. [139], [140].

The general principle of the formation is ingeniously simple; first an emulsion of water-in-oil is formed in which lipids are present in the oil phase. Such lipids will tend to orient onto the emulsion droplets with their hydrophilic heads facing the droplet and hydrophobic tails facing the oil; the emulsion will be stabilised by this process, preventing the rapid merging of droplets that would normally occur. For this to occur some incubation time is needed. Separately, oil containing lipid can be incubated against a flat aqueous interface where the lipid will tend to orient along the interface with hydrophilic heads facing the aqueous medium. When these two oil phases are combined, the aqueous lipid monolayer droplets

can be induced to pass through to the lower aqueous phase by gravity. At the interface, these droplets hence pick up a second monolayer and thus form a lipid bilayer around the aqueous droplets. This method also has similarities to one in which the motion of the vesicles through the second monolayer is induced by rotation around a central axis; continuous droplet interface encapsulation [162].

Giant vesicles were formed initially based on examples in the literature, with adaptations and innovations made over many preparations to both suit the needs of the project and also to reduce labour-intensiveness of the protocols. The finalised methodology involving vortex-mixing of emulsion is described in Chapter 2, along with an earlier standardised iteration involving extrusion of emulsion. Viewing and assessment of formed giant vesicle samples was generally performed under the microscope, with adaptations to the microscope set-up to advantage such assessments including the dark field insert device described in Chapter 2 for the simultaneous viewing of fluorescent and backscatter darkfield light-paths. Images of giant vesicles in brightfield and differential-interference contast (DIC) (Figure 4.1) highlight that contrast-enhancing methods are helpful for viewing the giant vesicles. The use of ficoll as an internal density agent presumably also helps contrast. In practice fluorophores were generally incorporated in order to simplify viewing and further elucidate structure. The heterogeneity in size and structure inherent to the method as it currently stands is displayed in Figure 4.1 and many of the figures to follow. Methods for more homogeneous preparations have been described in the literature [163]–[166] but the development time was thought too involved to look further into such

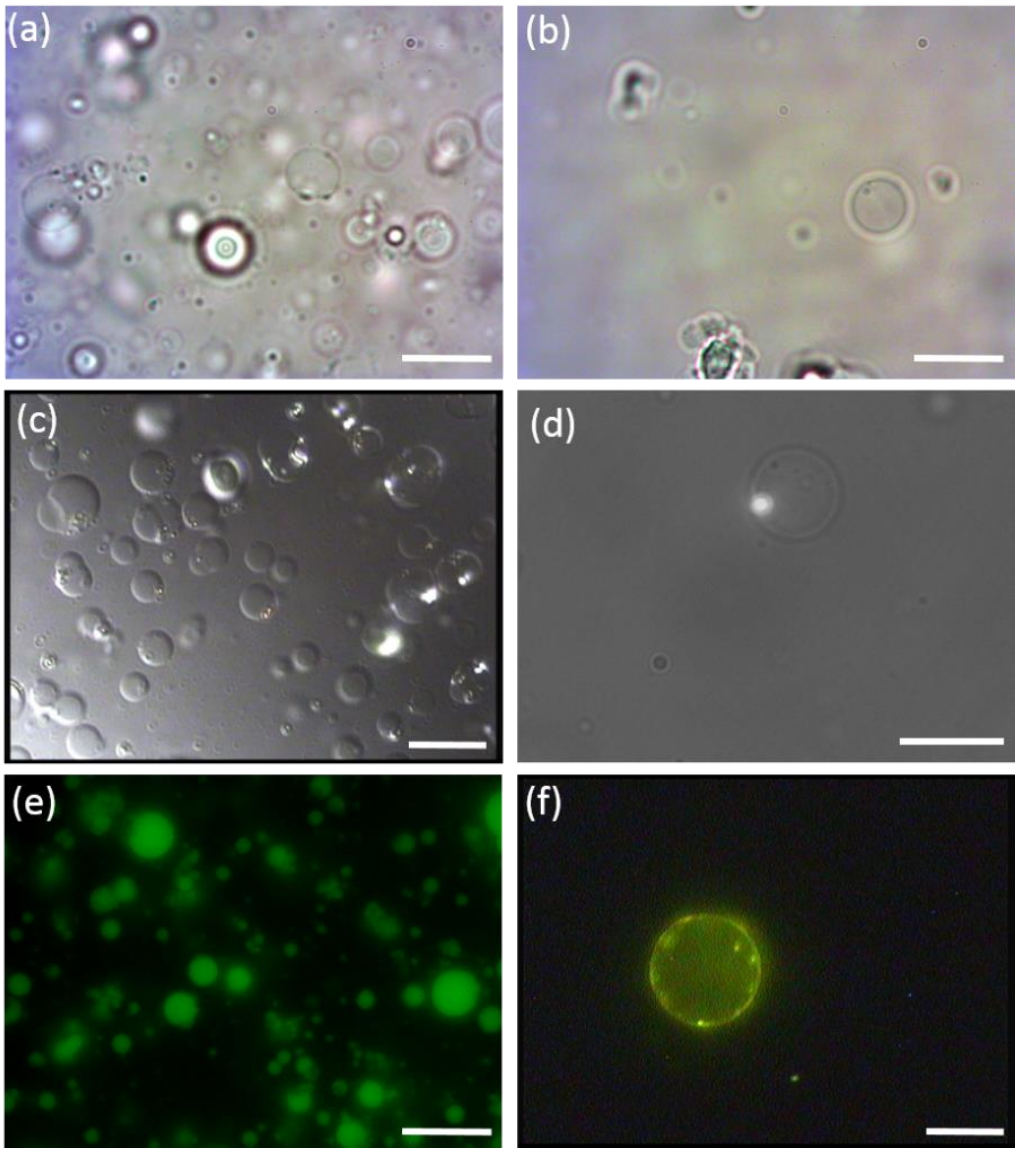

Figure 4.1

Giant vesicle preparations. (a) and (b) show brightfield images away from the coverslip surface. (c) shows the enhanced contrast available from DIC and is taken at the coverslip surface; this preparation contains 100 nm diameter gold nanospheres internally – this is discussed in detail in section 4.2.2. It is possible to form giant vesicles with arbitrary contents; (d) shows a combined brightfield and fluorescence view of a giant vesicle preparation containing a 1 μm diameter fluorescent bead. In general it proved most reliable to identify and characterise giant vesicles by use of fluorophores; (e) shows a preparation with the aqueous fluorophore pyranine in the internal space of the vesicles and (f) shows a fluorescent lipid (NBD-PE) forming an integral part of the bilayer. Brighter patches could represent regions of entrapped oil and associated fluorescent lipid; presence of such patches would not be expected to affect proton permeability though presumably could affect fusion behaviour at affected regions (see section 4.3 for fusion studies). The heterogeneity of sizes are visible in many of the images. Images taken with the following cameras with variable settings; (a,b,e) Toupcam UCMOS05100KPA; (d) Thorlabs 340M-GE; (c,f) Watec WAT-2215. Scale bars are 10 μm.

approaches; greater homogeneity has been described in the literature than I have generally observed but this should not be critical to the development of the methodology. Another approach that could be compatible with the aim of encapsulating gold nanospheres would be an inkjet method [167]. Heterogeneity seen experimentally by the emulsion method in this study also applies to the lamellarity of formed giant vesicles (discussed section 4.2.4); interestingly, multi-compartment giant vesicles formed by the emulsion method have also been of interest in the literature [168]. With further development, undesired heterogeneity should be resolvable since such approaches have been demonstrated in the literature – as ever, such development had to be balanced with the aim to further develop all areas leading to a working single-molecule experiment.

4.2.1 Establishment of the Protocol for GUV formation

The essential structure of the protocol through emulsion formation, followed by passage through a lipid monolayer formed between an aqueous buffer and oil, had been established in other research groups [139], [140] but the finalised form of the protocol presented in Chapter 2 came about through substantial trials of many different conditions. I will attempt to summarise the experience gained here in not too many words.

0.05 mg/ml – 0.4 mg/ml is the range of lipid concentrations in oil that have been used to successfully form giant vesicles; 0.2 mg/ml was first used successfully and was chosen simply as a mid-point between a fairly broad range used in the literature. It was expected based on discussion and speculation in the literature

that raising the concentration too high would compromise the overall unilamellarity of giant vesicles formed and so in general it had been aimed to keep the concentration around the minimum viable level; however a recent paper has claimed that this is not the case [169] and so it may well be an unfounded concern. That 0.2 mg/ml worked from the start would seem to reinforce this. However, issues were later encountered in which the concentration seemed less reliable and was raised to 0.4 mg/ml – this was actually tracked to a poor resuspension of lipids from their dried state into the oil itself (hence, some lipids remained on the wall of the container – this could be monitored by the use of fluorescent lipids). Glass vials and standard plastic eppendorfs were both also tested; the use of low-bind plastic eppendorfs as described in Chapter 2 was found to give a reliable resuspension of lipids into oil. Even so, the vortex treatment, use of a pipette to aid resuspension, and bath sonication described in Chapter 2 were still found to be required for reliable and consistent resuspension. Sonication for long periods (90 mins or more) have been described in the literature to promote resuspension; this was disfavoured since it was speculated damage to lipids might result. With the final protocol quoted in Chapter 2, consistent formation results are seen. Although it has been possible to reduce concentration to 0.05 mg/ml, this results in fewer giant vesicles formed and less reliably with no apparent change in lamellarity of structures (which would seem to agree with the findings of Chiba et al. [169]). Hence 0.2 mg/ml of lipid in oil became the standard.

The incubation time use for the interface between aqueous buffer and oil-with-lipid was set at 60 mins from the start, based on the literature, and not varied in order to more readily assess the impact of other variations. Upon addition of oil-with-lipid at 0.2 mg/ml to the aqueous buffer, the formation of a flat interface within 1 min has been found to indicate good resuspension of lipids.

Paraffin oil (see description in section 2.8.1) was used over other oils initially tested – hexadecane, dodecane, and squalene (based on references in the literature) due both to its viscosity being lower than some other oils, so based on initial tests it proved more practically straightforward to use, as well as being relatively cheap. The yield of giant vesicles also appeared to be at least as good as in other oils, so its use was standardised from the earliest tests on.

pH conditions and the presence of divalent cations were found to impact formation of giant vesicles and this is presumed to be related to the use of anionic charged lipids in their formation. From the earliest stages tests were performed with a lipid composition of 20% POPA 80% Soybean PC. This was presumed to be a sensible concentration of charged lipids even before fusion with content mixing at this level had been demonstrated; interestingly, Pautot et al. have discussed that charged lipids demonstrate faster formation of stable monolayer interfaces than zwitterionic lipids [170]. pH 8 or 7.5, at 100 mM salt or 20 mM all reliably gave formation of giant vesicles. A pH 7 condition formed a flat interface between oil-with-lipid and aqueous buffer significantly more slowly so was abandoned. Use of $MgCl_2$ up to 2 mM concentration, the concentration typically used for F_1F_O function, was found to inhibit the formation of giant

vesicles – presumably due to interaction between the Mg^{2+} and the anionic lipids. Hence either no $MgCl_2$ was used, or 0.1 mM $MgCl_2$ became a reliable concentration for formation. Interestingly, when it was desired to concentrate formed giant vesicles by centrifuge then $MgCl_2$ to a concentration of 0.1 mM was found to aid formation of a pellet compared to cases when it was not present (with otherwise the same buffer conditions); it is assumed to help overcome charge repulsion between giant vesicles. For this reason it was often favoured (though in practice it was still possible to form a pellet without it – just at higher g-force; this is described in Chapter 2).

In general giant vesicles were found to be fairly robust to centrifugation treatments and after formation into a 3 ml volume were generally concentrated by pelleting and resuspension into around 100 µl. Repeated centrifugation would result in a lessening pellet each time, so was avoided.

Fusion studies shown in section 4.3.1 demonstrate that a salt condition of 20 mM was favourable compared to 100 mM; interestingly this converged with findings that giant vesicles with gold nanospheres internally formed more reliably, and a higher proportion were seen with freely-moving gold rather than stationary or otherwise apparently stuck nanospheres, in 20 mM salt than 100 mM. Hence, based on these findings with Mg^{2+}, pH, and salt the final condition typically used for many of the described experiments was 20 mM KCl 10 mM MOPS 0.1 mM $MgCl_2$ pH 8.0.

The use of ficoll as a density agent in the formation of GUVs was an innovation not found in the literature; generally osmotically balanced concentrations of

sucrose and glucose have been used. This was felt to be unnecessarily complicated, since it was not desired to have external components that might interfere with binding at a surface and so internal ficoll was used on the first attempts and found to be effective. A concentration of 17% ficoll-400 (w/v) was selected with reference to information available from the supplier on the density and osmotic pressure effects of ficoll at varying concentration; it is a 1/3 dilution of a 50% solution made in water (its maximum solubility). It is not expected to introduce osmotic effects at this concentration, though the increased viscosity will be expected to affect the drag on the F_O motor from the attached bead. Based on past studies, 17% ficoll will have a relative viscosity up to 10× that of water [171]. The drag coefficient (f) will scale linearly with viscosity (η) but with a rotational drag component scaling with the cube of the bead radius (r_b) and a second eccentricity component scaling linearly with the bead radius (but depending also on the square of the eccentricity of the orbit r_e). This is $f = 8\pi\eta r_b^3 + 6\pi\eta r_b r_e^2$ [172]. Hence 10× the viscosity would have the same effect as increasing the bead size around 2-4× (depending on eccentricity). Based on past characterisations of F_1 under differing loads [59], anything below 100 nm radius in water might be expected to be effectively zero-load. Hence as long as we use a lower bead size (say 60 nm) then the effect on drag of the increased viscosity should still not be much above the zero-load condition; the ficoll concentration could presumably later be reduced and centrifugation conditions increased to compensate if this were of interest. 17% ficoll was reliable and used consistently for the characterisation presented here and would not be expected to prejudice initial attempts to view rotation (only later when viewing of rotation under an

effectively zero-load condition would be of interest, then this could be further optimised by reducing ficoll concentration). Formation utilised a relatively high g-force to pass the lipid-stabilised emulsion through the second monolayer compared to the literature; around 3500 g. Lower g-force tests resulted in lower formation yields.

The protocol presented in Chapter 2 uses a vortex to produce a proper dispersion of emulsion, combined with a sonication step. In initial results a protocol using extrusion to form the emulsion was used (described section 2.8.1). Essentially no discernible difference between results was perceived in terms of yield or size of GUVs between the final protocol and the earlier protocol. The inclusion of the sonication step in the vortex protocol was found to be important to reduce oversized emulsion objects to a size that resulted in proper transfer into the aqueous phase and formation of giant vesicles. Although the finalised protocol allowed for relatively straightforward preparations, it is speculated that some of the heterogeneity seen in preparations could be traced to the emulsion formation step – since heterogeneity is also observed there in cases when it was examined (see section 4.2.4, Figure 4.5). Hence greater control over the emulsion step would be expected to yield improved homogeneity in size and lamellarity of giant vesicle formations.

4.2.2 Internalisation of Functionalised Gold Nanospheres in Giant Vesicles

Of particular interest was the internalisation and retention of gold nanospheres 40-100 nm diameter into giant vesicles for darkfield studies of rotation. Since the discussed method of giant vesicle formation includes the use of a centrifuge to

force emulsion droplets through oil into the aqueous phase, it was not initially known whether this might have the potential to force the much denser gold nanosphere to pass through the lipid bilayer and thus open the vesicle to the environment. However, it was found that indeed such vesicle objects were reasonably robust to such treatment and would retain gold nanospheres in intact giant vesicles under the conditions tested.

Although reference to protocols involving the incorporation of microspheres such as fluorescent polystyrene was found [173], I am not aware of any prior protocols involving the use of gold nanospheres internal to giant vesicles. During the refinement of the protocol then where the g-forces could be reduced and the yield of giant vesicles not compromised, this was generally done with the expectation that it could potentially improve results when using gold nanospheres. Although to some extent gradually lowered centrifugation speeds (to the level in the finalised protocol presented in Chapter 2) were observed to aid in the reduction of deformed giant vesicle objects, it was not apparent that the yield of gold-containing giant vesicles was much affected.

To assess the presence of gold internally, some initial attempts were made to quantify gold presence using absorption measurements but these were never fully developed and seemed overly-complicated for the purpose. It was preferred to simply view samples under the microscope to gain a more qualitative feel for the preparation; to observe the gold freely moving within the giant vesicle, with a good yield of giant vesicles of appropriate size (around 2 μm diameter and up).

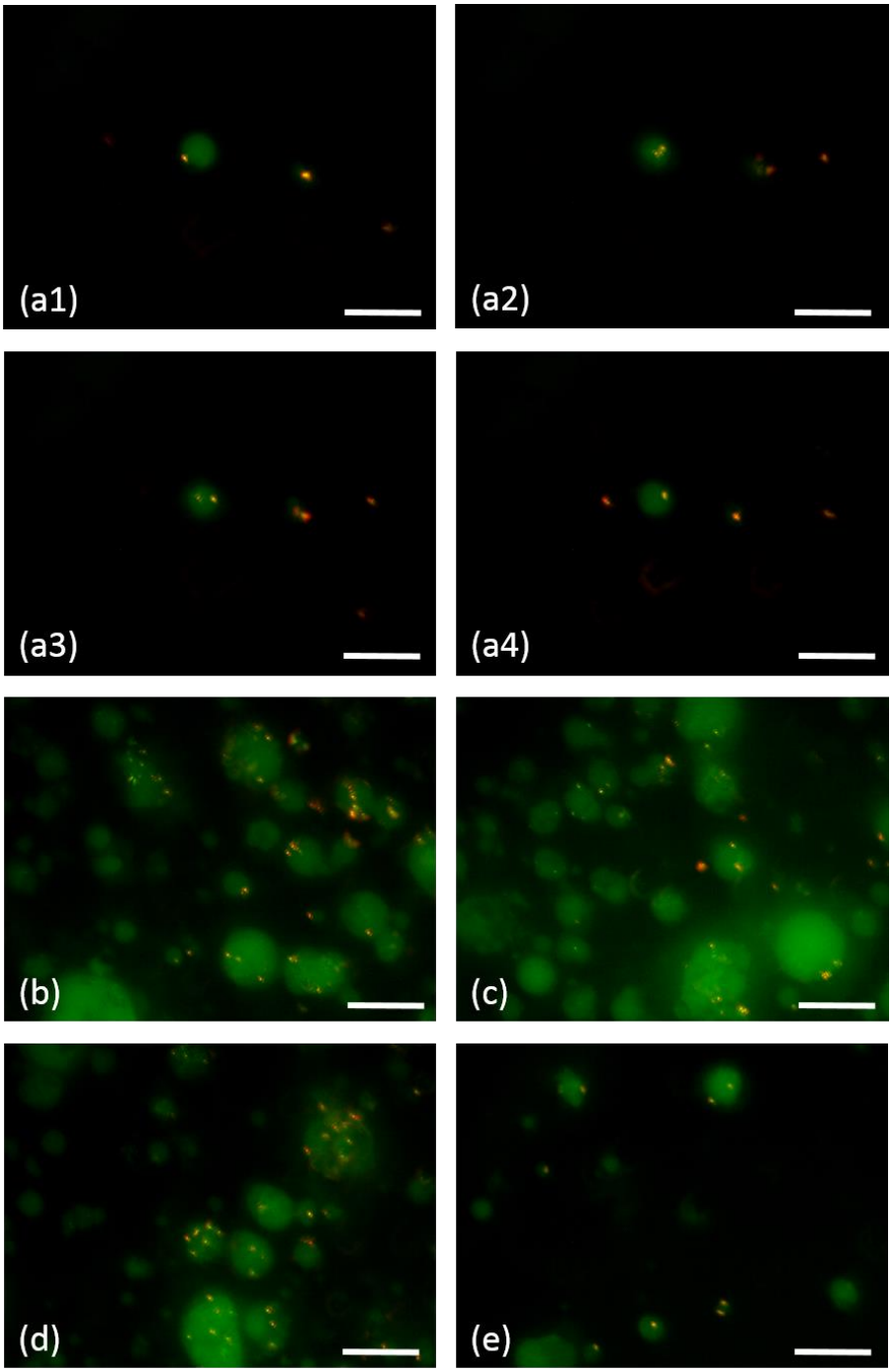

Figure 4.2

Giant vesicles loaded with 100 nm diameter gold nanospheres and pyranine in the internal aqueous space. Viewed with the darkfield insert (section 2.2.1) allowing simultaneous viewing of fluorescent and backscatter darkfield light paths. Each yellow/orange spot is one gold nanosphere (or a cluster of more than one). Images (a1-4) show the same field of view in time sequence, demonstrating the free movement of at least three identifiable separate gold nanospheres internal to one giant vesicle. That the gold moves freely within is readily apparent when viewing live or by video. (b)-(e) further fields of view at a surface, demonstrating typical heterogeneity of preparations. Images taken with Toupcam UCMOS05100KPA camera with "Bodipy" fluorescent cube spectral parameters (as listed in the appendix) as well as white LED illumination for the secondary path provided by the darkfield insert; camera conditions variable (typically 100ms no gain, with 3% arclamp fluorescent intensity). Scale bars are 10 μm.

Although it is possible to view gold nanospheres down to 60 nm diameter with brightfield microscopy, they are not straightforward to distinguish from other objects. Highest contrast can be obtained with darkfield; the desire to view gold objects with darkfield whilst demonstrating their presence internally to a giant vesicle using an aqueuous fluorophore internal to the vesicle led to the development of the backscatter darkfield insert device jointly by myself, Dr Ishmukhametov, and Dr Berry (discussed in section 2.2.1). Images taken using this device are displayed in Figure 4.2.

Gold nanospheres enclosed in such vesicles typically often move quickly around the volume of the spherical giant vesicles in an apparently random walk (though some proportion, perhaps up to half – but depending on preparation, are not freely moving and appear stationary; reducing the salt conditions to 20 mM KCl – from an original 100 mM KCl - appeared to reduce the stationary proportion and so was standardised). This free movement within the internal space is readily apparent and obvious by live viewing or video; I have attempted to demonstrate this in sequential still images in Figure 4.2 with a vesicle containing at least three distinct freely-moving gold nanospheres which can clearly be seen to move into and out of focus. As can be seen, typically some giant vesicles – identified by the presence of the aqueous fluorophore pyranine – would not contain gold (the majority of smaller vesicles below 2 μm diameter would not). Most of the larger giant vesicles (over 5 μm) would contain more than one and some free gold can also be seen externally (perhaps due to rupture). However, one could

straightforwardly increase or decrease the quantity of gold input to the inner contents volume to vary these observations (see section 2.8.1).

The free gold observed outside of vesicles, which inevitably settles at the coverslip surface, is a distraction for single-molecule darkfield measurements and a method for its removal is discussed in section 5.5. It is straightforward under the microscope to seek out those vesicles of more reasonable size (which we might define as above 2 μm diameter) and ignore the rest and many can be seen in a good preparation (particularly if concentrated by centrifuge as described section 2.8.1).

4.2.3 Stability of Giant Vesicles

When prepared with internal pyranine, giant vesicles have been observed to retain that pyranine over more than 24 hrs (both at room temperature and 4 °C storage); over several days it becomes apparent due to the reduction in the number of giant vesicles seen in a sample (and increase in background fluorescence) that an appreciable number of vesicles have ruptured. Giant vesicles were not typically used beyond three days after formation. Pyranine was not observed to leak from giant vesicles other than due to their actual rupture, however; this contrasts sharply with the only comparable giant vesicle-based single-molecule F_1F_O study in the literature, in which giant vesicles retained a fluorescent dye for only "hundreds of seconds" [98] (attempts to observe ATP synthesis in this publication were stated to have failed for this reason – since the membrane was leaky then no membrane potential could be induced).

Additionally, it was found to be possible to freeze giant vesicle samples in liquid nitrogen for storage, including those containing gold nanospheres. This was achieved with the incorporation of 10% glycerol into both the lower aqueous phase and the 'inner contents'; best results were achieved when a slightly higher concentration of glycerol (typically 12%) was added to the 'inner contents' volume (hence further increasing density).

Good results were seen when samples were frozen and then immediately thawed – judging by eye around half of the number of giant vesicles per field of view survived the process. However results over longer-term storage were more variable (sometimes down below 1 in 10 of the surviving number, or even no surviving giant vesicles at all). With such variable results, this was not investigated further. Nevertheless as a proof-of-principle it could be promising where long-term storage of giant vesicles is of interest. It was pursued here in order to save on preparation time, but the innovation of the vortex emulsion method as described previously significantly reduced preparation time and rendered this less of interest – it was then a relatively straightforward matter to prepare samples on the day of intended use.

Based on what is known so far giant vesicles will certainly be stable over the course of the finalised single-molecule experiments and no evidence has been seen of leakage of incorporated dyes that might indicate a non-energisable membrane thus far, but this has not been heavily investigated since it will not prejudice our initial aim to study hydrolysis-driven rotation.

4.2.4 Lamellarity of Giant Vesicles

In order to investigate lamellarity of giant vesicles, which is to say the extent to which they consist of a single lipid bilayer or have more complex structures, a fluorescent lipid may be incorporated into the membrane during formation. Giant vesicles were formed in the standard manner but including 0.25% by weight of NBD-PE, a fluorophore conjugated to a lipid molecule which is therefore incorporated into each of the two monolayer leaflets of the bilayer. From this we see in Figure 4.3 that there is heterogeneity in lamellarity, as has been seen in size.

A well-established bulk test of lamellarity of vesicles (how many lipid bilayers are present) involves the quenching of this NBD fluorophore by an external agent. By including the fluorescent lipid in both the inner and outer leaflets of the lipid bilayer, we obtain a base level of fluorescence by considering the total fluorescence of a bulk sample of many giant vesicles using a fluorimeter. When introducing a highly efficient quenching agent, we may observe the response of the fluorescent output. Since in a unilamellar population of vesicles we expect roughly equal fluorescence from the external and internal leaflets of the lipid bilayer, and since an external quenching agent is not expected to cross the lipid bilayer and contact the internal leaflet, it would be expected that the fluorescence level would drop to half its original level in such a population. However, a view of giant vesicles containing this fluorophore shown in Figure 4.3 demonstrates that this test will likely not be expected to yield sensible results for such a preparation – since there is such heterogeneity that many structures exhibit high levels of the fluorophore (potentially consisting of droplets of oil containing high amounts of

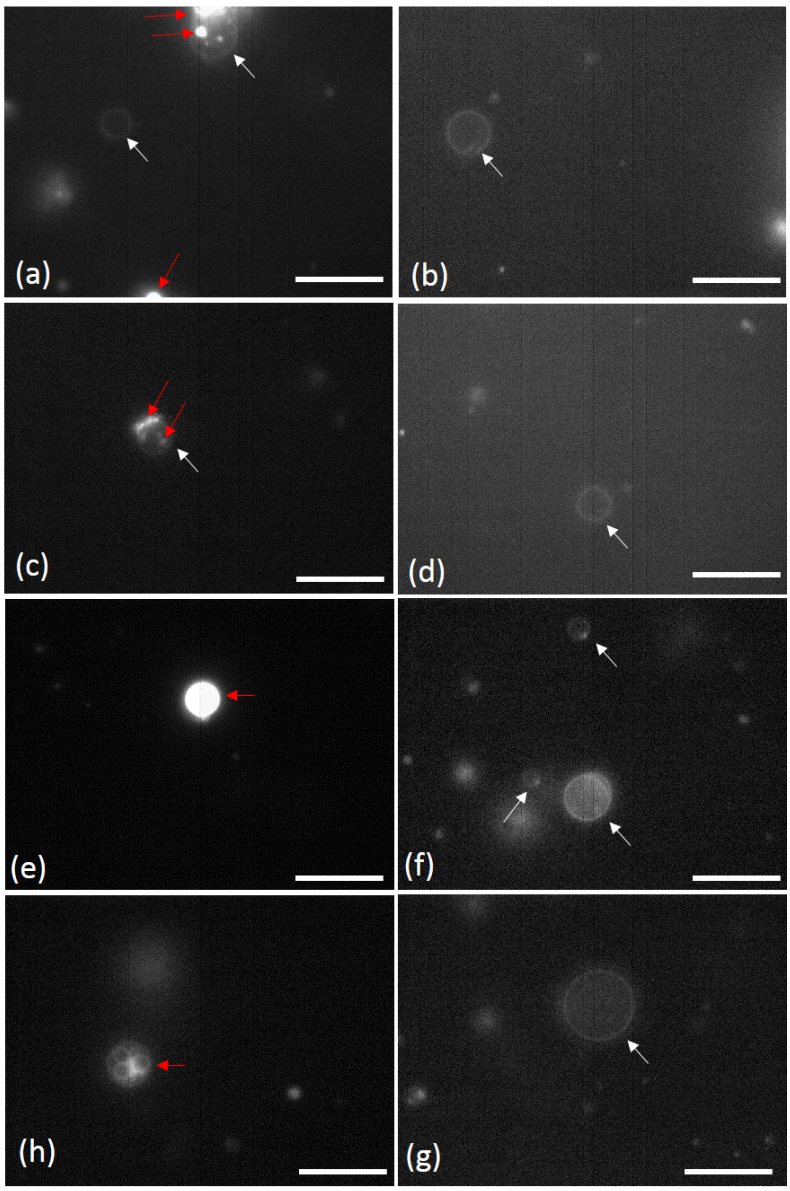

Figure 4.3
Giant vesicles with NBD-PE fluorophore present in the membrane at 0.25% weight fraction. (a)-(d) shows one preparation and (e)-(g) a second which is the same preparation used in the assay shown in Figure 4.4. Although each set of images used the same fluorescent input and camera settings (100 ms and full gain), signals rapidly bleach and are captured as they do so. Presumed unilamellar giant vesicles are identified with white arrows, anomalies are noted in red. Some objects such as in (a) and (c) appear generally unilamellar but contain highly-fluorescent regions noted. Some objects such as in (e) are extremely bright and do not bleach rapidly; they are thought to consist of oil droplets heavily laden with fluorescent lipid. Although many objects exhibit clean unilamellar structures; most appear to be a hybrid including some extra structures such as (a) and (c). A small number of apparently multivesicular objects such as that in (h) are also seen. Both preparations are anionic at 0.2 mg/ml of lipid as standard. First set formed in 20 mM KCl 10 mM MOPS 0.1 mM $MgCl_2$ pH 8.0 and the second without $MgCl_2$ (no significant differences were observed between these preparations). Images taken with Thorlabs 340M-GE camera with "Bodipy" cube fluorescent spectral parameters (as listed in the appendix) and variable camera settings (typically 100ms full gain, with 100% arclamp fluorescent intensity). Images have been adjusted to correct for an artifact in the camera that leads one half to be of lower

the lipid suspended that have passed through into a giant vesicle structure). In fact the quenching assay, shown in Figure 4.4, suggested that around 2/3 of lipids were external compared to 1/3 internal (however the trace is not completely parallel with the axis, so it is asymptotic to a lower point). Based on viewing of the samples under the microscope, presented in Figure 4.3, this result would be expected to be skewed by the presence of highly fluorescent structures as seen in Figure 4.3 that are presumed to be contaminating oil droplets highly-loaded with fluorescent lipids. These structures bleached under fluorescent illumination only very slowly, in marked contrast to other objects imaged in Figure 4.3 which bleached within seconds. Such structures could be speculated to contain freely-moving lipid molecules that may interact at the surface of the droplet with the aqueous quenching compound; this could perhaps explain the extremely slow

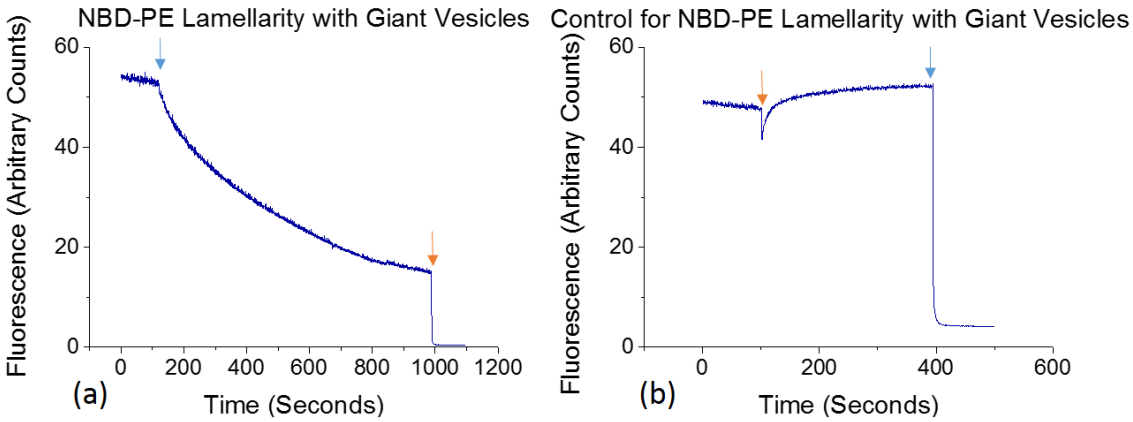

Figure 4.4

Giant vesicle lamellarity bulk test. Anionic giant vesicles formed at 0.2 mg/ml as standard in 20 mM KCl 10 mM MOPs pH 8.0; 1.4 ml of the 3 ml formed in this prep used for each of the two tests and present at the start of the experiment. In each case the blue arrow indicates the addition of 50 µl of 1 M sodium hydrosulfite to the 2 ml reaction volume in the fluorimeter (including magnetic stirring), and the orange arrow the addition of 200 µl of Triton X-100 reduced (to 1% final concentration) to lyse all vesicles. Hence in (a) it can be seen that external lipid leaflets would seem to account for around 2/3 of the total fluorescence; the slow pace of this quenching and the views under the microscope in Figure 4.3 attests to the perceived unreliability of this measurement as taken in bulk. (b) is a control which shows that the addition of detergent Triton X-100 reduced does not significantly affect the fluorescence level by itself.

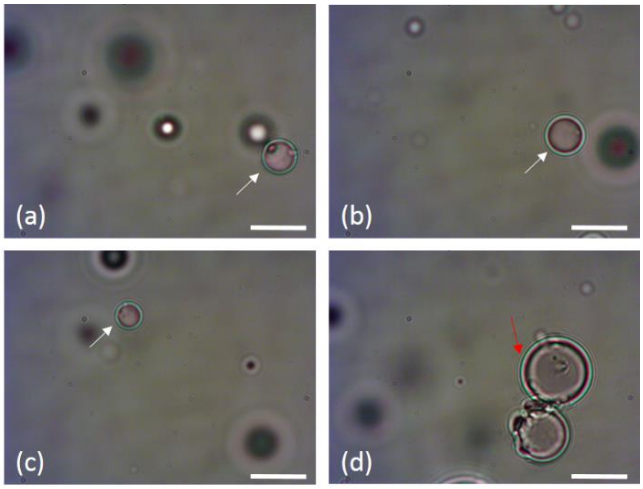

Figure 4.5
Brightfield image of lipid-stabilised emulsion for giant vesicle preparation (water-in-oil). Although most objects appear as expected, occasionally some objects such as that seen in (d) are seen which might be expected to become multivesicular when passed through the second monolayer. Images taken with Toupcam UCMOS05100KPA camera with variable settings (typically 100ms no gain). Scale bars are 10 μm.

quenching rate seen in Figure 4.4. Although care was taken to minimise the presence of such droplets in the removal of aqueous samples through the oil layer, in practice some were always seen. It is currently assumed that some of the structures identified in Figure 4.3 are indeed unilamellar; this is suggested by the format of the fluorescence under the microscope and is expected based on past literature.

Whilst initially it was thought that to properly interpret this quenching assay it might be necessary to perform this or another similar (several others are available [174], [175]) lamellarity assay under the microscope by use of buffer exchange and careful control of illumination conditions, Chiba et al. have recently (July 2014 [169]) demonstrated a relatively simple analysis based on comparison of theoretical calculations to fluorescence intensity as viewed in the microscope (there are also precedents to this analysis such as Akashi et al. [176]). Interestingly, it was found that under Chiba et al.'s (slightly differing but highly similar in essence) emulsion preparation conditions that most vesicles formed were unilamellar irrespective of the lipid concentration. Application of Chiba et al.'s methodology of image analysis may be expected to yield further

understanding of the lamellarity of the system; based on the findings of this and various past studies into giant vesicles by the emulsion method [139], [140], and the data shown here, it is expected that some fraction of the giant vesicle population is unilamellar (and some forms more complex structures). Viewing of the emulsion phase demonstrates that occasionally objects are seen which appear to have more than one emulsion droplet associated together; we may speculate that on occasion such objects pass through the oil phase and establish a second lipid monolayer to form a multivesicular structure consisting of more than one aqueous droplet. Such an object is seen in the emulsion images shown in Figure 4.5 and can be compared to the apparently multivesicular object seen in Figure 4.3h.

4.3 Charge-Based Lipid Fusion Studies

Having established the formation of GUVs containing freely-moving functionalised gold nanospheres, we turn ourselves to the issue of the insertion of functional F_1F_O into the bilayer.

4.3.1 Assessment of Fusion by Content Mixing

Assessments of fusion involving the transfer of lipids can conflate total fusion events with hemifusion or contact events, in which lipid bilayer leaflets may be exchanged but full fusion resulting in content mixing does not occur. In order to give an unambiguous assessment of content mixing, and hence the formation of a new and stable vesicle object, several assays have been developed in the literature involving the entrapment of compounds into the inner volume of vesicles that, when mixed, demonstrate a measurable change in fluorescent signal. These

include the interaction of terbium with dipicholinic acid (Tb/DPA assay) [177], 1-aminonaphthalene-3,6,8-trisulfonic acid with N,N'-p-xylylenebis (pyridinium bromide) (ANTS/DPX assay) [178], luciferase with ATP [179], as well as many others. Initial tests with Tb/DPA were found to give misleading false-positive artifacts that were thought to be related to the use of oppositely charged lipids, whereas much of the earlier development of such assays utilised mutually anionic vesicles induced to fuse by the addition of divalent cations (particularly Ca^{2+}) which would hence induce different interactions with the lipids. One method that had been previously demonstrated to be compatible with oppositely charged lipid mixtures is the interaction of calcein with cobalt [136], [137] and that is the assay here demonstrated. This assay furthermore has the advantage of being compatible with microscopy (Tb/DPA requiring an ultraviolet excitation).

The fluorescence of calcein may be quenched by the addition of cobalt (Co^{2+}), which forms a non-fluorescent complex – however the chelation of cobalt by EDTA is a stronger interaction; hence upon mixing of EDTA with the calcein-cobalt complex, cobalt will preferentially complex with EDTA – and calcein will then be free and exhibit its previously-quenched fluorescence. Due to their charge interactions, EDTA may be stably entrapped in negatively charged lipid vesicles and calcein-cobalt in positively charged lipid vesicles. The removal of external compounds allows the internal signal to be seen clearly and the addition of cobalt externally (in concentrations low enough not to cause artifact-inducing interaction with negatively-charged lipids) will ensure any calcein that might be released due to vesicle bursting is effectively quenched.

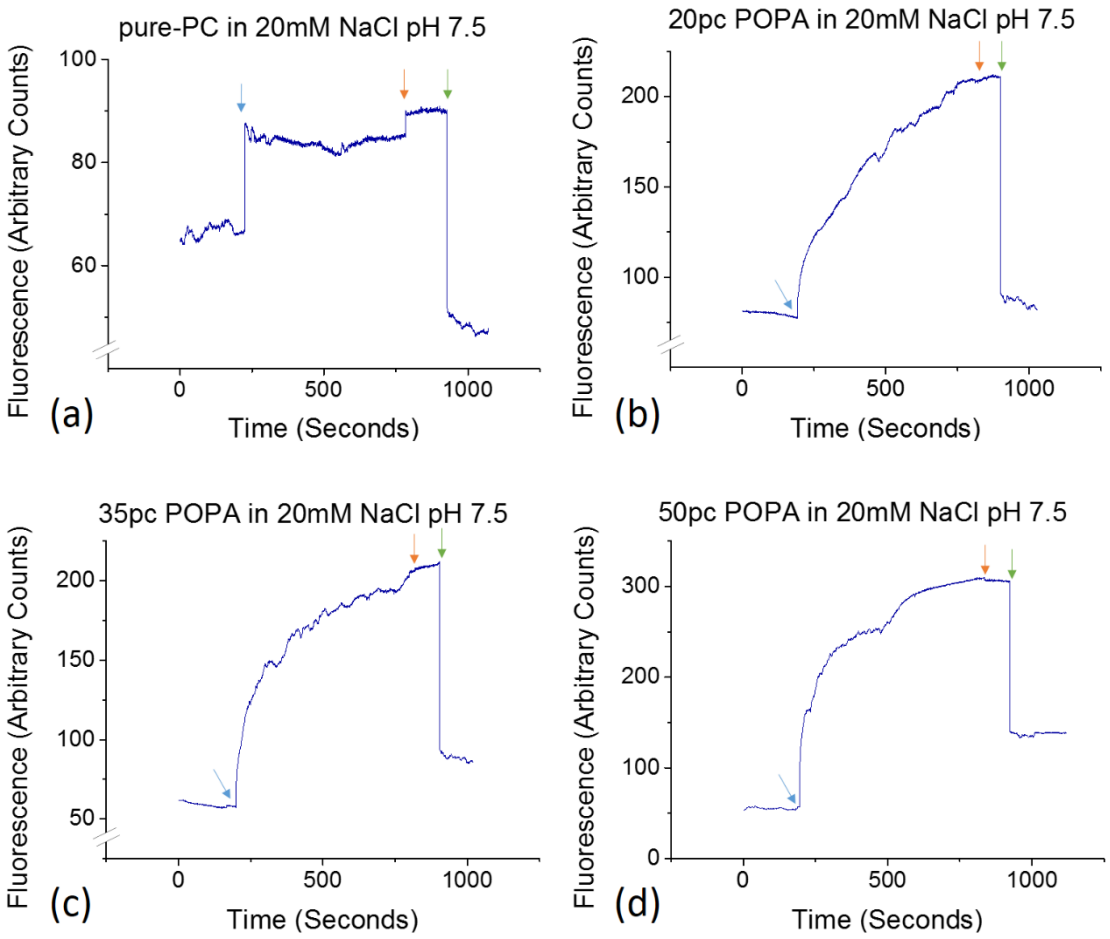

Figure 4.6
Fusion with content mixing under cobalt-calcein assay. In each case, 10 µl of cationic liposomes (50% DOTAP) containing cobalt-calcein complex are present and the blue arrow indicates addition of 20 µl of anionic liposomes containing EDTA. Rising signal indicates fusion of objects causing chelation of cobalt by EDTA and corresponding increase in fluorescence of calcein. Since cobalt is present externally at 100 µM, rupture of vesicles and release of calcein cannot account for this signal increase. The orange arrow indicates further addition of cobalt externally to 200 µM – that the signal does not change indicates that the fluorescent signal is indeed totally internal to liposomes and the added cobalt cannot reach the free calcein. Addition of detergent Triton X-100 at the green arrow opens all vesicles and the immediate drop in fluorescent signal indicates the rapid formation of cobalt-calcein complex as the free calcein is released from vesicles. For the anionic liposomes added: (a) shows a control with 100% Soybean PC liposomes (b) 20% POPA 80% Soybean PC (c) 35% POPA 65% Soybean PC and (d) 50% POPA 50% Soybean PC when using buffer 20 mM NaCl 10 mM Tris pH 7.5.

In the experiment documented, liposomes were formed as described in section 2.7.1 with a fixed 50% DOTAP 50% Soybean PC for the cationic liposome set and a variable concentration of anionic lipids mixed with soybean PC representing 50% POPA 50% Soybean PC, 35% POPA 65% Soybean PC, 20% POPA 80%

Soybean PC, and 0% POPA 100% Soybean PC sets. Anionic liposomes, after removal of external EDTA by sephadex column, were added to the sample volume in which cationic liposomes (washed of external calcein by ultracentrifugation) were present with an excess of external cobalt (100 μM). An increasing signal upon addition of anionic liposomes demonstrates fusion and mixing of calcein-cobalt complex (internal to cationic liposomes) with EDTA (internal to anionic liposomes); as a control the addition of further external cobalt from 100 μM to 200 μM final concentration demonstrates that the increasing fluorescent observed is indeed internal to liposomes, since no significant change to the fluorescent level is seen (which would occur if the free calcein were external and thus able to be affected by the addition of external cobalt). The addition of Triton X-100 to 1% final concentration (v/v) lyses all vesicles and the immediate reduction of fluorescent intensity to at or around the starting level furthermore affirms that all fluorescence previously above this level was internal to liposomes and that external cobalt is more than sufficient to rapidly quench any leaked calcein. As expected, no fusion is indicated on the neutral PC liposome sample – however it should be noted that high levels of turbidity in this sample (affirmed on a repeat) could indicate improper formation of liposomes consisting purely of zwitterionic lipids from Soybean PC in the presence of EDTA without anionic POPA. There was insufficient time to further investigate entrapment of EDTA by these vesicles; that content mixing occurs in all anionic cases is clear and unambiguous and so the non-anionic control was not considered necessary and is included here as a point of interest. Since levels of entrapped EDTA in vesicles were not investigated, it is not immediately clear

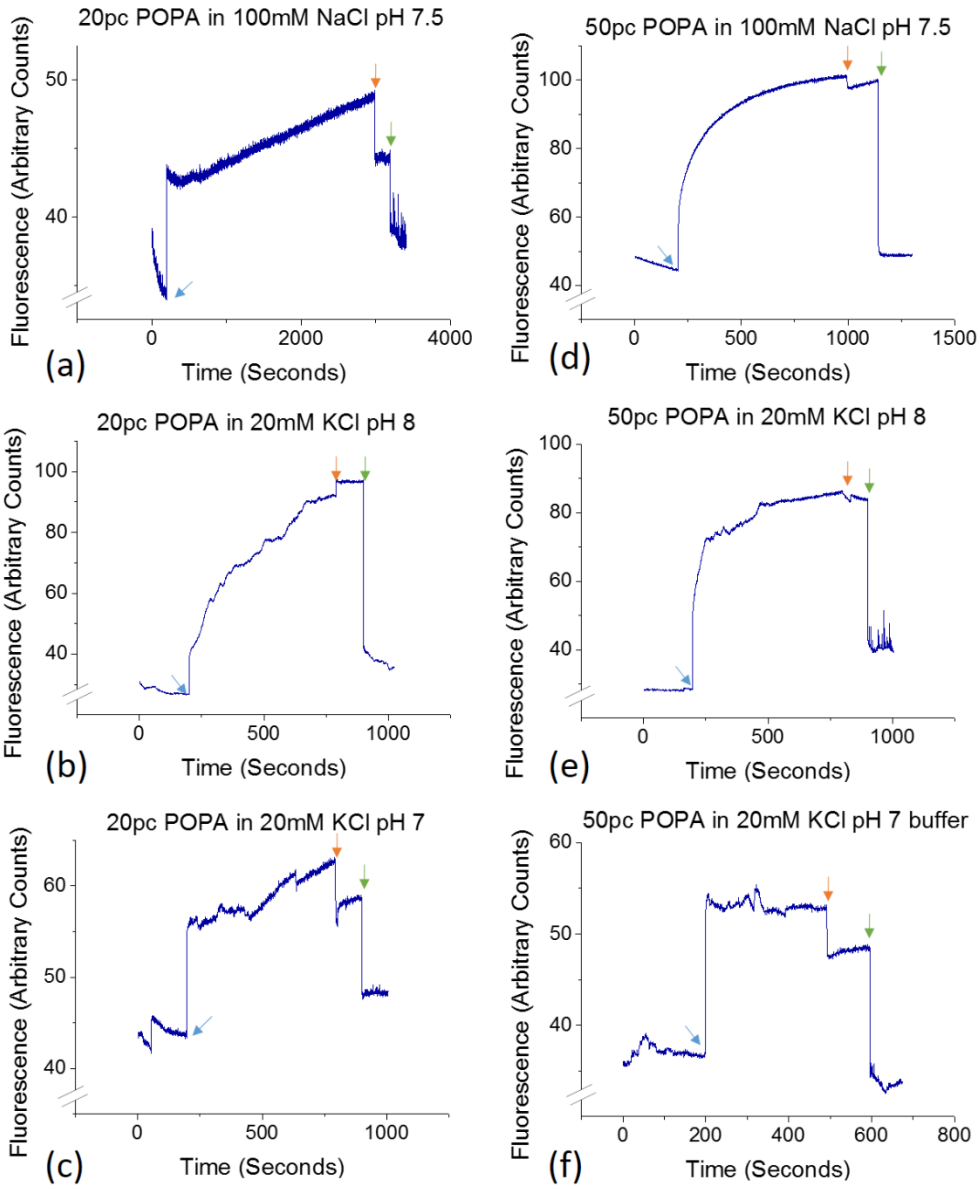

Figure 4.7

Comparative traces of fusion under differing buffer, salt, and pH conditions. In all cases 10 µl of cationic liposomes and 100 µM cobalt are present at the start of the experiment and the blue arrow indicates the addition of 20 µl of the anionic liposomes (which are either 20% POPA 80% Soybean PC liposomes or 50% POPA 50% Soybean PC liposomes as indicated). The orange arrow indicates addition of further cobalt to 200 µM; no change in signal would affirm that the fluorescent calcein is internal to liposomes and inaccessible to external cobalt. Green arrow indicates addition of detergent Triton X-100 to lyse all vesicles; previously internal free calcein is now available to external cobalt. (a) shows 20% POPA liposomes in 100 mM NaCl 10 mM Tris pH 7.5; fusion is not seen based on this trace. (b) 20% POPA liposomes in 20 mM KCl 10 mM MOPS pH 8.0; fusion is positively identified. (c) 20% POPA liposomes in 20 mM KCl 10 mM MOPS pH 7.0; fusion is not seen. (d) 50% POPA liposomes in 100 mM NaCl 10 mM Tris pH 7.5; fusion is positively identified. (e) 50% POPA liposomes in 20 mM KCl 10 mM MOPS pH 8.0; fusion is positively identified. (f) 50% POPA liposomes in 20 mM KCl 10 mM MOPS pH 7.0; fusion is not seen. Comparison between these traces, and also with those of Figure 4.6, hence indicates that 20 mM salt and pH of 7.5 or 8 provide the more optimal conditions for fusion when compared to 100 mM salt or pH 7.0 conditions.

that higher overall signals of fluorescence seen in the 50% POPA sample can validly be interpreted as higher levels of fusion; it could simply represent higher entrapped volumes. Though equal volumes of each sample were added to the reaction chamber, their interaction with EDTA or with the sephadex column passage were not investigated (for example, by the testing of total lipid concentrations in each sample) since it was sufficient to see a positive signal of fusion. However, we can validly interpret fluorescence levels seen when equal volumes of the same anionic liposomes are added to cationic liposomes under differing buffer/salt conditions. Although the liposomes used for these tests were formed under 100 mM NaCl 10 mM Tris pH 7.5 buffer condition, as 200 nm diameter SUVs they will not be expected to be osmotically sensitive.

To compare pH/salt conditions we see the effect of otherwise equal conditions of cationic (50% DOTAP 50% Soybean PC, 10 µl) and anionic (20% POPA 80% soybean PC condition, 20 µl) liposomes and compare the final fluorescent level and the shape of the fluorescent response. This is seen in Figure 4.7. Figure 4.6b demonstrates a 20 mM NaCl 10 mM Tris pH 7.5 condition and Figure 4.7b demonstrates a 20 mM KCl 10 mM MOPS pH 8.0 condition; the latter had been developed for use with giant vesicles. Since Mg^{2+} was not compatible with the assay due to its competition with Co^{2+}, it was not possible to test the effect of this component on fusion which had commonly been utilised in giant vesicle development (discussed in Section 4.2.1). Of note however is the reduction to the point of cessation of fusion in this 20% POPA liposome condition under the buffer conditions 100 mM NaCl 10 mM Tris pH 7.5, presented in Figure 4.7a, and

also its heavy reduction (interpreted as total or near-total cessation of content mixing) in the condition 20 mM KCl 10 mM MOPS pH 7.0 shown in Figure 4.7c. Hence it is clear that by comparison of Figure 4.6b with Figure 4.7a, 20 mM salt strongly promotes fusion compared to 100 mM. From comparison of Figure 4.6b with Figure 4.7b and Figure 4.7c, we may say that pH 8 and pH 7.5 strongly promote fusion compared to pH 7. In fact, even under 50% POPA then fusion was not clearly seen with pH 7 condition (Figure 4.7f); fusion was undoubtedly seen with 50% POPA under 100 mM NaCl 10 mM Tris pH 7.5 (Figure 4.7d).

Since 20% POPA 80% Soybean PC has been developed as the preferred condition for giant vesicle formation (discussed in section 4.2.1), then it is clear that a condition of 20 mM salt at either pH 7.5 or 8 (and not 7) will promote the content mixing expected to deliver the F_1F_O from its incorporated liposome into the membrane of a giant vesicle.

Giant vesicles formed by the emulsion method I have developed and described in section 4.2 are observed to have diameters of up to 10 μm or more. Although it has been demonstrated here positively and clearly that the lipid mixtures described do indeed undergo full fusion with content mixing under the conditions described, the dynamics of fusion between a small (around 100 nm diameter) cationic protein-containing liposome and a 10 μm anionic giant vesicle could well be expected to differ from the fusion conditions demonstrated in which both cationic and anionic liposomes were formed at equal size (200 nm diameter). In order to investigate if fusion with content mixing still occurs in this case of differently-sized objects, giant vesicles were formed as described in

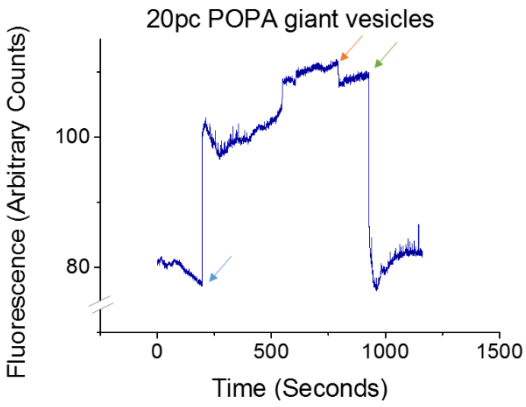

Figure 4.8
Calcein fusion test for 20% POPA giant vesicles containing 10 mM EDTA internally. 10 µl cationic liposomes and 100 µM cobalt are present at the start of the experiment. At the blue arrow giant vesicles are added to the 2 ml reaction volume; at the orange arrow cobalt is added to 200 µM; at the green arrow 200 µl of 10% Triton X-100 is added. A weak increasing signal is seen, and addition of cobalt does not see a return to the starting level - indicating fusion. The large jump on addition of giant vesicles could indicate a rapid fusion, or could be an artifact related to external EDTA.

section 2.8.1 according to the standard method, but in a buffer condition of 20 mM NaCl 10 mM Tris pH 7.5 and also containing 10 mM EDTA in the internal volume. A fluorimeter trace taken using the whole of one preparation of giant vesicles is seen in Figure 4.8, which gives a tentative appearance indeed of fusion though it is a weak signal not much above the noise level; the addition of the extra cobalt to 200 µM measurably reduces the fluorescence but not to the starting level, implying some of the rising signal seen is indeed internal. Since the volume scales as the cube of the radius and the surface area (and hence lipid number) scales as the square, it may be that fewer fusion events can occur with respect to equal volumes of calcein compared with what is seen in Figure 4.6 (any one fusion event will involve calcein becoming highly diluted into the much larger giant vesicle volume). In this case viewing under the microscope gives us a substantially clearer view of what is happening than the use of the fluorimeter. By first diluting a small volume of the cationic liposomes preparation previously used 5× with water to create an external buffer condition of 20 mM NaCl 2 mM Tris pH 7.5, 100 µM cobalt chloride was added similarly to the previous fluorimeter tests. An equal volume of the giant vesicles (also with 100 µM added

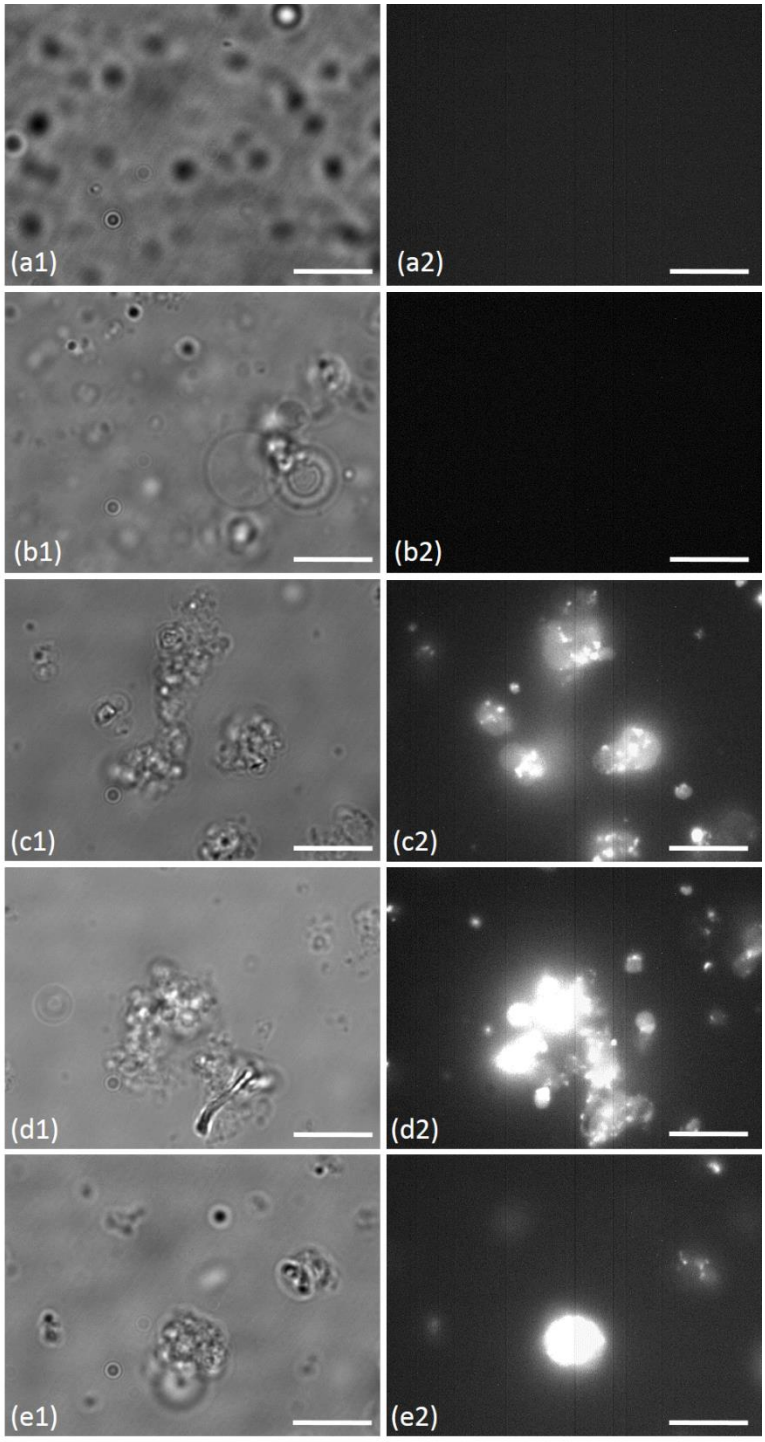

Figure 4.9
Fusion with content mixing under the microscope. All fluorescent images (a2-e2) taken under equal fluorescent illumination and camera settings (200 ms full gain, with 3% arclamp fluorescent intensity) on Thorlabs 340M-GE camera with "Bodipy" cube fluorescent spectral parameters (as listed in the appendix), and have been adjusted to correct for an artifact in the camera that leads one half of the image to be of lower brightness. (a1-e1) the corresponding field of view in brightfield illumination. (a) cationic liposomes with cobalt-calcein (note background level). (b) anionic giant vesicles loaded with EDTA internally. There is no fluorescence at all, hence no background level. (c-e) the result when the two are mixed in equal volumes; clumping of objects is clearly seen in brightfield views (c1-e1) and clear signal is seen in fluorescent views (c2-e2) that was not present in either of (a2, b2). Fusion with content mixing results in highly-fluorescent calcein due to the chelation of cobalt by EDTA internal to giant vesicles. It is clear by comparing brightfield and fluorescent traces that such fluorescence is internal. Performed in 20 mM NaCl 10 mM Tris pH 7.5 with 100 μm cobalt externally. Scale bars are 10 μm.

external cobalt) was then added and mixed and viewed under the fluorescent microscope. The results are clear and striking and shown in Figure 4.9.

All images are shown with equal epifluorescent illumination intensity and equal camera settings of exposure and gain; firstly we establish that both the cationic liposomes and giant vesicles show no fluorescence under these conditions. Upon mixing and viewing, we observe two clear phenomena; one is the aggregation of giant vesicles into large clumps and the second is that these clumps exhibit a clear internal fluorescent signal. Clumping phenomena clearly relate to the mutual attraction of cationic and anionic vesicles for more than one object at a time; these presumably could be mediated by varying relative concentrations of each – this has relevance for the final design of the rotation experiment as described in Chapter 5. That content mixing occurs is clear by the high levels of internal fluorescence seen which can only occur upon the mixing of calcein-cobalt with EDTA to generate free calcein internal to giant vesicles. Such fluorescence was seen to be long-lived and clusters of cationic liposomes and anionic giant vesicles were stable.

Many such objects could be easily found within the sample volume under the microscope. Bursting open of such fused objects would be accompanied by an immediate drop in the fluorescence as free calcein was re-complexed with external cobalt; although this was not observed the studies performed were not comprehensive enough to rule this outcome out and past studies by other researchers using high-speed cameras to view fusion events suggest that such bursting is not an uncommon outcome, depending on lipid compositions [113]. It

is straightforward to compare brightfield images in Figure 4.9 to confirm that all fluorescence observed is internal to giant vesicles.

Based on these results we expect to see the same fusion with content mixing to occur between cationic proteoliposomes and anionic giant vesicles at these lipid mixture levels of 50% DOTAP 50% Soybean PC and 20% POPA 80% Soybean PC. We should take note that buffer conditions in which salt is at 20 mM and pH is at 7.5 or 8 have been clearly demonstrated to lead to content mixing fusion, but based on liposome studies presented we may expect to see much more limited fusion (if any) at 100 mM salt or at pH 7 with these lipid compositions. This will be of interest in the design of final experimental conditions.

4.3.2 Selection of the Fusogenic Lipid Complementary Mixtures

The selection of POPA as an anionic lipid was largely due to the previous work of a DPhil student within the research group Dr Wei Meng Ho and his work investigating this lipid for Ca^{2+}-induced fusion, meaning it was already present in the laboratory. The use of DOTAP as a complementary cationic lipid was based on comparison of its structure with that of PC and its prior use by others with liposome-based fusion studies [111], though no reference to its prior complementation with POPA has been found.

Since both lipids are charged (and DOTAP is totally synthetic), some effect on protein function was always to be expected and this has been explored in Chapter 3 for the case of DOTAP. Again the choice of DOTAP for the protein delivery vehicle and POPA for the larger giant vesicle or extruded-liposome object was also fairly arbitrary and could have been approached the other way around. A

smaller concentration of charged lipids has typically been used for the giant vesicle and a higher concentration for the proteoliposome. There are several reasons for this. Since the giant vesicle is larger, it was speculated that a lower overall percentage of charged lipid would be needed for a marked fusion effect from the beginning – before content mixing had actually been observed. Secondly it was speculated that since the giant vesicle, post-fusion with a relatively small proteoliposome, would effectively dilute the charged lipids of the proteoliposome into its larger surface area the protein might well prove more stable and functional in such an environment than has been observed in the case of cationic proteoliposomes with a high (50%) amount of charged lipids. This has not been much explored. Finally, and perhaps most practically, 50% POPA giant vesicles formed with lower yield than 20% POPA giant vesicles and conditions could not be found in which to form a pellet to concentrate the 50% POPA giant vesicle sample – hence it was more difficult to handle and characterise such highly-charged giant vesicles.

Certainly it is expected that further optimisation of these lipids could yield improvements both in the rate of fusion and in the stability of F_1F_O. What is clear is that the expected fusion occurs with these mixtures; and we have already shown in Chapter 3 that F_1F_O is functional in the cationic mixture used for delivery.

4.3.3 Fusion Observed via Exchange of Fluorescent Bilayer Leaflets

The transfer of fluorescently-conjugated lipid from a cationic liposome or proteoliposome to a previously non-fluorescent anionic giant vesicle has been

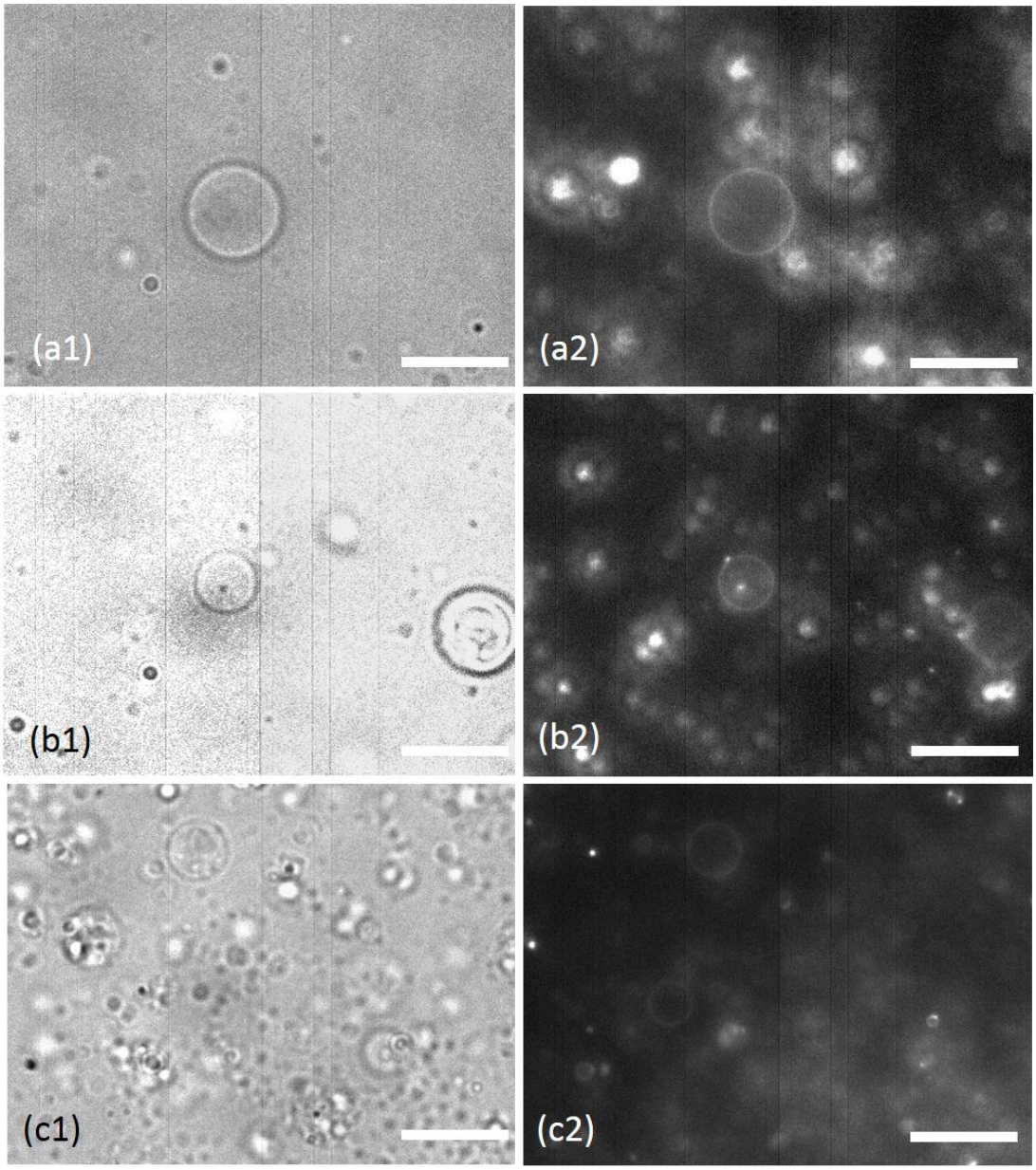

Figure 4.10

Fusion observed by mixing of bilayer leaflets. Anionic giant vesicles, identified in bright field images (a1-c1), contain no fluorophores upon formation. Cationic proteoliposomes, bound to the surface (this is described in Chapter 5) contain 0.25% weight fraction fluorescent Bodipy-cholesteryl; upon incubation fluorescent cholesterol is transferred to the giant vesicles – this is seen in the corresponding fluorescent images (a2-c2). Defocussed fluorescence from surface-bound proteoliposomes is also seen. This has been observed many times; images (a,b) from one preparation and (c) from a second; both formed under earlier conditions of 0.4 mg/ml lipid (though actual concentration most likely lower; see discussion on giant vesicle formation conditions) with 20% POPA under 20 mM KCl 10 mM MOPS 0.1 mM $MgCl_2$ pH 8.0 including 10% glycerol (this has also been observed without glycerol). Images taken with Thorlabs 340M-GE camera; images (a2-c2) with "Bodipy" cube fluorescent spectral parameters (as listed in the appendix) and fixed camera settings (100 ms and full gain, with 100% arclamp fluorescent intensity). Images have been adjusted to correct for an artifact in the camera that leads one half of the image to be of lower brightness Scale bars are 10 μm.

observed many times. This observation was made prior to the demonstration of full content mixing outlined in section 4.3.1. Since the transfer of lipid leaflets could occur in hemifusion, or even a contact event which results in later separation of the two vesicle objects, such demonstrations offer less clear demonstrations for fully functional F_1F_O delivery to a giant vesicle; but, nevertheless, when combined with demonstrations of content mixing were often studied as an indicative guide that fusion events had taken place. This is also outlined in Chapter 5, where such transfer of lipid observed under the fluorescence microscope was used to assess the conditions under which mixing of bound proteoliposomes at a surface and free giant vesicles promoted this lipid transfer and so, it is inferred, promoted the fusion with content mixing of giant vesicles to proteoliposomes. Indeed, such tests provided the first indications that fusion was dependent on buffer conditions, which has been clearly demonstrated by content mixing assays in section 4.3.1.

Figure 4.10 demonstrates this effect; cationic proteoliposomes which contain cholesteryl-Bodipy fluorophore incorporated into the bilayer are first bound to a surface (see section 5.3.1). Non-fluorescent anionic giant vesicles are then flowed into the sample volume and fuse at the surface, observed by the transfer of fluorescent lipid to the giant vesicles as seen. This fluorescent signal bleached rapidly but was just observable. As stated it has been seen many times under many conditions and was not generally seen when 100% Soybean PC liposomes/proteoliposomes were used (only in one single case was this observed out of many fields of view observed – perhaps resulting from contact without

fusion, but this was not studied further or in much detail). Given more time, the calcein with content mixing study could be tested with proteoliposomes at a surface.

4.3.4 Functional Protein Delivery by Fusion

In one method to demonstrate that functional protein can be delivered from one vesicle object to another, larger anionic liposomes (800 nm extrusion) are tested with smaller cationic proteoliposomes (100 nm) or equivalent neutral proteoliposomes as a control. The benefit in this case of using a larger 800 nm extrusion for anionic liposomes is that they can be separated easily by table-top centrifugation. 100 nm proteoliposomes are not pelleted by such low-speed centrifugation, requiring ultracentrifugation and long run-times to form a pellet. Longstanding experience shows that 800 nm extruded liposomes are stable to repeated centrifugations, though experience shows anionic 800 nm liposomes require longer run-times to ensure firm pelleting without significant loss of pellet size on repeated centrifugations when compared to neutral 100% soybean PC liposomes, presumably due to charge repulsion.

Although the use of 100% Soybean PC proteoliposomes as a control ostensibly allows us to compare like-for-like addition of fusogenic to non-fusogenic proteoliposomes, it has been discussed in Chapter 3 that equal volumes are not found to exhibit equal ACMA quenching particularly when measured more than 12 hours after protein insertion. Though, it is interesting to note, that by using equal volumes then this could be considered as a methodology to place our

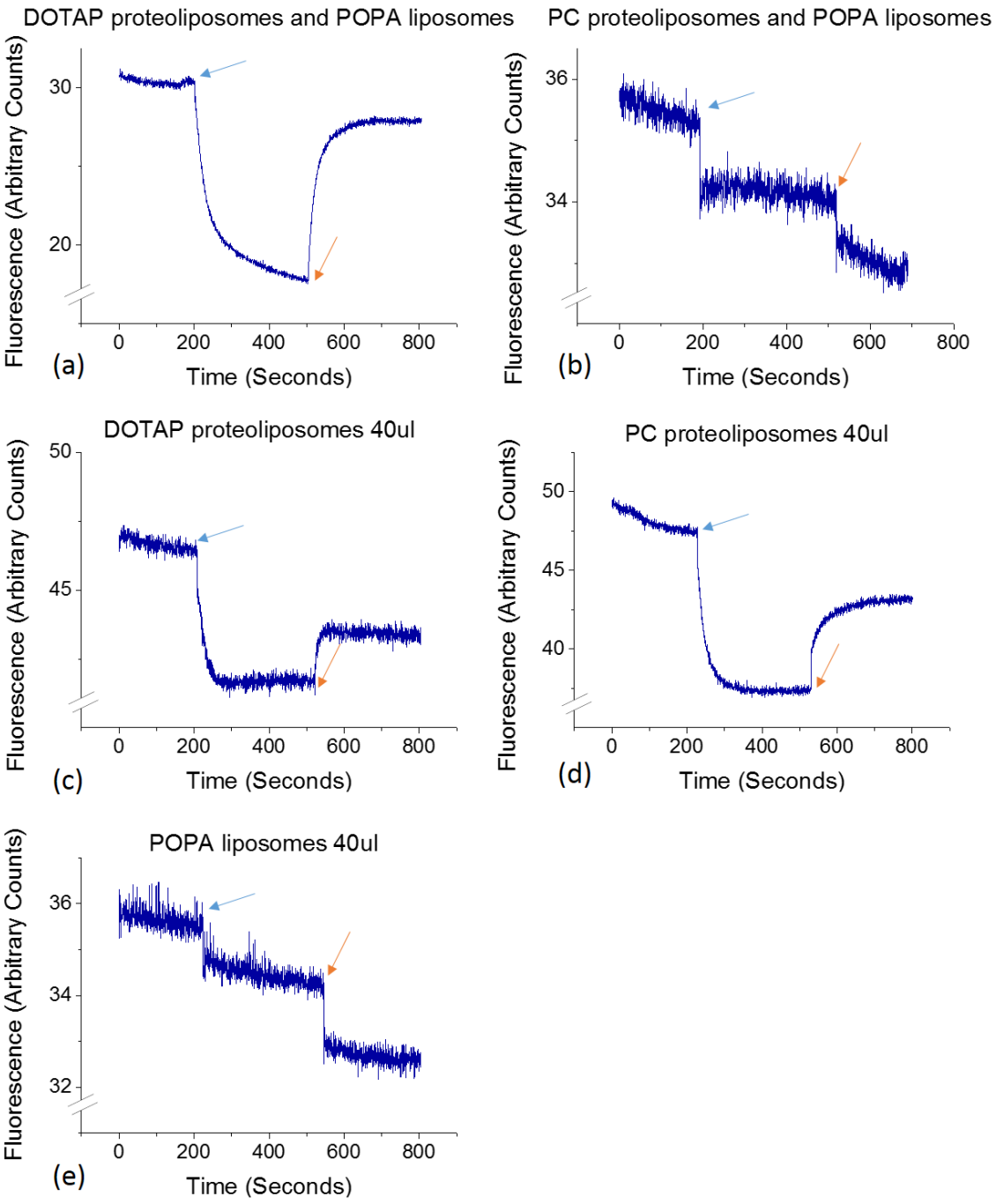

Figure 4.11

ACMA quenching on fusion test. In both charts the blue arrow indicates when ATP is added and the orange arrow indicates FCCP addition, decoupling the proton-motive force. Anionic 20% POPA 80% Soybean PC 800 nm extruded liposomes are mixed with equal volumes of (a) 100 nm cationic 50% DOTAP 50% Soybean PC or (b) neutral 100% Soybean PC proteoliposomes, incubated and then larger objects are separated by centrifugation (unfused proteoliposomes remain in solution). A clear signal of protein function is seen in the fusogenic case (a) that is not present in the non-fusogenic case (b). Charts (c) and (d) show the positive ACMA quenching of the fusogenic and non-fusogenic proteoliposomes respectively, and (e) shows the anionic liposomes on their own indicating no ACMA quenching prior to incubation of proteoliposomes.

intended test at a potential disadvantage; the observation of success under such conditions could then be considered doubly-validating.

It was under such conditions that proton pumping activity in what we may term a post-fusion product was first tested; 100 µl of anionic (20% POPA 80% Soybean PC) 800 nm liposomes were incubated with 300 µl of cationic (50% DOTAP 50% Soybean PC) proteoliposomes or neutral (100% Soybean PC) proteoliposomes (formed 24 hrs previously and left at room temperature) and separated by centrifugation; results are presented in Figure 4.11.

To clarify the conditions used: liposomes and proteoliposomes were formed in the standard manner described in section 2.6.1, though with a 100 mM KCl 50 mM MOPS 0.5 mM $MgCl_2$ pH 8 buffer. Liposome mixtures were incubated together for 1 hr and then subjected to centrifugation; 16 000 g 10 mins 15 °C forms a pellet of 800 nm liposomes. The pellet was resuspended in 1 ml of buffer and centrifuged a second time and resuspended in 100 µl. 40 µl of that sample was then placed in the fluorimeter (see Figure 4.11). This test was performed in 100 mM KCl; at the point these tests had been performed it was not known that 20 mM KCl provided a more optimal condition for fusion (demonstrated in section 4.3.1) and 100 mM KCl was chosen for optimal protein function. That a clear positive signal is still seen is nevertheless encouraging and it seems likely that at 20 mM a smaller amount of proteoliposomes could have been added to achieve the same effect.

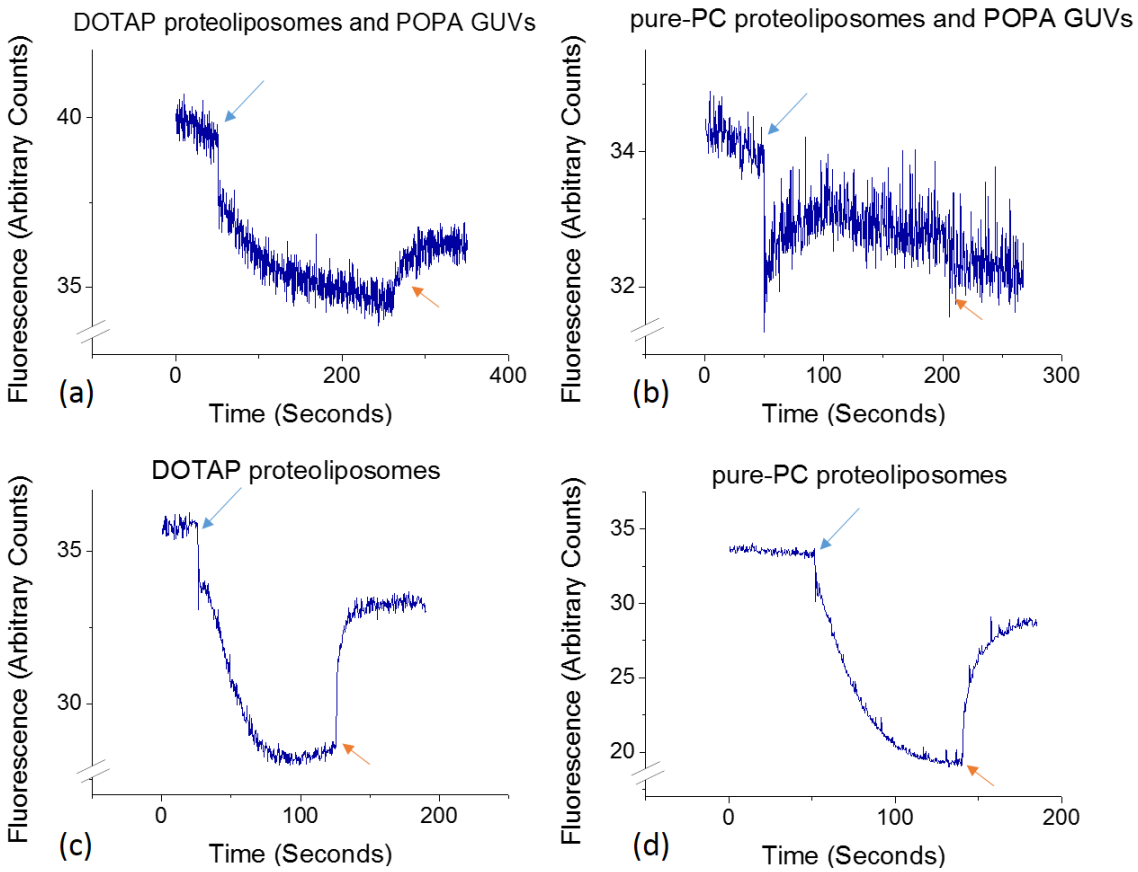

Figure 4.12
Comparative ACMA quenching cationic and neutral proteoliposomes mixed with 20% POPA 80% Soybean PC anionic giant vesicles. Post-fusion and separation by centrifugation, (a) shows a clear signal of ACMA quenching for the cationic case whereas (b) does not. Clarifying the initial proteoliposomes input, (c) shows 60 µl of cationic 50% DOTAP 50% Soybean PC proteoliposomes, (d) shows 30 µl of neutral 100% Soybean PC proteoliposomes.

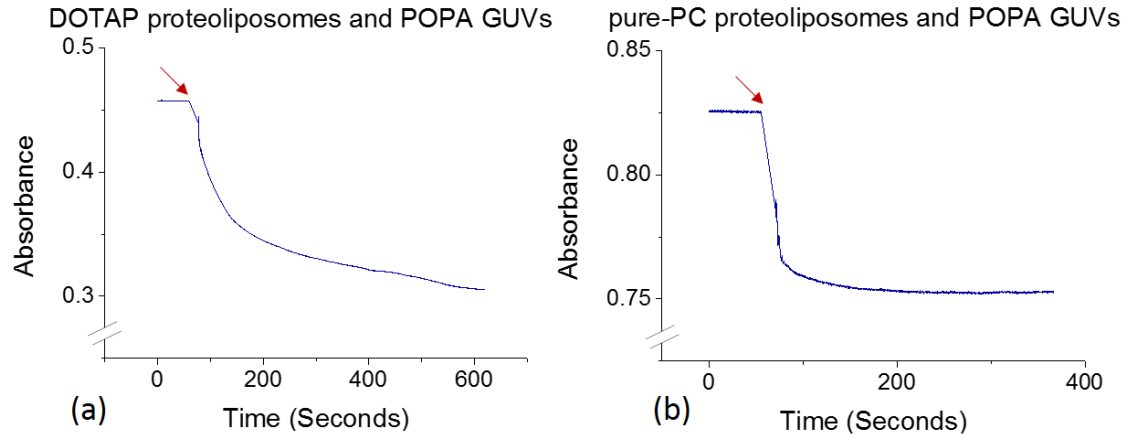

Figure 4.13
Taking the post-fusion samples assayed in Figure 4.12 to test ATP hydrolysis activity by NADH, (a) shows ongoing hydrolysis for the cationic case (previously assayed for ACMA quenching in Figure 4.12a) whilst (b) for the neutral case does not (previously assayed for ACMA quenching in Figure 4.12b).

As can be seen, no apparent transfer of F_1F_O is observed with neutral proteoliposomes whereas a clear signal is seen in the cationic case. For equal volumes of each proteoliposome tested, cationic proteoliposomes show significantly weaker ACMA quenching. However, equal volumes were used for both the test and control. Anionic liposomes on their own show no ACMA quenching, as expected since no protein is present before the fusion takes place.

Similarly, an early ACMA study was performed with anionic GUVs separated by centrifugation; activity in the post-fusion product was then tested, showing similar results but with a weaker signal – hence I have presented both (see Figure 4.12 for this test). To clarify the conditions used for the GUV test: six anionic (20% POPA 80% Soybean PC) giant vesicle preparations of 3 ml each were concentrated by means of centrifuge and mixed together to form 140 µl total of densely-packed vesicles. One set of cationic (50% DOTAP 50% Soybean PC) proteoliposomes and one set of neutral (100% Soybean PC) proteoliposomes were prepared. Based on weaker ACMA quenching signal for cationic proteoliposomes, in this case one-fourth the amount of neutral proteoliposomes was used compared to the cationic case. 850 µl of cationic proteoliposomes were added to 70 µl of the concentrated giant vesicles and 220 µl of neutral proteoliposomes to the other 70 µl giant vesicles. These were incubated for 5 mins (subsequent studies on content mixing assure us that fusion is essentially complete in this time) and buffer (100 mM KCl 50 mM MOPS 0.5 mM $MgCl_2$ pH 8.0) was added to 1.5 ml total volume and each sample spun 16 000 g 15 mins 15 °C. All liquid was carefully removed and the pellets resuspended in 2 ml 100 mM KCl 50 mM MOPS

2 mM $MgCl_2$ pH 8.0. These were then tested in the fluorimeter (Figure 4.12), where no apparent transfer of F_1F_O is observed with neutral proteoliposomes whereas a positive signal is seen in the cationic case.

Following this, an NADH assay was also performed to assess ATPase activity on the same samples (shown in Figure 4.13). The post-fusion product as tested for ACMA quenching was placed under NADH assay conditions with ATP regenerating system in a 2 ml volume and ATP to 1 mM. 200 µl (of the 2 ml total sample of each) was added to the sample volume; the initial reduction in absorbance can most likely be interpreted as ADP present in the post-fusion product sample volume. This is then followed in the neutral proteoliposome sample as a steady levelling of the signal as no more ADP is converted back to ATP by the regenerating system – indicating no protein activity. In the cationic proteoliposome sample however a clear downward trend indicates continues conversion of ADP to ATP by the regenerating system due to its ongoing hydrolysis by F_1F_O. Based on this one could arrive at a very rough order-of-magnitude idea of the level of fusion by comparing the level of activity and, by assuming a linear response, estimate the quantity of protein present and compare to an assumed starting level present in the proteoliposomes input to the experiment to fuse with GUVs (however the F_1F_O content of cationic proteoliposomes has not been measured directly in this study, so we must assume a 100% insertion of F_1F_O from a solubilised state into cationic proteoliposomes) – in this case we can arrive at a figure of around $5x10^{-6}$ mg F_1F_O in the 200 µl volume (extrapolating back from activity levels seen in section

3.2.3), and given an assumed starting amount of 0.25mg F_1F_O (based on 850 µl proteoliposomes used, but bearing in mind only 200 µl of the 2 ml volume was used – hence one tenth) then this would represent 0.4% transfer of the starting level of F_1F_O via fusion. This is certainly expected to be an under-estimate of the transfer level based on insertion of F_1F_O into cationic proteoliposomes potentially being substantially lower than 100%, and so represents a very rough initial estimate and further work would be needed to arrive at a more confident final number and hence an efficiency of protein insertion via fusion (this number is presented more as a demonstration of a potential methodology to be investigated).

These tests have clearly shown that functional F_1F_O is present in the post-fusion product in both cases; however this does not directly show protein insertion into a new single unilamellar object. A hemi-fusion event in which proteoliposomes attach to anionic GUVs (or large extruded vesicles), perhaps with some mixing of bilayer leaflets but with separate aqueous compartments, would yield the same result. This stems from ACMA's mode of operation in which it permeates the bilayer (meaning such distinctions cannot be separated) – however, it is extremely sensitive and this is why it was utilised. These tests are presented as early attempts to demonstrate fusion with insertion of F_1F_O and are of interest to demonstrate that F_1F_O is clearly seen to be present and functional in the post-fusion environment in which charged cationic and anionic lipids are mixed.

Given these caveats, I have not further explored these tests under the now-known optimal condition of 20 mM KCl compared to 100 mM KCl used here. It is

sufficient that we have found that F_1F_O is functional in the post-fusion product and is delivered in a lipid-dependent manner. For further insights, I would speculate that alternative tests using aqueous pH-sensitive dyes (such as pyranine) within the giant vesicle volume may allow for testing of functional protein activity after fusion-based insertion (as long as an ionophore is used to dissipate $\Delta\psi$) in a manner that should be free of such potential ambiguities (although pyranine may not be sensitive enough for such studies; this is a matter of current interest). I have speculated further on this in section 6.4 on future work. However for the current work we can combine the content mixing studies, presented in section 4.3.1, with the studies presented here demonstrating F_1F_O function in a post-fusion product.

4.4 Summary and Conclusions

A strategy for the formation of giant vesicle objects with an emulsion-based method has been developed, based on antecedents in the literature, with the novel step of including gold nanospheres in the enclosed volume. Such giant vesicles are stable over at least 24 hrs and can even be frozen and thawed; an entrapped aqueous fluorophore was not seen to leak out over this period, suggesting a properly enclosed membrane that is hence expected to be properly energisable. Insertion of a fluorophore-labelled lipid has suggested that a population of objects is unilamellar, and some objects are found to be more complex multivesicular objects. Based on recent developments in the literature, it should be possible to formally identify unilamellar objects under the microscope and optimise giant vesicle formation to promote this subset over other objects.

This has not been an immediate priority as a subset of objects appear to be unilamellar, and multivesicular objects should still in principle be compatible with the proposed system – though it would decrease the probability of any one gold nanosphere coming into contact with any one F_1F_O molecule since these must occupy the same vesicular space. When functionalised gold nanospheres are incorporated into vesicles, they are readily observed to move freely within the giant vesicle volume in many cases by use of the backscatter darkfield insert which I co-developed for this purpose (described section 2.2.1).

A complementary lipid pair of POPA (anionic) and DOTAP (cationic) in a mixture with Soybean PC (neutral lipid mixture) has been used to establish charge-based lipid fusion with content mixing, which was demonstrated using the calcein-cobalt assay. Fusion has been observed between 50% DOTAP 50% Soybean PC cationic liposomes and a variety of anionic mixtures including 20%, 35%, and 50% POPA (with the remainder Soybean PC). It has been found that reduction of salt concentration from the 100 mM KCl standard (optimised for F_1F_O function) to 20 mM KCl strongly promoted fusion. It is furthermore noted that pH 7.5 and 8 conditions provided strong fusion while a pH 7 condition proved weak. It is noted that F_1F_O has been shown to be functional in a 20 mM KCl buffer condition; this was demonstrated in Chapter 3 (section 3.3.1). Fusion with content mixing between anionic giant vesicles (around 0.5 μm – 10 μm) and cationic small unilamellar extruded vesicles (200 nm) has also been shown with fluorimeter traces and, most clearly, with fluorescence microscopy using optimised conditions from the previous liposome study.

The transfer of membrane-embedded fluorescent cholesterol from the cationic proteoliposome to the anionic giant vesicle (which is formed with no associated fluorophores) is demonstrated. This clearly demonstrates mixing of the bilayer leaflets and is demonstrated as a straightforward method for the rapid observation of fusion. Since this is observed with proteoliposomes it also further reinforces that we expect the same fusion behaviour from cationic proteoliposomes as has been seen in cationic liposomes of similar size.

Further investigations were undertaken which demonstrate fusion of cationic proteoliposomes with both anionic large vesicles (800 nm extruded liposomes) and giant vesicles, with delivery of functional F_1F_O tested by the highly-sensitive ACMA quenching method. Although it is noted that this test does not exclude the possibility that proton-pumping is observed solely due to hemifusion events, the prior demonstration of full content-mixing is asserted to demonstrate that content mixing and hence delivery of functional F_1F_O to the giant vesicle is expected to occur. It is speculated that some fraction of functional protein observed after fusion could exist in a hemifused state and some fraction in a fully-inserted state; that at least some will fully insert seems clear based on content-mixing results. It is noted that, as far as the author is aware, no previous study of charge-based fusion for the transfer of transmembrane proteins from one vesicle object to another has been published. This system can be contrasted to the more complex SNARE-protein-based fusion system demonstrated recently by Nordlund et al. [107]. I have discussed methods that could further probe this protein function as future work.

It is not suggested that the lipid compositions presented here are the most optimal; simply that they do perform the required functions of fusion in which the two complementary lipid objects merge with complete mixing of bilayer leaflets and inner contents (and hence delivery of transmembrane proteins embedded in those leaflets, much as fluorescent lipid is observed to also transfer). Further exploration to increase protein stability (as discussed in Chapter 3) or to improve rates at which full fusion occurs would be expected to yield improvements in the system as outlined here.

In a few words: I have developed a giant vesicle system, with internal functionalised gold nanospheres, and I have developed a method to insert F_1F_O into this giant vesicle and retain its function without compromising the structure of the giant vesicle in the process.

Chapter 5 Building a Single-Molecule Approach at a Surface

5.1 Introduction

Having developed the basis for a gold nanoparticle entrapped in an enclosed giant lipid vesicle and a fusion-based protein delivery system, we turn ourselves to the issue of how to put this together under the microscope. First will need to be developed a system whereby the protein-giant vesicle 'post-fusion product' can be attached to a surface specifically and via the protein itself – three binding points in a roughly triangular arrangement provide a firm hold that ensures rotational motion of the protein can be observed. For this purpose his-tags present on the β-subunits of the mutant F_1F_O can be used. Alternatively biotin-tags on the α-subunit using an available dual α- and c-subunit cysteine modified mutant could be used, though such a binding would require an intermediate binding of streptavidin (or neutravidin) and was considered less preferable during development.

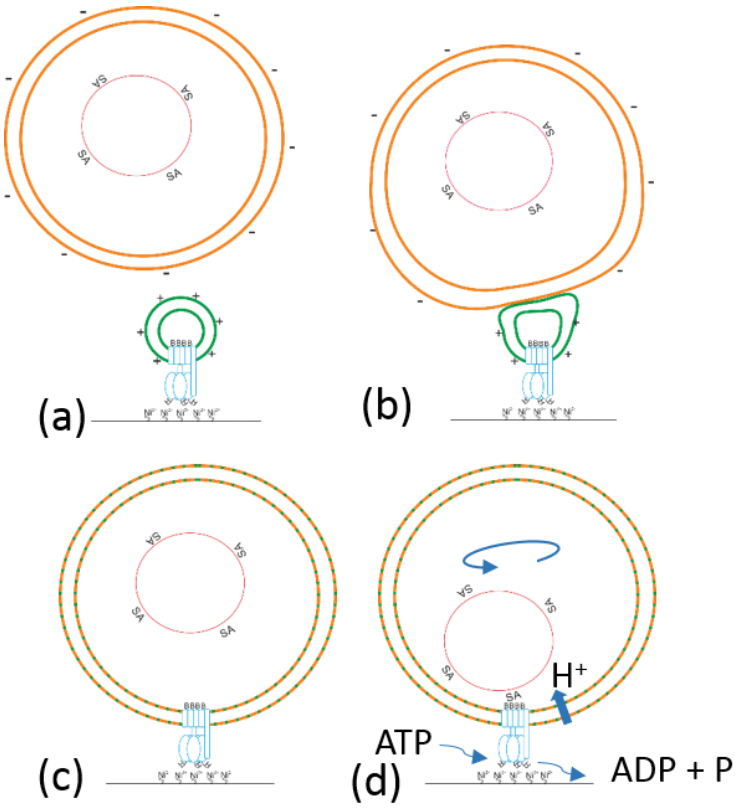

Figure 5.1
Overall schematic view of the initial single-molecule method for observation of hydrolysis-driven rotation. (a) a positively-charged fusogenic proteoliposome is bound specifically to the coverslip via the Ni^{2+}-his tag interaction and a negatively-charged fusogenic GUV loaded with a functionalised gold nanospheres is brought in proximity (b) fusion begins (c) fusion has resulted in a new unilamellar object (d) avidin-functionalised gold binds to the biotin-site on the c-subunits of the protein and ATP is introduced into the chamber; the F_1F_O hydrolyses ATP, pumps protons, and the c-ring rotates – darkfield microscopy is utilised to view this rotation as it is transmitted to the gold nanosphere. Upon establishment of observation of this rotation, observation of rotation by synthesis should be a relatively straightforward extension and approaches to this are discussed in Chapter 6.

It would presumably be possible to fuse objects first and then bind to the surface – it has been seen in Chapter 4 that fusion in this manner can lead to aggregation of multiple giant vesicles (see Figure 4.9). Presumably this can be controlled by regulating relative concentrations, however by binding the proteoliposomes to the surface first, we can straightforwardly show that this takes place via the protein; and from there a gold-loaded giant vesicle can be added and allowed to spontaneously fuse with the proteoliposome via the charge-based fusion explored

in section 4.3. This should mean that the expected binding of the streptavidin-coated gold nanoparticle, internal to the giant vesicle, to the biotinylated c-ring of the F_1F_O takes place on a protein that is also bound via his-tags to the surface. Since unbound cationic proteoliposomes will be washed out of the chamber volume prior to the entry of anionic giant vesicles, no clumping will be possible.

We might speculate that if several F_1F_O are present per proteoliposome there exists the possibility that a streptavidin-functionalised gold nanosphere could bind to more than one F_1F_O at a time and thus its rotation be impaired or impossible. Control of proteoliposome formation can ensure that on average only one protein is present per proteoliposome; this might also mean fewer chances for proteoliposomes to bind to the surface if only one protein is present rather than many, hence initially studies were undertaken with highly-protein-loaded proteoliposomes, with the expectation to be able to reduce this later once conditions for positive binding are clear.

5.2 Flow slide system

In order to allow rapid buffer change with known volumes and repeatable conditions, I have developed a flow slide system in which standard glass slides were modified with plastic tubing to allow inlet and outlet ports. Glass coverslips are attached with double-sided tape, into which a channel is cut between the inlet and outlet ports. This system allowed for a syringe to be held to the inlet pipe for ingress of buffer or sample flows, while the outlet pipe would be left open for flow to exit.

Since the chamber volume formed by double-sided tape in this design is around 10-20 µl, with an additional roughly 5 µl dead volume in the pipes either side of the chamber, 50 µl would typically be added as a standard sample volume to ensure total coverage of the chamber volume and associated pipe volumes and prevent any diffusive changes in concentration throughout the experiment. For washes with buffer, typically 150-200 µl would be flowed through the chamber within a few seconds.

For later experiments involving giant vesicle fusion to proteoliposomes on a surface, it was found that this arrangement provided too rapid a flow for giant vesicles, which could readily be seen to deform and even tear open under shear stress when at a surface. I therefore arranged a modified system based on gravity flow; the inlet port was open to the environment and could hold up to 200 µl of fluid. The outlet pipe was a long piece of tubing attached with a valve to allow it

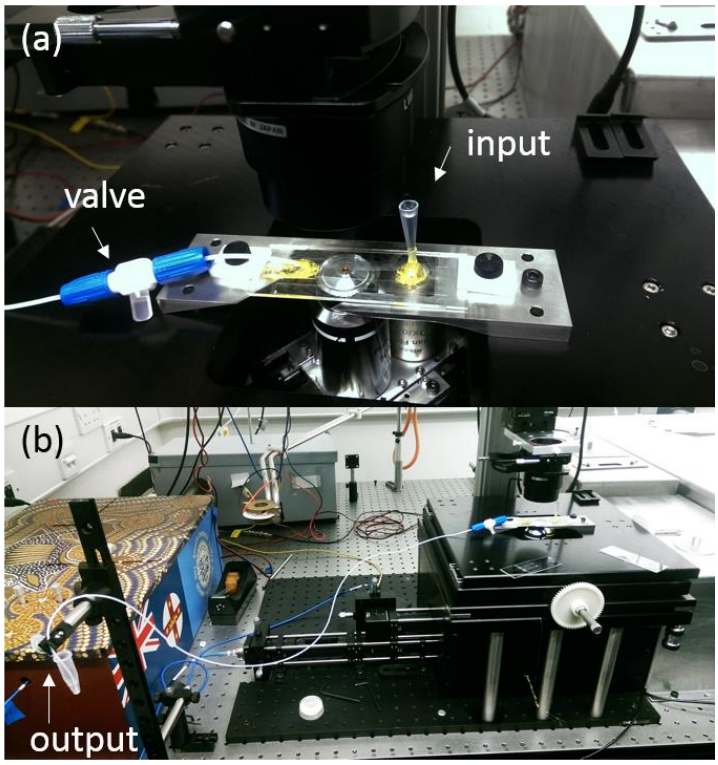

Figure 5.2
Gravity-based flow slide in place on the laser darkfield microscope. Output is height-adjustable to control flow rate; typically a rate around 10 µl per minute is used, based on the aim to minimise deformation caused to giant vesicles at the surface by flow. The input is capable of holding a 200 µl well.

to be sealed and removed as needed; hence liquid would flow from the inlet at a rate determined by the relative height of the outlet interface and the inlet interface. The flow could be monitored by viewing the motion of free non-surface attached objects through the sample volume live under the microscope. A valve was included such that flow could be stopped and restarted, which in particular allowed the flow slide system to be readily set up on the fluorescence microscope and then to be moved directly to the laser darkfield microscope robustly and without any apparent damage.

5.3 Modification of a Glass Surface for Specific Binding

For single molecule experiments performed in the research group, it is established to bind the purified F_1 to a surface via the his-tags available on the mutant utilised (on α-subunits), using a chemical modification of glass to attach nickel via an NTA-group. This methodology has existed in the literature for many years [63]. However, this was not found to be compatible with cationic proteoliposomes containing F_1F_O (for which his-tags are sited on the β-subunits), which were found to be highly apt to burst and spread on a glass surface - see Figure 5.4. Several methodologies were explored experimentally to prevent this behaviour including the use of common blocking agents to the glass surface such as bovine serum albumin (BSA), polyethylene glycol (PEG) introduced through chemical modification of the coverslip (well-established in Achillefs Kapanidis' group in Oxford biophysics [180] and originating here [181]), and variation of pH of the buffer solution. In data not presented, whilst chemical modification of glass to introduce PEG and also the use of BSA were found to work well to

prevent sticking and bursting of zwitterionic 100% Soybean PC proteoliposomes, charged cationic proteoliposomes (50% DOTAP 50% Soybean PC) were found to be much more persistent in their non-specific binding.

A solution was eventually found in commercially-available crafted-polymer polylysine-polyethylene glycol (PLL-PEG) molecules, including functionalisation with NTA for nickel binding. These bind to glass via an electrostatic interaction between the glass surface and the polylysine (coincidentally the use of polylysine as a sticking agent to glass coverslips is well established in the Berry group for the attachment of bacterial cells [182]). Further details on the chemistry of these crafted polymers can be found in the original paper describing their synthesis [141], and a schematic view is offered in Figure 5.3.

By mixing plain unfunctionalised "plain-PLL-PEG" and NTA-functionalised "PLL-PEG-NTA" polylysine crafted-polymers in the manner described in Chapter 2, we may readily arrive at a functionalised glass surface after a short incubation in a low-pH buffer. No prior preparation of glass was found to be necessary; methods in the literature including the use of plasma cleaning to enhance the inherent surface charge of glass [93] were not found to yield much improvement in binding coverage of these PLL-PEG, as measured by the reduction of non-specific binding of test objects in early comparisons (not presented); this was favoured due to the minimal preparation time. We might speculate that this behaviour could depend to some extent on the properties of the particular glass formulation of coverslips used; other brands or types were not tested. Most significantly, these "PLL-PEGs" were able to essentially eliminate non-specific binding of the cationic

proteoliposomes – perhaps related to their inherently charged nature. Data demonstrating this behaviour will be presented in the following sections.

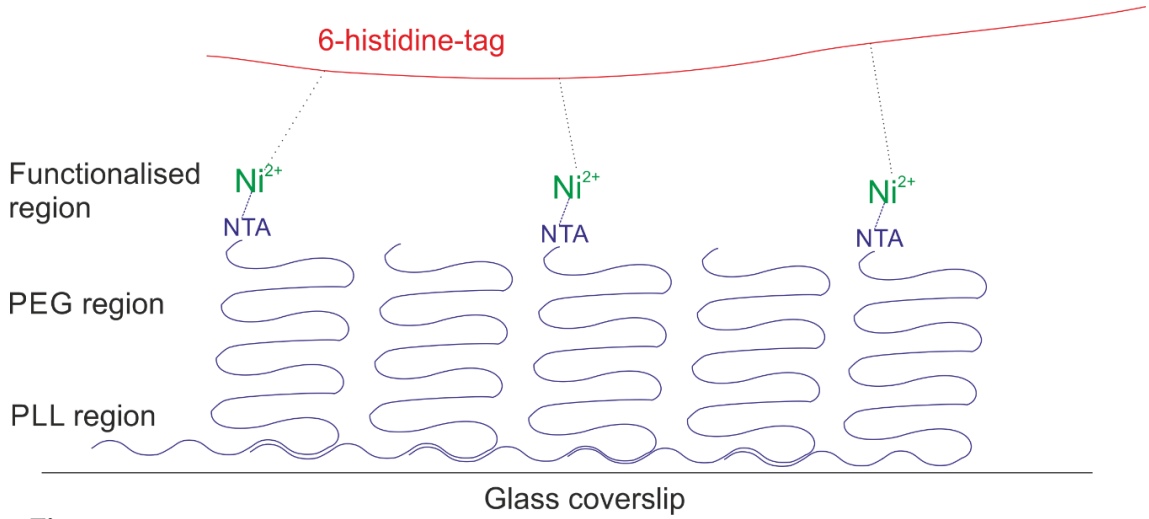

Figure 5.3
Schematic view of the PLL-PEG and PLL-PEG-NTA on a glass coverslip. Incubation with Ni^{2+} allows for binding of modified proteins via the poly-histidine moiety. This figure is based on one in the original paper describing these molecules and including more detail about their structure [141].

5.3.1 Specific Binding of Fusogenic Proteoliposomes

Having established that PLL-PEG is able to prevent non-specific binding of cationic proteoliposomes to a glass coverslip (see Figure 5.4), specific binding via the F_1F_O is of crucial interest. Using a roughly 10% mixture of functionalised PLL-PEG-NTA with 90% plain PLL-PEG as described in section 2.9.1, tunnel slides were coated. Using a set of cationic proteoliposomes with incorporated 0.5% weight fraction of cholesteryl-Bodipy fluorescent lipid, individual proteoliposomes may easily be visualised under the fluorescence microscope.

A positive binding test was performed by the addition of 10 mM $NiCl_2$ after incubation of PLL-PEG-NTA (as described in section 2.9.1); a negative test was performed by using the same conditions of PLL-PEG-NTA binding but simply by

omitting the addition of $NiCl_2$ as the final step. His-tags will hence not be expected to interact with this surface. Finally by the addition of high levels of imidazole in the positive test case then the release of proteoliposomes can be observed as a secondary control.

It is worth noting here that glycerol at a 10% concentration, often used in the storage of proteoliposomes in liquid nitrogen as a cryoprotectant (and occasionally experimented with for the storage of giant vesicles, as discussed in section 4.2.3), was found to interfere with this PLL-PEG interaction and led to high levels of non-specific binding at pH 8.0 that were subsequently reduced at pH 6.0. Glycerol had initially been used in some experiments to provide consistent buffer conditions, but was later removed when it was identified as the source of this binding. It is presumed to introduce some charge shielding effect, but this was not further investigated. Its inclusion caused inconsistent results before being identified and consequently it was always omitted from the finalised protocols as presented.

For this reason, and also for its effect on fusion (as seen in section 4.3.1), pH was initially of interest and has been investigated here under buffer conditions of 100 mM KCl, 25 mM Tris, 25 mM Bis-Tris, 0.1 mM $MgCl_2$ with four different pH conditions of 6.0, 7.0, 8.0 and 9.0 (the choice of a two-buffer system was used to span the pH range more effectively than the typical 50 mM MOPS used at pH 8.0). Under the experiment presented in Figure 5.5 (and also Figure 5.4) cationic proteoliposomes were initially formed as described in section 2.6.1 and stored in liquid nitrogen. They were then thawed and diluted into the buffer above at the

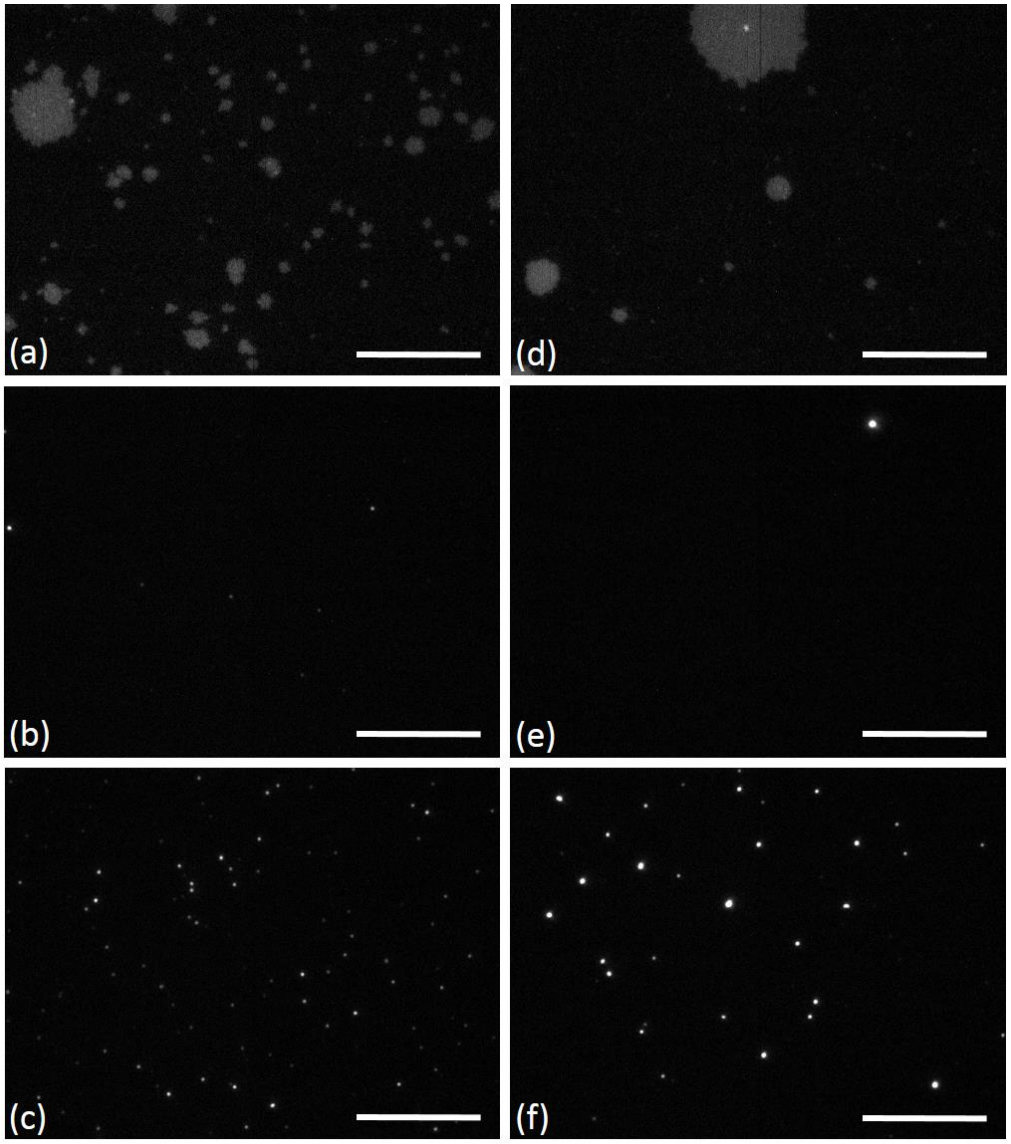

Figure 5.4

Comparison showing typical fields of view for cationic (50% DOTAP 50% Soybean PC) proteoliposome binding under the same proteoliposome dilution, fluorescent illumination, and camera settings (100 ms full gain, with 3% arclamp fluorescent intensity) for direct comparison - use Thorlabs 340M-GE camera with "Bodipy" cube fluorescent spectral parameters (as listed in the appendix). Images have been adjusted to correct for an artifact in the camera that leads one half to be of lower brightness. Using 250x dilution of proteoliposomes in 100 mM KCl 25 mM Tris 25 mM Bis-Tris 0.1 mM $MgCl_2$ and 5 mins incubation time, images (a-c) show a pH 7.0 condition and (d-f) a pH 8.0 condition. Images (a,d) show no functionalisation of the coverslip surface; bursting and spreading of proteoliposomes across the glass is readily apparent. Images (b,e) show the difference with PLL-PEG-NTA surface where the NTA has not been functionalised with Ni^{2+}, rendering this a passive surface – non-specific sticking is essentially eliminated (note that all other types of surface passivation failed to yield results as clear as this for cationic liposomes, though many were capable of this result with neutral 100% Soybean PC liposomes). Images (c,f) show specific binding of proteoliposomes where the surface has been incubated with Ni^{2+}, allowing his-tag binding of the F_1F_O to the surface. Such binding was sensitive to imidazole. Similar fields of view were obtained under pH 6.0 and 9.0 conditions; this data is summarised in Figure 5.5. Scale bars are 10 μm.

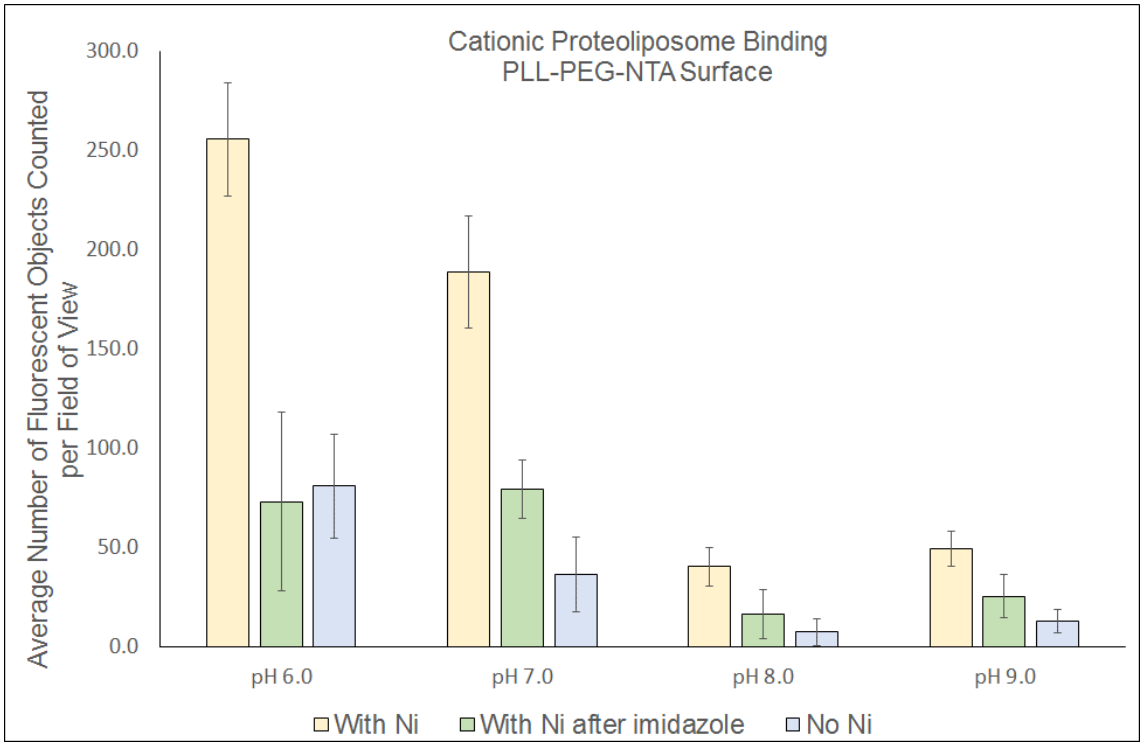

Figure 5.5
Summary of results of object-counting of fluorescent proteoliposome binding. Measured 3 repeats of each binding condition, and 20 fields of view on each repeat. Error bars indicate the average of one standard deviation over the three repeats. Compare to Figure 5.4 for original data form input to this analysis (performed in ImageJ). Yellow bar is the positive test where $NiCl_2$ is incubated with the functionalised PLL-PEG-NTA surface prior to addition of proteoliposomes. Green bar is when no $NiCl_2$ is added to the PLL-PEG-NTA surface prior to incubation with proteoliposomes. Blue bar is the same condition as the yellow bar but after incubation with 200 mM imidazole. pH 6.0 and 7.0 both offer excellent differentiation; given that protein function is expected to be more optimal at pH 7.0 then this provides the best condition as a compromise between retention of function and differentiated binding.

stated pH from 6.0-9.0 with a dilution factor of 250×. Lower dilution factors tended to give more non-specific binding, which threatened to overwhelm the clear signal of specific binding.

Slide preparations are described in section 2.9.1. The results presented in Figure 5.5 are taken from a random 20 fields of view of each condition, with three separate repeat experiments performed for each condition presented (hence an average of 60 fields of view for each condition). Although field-of-view selection was done manually, best effort was made to ensure the selection was without

bias. These 60 fields of view for each condition are then averaged to present the number of objects found by using a standard spot-counting algorithm in ImageJ (Triangle Method). The error bars indicate the average of one standard deviation for each set of images. The relative size of different spots is not considered in this analysis.

Since pH 8.0 was the standard used for optimal protein function, initial experiments had generally been performed in this condition. However while it is clear that binding occurs via the Ni-his tag interaction under pH 7 (and also pH 6), this binding is poorly distinguishable under pH 8 (and also pH 9). Note however that in section 4.3.1, pH 7.0 was found to be inhibitory for fusion compared to 7.5 or 8.0. Hence a change in buffer conditions is expected in the final experiment. Note also that a reduction in salt conditions from 100 mM to 20 mM was found in section 4.3.1 to enhance fusion conditions significantly. This was concluded after the data presented here was established and so binding tests at 20 mM salt have not been presented; possibly this may offer an even stronger condition than that shown, though we might speculate though that – since lower salt would reduce charge shielding – the opposite actually seems more likely.

Hence, based on the results presented in Figure 5.5 (and see also Figure 5.4 for typical fields of view) we can conclude that specific binding of cationic proteoliposomes via the his-tag on the β-subunits of F_1F_O has been observed.

5.3.2 Note on the Purification of F_1

Some of the following sections utilise purified mutant *E. Coli* F_1; this acted both as a positive test of rotational studies and also as a simple structural binding model

as it included both his-tags (on α) and a biotin-labelled cysteine (on γ). This F_1 was purified on occasion by the author or by Dr Ishmukhametov (or jointly). Since it was not used as frequently as F_1F_O, storage was generally up to 12 months before purification would be performed again. The method is described in section 2.4.2. The results presented in this chapter were performed on a purification with measured concentration by BCA of 1.0 mg/ml, and typical ATP hydrolysis results from this purification method returned around 15 units/mg (or 125 ATP per second per F_1) at room temperature (20-25 °C).

5.3.3 Specific Binding and Unbinding of Purified F_1 via Poly-Histidine-Tag and Nickel Interaction

Previously (Figure 5.5) it was demonstrated that the PLL-PEG-NTA surface operates for specific binding of proteoliposomes over a broad pH range, though at higher pH (8.0 and 9.0) poor differentiation is offered. In order to further investigate the response of PLL-PEG-NTA itself, the binding of purified biotin-tagged F_1 followed by avidinated quantum dots was used as a control test – this provides a clear indication of binding via the his-tag since high imidazole is shown clearly in Figure 5.5 to lead to the release of the majority of bound objects across all four pH ranges tested. An alternative would have been to directly test his-tag affinity to the surface through the use of a fluorescent protein including a his-tag; the two-step process of binding F_1 via its his-tag and then binding avidin-quantum dots via the biotin-tag on the α-subunit of F_1 was more straightforward owing to all components being readily available. Since pH became of interest in testing binding conditions, it was important to test these conditions under different pH ranges since it was not known if due to the charge-based method of

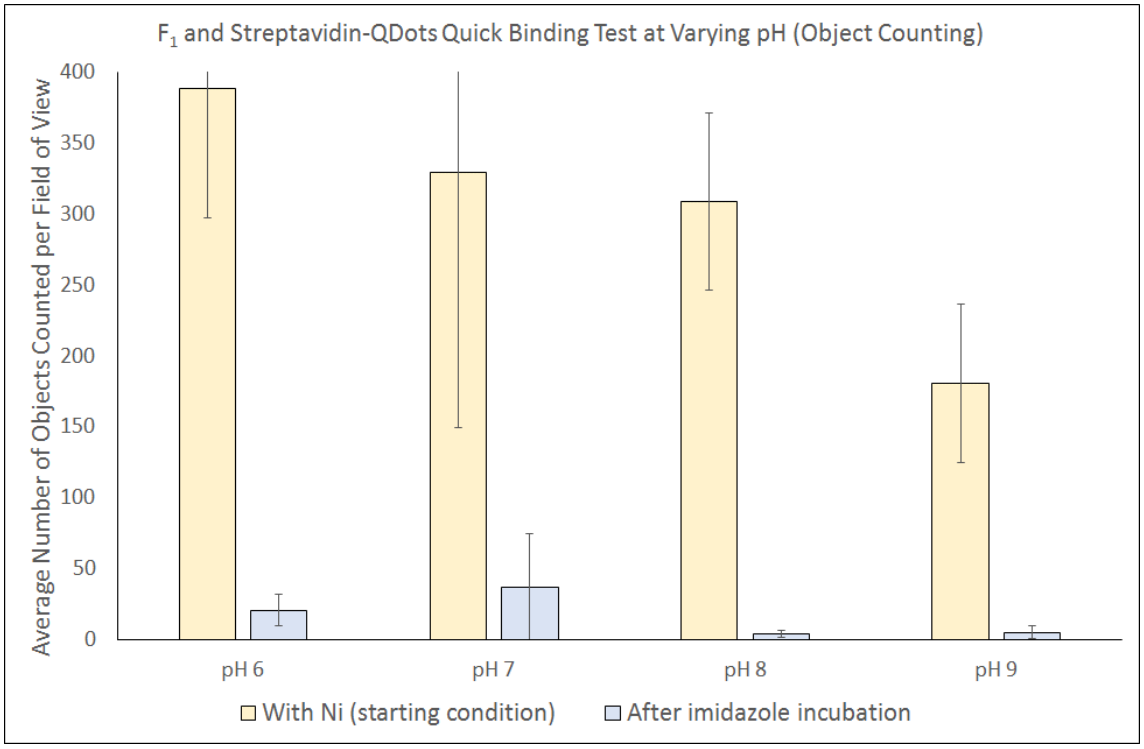

Figure 5.6
F_1 binding test at varying pH on PLL-PEG-NTA. Average number of quantum dot fluorescent objects counted per field of view at the coverslip surface in a comparison of PLL-PEG-NTA-Ni coated glass surface when F_1 added and incubated and washed, then quantum-dot-streptavidin incubated and washed (see Chapter 2 for conditions used). The blue bar for each pH condition compares when high imidazole buffer is flowed through the chamber volume. Under all pH conditions tested, the majority of objects are released under the 200 mM imidazole condition indicating that binding seen at the start was specific and via the his-tag-Ni interaction (which is overcome by imidazole). In conclusion, the PLL-PEG-NTA-Ni behaves as expected under the pH range 6-9.

binding of the PLL-PEG polymer (lysine having a pK around 10) then it might prove less effective at higher pH such as 8 or 9. Twenty random fields of view were imaged for each condition and the averages presented in Figure 5.6 with error bars indicating one standard deviation over those measurements. That release is still effective at these pH values is clear, which would not be the case were the objects to be bound non-specifically. To clarify, this test is offered as a compliment to Figure 5.5 in order to shed further light on the response as pH is raised, in which the number of objects counted under the positive test appears to decrease. This is also seen in Figure 5.6 and we might speculate could relate a

lower efficiency of Ni^{2+} binding to the surface under higher pH conditions. Alternatively this could represent a more complicated interaction which is distinct to each case. Chronologically, the test in Figure 5.6 was performed first as a rational first step prior to testing proteoliposome binding at varying pH. This also offers an initial test of F_1 binding prior to the single-molecule F_1 study to follow.

5.4 Specific binding of F_1 and observation of rotation

The long-established chemical-modification of glass to introduce an NTA-group for nickel-binding is known to offer a firm grip on non-membrane purified F_1 that allows for resolution of substeps in its rotation when a gold bead is attached to the protein and viewed in darkfield microscopy, using the laser darkfield microscope and high-speed camera available in the research group (described in section 2.2). Since the PLL-PEG-NTA system here investigated had not previously been used for this purpose either in this research group or in the literature, it was unknown whether the PLL-PEG system might prove incompatible with the observation of rotation. To test this, purified F_1 was used using the laser darkfield backscatter microscope. This essentially provides a positive control of the suitability of the binding mechanism for single-molecule rotation studies and also allowed a positive control for the analysis software used to detect rotation.

A rotational study was set up as described in section 2.9.2, with F_1 bound to the surface via his-tags and biotinylated gold 60 nm beads attached via neutravidin-binding to F_1. ATP regenerating system was flowed into the chamber volume and

the gold viewed under laser darkfield microscopy at the coverslip surface. Images were taken at 2.5kHz of random fields of view and analysed later by a Matlab code custom-made for this purpose by Dr Bradley Steel to search for spinning gold by the assessment of rotational bias and speed.

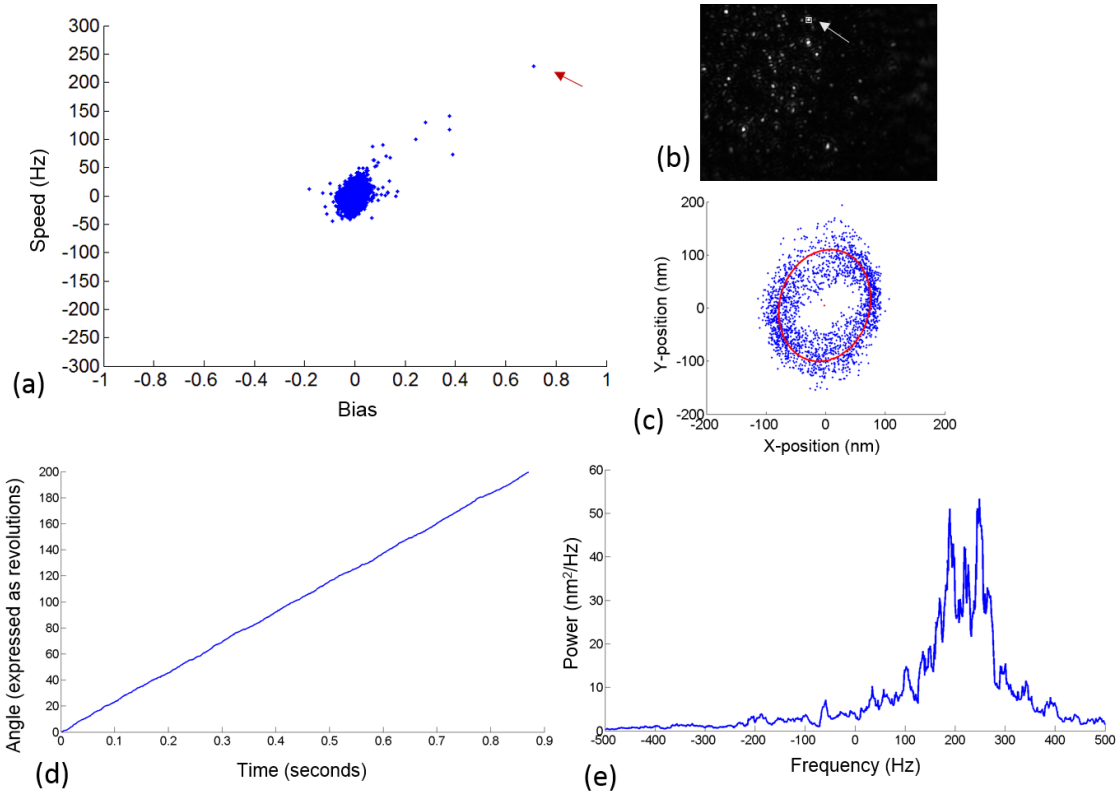

Figure 5.7

Summary of F_1 rotational data. (a) shows data from all 16 1-second videos of different fields of view, displayed based on calculated rotational bias and speed of identified beads (each spot representing one bead as identified by the software). Most objects are clustered around 0 and are not classed as rotating. Objects with a bias above around 0.2 may be rotating but must be analysed more closely. One object in particular stands out with bias 0.71 and speed 230 Hz. This is focussed on in (b-e). (b) shows this bead in the field of view as input to the software; the field is 512×384 pixels so 44 µm × 33 µm. (c) shows the calculated centre of the bead in each frame, based on a Gaussian fit; the bead is clearly seen to move around a centre point as expected – the radius of the ellipse fit (red) of rotation given that 60 nm beads were used suggests a cluster of 2 or more beads rather than a single. Based on (c), an angle can be calculated at each point on the rotation; that this angle consistently increases in one direction is demonstrated in (d). (e) is the power spectrum and demonstrates a clear asymmetry with a peak around 230 Hz and so is in agreement with the speed calculated from the angle-time trace. This is a good, clean 'spinner' and represents functionalised gold nanosphere(s) attached to rotary F_1 on a PLL-PEG-NTA-Ni surface.

As can be seen in Figure 5.7 unidirectional rotation of beads was indeed seen; in particular one object has been highlighted here which demonstrates strong rotation speed and bias. This provides a sensible control before moving on to the final experimental arrangement. That so few of the presumably many F_1 with attached gold are seen to rotate ('spinners') is fairly typical and is thought to relate partly to the prevalence of inhibited states, as discussed in Chapter 1, as well as partly to the optimisation of the experimental conditions.

In order to help us to understand what to expect from a single-molecule study on F_1F_O, it is helpful to view data on F_1. In Figure 5.7a I have given a summary of all beads identified by the software from the 16 videos taken against their rotational bias and speed. From this our spinner of particular interest is identified; it has a clear rotational bias of 0.7 and a speed of 230 Hz. Figure 5.7c shows the position of the centre of the bead as calculated by a Gaussian fit to the intensity profile, as tracked over the course of the 1-second video (this algorithm is by Thompson et al. [183]). By assigning an angle to an ellipse-fit of this position data (red line) we can plot the angle as it changes over time (Figure 5.7d); although rotation is expected to be circular, an ellipse allows analysis of data from rotation that occurs at a tilted angle to the coverslip [184]. Assumptions are not made regarding the expected size of the ellipse, which simply fits the data, so a large radius of ellipse would be taken as representing an orbit of multiple beads in a cluster attached to one molecule. A clear consistent increase in angle over time (hence unidirectional rotation) is observed. The complex power spectrum seen in Figure 5.7e is calculated from the Fourier transform of this rotational data (by

assigning positions from Figure 5.7c in an *x+iy* format) [185]. By integrating the power spectrum in the forward versus the backwards direction a number is assigned for the rotational bias (this was plotted in Figure 5.7a). The power spectrum can offer a clearer speed result than that calculated from an angle analysis alone (i.e. Figure 5.7d), since the speed appears as a peak. There is a clear circle shape to the position trace given (Figure 5.7c), making analysis more straightforward – the speed taken from angle-over-time (Figure 5.7d; this is the speed that was assigned in the plot Figure 5.7a) hence agrees with the peak of the complex power spectrum in this case (Figure 5.7e).

The F_1F_O will be expected to rotate in the same direction under hydrolysis as the isolated F_1, since the orientation will be the same (the convention in the literature is to refer to the hydrolysis direction of F_1 as anti-clockwise, representing the view from above the γ-subunit down onto the immobilised F_1).

5.5 Arrangement of the Final Experimental Conditions

The essential form of the final proposed single-molecule experiment has been arrived upon; a condition has been found in which cationic proteoliposomes may be bound to the coverslip surface via the his-tag on mutant F_1F_O and anionic giant vesicles have been formed containing functionalised gold nanospheres. Fusion with content mixing has been observed and optimised in Chapter 4. Since we have discussed that free proteoliposomes will first be removed from the sample volume by washing prior to introducing giant vesicles, these complimentary objects will only have the opportunity to fuse once giant vesicles

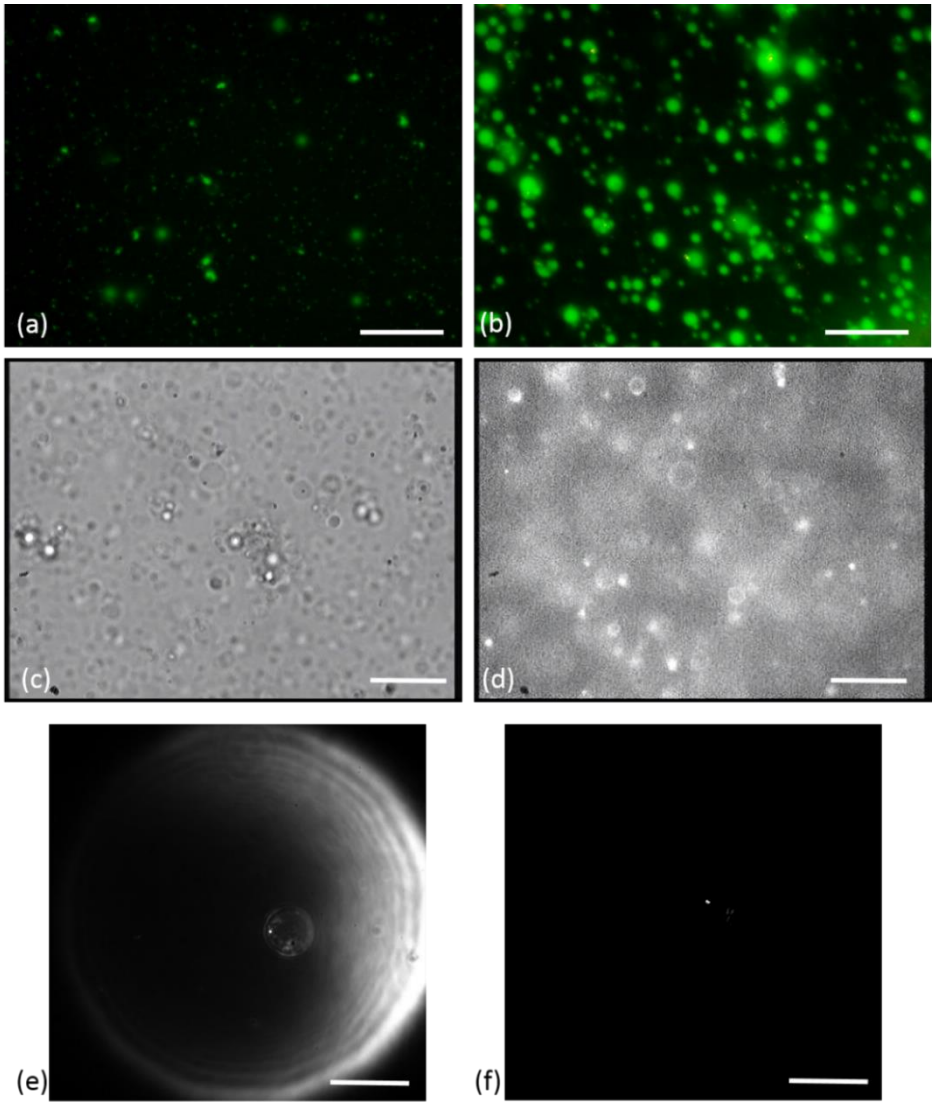

Figure 5.8

(a-d) shows demonstrations of a finalised system in two cases as ready to transfer to the laser darkfield microscope. (e-f) views in the laser darkfield microscope. In (a) and (b) we see comparative images at the coverslip surface (a) immediately after giant vesicles have been infused into the sample volume and (b) after a 100 g 10 mins centrifugation treatment to bring objects down to the surface. Since giant vesicles have entrapped pyranine, we cannot observe fluorescent lipid transfer in this case. The increase in giant vesicle objects at the surface after centrifugation is clear. In (c,d) we see the same field of view in (c) brightfield and (d) fluorescence showing the transfer of fluorescent lipid (this was also described in section 4.3.3). Gold nanospheres are internal to giant vesicles; these are seen as black dots in brightfield in (c) and yellow dots in the backscatter darkfield insert device in (b). In (e,f) we see the same field of view (e) a partial forward-scatter darkfield with brighfield arrangement and (f) laser backscatter darkfield using the supercontinuum light source (proof of principle; see section 2.2.2). Note the gold nanosphere seen clearly in backscatter with no scattering from the giant vesicle. This is not a typical field of view (generally more GUVs in a field of view) but was selected as the GUV is large and easy to see. Images (a,b) use Toupcam UCMOS05100KPA camera, images (c,d) use Watec WAT-902H Ultimate, images (e,f) use Photron Fastcam 1024PCI. (a,b,d) use "Bodipy" fluorescent cube spectral parameters (as listed in the appendix), variable camera settings. Scale bars are 10 μm.

have settled to the bottom of the sample volume. Such fusion events have been observed by the transfer of fluorescent lipids as described in section 4.3.3.

Since giant vesicles contain 17% ficoll, they are more dense than their surroundings; however it has been observed to take around 1 hr for most to reach the bottom. Significantly faster results were found by utilising a centrifuge. By use of the flow slide design including a stop valve, it was found that the entire slide along with its flow tube arrangement could be taken into a swinging-bucket centrifuge and spun at 100 g 10 mins – which was found to bring essentially all giant vesicles down to the coverslip surface without any apparent damage. Figure 5.8 gives an indication of the effect. When this treatment was combined with the use of non-fluorescent giant vesicles it appeared to promote fusion, as observed by the transfer of fluorescent lipid from fluorescent-cholesterol-loaded cationic proteoliposomes to giant vesicles. It is speculated that the increased downward force could actually promote fusion, though this has not been much explored beyond the observation that higher numbers of such fluorescent giant vesicles tended to be seen under the centrifugation condition. The flow slide can then be transferred directly to the laser darkfield microscope.

5.5.1 Bioenergetic Considerations in the Single-Molecule Approach

Initially the proposal is to observe hydrolysis-driven rotation of the F_1F_O by observation of the attached gold nanospheres in laser darkfield microscopy; efforts towards this are described in Chapter 6. It has been expected that studies on ATP synthesis could follow once this step has been observed; the giant vesicle is expected to provide a sealed environment with control over ΔpH and $\Delta\psi$.

To study hydrolysis, ATP must be introduced into the slide chamber once the giant vesicle-F_1F_O system has been arranged. However we must also consider that protons will be pumped from the outside medium to the interior of the giant vesicle due to the action of F_O. As protons are built up over time, there will be an opposing pmf that develops and will be expected to inhibit the protein function in the hydrolysis direction. For this reason FCCP can be used in proteoliposome studies to induce higher function in ATP hydrolysis mode, since it dissipates this opposing pmf and allows the rate of ATP hydrolysis to be seen limited only by ATP concentration and the protein function.

For a rapid calculation for an order-of-magnitude estimate of this effect, we can make the assumption of a capacitance in the bilayer of around 1 μFcm^{-2}. Bilayer capacitances of this order have been found in many specific measurements from squid giant nerve fibres [186] to planar bilayer measurements [187], [188] and droplet-hydrogel bilayers [83], [189]. We know that a membrane potential of the order of 200 mV will be sufficient for ATP synthesis (see discussion in section 1.1); hence as membrane potential approaches this value hydrolysis might be expected to slow and eventually stop (though, of course, this is not an absolute number and will depend on the relative free energy available from hydrolysis of ATP compared to traversal of protons through F_O – what we seek is simply a rough estimate of whether this stated effect could be within an order of magnitude of the level to affect hydrolysis rates within a 30-60 min timeframe). The charge, from $Q=CV$, necessary to build up such a potential would be dependent on the surface area of the bilayer. We have previously (section 3.2.3) measured ATP

hydrolysis bulk activity rates that indicated around 70 Hz rotation and this will correspond to 700 H^+ transported into the GUV per second per F_1F_O (presumably this rate would gradually slow, rather than remain constant as we assume for this calculation). It will be most sensible to include saturating levels of ATP (i.e. 1 mM or above) and ATP regenerating system to give the maximum rates possible.

If we deal with a small GUV, 1 μm diameter, this would correspond to around 40 000 protons or around one minute to reach 200 mV for one inserted F_1F_O. For a larger GUV of 10 μm diameter, this would correspond to around 4 million protons or over 1 hr.

With these caveats stated, based on this order-of-magnitude calculation it will be prudent to include an ionophore in initial experiments at a concentration sufficient for at least one such molecule to insert per giant vesicle (each FCCP can transport around 1000 H^+ per second) to thus very simply eliminate pmf and give the highest chances of success for the viewing of hydrolysis-driven rotation. Presumably once established, it would be of interest to study the expected slowing effect on rotation as the opposing pmf builds up in the absence of ionophore.

5.6 Summary and Conclusions

After initial experimentation with a variety of methods, a system based on commercially-available crafted-polymer polylysine-polyethylene glycol molecules functionalised with NTA has allowed for specific binding of cationic proteoliposomes to a glass coverslip with clear specificity via the his-tags on the mutant F_1F_O β-subunits. A pH 7.0 condition has been chosen for this binding as

protein function is not expected to be impaired by exposure to this pH range and specificity of binding was very clear and strong; pH 8.0, which had been used as a standard for protein function, offered a considerably weaker specificity condition. pH 6.0 offered an apparently stronger binding but is expected to be less compatible with protein function. That this binding occurs via the his-tag interaction is clear from its sensitivity both to a lack of Ni^{2+} on the surface and, when Ni^{2+} is present, then to the addition of imidazole (which disrupts the his-tag interaction).

A condition to easily and quickly induce fusion of giant vesicles to proteoliposomes at the surface has been found, in which the coverslip itself is placed briefly into a swinging-bucket centrifuge. This causes giant vesicles to settle at or near the surface and fusion is observed via the transfer of fluorescent cholesterol from proteoliposomes bound at the surface to initially non-fluorescent giant vesicles. The design of the flow-slide system includes a valve that prevents buffer from leaving the slide during this treatment; using this the sample is not found to be damaged by the centrifuge treatment.

It is noted that studies on fusion presented in Chapter 4 concluded that a pH 7.0 condition inhibited fusion compared to pH 7.5 or 8 (see section 4.3.1). Since the flow-slide system allows for straightforward buffer exchange, it is expected that single-molecule studies will proceed by the binding of proteoliposomes first under a condition of 100 mM KCl 50 mM MOPS 0.1 mM $MgCl_2$ pH 7.0, as presented here, followed by a buffer exchange to 20 mM KCl 10 mM MOPS pH 8.0 for fusion (this buffer was tested for fusion in section 4.3.1). It has been

preferred to remove all $MgCl_2$ from the final fusion conditions since it has not been possible to test the influence of this component on content mixing in the studies presented in Chapter 4 (owing to artifacts caused by its interaction with the assay used to assess fusion). $MgCl_2$ can then be reintroduced after some incubation time along with ATP regenerating system to allow F_1F_O to undergo hydrolysis-driven rotation (since Mg^{2+} is required for this to occur).

The use of a gravity-based flow slide system allows buffer exchange at a rate that is not damaging to giant vesicle structures; around 10 µl per minute causes no apparent deformation when viewed live under brightfield illumination. The bioenergetics considerations of ATP hydrolysis have allowed an experimental arrangement for single-molecule F_1F_O rotation by hydrolysis in a fused giant vesicle object containing gold nanospheres to be arrived upon, including incubation with the proton ionophore FCCP to prevent the development of a pmf (due to the action of F_O) that would otherwise be expected to inhibit hydrolysis over the time required for a single-molecule darkfield experiment.

Chapter 6 F_1F_O Single Molecule Rotation Studies, Final Conclusions, and Future Work

6.1 Introduction

The multiple steps to arrive at a point by which we may construct a single-molecule experiment on F_1F_O have been described across the course of the previous chapters; in particular, Chapter 5 has outlined some of the more practical considerations related to the particular experimental arrangement. In the event, the amount of time it has been possible to dedicate to this final experiment as a proof of the overall methodology has been limited due to the development time of other stages. There has always been a trade-off between optimising the best conditions for the single-molecule experiment to be successful and actual attempts to try the single-molecule experiment under the then-current optimisation. The aim has been to demonstrate ATP hydrolysis-driven rotation of the F_1F_O by single-molecule rotation, utilising the laser backscatter darkfield microscope and analysis software designed for F_1 studies. The use of the darkfield microscope ensures low-noise recordings can be taken with high speeds (up to 109 500 Hz) over fields of view including multiple gold

nanospheres at a time. In these initial studies, the expected speed of F_1F_O rotation cannot be readily assumed a priori and so all studies conducted so far have been performed at 2.5kHz recording. This is based on the research group's experience with single-molecule F_1 studies; in F_1F_O in hydrolysis mode rotation will certainly not be expected to be faster than that seen with hydrolysis-driven rotation of isolated F_1. Such considerations will be important to ensure we do not undersample and so misinterpret rotation; the analysis software can only operate by assuming that a bead does not rotate more than π radians between frames. There are practical implications of this high sampling rate, including short recording times for each field of view before data is then downloaded from the camera (compromised to 16 fields of view of around 1 second recording, though different arrangements with longer recording times and different sizes of field of view would be possible).

Data will be presented here from one day of experiments, which was the first so far performed after full optimisation of previous steps presented; in particular, improvement of biotin-labelling on the c-subunits as outlined in Chapter 3, as well as much of the optimisation of giant vesicle formation presented in Chapter 4. Previous attempts at this single molecule study had used earlier, less optimal versions of these systems. Since previous attempts had slightly varying methods in their preparation, I have presented in Chapter 2 the exact protocol which was used to prepare the particular day of experiments I present here. Previous experiments did not, in any case, contain anything that could be called spinning; though a few compelling traces demonstrating three-fold symmetry with largely

unidirectional rotation at very low speed (1-2 Hz) were seen in these earlier attempts which gave encouragement.

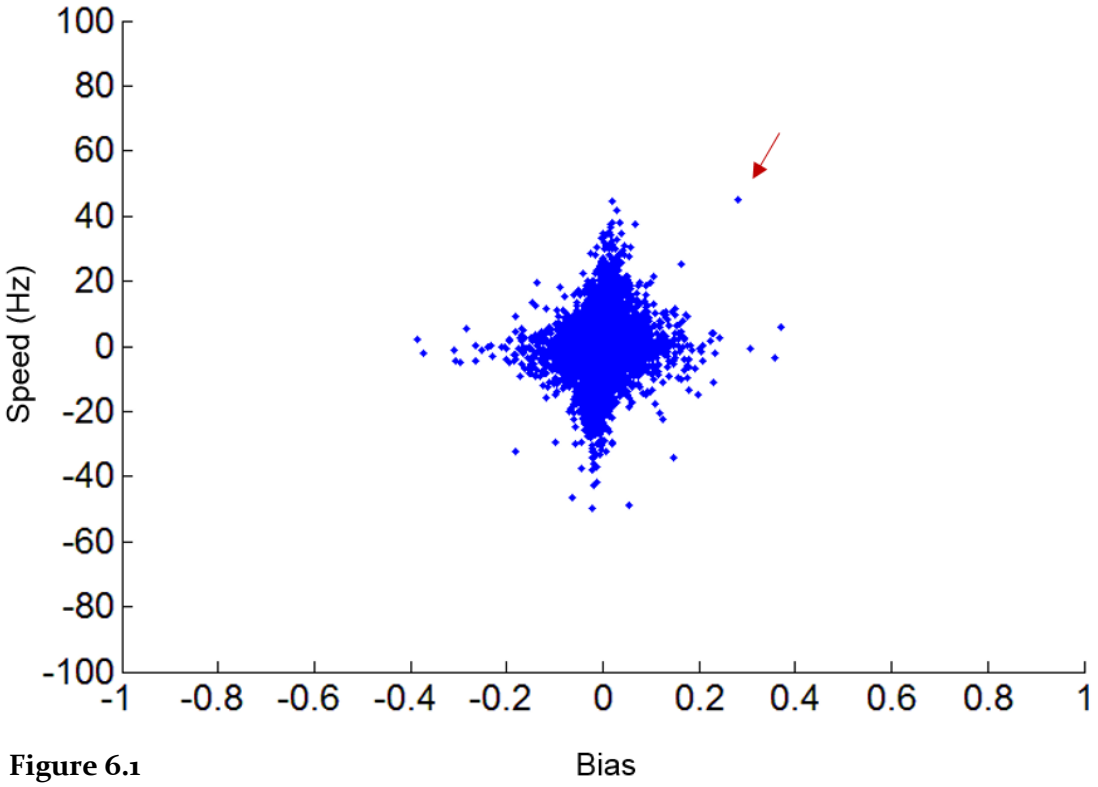

Figure 6.1
Summary speed-bias plot of 128 fields of view taken on a single day of a giant vesicle F_1F_O experiment. Preparation as described in section 2.9.3. Each point is one gold nanosphere identified by the Matlab software. Candidates of interest are represented in the top-right hand corner based on sign conventions for the expected rotation (as seen also in Figure 5.7a). One object of particular interest is identified; bias 0.28, speed 43 Hz.

6.2 F_1F_O Single-Molecule Study Data

A speed-bias plot is shown in Figure 6.1 which summarises all 128 fields of view recorded in the experiment presented (each video 432 × 284 pixels, corresponding to 37 μm × 24 μm). Each point has been identified as a gold bead and analysis has output a bias of rotation in one direction and a speed (it is thought that this is an over-estimate of the number of beads, due to imperfect optimisation of the contrast – this will not prejudice analysis, though it increases

computational time required). Based on experience with F_1, there is little to be expected in anything with bias below 0.2. Note that we expect that rotation in the F_1F_O case will be in the same direction under hydrolysis as was seen in F_1 – hence we look to the upper right quadrant of Figure 6.1.

One single point stands out of interest and this has been identified as rotating on closer analysis as seen in Figure 6.2 This trace shown in Figure 6.2 exhibits a clear unidirectional increase in angle over time, with some apparent back-steps. Based

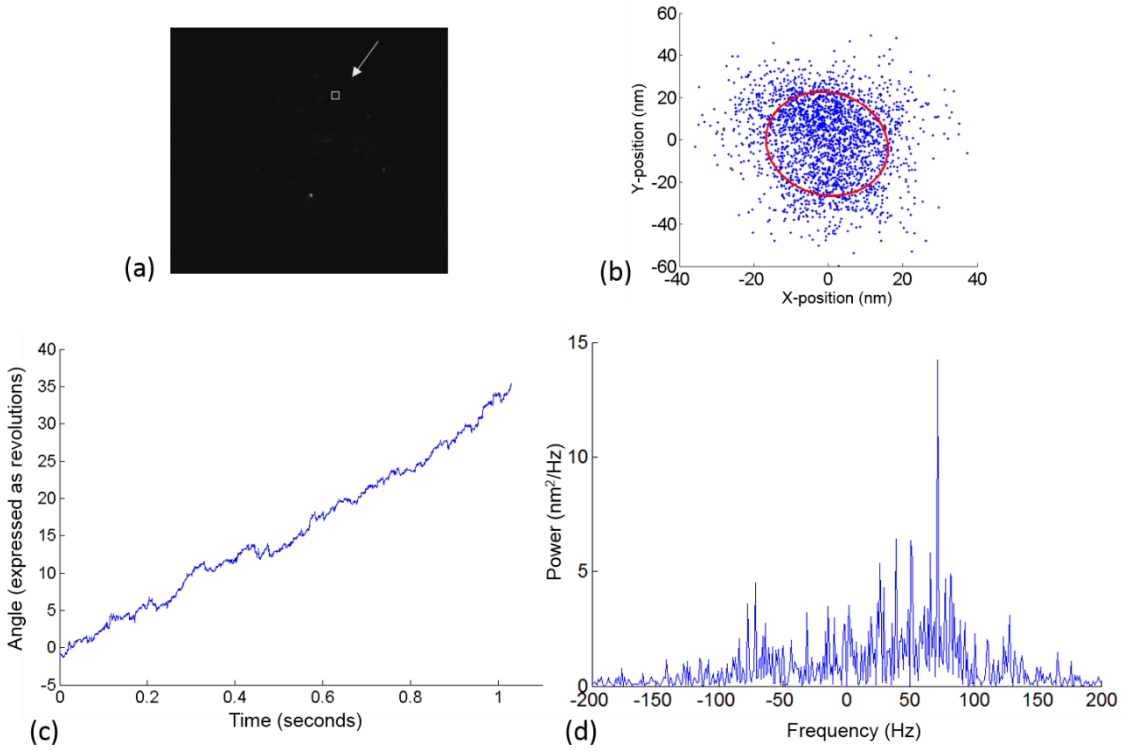

Figure 6.2

A summary of analysis on the single bead identified as of particular interest in Figure 6.1. (b) shows the centre of the Gaussian fit for the bead as it is tracked over time. Based on an ellipse-fit to the data (red) an angle can be calculated for each point [184]. (c) shows that this angle consistently increases over the measured time with a fairly constant rate, with only a few back-steps. The calculated bias in this direction of rotation is 0.28 and the speed is 43 Hz. (d) shows the power spectrum, giving a clear peak around 70 Hz, higher than that calculated from the angle-fit trace (b). For beads not exhibiting clear circular paths, such as this one, a power spectrum-fit is considered a more reliable indication of speed than the angle-fit. (a) shows the field of view as input to the software with the bead of interest highlighted (contrast sub-optimal but sufficient; owing to shutter conditions); each field is 432×284 pixels, corresponding to 37 μm × 24 μm.

on angle-time, the speed has been calculated to be around 43 Hz. However, viewing of the subtracted power spectrum indicates a clear peak closer to 70 Hz. This is a more reliable indication of speed, since this trace does not exhibit a clear circular shape in the position of the Gaussian fit to the centre of the bead (Figure 6.2b). This peak was not seen in other beads recorded in the same field of view – indicating it is not a spurious noise from, for example, a rotation of the slide itself. Hence we can say with some confidence that this trace does indeed represent a bead attached to a rotating single molecule.

Since the current experimental arrangement was designed for an initial high-throughput of traces on a single day to look for an assumed rare-event of a spinning bead attached to the c-ring of F_1F_O internal to a giant vesicle, a high number of fields of view were recorded in succession and analysed separately after the experiment was complete. Although it has been discussed that both brightfield on the laser darkfield microscope and the potential to view fluorescence by attachment of the supercontinuum laser and wavelength selection system (described section 2.2.2) offer methods to take sequential or simultaneous images of fields of view recorded in darkfield for later comparison and identification of whether candidate spinners are actually located within a giant vesicle as expected, this was not performed in the experiment presented. This is due to the expectation that a high throughput would yield the best opportunity to first see a positive case of a rotating bead; once this was observed, as it clearly seems to have been here, then such techniques for deeper analysis could follow to understand whether the rotating bead is actually inside a giant

vesicle as intended. Without such extra data on the field of view taken, we cannot know if, for example, this one trace identified could represent an F_1F_O with attached bead stuck within a lipid fragment rather than an enclosed vesicle. Such lipid fragment results have previously been published in the field. Hence this one positive trace is not intended to be identified as a demonstration of the methodology presented in the thesis, but rather as the current state of the results and with the intention to display the level of understanding of the system at the present time. Although some other points of potential interest can be seen in Figure 6.1, nothing on closer analysis appeared to be rotating as clearly as that identified in Figure 6.2 (this comes as no surprise however – we must always have expected such spinners to be a rare event given that no more ~10 GUVs are ever likely to be able to fit within the 37 μm × 24 μm field of view (and current conditions do not reach this speculated maximum density).

Furthermore, as has been discussed, the current set of data has been taken 'blind' – i.e. all viewed under darkfield, with no distinction made between gold internal to a GUV or external. External gold could presumably only ever exhibit noise – a non-specific binding of gold nanospheres even to the exposed α- or β-subunits, which seems unlikely given the liposomes blocking access, would not exhibit rotation since these are held firm to the surface by the his-tag. Hence it seems that the only other likely explanation for the spinner seen than an internalised gold nanosphere is the suggested possibility of an F_1F_O embedded in a lipid fragment that is hence open (perhaps due to the rupture of a GUV). Although I

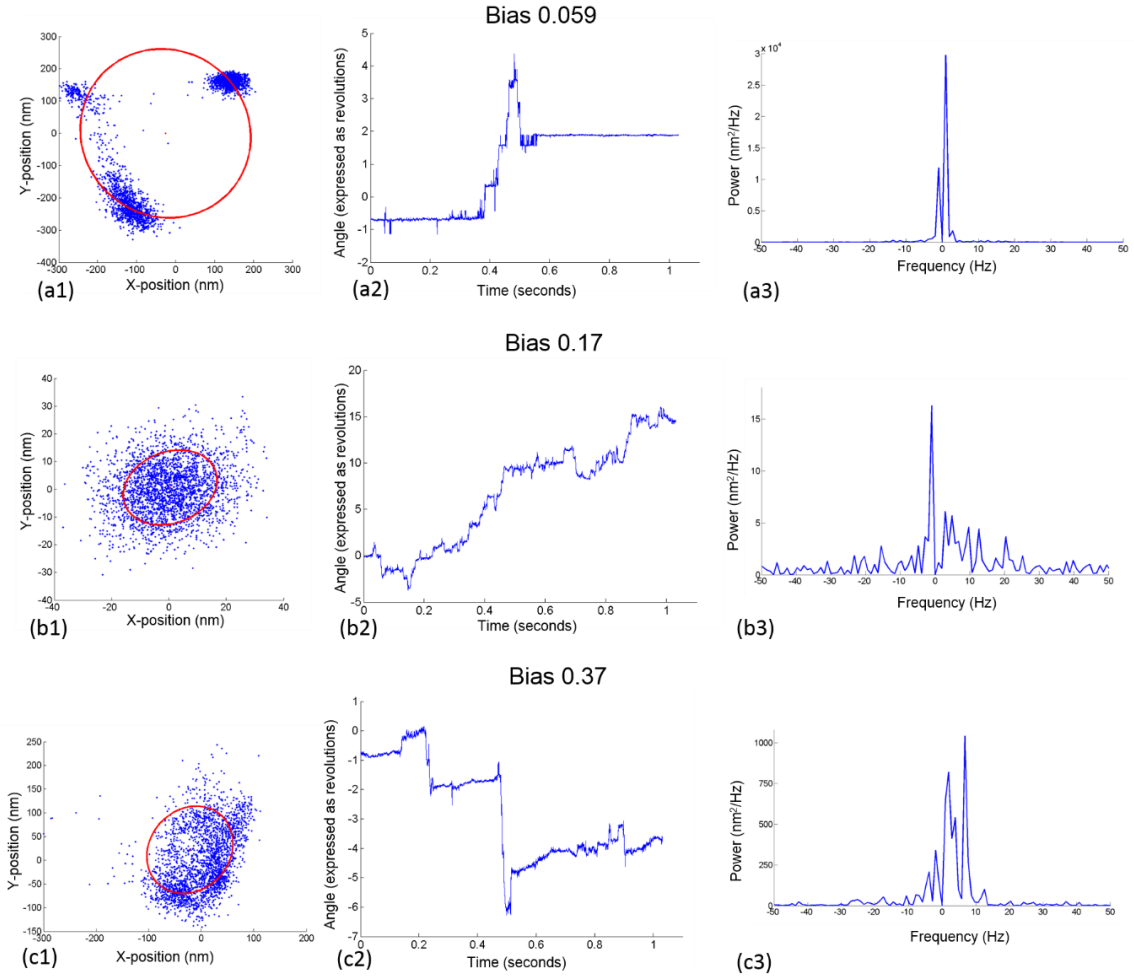

Figure 6.3

Some further points of interest taken from those summarised in Figure 6.1. Speculative analysis is here offered. In each set 1 is the positions of the Gaussian fit to the centre of the bead in each frame, 2 is the angle-time trace, and 3 is the power spectrum. The calculated bias is shown for each. (a) appears to show three dwells as might be expected for the three hydrolysis states; perhaps this represents a non-functional protein or one in a series of inhibited states; based on the radius observed, given 60 nm beads used this could only sensibly represent rotational data if we assume a cluster of perhaps three beads. (b) seems to rotate nearly unidirectionally, however the only clear peak in the power spectrum is in its back-steps – otherwise it moves in the expected direction with a variety of speeds. Similarly, this bead is perhaps attached to a non-functional protein. (c) has been selected by the analysis software as having the highest rotational bias at 0.37; it is a good example of where analysis by eye would reject this data, but by viewing the power spectrum we see a peak around 8 Hz possibly indicating a weak rotation that is perhaps masked in the angle-time trace by points which cross the centre, dominating the trace with apparent back-steps. The radius of the ellipse fit is also high and would represent multiple beads in a cluster. Given the weakness of the data, it is not offered as a positive spinner.

do not have other clear spinners to display from this dataset, some further traces of possible note are displayed in Figure 6.3.

The traces from the bead in Figure 6.3a display a clear three dwell states, which we might speculate could correspond to an F_1F_O undergoing what appear to be short periods of rotation at high speed followed by long periods in a locked position. There is also a significant back-step which can be seen in the angle-time trace. It seems highly probable that this trace represents a bead attached to an F_1F_O (owing both to the rotation and the symmetry), but the protein is perhaps inhibited or otherwise non-functional. Prior to the experiment presented here, traces of the kind in Figure 6.3a had been seen a small handful of times in attempts at this experiment and represented the best data up to that point. Since it seemed from such traces that gold attachment to F_1F_O had most likely occurred, but the protein was in a non-rotating state, an approach of optimisation of conditions followed by a large number of fields of view recorded was taken leading to this presented experiment. Figure 6.3b appears in angle-time to be undergoing rotation with some backstepping, but on the power spectrum we see a series of positive speed peaks – and the clearest peak actually corresponds to back-stepping (i.e. negative frequency). Perhaps this represents an improperly functional protein, or the rotation could be improperly seen if the three his-tags do not provide a firm anchoring (e.g. 1 out of the 3 transiently) which would obscure the trace. Figure 6.3c is interesting because the power spectrum would seem to show a fairly clear positive rotation peak 8 Hz, but the angle-time appears poor because of back-stepping and the Gaussian fit of the

bead centre also appears to include some spurious points far from the centre of rotation. It may demonstrate a weak rotation, but it is difficult to make firm conclusions based on such apparently noisy traces.

These three additional traces represent a good summary of the best of much of the rest of the data of interest from this experiment and previous attempts. It has been discussed that several are thought to possibly represent gold nanospheres attached to F_1F_O but not demonstrating a clear signal of unidirectional rotation; from F_1 studies we expect the majority of particles could well be in an inhibited state for the majority of the time. Hence it will be a probabilistic approach depending on how many such functional proteins-with-gold can be taken in a field of view and how many fields of view can be taken. That one positive spinner has been seen has been taken as highly encouraging and there is much future work for further optimisation of the experiment.

6.3 Final Summary and Conclusions of the Thesis

To draw a summary here of the whole of the presented work; a novel multi-step methodology for the single-molecule study of the rotation of F_1F_O ATP synthase by darkfield microscopy has been proposed, developed, refined, and finally tested in full in a limited number of cases with results that are suggestive but which will require further investigation.

F_1F_O has been expressed and purified from *E. Coli* mutant strains with strong yield and purity, with all subunits intact and identified, and high levels of activity have been shown. Though these mutants had been previously developed, it has

been shown that the labelling of the closely-packed c-subunit cysteines with a maleimide-biotin tag required highly-reducing conditions to achieve high levels of labelling. This was a novel step and protein function proved unimpaired by this treatment.

A novel mixture of natural soybean lipid extract and complementary cationic and anionic pure charged lipids have been used to show fusion of vesicles with content mixing. Conditions have been found to optimise this fusion, which have also been shown to be compatible with F_1F_O function. It has been shown that F_1F_O is functional in proteoliposomes of this same mixture of cationic charged lipids and natural lipid extract, though the function has been shown to degrade over time as compared to insertion into liposomes made of (zwitterionic) soybean lipid extract only.

A giant lipid vesicle formation method by an emulsion of water-in-oil has been developed, based on precedents in the literature and utilising the fusogenic lipid mixture previously discussed. Owing to the emulsion method, the interior contents of giant vesicles can be well-defined against the exterior – meaning that high-value contents could be entrapped without the equalisation between interior and exterior contents that are a typical feature of other vesicle formation methods. In a novel step this has been used to show the entrapment of gold nanospheres, functionalised with the biotin-binding protein streptavidin (also neutravidin), of both 60 nm and 100 nm diameter – suitable for darkfield microscopy. Such giant vesicles have been shown to be robust to centrifugation treatment, such that they can be formed and concentrated reliably, and gold

nanospheres have been observed to move freely about the giant vesicle interior space in many cases. Characterisation of the lipid leaflets by inclusion of a lipid-conjugated fluorophore have suggested that many giant vesicles are unilamellar, though multivesicular objects and some highly-fluorescent objects thought to be oil droplets are also seen. Fusion between such anionic giant vesicles and cationic small unilamellar vesicles has shown full content mixing both in the fluorimeter and, most clearly, under the fluorescence microscope. Aggregation of objects under fusion was also clearly seen under the microscope, which suggested that a sequential build-up of cationic and anionic objects at the coverslip surface would be the best way to proceed for a single-molecule experiment.

Concurrently to the development of giant vesicles containing gold, two microscopy designs have been co-innovated along with others in the research group. One consists of a method to adapt a standard arc-lamp fluorescence microscope to also perform backscatter darkfield simultaneously by insertion of a secondary lightpath; several images have been shown displaying the use of this device for studying the movement of gold nanospheres within fluorophore-labelled giant vesicles, an application for which it has proven highly useful. The other innovation has been the development of a method for arbitrary selection of wavelengths from a supercontinuum broad-band laser input, with the potential to select multiple single wavelengths as well as broad bands across a range of wavelengths. This also has the potential to allow fluorescence viewing combined with the laser darkfield microscope. Such approaches are of interest to fully

characterise fields of view when analysing rotation under darkfield microscopy and will be of interest for future work.

Cationic small unilamellar vesicles into which F_1F_O has been inserted ('proteoliposomes') have been shown by thin-layer chromatography to have the same lipid composition after protein insertion, which is of interest due to the levels of potentially-contaminating lipids present in the solubilisation buffer in which F_1F_O is stabilised. This is taken as an initial study of interest to indicate that cationic F_1F_O proteoliposomes can be considered to exhibit the same fusion with content mixing behaviour with anionic giant vesicles as previously described for cationic liposomes.

By centrifugation separation then F_1F_O has been shown to be inserted into a new post-fusion product and remain functional with these lipid mixtures. Although it must be noted that the results as so far demonstrated on functional protein delivery could also be explained by hemifusion events, the previously-discussed results on content mixing are offered to demonstrate that a full new unilamellar post-fusion product with F_1F_O embedded is expected. Transfer of fluorescent lipid from fluorescent proteoliposomes to initially non-fluorescent giant vesicles has also been observed, reinforcing that fusion is observed at the coverslip surface with sequential addition of components (hence removing the possibility of aggregation as observed in bulk).

A gravity-based flow slide system has been developed to be compatible with giant vesicles, which have been observed to be intolerant to rapid flow through a coverslip volume when located at a surface. This has allowed both slow buffer

exchange and, by incorporating a stop-valve, the transfer of samples between microscopes.

A method by which cationic proteoliposomes can be bound to a glass coverslip surface in a stable manner via the his-tag present on the utilised F_1F_O mutant has been found, which is notable given their persistent non-specific binding to other surface modifications tested. This allows a firm binding of the F_1F_O to a surface on one side (the protruding F_1), which should allow the rotation of the functional protein to be transmitted to a functionalised gold nanosphere bound to the F_O c-ring on the interior of the post-fusion vesicle (expected to form upon introduction of anionic gold-containing giant vesicles into the chamber volume and subsequent fusion with cationic proteoliposomes at the surface). In order to speed the time of fusion at the surface between cationic proteoliposomes and anionic giant vesicles, mild centrifugation techniques have been explored in which the slide and coverslip apparatus itself can be taken from the microscope and subjected to forces of several tens of g for several minutes. By observation of the transfer of fluorescent bilayer-incorporated lipids from cationic proteoliposomes to previously non-fluorescent anionic giant vesicles, this centrifugation has been observed to encourage fusion at the surface without apparent damage to giant vesicles.

Given a pre-existing high space-and-time-resolution laser backscatter darkfield microscope and Matlab analysis software used within the research group for the study of single-molecule purified F1, this has been used to probe the final experimental condition once cationic proteoliposomes are bound; anionic giant

vesicles containing functionalised gold nanospheres are introduced to the chamber volume, centrifugation brings them to the surface, and ATP regenerating system is introduced into the chamber volume. As is typically expected, a large number of apparently non-rotating beads are seen in the subsequent analysis – and one particular bead out of 128 fields of view captured is seen to undoubtedly demonstrate rotation in the expected direction at a speed of some 70 Hz. This is not offered as a demonstration of proof of the experimental arrangement, since it has not been confirmed at this point that the spinner seen was internal to a giant vesicle as expected. This spinner might be speculated to sit in a lipid fragment, rather than an enclosed vesicle as proposed; this is not known at this stage. This is rather offered as a demonstration that the experimental arrangement is of interest and more work is required to continue experiments with greater additional data on fluorescent and/or brightfield views of each field of view to allow such determination of interesting rotating beads observed (assuming more such rotating beads can be observed in future experiments, since at the moment we discuss only a single object observed, though further suggestive traces are also shown). There is much to be done in this regard and it is hoped that if the system can indeed demonstrate ATP-hydrolysis-driven rotation of F_1F_O in a vesicle object in a repeatable and robust manner then many further experiments, particularly the observation of ATP-synthesis-driven rotation, become within reach. If this single-molecule study can be confirmed by repeats and further study to reach a reliable and robust level then it becomes of interest as a technique to many research groups working in this field.

6.4 Future Work

The immediate future work is to investigate further the single-molecule study as presented, with repeats and with additional brightfield and/or fluorescent views of each field of view recorded for better characterisation of the nature of nanospheres imaged. The experimental arrangement will need optimisation; rapid analysis of fields of view with Matlab at the microscope could be performed to ensure that any objects of interest can be probed further and immediately as soon as they are found. Besides identifying if such a rotating gold nanosphere of interest is indeed located within a giant vesicle, this could include alterations to the external conditions by buffer exchange to, for example, vary ATP concentration. If such rotating gold nanospheres can indeed be observed to be internal to giant vesicles, and if such objects can be found with reliability, then many such objects will need to be recorded in order that conclusions about the nature of the rotation observed can begin to be made. For example the range of speeds at which the rotation is observed, and the factors affecting that speed, as well as any steps observed in the rotation will be of immediate interest. It may prove more practical to perform live analysis on single beads, using a quadrant photo-diode or similar arrangement (such possibilities are available within the research group).

It has been seen that the charged cationic lipid mixture used induces damage to the F_1F_O over time and it will be of interest to see whether alteration of the lipid mixture could prevent or slow this effect without unduly inhibiting the fusion seen. Additionally, it is not currently well-understood to what extent the post-fusion F_1F_O, once incorporated into the giant vesicle consisting of a mixture of

zwitterionic, anionic, and cationic lipids, may still exhibit this degradation of ATP hydrolysis rate or if the effect might be halted or reversed once the lipid environment changes. Further work on the development of the lipid mixture is of interest, in both modifying the soybean PC used to a purer format and also varying the cationic lipid with the aim to improve upon the protein function results presented in section 3.3.3. It is thought that studies using a pH-sensitive dye (such as pyranine) to monitor the interior of a giant vesicle, whilst including an ionophore such as valinomycin to negate $\Delta\psi$ effects, might allow more clear probing of the post-fusion functioning of F_1F_O by monitoring the pH change as protons are pumped inwards (but no $\Delta\psi$ is induced due to K^+ traversing outwards via valinomycin). As well as allowing investigation of protein stability in the post-fusion product, this should also allow a more definite demonstration of functional F_1F_O delivery by charge-based fusion to a giant vesicle than has been presented with the (much more sensitive, but also somewhat ambiguous given potential conflation with hemifusion events) ACMA quenching assay. Such an experiment to measure pH changes internal to a giant vesicle, if it should be achievable in bulk tests, could presumably also be undertaken under the microscope.

Further studies would naturally progress to the study of ATP-synthesis-driven rotation; this is the essential feature of the system presented, since hydrolysis-driven rotation of F_1F_O can and has been observed in lipid fragments and in detergent-stabilised states. By the inclusion of ionophores such as valinomycin, it should be possible to induce a diffusion potential across the vesicle bilayer by

means of exchanging the exterior salt conditions. Such a potential would then be expected to drive ATP synthesis, in the same manner as many such experiments have demonstrated in the case of bulk studies in proteoliposomes [14]. By co-reconstitution of a primary proton pump, it should be possible to construct a system in which a continuous pmf can be generated – in the case of light-driven pumps such as proteorhodopsin or bacteriorhodopsin this would then be light-dependent and hence one could presumably readily vary the pmf at will and study its effect on F_1F_O rotation. Similarly to the development of ATP hydrolysis-driven single molecule studies presented, methods for measurement of ATP synthesis by purified F_1F_O as exist in the literature would be established in bulk prior to single-molecule level studies. By the inclusion of pH- or membrane-potential-sensitive dyes (such as oxonol VI for $\Delta\psi$ and pyranine for ΔpH [190], [191]) it should be possible to map these values to F_1F_O rotation and hence study the effect of each; this is a key inherent feature of the approach compared to planar bilayer studies since the ΔpH and $\Delta\psi$ should be well-defined by the giant vesicle's boundary. By the varying inclusion of differing ionophores, such as the aforementioned valinomycin (for K^+) or FCCP (for H^+) amongst others, it should be possible to disentangle the ΔpH and $\Delta\psi$ components of pmf and study the effects of each on synthesis-driven rotation independently. It should be possible to study the equilibrium between ATP synthesis and hydrolysis and determine clear studies of the regulation between the two states. Step sizes expected to be observed in rotation, presumably 10-fold based on the work of others so far, will be of interest along with elucidation of any further sub-steps that might be seen under the high time-resolution offered by the laser darkfield microscopy

approach (such as studied under hydrolysis by Ishmukhametov et al. [27]). The effects of inhibitors on these factors will be of interest.

With such characterisation of rotation in the utilised *E. Coli* mutant strain, it would then be of interest to also compare different varieties of the protein – including Na^+ driven F_1F_O, varying c-subunit compositions, and also induced mutations or cross-linking of subunits. It should also be possible to study isolated F_O, assuming a mutation can be induced such that the isolated F_O in a proteoliposome can be bound to a surface, similarly to what has been shown here for F_1F_O via the his-tag on F_1. For example, using a his-tag or biontinylation via cysteine on the c-subunits and then attaching a gold nanosphere onto the protruding b-subunit, then the rotation of F_O (as an abc-subcomplex) could be studied.

Appendix

During the initial stages of the DPhil, I worked on a different but related project in which the aim was not so much to study the F_1F_O but rather to utilise it as a motor to drive a nanotechnological concept of a rotary swimmer. Although this work was eventually abandoned in favour of the project presented in the main body of the thesis, not least because progress had been disappointing, nevertheless I present here two protocols I developed during this period, in the hope that they could be of use to others. Other data from the progression of the project's aims will not be presented.

The concept of this project was to use a purified bacterial flagellum to attach to the rotary F_1 (as an initial proof of concept) and then later to a membrane-bound F_1F_O. For the F_1, one can see the relation to the initial proof-of-rotation paper in 1997 in which an actin filament was used [51]. Staining of bacterial flagella with non-specific dyes followed standard protocols and purification of the flagellar filament is here presented. The difficulty, other than the binding step, would be to arrange the system such that the rotation ended up driving the filament directly about its axis so that propulsion would result. In practice that issue was never resolved. A bead could be used to provide a bulwark against counter-rotation; a protocol to modify a polystyrene bead with Ni-NTA was developed based on precedents in the literature and mutant F_1 was demonstrated to bind specifically and was active. By using the beads as a method to continually bind

and wash unbound components, the binding of F_1 and filaments sequentially was shown via SDS-PAGE.

This *E. Coli* mutant included a biotin-modification on the hook introduced by Dr Mostyn Brown. This was characterised in the isolated sample by use of a Western blot, and also as discussed was shown to bind F_1 via streptavidin.

Protocols

Purification of *E. Coli* flagellar filament-hook-basal body

Largely derived from Kubori et al. [192] but with additions (note the cited paper refers to Salmonella rather than *E. Coli*).

All experiments performed in walk-in fridge at 4 °C unless otherwise stated. 2x 1 L of mutant *E. Coli* grown overnight in tryptone broth (TB) at 30 °C with 225 rpm shaking to an optical density (OD600) of 1.0 (0.8-1.2 works fine). Split into two 1 L centrifuge tubes and spin at 5100 rpm 23 mins 4 °C (in 8.100 rotor). Supernatant discarded. 60 ml of 0.5 M sucrose, 0.1 M Tris pH 8.0 (as measured at room temperature) added to each tube and left on 100 rpm shaker to resuspend pellet (~1 hr). Combine two tubes in a 1 L flask. Add 10 ml of 2 mg/ml lysozyme (in distilled water), followed by 2 ml of 1 M EDTA pH 8.0 (as measured at room temperature) and leave in fridge for ~45 mins with mild agitation. Add 20 ml of 10% Triton X-100 (in 0.1 M Tris pH 8.0, note detergent solution must be made up fresh on the day) and swirl mixture gently by hand until colour change is apparent and total (30 sec). Add 2 ml of 1 M MgCl2. Add 4 µl of DNase 1 (not

present in Kubori et al.). Incubate at 30 °C for 30 mins at 225 (or less – as available) rpm followed by a 37 °C incubation for 10 mins at 225 (or less) rpm. Can leave at this stage overnight on gentle agitation (not required). Raise pH to 10-11 by adding 5 M NaOH dropwise with care (using pH paper to test). Ultracentrifuge at 28000 rpm 60 mins 4 °C (in 45Ti rotor) and discard supernatant. Resuspend pellet in 100 mM KCl, 500 mM sucrose, 0.1% Triton X-100, pH 10-11 (with KOH, as measured at room temperature) using a magnetic stirrer (~2-3 hrs or more, can leave overnight). Centrifuge at 8000 rpm 10 mins 4 °C (in 45Ti rotor) to remove undissolved material (ie discard pellet) before a 28 000 rpm 60 mins 4 °C spin (in 45Ti rotor). Remove the pellet into 500 µl of 10 mM Tris, 5 mM EDTA, 0.1% Triton X-100, pH 8.0 (as measured at room temperature) and leave to resuspend on rollers overnight before performing transmission electron microscopy (TEM).

Ni-NTA Modification of amino polystyrene beads

Largely derived from Yasuda et al. [60], but note the protocol in the cited paper is vague on several key points which required trial-and-error to resolve. The protocol as given here should hopefully be easy to follow for anyone for whom this could be of interest.

Make 100 ml of 100 mM MOPS pH 7.5 with 2.0927 g solid MOPS. pH with meter, filter-sterilise 40 ml and transfer to falcon tube. Make 500 µl of 100 mM AB-NTA pH 7.5 with 0.013113 g solid AB-NTA and 500 µl 100 mM MOPS. AB-NTA will

require vigorous vortexing to pass into solution. pH the solution carefully with pH paper, using MOPS as a reference colour for the target pH; this requires around 40 µl of 2 M KOH. Make 500 µl of 10 mM sulfo-EGS pH 7.5 with 0.0033023 g solid sulfo-EGS and 500 µl 100 mM MOPS. Test with pH paper, but should not require adjustment to meet target pH. Make 10 ml of 10 mM glycine, 10 mM $NiCl_2$, pH 7.5 with 0.007507 g glycine and 0.023769 g of $NiCl_2{\cdot}6H_20$. pH very carefully with around 60 µl 2 M KOH using pH meter. pH paper will not be reliable since the solution is unbuffered. Note the addition of MOPS as a buffer has previously been shown to render the solution ineffective to transfer Ni^{2+} ions. Take 200 µl 1 µm amino-polystyrene beads at 2.6% into a 1.7 ml eppendorf and add 300 µl 100 mM MOPS pH 7.5. Standard spin is 10 000 rpm 1 min to pellet beads. Spin and wash in 500 µl 100 mM MOPS pH 7.5 four times. Spin and resuspend in 10 mM sulfo-EGS solution and place on shaker for 20 mins. Spin and wash in 500 µl 100 mM MOPS pH 7.5 four times. Spin and resuspend in AB-NTA solution and place on shaker for 60 mins. Spin and wash in 500 µl 100 mM MOPS pH 7.5 four times. Spin and resuspend in 500 µl $NiCl_2$ solution and incubate 5 mins (shaker unnecessary over this time frame). Repeat this process three more times with 5 min incubations each time. Spin and wash in 500 µl 100 mM MOPS pH 7.5 four times. Final volume 500 µl. The success of the protocol is generally readily apparent by a green tinge to the bead pellet, indicating retention of Ni. Transfer into a new eppendorf for storage.

Fluorescent Spectral Parameters

The "Bodipy" filter cube, so-called as it was originally selected for the Bodipy fluorophore but proved to give clearly visible levels of fluorescence for pyranine and NBD-PE fluorophores also, was the cube used for all fluorescent images presented in Chapters 4 and 5.

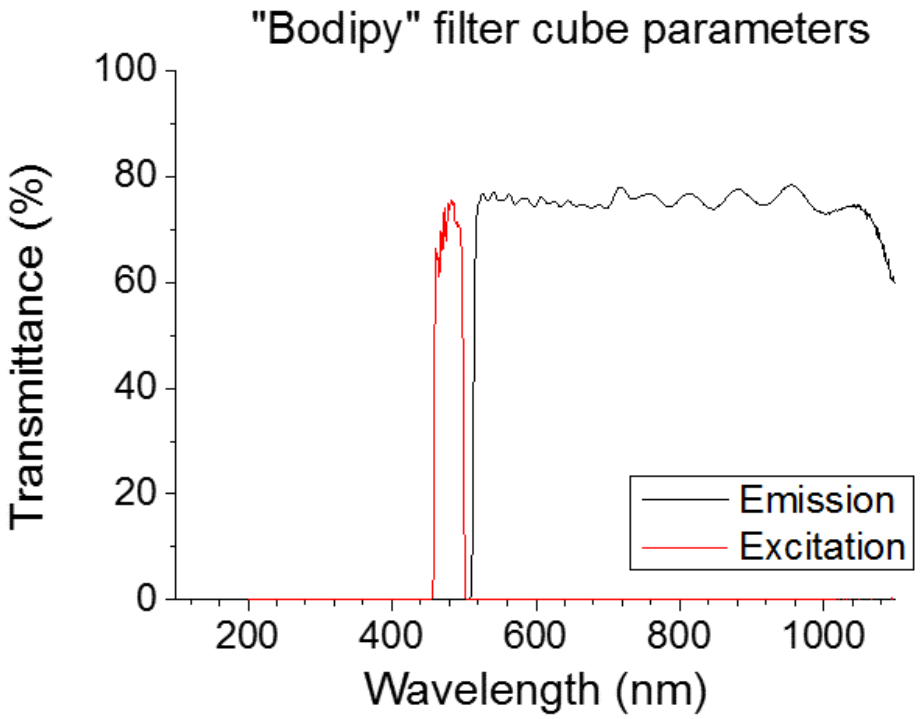

Figure A-1. Transmittance properties across 200 nm – 1100 nm wavelengths as measured in a spectrometer of the fluorescent filter cube set (dichroic, excitation, and emission filter) used for all fluorescent images presented in this thesis. Excitation is provided by a mercury arc-lamp which, based on data provided by the manufacturer (Nikon) provides broadly constant intensity over the roughly 460 nm – 500 nm region in which excitation is highly transmitted.

Plasmid Sequences

The following sequences and plasmid map were obtained courtesy of Dr Robert Ishmukhametov and represent the four F_1F_O mutants used in this study; cysteine free, α-subunit cysteine insertion, c-subunit cysteine insertion, and both α- and c-subunit cysteine insertion. Note his-tags are present in all cases on the β-subunits

inserted four amino acids from the N-terminus; this can be seen as "caccatcaccatcatcat" – both "cac" and "cat" representing histidine.

pVF2 plasmid for cysteine-free F_1F_O – entire sequence

agctttcaaagttctggcgatgttggtgttactggtggtggcgttggcggttttaaaggcggtattcttgccgctgatcg
ttacgtgggttttggtgctggtggttcagatactggcaccggctgtaattaacaacaaagggtaaaaggcatcatggc
ttcagaaaatatgacgccgcaggattacataggacaccacctgaataaccttcagctggacctgcgtacattctcgct
ggtggatccacaaaaccccccagccaccttctggacaatcaatattgactccatgttcttctcggtggtgctgggtctg
ttgttcctggttttattccgtagcgtagccaaaaaggcgaccagcggtgtgccaggtaagtttcagaccgcgattgag
ctggtgatcggctttgttaatggtagcgtgaaagacatgtaccatggcaaaagcaagctgattgctccgctggccctg
acgatcttcgtctgggtattcctgatgaacctgatggatttactgcctatcgacctgctgccgtacattgctgaacatgt
actgggtctgcctgcactgcgtgtggttccgtctgcggacgtgaacgtaacgctgtctatggcactgggcgtatttatc
ctgattctgttctacagcatcaaaatgaaaggcatcggcggcttcacgaaagagttgacgctgcagccgttcaatcac
tgggcgttcattcctgtcaacttaatccttgaaggggtaagcctgctgtccaaaccagtttcactcggtttgcgactgtt
cggtaacatgtatgccggtgagctgattttcattctgattgctggtctgttgccgtggtggtcacagtggatcctgaatg
tgccgtgggccattttccacatcctgatcattacgctgcaagccttcatcttcatggttctgacgatcgtctatctgtcg
atggcgtctgaagaacattaatttaccaacactactacgttttaactgaaacaaactggagactgtcatggaaaacct
gaatatggatctgctgtacatggctgccgctgtgatgatgggtctggcggcaatcggtgctgcgatcggtatcggcat
cctcgggggtaaattcctggaaggcgcagcgcgtcaacctgatctgattcctctgctgcgtactcagttctttatcgtt
atgggtctggtggatgctatcccgatgatcgctgtaggtctgggtctgtacgtgatgttcgctgtcgcgtagtaagcgt
tgcttttatttaaagagcaatatcagaacgttaactaaatagaggcattgtgctgtgaatcttaacgcaacaatcctcg
gccaggccatcgcgtttgtcctgttcgttctgttcgccatgaagtacgtatggccgccattaatggcagccatcgaaaa
acgtcaaaaagaaattgctgacggccttgcttccgcagaacgagcacataaggaccttgaccttgcaaaggccagc

gcgaccgaccagctgaaaaaagcgaaagcggaagcccaggtaatcatcgagcaggcgaacaaacgccgctcgca

gattctggacgaagcgaaagctgaggcagaacaggaacgtactaaaatcgtggcccaggcgcaggcggaaattga

agccgagcgtaaacgtgcccgtgaagagctgcgtaagcaagttgctatcctggctgttgctggcgccgagaagatca

tcgaacgttccgtggatgaagctgctaacagcgacatcgtggataaacttgtcgctgaactgtaaggagggaggggc

tgatgtctgaatttattacggtagctcgcccctacgccaaagcagcttttgactttgccgtcgaacaccaaagtgtaga

acgctggcaggacatgctggcgtttgccgccgaggtaaccaaaaacgaacaaatggcagagcttctctctggcgcg

cttgcgccagaaacgctcgccgagtcgtttatcgcagttgctggtgagcaactggacgaaaacggtcagaacctgat

tcgggttatggctgaaaatggtcgtcttaacgcgctcccggatgttctggagcagtttattcacctgcgtgccgtgagt

gaggctaccgctgaggtagacgtcatttccgctgccgcactgagtgaacaacagctcgcgaaaatttctgctgcgat

ggaaaaacgtctgtcacgcaaagttaagctgaatgccaaaatcgataagtctgtaatggcaggcgttatcatccgag

cgggtgatatggtcattgatggcagcgtacgcggtcgtcttgagcgccttgcagacgtcttgcagtcttaaggggact

ggagcatgcaactgaattccaccgaaatcagcgaactgatcaagcagcgcattgctcagttcaatgttgtgagtgaa

gctcacaacgaaggtactattgtttctgtaagtgacggtgttatccgcattcacggcctggccgatgctatgcagggtg

aaatgatctccctgccgggtaaccgttacgctatcgcactgaacctcgagcgcgactctgtaggtgcggttgttatgg

gtccgtacgctgaccttgccgaaggcatgaaagttaaggctactggacgtatcctggaagttccggttggccgtggc

ctgctgggccgtgtggttaacactctgggtgcaccaatcgacggtaaaggtccgctggatcacgacggcttctctgct

gtagaagcaatcgctccgggcgttatcgaacgtcagtccgtagatcagccggtacagaccggttataaagccgttga

ctccatgatcccaatcggtcgtggtcagcgtgaattgatcatcggtgaccgtcagacaggtaaaaccgcactggctat

cgatgccatcatcaaccagcgcgattccggtatcaaagctatctatgtcgctatcggccagaaagcgtccaccatttc

taacgtggtacgtaaactggaagagcacggcgcactggctaacaccatcgttgtggtagcaaccgcgtctgaatccg

ctgcactgcaatacctggcaccgtatgccggtgccgccatgggtgaatacttccgtgaccgcggtgaagatgcgctg

atcatttacgatgacctgtctaaacaggctgttgcttaccgtcagatctccctgctgctccgtcgtccgccaggacgtg

aagcattcccgggcgacgttttctacctccactctcgtctgctggagcgtgctgcacgtgttaacgccgaatacgttga

agccttcaccaaaggtgaagtgaaagggaaaaccggttctctgaccgcactgccgattatcgaaactcaggcgggt

gacgtttctgcgttcgttccgaccaacgtaatctccattaccgatggtcagatcttcctggaaaccaacctgttcaacg

ccggtattcgtcctgcggttaacccgggtatttccgtatcccgtgttggtggtgcagcacagaccaagatcatgaaaa

aactgtccggtggtatccgtaccgctctggcacagtatcgtgaactggcagcgttctctcagtttgcatccgaccttga

cgatgcaacacgtaaccagcttgaccacggtcagaaagtgaccgaactgctgaaacagaaacagtatgcgccgatg

tccgttgcgcagcagtctctggttctgttcgcagcagaacgtggttacctggcggatgttgaactgtcgaaaattggc

agcttcgaagccgctctgctggcttacgtcgaccgtgatcacgctccgttgatgcaagagatcaaccagaccggtgg

ctacaacgacgaaatcgaaggcaagctgaaaggcatcctcgattccttcaaagcaacccaatcctggtaacgtctgg

cgggtacccttagggcaggccgcaaggcattgaggagaagctcatggccggcgcaaaagacatacgtagtaagat

cgcaagcgtccagaacacgcaaaagatcactaaagcgatggagatggtcgccgcttccaaaatgcgtaaatcgcag

gatcgcatggcggccagccgtccttatgcagaaaccatgcgcaaagtgattggtcaccttgcacacggtaatctgga

atataagcacccttacctggaagaccgcgacgttaaacgcgtgggctacctggtggtgtcgaccgaccgtggtttgg

cgggtggtttgaacattaacctgttcaaaaaactgctggcggaaatgaagacctggaccgacaaaggcgttcaagcc

gacctcgcaatgatcggctcgaaaggcgtgtcgttcttcaactccgtgggcggcaatgttgttgcccaggtcaccggc

atgggggataacccttccctgtccgaactgatcggtccggtaaaagtgatgttgcaggcctacgacgaaggccgtct

ggacaaactttacattgtcagcaacaaatttattaacaccatgtctcaggttccgaccatcagccagctgctgccgtta

ccggcatcagatgatgatgatctgaaacataaatcctgggattacctgtacgaacccgatccgaaggcgttgctggat

accctgctgcgtcgttatgtcgaatctcaggtttatcagggcgtggttgaaaacctggccagcgagcaggccgcccgt

atggtggcgatgaaagccgcgaccgacaatggcggcagcctgattaaagagctgcagttggtatacaacaaagctc

gtcaggccagcattactcaggaactcaccgagatcgtctcgggggccgccgcggtttaaacaggttaactagtagag

gatttaagatgagaggatctcaccatcaccatcatcatggcatggctactggaaagattgtccaggtaatcggcgccg

tagttgacgtcgaattccctcaggatgccgtaccgcgcgtgtacgatgctcttgaggtgcaaaatggtaatgagcgtc

tggtgctggaagttcagcagcagctcggcggcggtatcgtacgtaccatcgcaatgggttcctccgacggtctgcgt

cgcggtctggatgtaaaagacctcgaacacccgattgaagtcccggtaggtaaagcgactctgggccgtatcatgaa

cgtactgggtgaaccggtcgacatgaaaggcgagatcggtgaagaagagcgttgggcgattcaccgcgcagcacct

tcctacgaagagctgtcaaactctcaggaactgctggaaaccggtatcaaagttatcgacctgatggccccgttcgct

aagggcggtaaagttggtctgttcggtggtgcgggtgtaggtaaaaccgtaaacatgatggagctcattcgtaacatc

gcgatcgagcactccggttactctgtgtttgcgggcgtaggtgaacgtactcgtgagggtaacgacttctaccacgaa

atgaccgactccaacgttatcgacaaagtatccctggtgtatggccagatgaacgagccgccgggaaaccgtctgcg

cgttgctctgaccggtctgaccatggctgagaaattccgtgacgaaggtcgtgacgttctgctgttcgttgacaacatc

tatcgttacaccctggccggtacggaagtatccgcactgctgggccgtatgccttcagcggtaggttatcagccgacc

ctggcggaagagatgggcgttctgcaggaacgtatcacctccaccaaaactggttctatcacctccgtacaggcagt

atacgtacctgcggatgacttgactgacccgtctccggcaaccacctttgcgcaccttgacgcaaccgtggtactgag

ccgtcagatcgcgtctctgggtatctacccggccgttgacccgctggactccaccagccgtcagctggacccgctgg

tggttggtcaggaacactacgacaccgcgcgtggcgttcagtccatcctgcaacgttatcaggaactgaaagacatc

atcgccatcctgggtatggatgaactgtctgaagaagacaaactggtggtagcgcgtgctcgtaagatccagcgctt

cctgtcccagccgttcttcgtggcagaagtattcaccggttctccgggtaaatacgtctccctgaaagacaccatccgt

ggctttaaaggcatcatggaaggcgaatacgatcacctgccggagcaggcgttctacatggtcggttccatcgaaga

agctgtggaaaaagccaaaaaactttaacgccttaatcggagggtgatatggcaatgacttaccacctggacgtcgt

cagcgcagagcaacaaatgttctctggtctggtcgagaaaatccaggtaacgggtagcgaaggtgaactggggatc

taccctggccacgcaccgctgctcaccgccattaagcctggtatgattcgcatcgtgaaacagcacggtcacgaaga

gtttatctatctgtctggcggcattcttgaagtgcagcctggcaacgtgaccgttctggccgacaccgcaattcgcgg

ccaggatctcgacgaagcgcgagccatggaagcgaaacgtaaggctgaagagcacattagcagctctcacggcga

cgtagattacgctcaggcgtctgcggaactggccaaagcgatcgcgcagctgcgcgttatcgagttgaccaaaaaa

gcgatgtaacaccggcttgaaaagcacaaaagccagtctggaaacaggctggctttttttgcgcgtgtgacccgtcc

tgaatagcgttcacatagatcctgctgatataaaaccccccctgttttcctgtttattcattgatcgaaataagagcaaaa

acatccacctgacgcttaaattaaggtactgccttaattttctgcagacaaaaggcgtgacgatggtcgaaaatggcg

ctttcgtcagcggggataatccgttattgaacaatttatcctctgtccatttcacgatgaaaaaaatgtagttttttcaag

gtgaagcggtttgactctagagtcgactctagcggagtgtatactggcttactatgttggcactgatgagggtgtcagt

gaagtgcttcatgtggcaggagaaaaaaggctgcaccggtgcgtcagcagaatatgtgatacaggatatattccgct

tcctcgctcactgactcgctacgctcggtcgttcgactgcggcgagcggaaatggcttacgaacggggcggagattt

cctggaagatgccaggaagatacttaacagggaagtgagagggccgcggcaaagccgtttttccataggctccgcc

cccctgacaagcatcacgaaatctgacgctcaaatcagtggtggcgaaacccgacaggactataaagataccaggc

gtttccccctggcggctccctcgtgcgctctcctgttcctgcctttcggtttaccggtgtcattccgctgttatggccgc

gtttgtctcattccacgcctgacactcagttccgggtaggcagttcgctccaagctggactgtatgcacgaacccccc

gttcagtccgaccgctgcgccttatccggtaactatcgtcttgagtccaacccggaaagacatgcaaaagcaccactg

gcagcagccactggtaattgatttagaggagttagtcttgaagtcatgcgccggttaaggctaaactgaaaggacaa

gttttggtgactgcgctcctccaagccagttacctcggttcaaagagttggtagctcagagaaccttcgaaaaaccgc

cctgcaaggcggtttttcgttttcagagcaagagattacgcgcagaccaaaacgatctcaagaagatcatcttattaa

ggggtctgacgctcagtggaacgaaaactcacgttaagggattttggtcatgagattatcaaaaaggatcttcaccta

gatccttttaaattaaaaatgaagttttaaatcaatctaaagtatatatgagtaaacttggtctgacagttaccaatgctt

aatcagtgaggcacctatctcagcgatctgtctatttcgttcatccatagttgcctgactccccgtcgtgtagataacta

cgatacgggagggcttaccatctggccccagtgctgcaatgataccgcgagacccacgctcaccggctccagattta

tcagcaataaaccagccagccggaagggccgagcgcagaagtggtcctgcaactttatccgcctccatccagtctat

taattgttgccgggaagctagagtaagtagttcgccagttaatagtttgcgcaacgttgttgccattgctgcaggcatc

gtggtgtcacgctcgtcgtttggtatggcttcattcagctccggttcccaacgatcaaggcgagttacatgatccccca

tgttgtgcaaaaaagcggttagctccttcggtcctccgatcgttgtcagaagtaagttggccgcagtgttatcactcat

ggttatggcagcactgcataattctcttactgtcatgccatccgtaagatgcttttctgtgactggtgagtactcaacca

agtcattctgagaatagtgtatgcggcgaccgagttgctcttgcccggcgtcaacacgggataataccgcgccacat

agcagaactttaaaagtgctcatcattggaaaacgttcttcggggcgaaaactctcaaggatcttaccgctgttgaga

tccagttcgatgtaacccactcgtgcacccaactgatcttcagcatcttttactttcaccagcgtttctgggtgagcaaa

aacaggaaggcaaaatgccgcaaaaaagggaataagggcgacacggaaatgttgaatactcatactcttccttttc

aatattattgaagcatttatcagggttattgtctcatgagcggatacatatttgaatgtatttagaaaaataaacaaata

ggggttccgcgcacatttccccgaaaagtgccacctgacgtctaagaaaccattattatcatgacattaacctataaa

aataggcgtatcacgaggccctttcgtcttcaagaattttataaaccgtggagcgggcaatactgagctgatgagcaa

tttccgttgcaccagtgcccttctgatgaagcgtcagcacgacgttcctgtccacggtacgcctgcggccaaatttgat

tcctttcagctttgcttcctgtcggccctcattcgtgcgctctaggatca

Individual subunits (in each case these can be found as part of the sequence above, in the order in which they are here listed):

a-subunit

atggcttcagaaaatatgacgccgcaggattacataggacaccacctgaataaccttcagctggacctgcgtacattc

tcgctggtggatccacaaaacccccccagccaccttctggacaatcaatattgactccatgttcttctcggtggtgctgg

gtctgttgttcctggttttattccgtagcgtagccaaaaaggcgaccagcggtgtgccaggtaagtttcagaccgcgat

tgagctggtgatcggctttgttaatggtagcgtgaaagacatgtaccatggcaaaagcaagctgattgctccgctggc

cctgacgatcttcgtctgggtattcctgatgaacctgatggatttactgcctatcgacctgctgccgtacattgctgaac

atgtactgggtctgcctgcactgcgtgtggttccgtctgcggacgtgaacgtaacgctgtctatggcactgggcgtatt

tatcctgattctgttctacagcatcaaaatgaaaggcatcggcggcttcacgaaagagttgacgctgcagccgttcaa

tcactgggcgttcattcctgtcaacttaatccttgaaggggtaagcctgctgtccaaaccagtttcactcggtttgcga

ctgttcggtaacatgtatgccggtgagctgattttcattctgattgctggtctgttgccgtggtggtcacagtggatcct

gaatgtgccgtgggccattttccacatcctgatcattacgctgcaagccttcatcttcatggttctgacgatcgtctatc

tgtcgatggcgtctgaagaacattaa

c-subunit

atggaaaacctgaatatggatctgctgtacatggctgccgctgtgatgatgggtctggcggcaatcggtgctgcgatc

ggtatcggcatcctcgggggtaaattcctggaaggcgcagcgcgtcaacctgatctgattcctctgctgcgtactcag

ttctttatcgttatgggtctggtggatgctatcccgatgatcgctgtaggtctgggtctgtacgtgatgttcgctgtcgc

gtag

b-subunit

atgaagtacgtatggccgccattaatggcagccatcgaaaaacgtcaaaaagaaattgctgacggccttgcttccgc

agaacgagcacataaggaccttgaccttgcaaaggccagcgcgaccgaccagctgaaaaaagcgaaagcggaag

cccaggtaatcatcgagcaggcgaacaaacgccgctcgcagattctggacgaagcgaaagctgaggcagaacagg

aacgtactaaaatcgtggcccaggcgcaggcggaaattgaagccgagcgtaaacgtgcccgtgaagagctgcgtaa

gcaagttgctatcctggctgttgctggcgccgagaagatcatcgaacgttccgtggatgaagctgctaacagcgaca

tcgtggataaacttgtcgctgaactgtaa

δ-subunit

atgtctgaatttattacggtagctcgcccctacgccaaagcagcttttgactttgccgtcgaacaccaaagtgtagaac

gctggcaggacatgctggcgtttgccgccgaggtaaccaaaaacgaacaaatggcagagcttctctctggcgcgctt

gcgccagaaacgctcgccgagtcgtttatcgcagttgctggtgagcaactggacgaaaacggtcagaacctgattcg

ggttatggctgaaaatggtcgtcttaacgcgctcccggatgttctggagcagtttattcacctgcgtgccgtgagtgag

gctaccgctgaggtagacgtcatttccgctgccgcactgagtgaacaacagctcgcgaaaatttctgctgcgatgga

aaaacgtctgtcacgcaaagttaagctgaatgccaaaatcgataagtctgtaatggcaggcgttatcatccgagcgg

gtgatatggtcattgatggcagcgtacgcggtcgtcttgagcgccttgcagacgtcttgcagtcttaa

α-subunit

atgcaactgaattccaccgaaatcagcgaactgatcaagcagcgcattgctcagttcaatgttgtgagtgaagctcac

aacgaaggtactattgtttctgtaagtgacggtgttatccgcattcacggcctggccgatgctatgcagggtgaaatg

atctccctgccgggtaaccgttacgctatcgcactgaacctcgagcgcgactctgtaggtgcggttgttatgggtccg

tacgctgaccttgccgaaggcatgaaagttaaggctactggacgtatcctggaagttccggttggccgtggcctgctg

ggccgtgtggttaacactctgggtgcaccaatcgacggtaaaggtccgctggatcacgacggcttctctgctgtaga

agcaatcgctccgggcgttatcgaacgtcagtccgtagatcagccggtacagaccggttataaagccgttgactccat

gatcccaatcggtcgtggtcagcgtgaattgatcatcggtgaccgtcagacaggtaaaaccgcactggctatcgatg

ccatcatcaaccagcgcgattccggtatcaaagctatctatgtcgctatcggccagaaagcgtccaccatttctaacgt

ggtacgtaaactggaagagcacggcgcactggctaacaccatcgttgtggtagcaaccgcgtctgaatccgctgcac

tgcaatacctggcaccgtatgccggtgccgccatgggtgaatacttccgtgaccgcggtgaagatgcgctgatcattt

acgatgacctgtctaaacaggctgttgcttaccgtcagatctccctgctgctccgtcgtccgccaggacgtgaagcat

tcccgggcgacgttttctacctccactctcgtctgctggagcgtgctgcacgtgttaacgccgaatacgttgaagcctt

caccaaaggtgaagtgaaagggaaaaccggttctctgaccgcactgccgattatcgaaactcaggcgggtgacgttt

ctgcgttcgttccgaccaacgtaatctccattaccgatggtcagatcttcctggaaaccaacctgttcaacgccggtat

tcgtcctgcggttaacccgggtatttccgtatcccgtgttggtggtgcagcacagaccaagatcatgaaaaaactgtc

cggtggtatccgtaccgctctggcacagtatcgtgaactggcagcgttctctcagtttgcatccgaccttgacgatgca

acacgtaaccagcttgaccacggtcagaaagtgaccgaactgctgaaacagaaacagtatgcgccgatgtccgttg

cgcagcagtctctggttctgttcgcagcagaacgtggttacctggcggatgttgaactgtcgaaaattggcagcttcg

aagccgctctgctggcttacgtcgaccgtgatcacgctccgttgatgcaagagatcaaccagaccggtggctacaac

gacgaaatcgaaggcaagctgaaaggcatcctcgattccttcaaagcaacccaatcctggtaa

ϒ-subunit

atggccggcgcaaaagacatacgtagtaagatcgcaagcgtccagaacacgcaaaagatcactaaagcgatggag

atggtcgccgcttccaaaatgcgtaaatcgcaggatcgcatggcggccagccgtccttatgcagaaaccatgcgcaa

agtgattggtcaccttgcacacggtaatctggaatataagcacccttacctggaagaccgcgacgttaaacgcgtgg

gctacctggtggtgtcgaccgaccgtggtttggcgggtggtttgaacattaacctgttcaaaaaactgctggcggaaa

tgaagacctggaccgacaaaggcgttcaagccgacctcgcaatgatcggctcgaaaggcgtgtcgttcttcaactcc

gtgggcggcaatgttgttgcccaggtcaccggcatgggggataacccttccctgtccgaactgatcggtccggtaaa

agtgatgttgcaggcctacgacgaaggccgtctggacaaactttacattgtcagcaacaaatttattaacaccatgtct

caggttccgaccatcagccagctgctgccgttaccggcatcagatgatgatgatctgaaacataaatcctgggattac

ctgtacgaacccgatccgaaggcgttgctggataccctgctgcgtcgttatgtcgaatctcaggtttatcagggcgtg

gttgaaaacctggccagcgagcaggccgcccgtatggtggcgatgaaagccgcgaccgacaatggcggcagcctg

attaaagagctgcagttggtatacaacaaagctcgtcaggccagcattactcaggaactcaccgagatcgtctcggg

ggccgccgcggtttaa

β-subunit

atgagaggatctcaccatcaccatcatcatggcatggctactggaaagattgtccaggtaatcggcgccgtagttgac

gtcgaattccctcaggatgccgtaccgcgcgtgtacgatgctcttgaggtgcaaaatggtaatgagcgtctggtgctg

gaagttcagcagcagctcggcggcggtatcgtacgtaccatcgcaatgggttcctccgacggtctgcgtcgcggtct

ggatgtaaaagacctcgaacacccgattgaagtcccggtaggtaaagcgactctgggccgtatcatgaacgtactgg

gtgaaccggtcgacatgaaaggcgagatcggtgaagaagagcgttgggcgattcaccgcgcagcaccttcctacga

agagctgtcaaactctcaggaactgctggaaaccggtatcaaagttatcgacctgatggccccgttcgctaagggcg

gtaaagttggtctgttcggtggtgcgggtgtaggtaaaaccgtaaacatgatggagctcattcgtaacatcgcgatcg

agcactccggttactctgtgtttgcgggcgtaggtgaacgtactcgtgagggtaacgacttctaccacgaaatgaccg

actccaacgttatcgacaaagtatccctggtgtatggccagatgaacgagccgccgggaaaccgtctgcgcgttgct

ctgaccggtctgaccatggctgagaaattccgtgacgaaggtcgtgacgttctgctgttcgttgacaacatctatcgtt

acaccctggccggtacggaagtatccgcactgctgggccgtatgccttcagcggtaggttatcagccgaccctggcg

gaagagatgggcgttctgcaggaacgtatcacctccaccaaaactggttctatcacctccgtacaggcagtatacgta

cctgcggatgacttgactgacccgtctccggcaaccacctttgcgcaccttgacgcaaccgtggtactgagccgtca

gatcgcgtctctgggtatctacccggccgttgacccgctggactccaccagccgtcagctggacccgctggtggttg

gtcaggaacactacgacaccgcgcgtggcgttcagtccatcctgcaacgttatcaggaactgaaagacatcatcgcc

atcctgggtatggatgaactgtctgaagaagacaaactggtggtagcgcgtgctcgtaagatccagcgcttcctgtcc

cagccgttcttcgtggcagaagtattcaccggttctccgggtaaatacgtctccctgaaagacaccatccgtggcttta
aaggcatcatggaaggcgaatacgatcacctgccggagcaggcgttctacatggtcggttccatcgaagaagctgtg
gaaaaagccaaaaaactttaa

ε-subunit

atggcaatgacttaccacctggacgtcgtcagcgcagagcaacaaatgttctctggtctggtcgagaaaatccaggt
aacgggtagcgaaggtgaactggggatctaccctggccacgcaccgctgctcaccgccattaagcctggtatgattc
gcatcgtgaaacagcacggtcacgaagagtttatctatctgtctggcggcattcttgaagtgcagcctggcaacgtga
ccgttctggccgacaccgcaattcgcggccaggatctcgacgaagcgcgagccatggaagcgaaacgtaaggctg
aagagcacattagcagctctcacggcgacgtagattacgctcaggcgtctgcggaactggccaaagcgatcgcgca
gctgcgcgttatcgagttgaccaaaaaagcgatgtaa

Modifications to introduce cysteines:

The above sequences represent the entirely cysteine-free mutant; for the other mutants described in this thesis modifications exist to introduce cysteines on the c-subunit and α-subunit (and a third mutant which carries both). In all cases cysteines are inserted after the second amino acid from the N-terminus; these subunits then read as listed below – “tgc” representing cysteine.

c-subunit including cysteine insertion

atggaaTGCaacctgaatatggatctgctgtacatggctgccgctgtgatgatgggtctggcggcaatcggtgctg
cgatcggtatcggcatcctcgggggtaaattcctggaaggcgcagcgcgtcaacctgatctgattcctctgctgcgta
ctcagttctttatcgttatgggtctggtggatgctatcccgatgatcgctgtaggtctgggtctgtacgtgatgttcgct
gtcgcgtag

α-subunit including cysteine insertion

atgcaaTGCctgaattccaccgaaatcagcgaactgatcaagcagcgcattgctcagttcaatgttgtgagtgaag

ctcacaacgaaggtactattgtttctgtaagtgacggtgttatccgcattcacggcctggccgatgctatgcagggtga

aatgatctccctgccgggtaaccgttacgctatcgcactgaacctcgagcgcgactctgtaggtgcggttgttatggg

tccgtacgctgaccttgccgaaggcatgaaagttaaggctactggacgtatcctggaagttccggttggccgtggcct

gctgggccgtgtggttaacactctgggtgcaccaatcgacggtaaaggtccgctggatcacgacggcttctctgctgt

agaagcaatcgctccgggcgttatcgaacgtcagtccgtagatcagccggtacagaccggttataaagccgttgact

ccatgatcccaatcggtcgtggtcagcgtgaattgatcatcggtgaccgtcagacaggtaaaaccgcactggctatc

gatgccatcatcaaccagcgcgattccggtatcaaagctatctatgtcgctatcggccagaaagcgtccaccatttct

aacgtggtacgtaaactggaagagcacggcgcactggctaacaccatcgttgtggtagcaaccgcgtctgaatccgc

tgcactgcaatacctggcaccgtatgccggtgccgccatgggtgaatacttccgtgaccgcggtgaagatgcgctga

tcatttacgatgacctgtctaaacaggctgttgcttaccgtcagatctccctgctgctccgtcgtccgccaggacgtga

agcattcccgggcgacgttttctacctccactctcgtctgctggagcgtgctgcacgtgttaacgccgaatacgttgaa

gccttcaccaaaggtgaagtgaaagggaaaaccggttctctgaccgcactgccgattatcgaaactcaggcgggtg

acgtttctgcgttcgttccgaccaacgtaatctccattaccgatggtcagatcttcctggaaaccaacctgttcaacgc

cggtattcgtcctgcggttaacccgggtatttccgtatcccgtgttggtggtgcagcacagaccaagatcatgaaaaa

actgtccggtggtatccgtaccgctctggcacagtatcgtgaactggcagcgttctctcagtttgcatccgaccttgac

gatgcaacacgtaaccagcttgaccacggtcagaaagtgaccgaactgctgaaacagaaacagtatgcgccgatgt

ccgttgcgcagcagtctctggttctgttcgcagcagaacgtggttacctggcggatgttgaactgtcgaaaattggca

gcttcgaagccgctctgctggcttacgtcgaccgtgatcacgctccgttgatgcaagagatcaaccagaccggtggc

tacaacgacgaaatcgaaggcaagctgaaaggcatcctcgattccttcaaagcaacccaatcctggtaa

Plasmid map including unique restriction sites

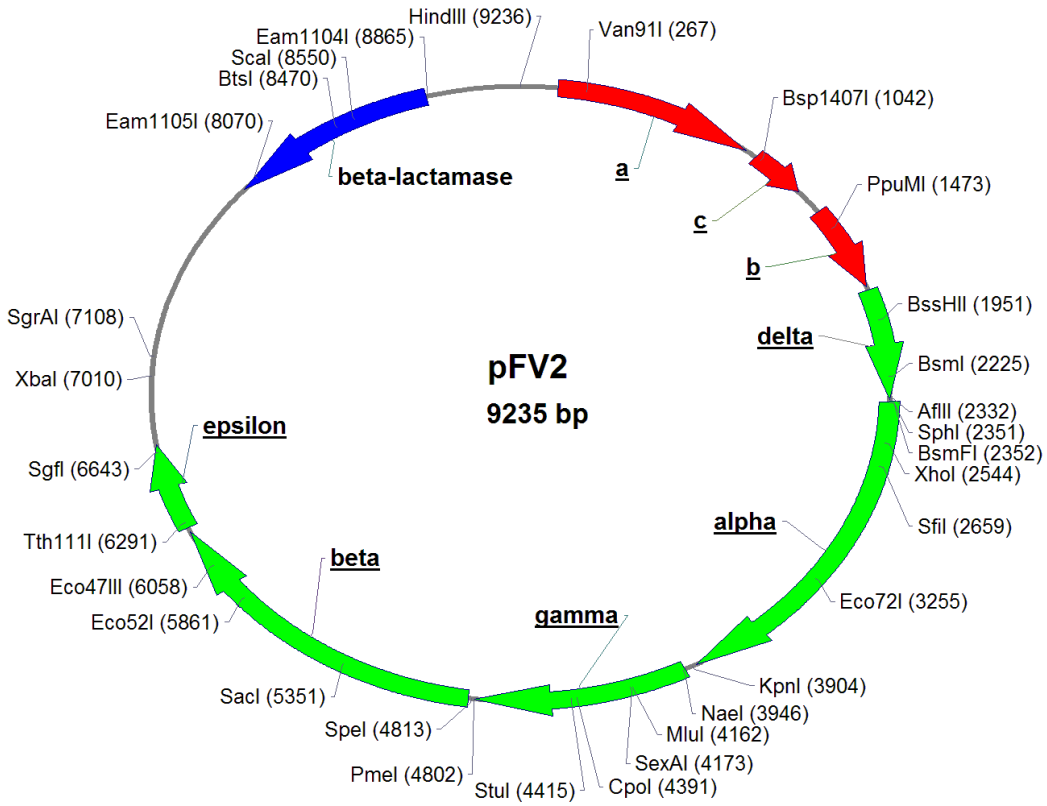

References

[1] D. G. Nicholls and S. Ferguson, *Bioenergetics*. Academic Press, 2013, p. 434.

[2] R. L. Cross and V. Müller, "The evolution of A-, F-, and V-type ATP synthases and ATPases: reversals in function and changes in the H+/ATP coupling ratio.," *FEBS Lett.*, vol. 576, no. 1–2, pp. 1–4, Oct. 2004.

[3] A. Y. Mulkidjanian, K. S. Makarova, M. Y. Galperin, and E. V Koonin, "Inventing the dynamo machine: the evolution of the F-type and V-type ATPases.," *Nat. Rev. Microbiol.*, vol. 5, no. 11, pp. 892–899, Nov. 2007.

[4] A. D. Bangham, "Membrane models with phospholipids," *Prog. Biophys. Mol. Biol.*, vol. 18, pp. 29–95, Jan. 1968.

[5] Y. Sowa and R. M. Berry, "Bacterial flagellar motor.," *Q. Rev. Biophys.*, vol. 41, no. 2, pp. 103–32, May 2008.

[6] H. T. Witt, E. Schlodder, and P. Gräber, "Membrane-bound ATP synthesis generated by an external electrical field," *FEBS Lett.*, vol. 69, no. 1–2, pp. 272–276, Oct. 1976.

[7] M. Bokranz, E. Morschel, and A. Kroger, "Phosphorylation and phosphate-ATP exchange catalyzed by the ATP synthase isolated from Wolinella succinogenes," *Biochim. Biophys. Acta - Bioenerg.*, vol. 810, no. 3, pp. 332–339, Dec. 1985.

[8] U. Junesch and P. Gräber, "The rate of ATP-synthesis as a function of ΔpH and Δψ catalyzed by the active, reduced H+-ATPase from chloroplasts," *FEBS Lett.*, vol. 294, no. 3, pp. 275–278, Dec. 1991.

[9] P. Turina, B. A. Melandri, and P. Graber, "ATP synthesis in chromatophores driven by artificially induced ion gradients," *Eur. J. Biochem.*, vol. 196, no. 1, pp. 225–229, Feb. 1991.

[10] G. Kaim and P. Dimroth, "ATP synthesis by the F1Fo ATP synthase of Escherichia coli is obligatorily dependent on the electric potential," *FEBS Lett.*, vol. 434, no. 1–2, pp. 57–60, Aug. 1998.

[11] B. A. Feniouk, M. A. Kozlova, D. A. Knorre, D. A. Cherepanov, A. Y. Mulkidjanian, and W. Junge, "The proton-driven rotor of ATP synthase: ohmic conductance (10 fS), and absence of voltage gating.," *Biophys. J.*, vol. 86, no. 6, pp. 4094–109, Jun. 2004.

[12] M. Toei, C. Gerle, M. Nakano, K. Tani, N. Gyobu, M. Tamakoshi, N. Sone, M. Yoshida, Y. Fujiyoshi, K. Mitsuoka, and K. Yokoyama, "Dodecamer rotor ring

defines H+/ATP ratio for ATP synthesis of prokaryotic V-ATPase from Thermus thermophilus.," *Proc. Natl. Acad. Sci. U. S. A.*, vol. 104, no. 51, pp. 20256–61, Dec. 2007.

[13] D. Pogoryelov, A. L. Klyszejko, G. O. Krasnoselska, E.-M. Heller, V. Leone, J. D. Langer, J. Vonck, D. J. Müller, J. D. Faraldo-Gómez, and T. Meier, "Engineering rotor ring stoichiometries in the ATP synthase.," *Proc. Natl. Acad. Sci. U. S. A.*, vol. 109, no. 25, pp. E1599–608, Jun. 2012.

[14] S. Fischer and P. Gräber, "Comparison of ΔpH- and Δϕ-driven ATP synthesis catalyzed by the H+-ATPases from Escherichia coli or chloroplasts reconstituted into liposomes," *FEBS Lett.*, vol. 457, no. 3, pp. 327–332, Sep. 1999.

[15] J. Weber, S. T. Hammond, S. Wilke-Mounts, and A. E. Senior, "Mg2+ coordination in catalytic sites of F1-ATPase.," *Biochemistry*, vol. 37, no. 2, pp. 608–14, Jan. 1998.

[16] A. E. Senior, S. Nadanaciva, and J. Weber, "The molecular mechanism of ATP synthesis by F1F0-ATP synthase," *Biochim. Biophys. Acta - Bioenerg.*, vol. 1553, no. 3, pp. 188–211, Feb. 2002.

[17] "Encyclopedia of Biophysics." [Online]. Available: http://www.springer.com/life+sciences/biochemistry+&+biophysics/book/978-3-642-16711-9. [Accessed: 22-Jul-2014].

[18] T. Bilyard, M. Nakanishi-Matsui, B. C. Steel, T. Pilizota, A. L. Nord, H. Hosokawa, M. Futai, and R. M. Berry, "High-resolution single-molecule characterization of the enzymatic states in Escherichia coli F1-ATPase.," *Philos. Trans. R. Soc. Lond. B. Biol. Sci.*, vol. 368, no. 1611, p. 20120023, Feb. 2013.

[19] J. P. Abrahams, A. G. Leslie, R. Lutter, and J. E. Walker, "Structure at 2.8 A resolution of F1-ATPase from bovine heart mitochondria.," *Nature*, vol. 370, no. 6491, pp. 621–8, Aug. 1994.

[20] G. Cingolani and T. M. Duncan, "Structure of the ATP synthase catalytic complex (F(1)) from Escherichia coli in an autoinhibited conformation.," *Nat. Struct. Mol. Biol.*, vol. 18, no. 6, pp. 701–7, Jun. 2011.

[21] H. Sielaff and M. Börsch, "Twisting and subunit rotation in single F(O)(F1)-ATP synthase.," *Philos. Trans. R. Soc. Lond. B. Biol. Sci.*, vol. 368, no. 1611, p. 20120024, Feb. 2013.

[22] J. E. Walker, "The ATP synthase: the understood, the uncertain and the unknown.," *Biochem. Soc. Trans.*, vol. 41, no. 1, pp. 1–16, Feb. 2013.

[23] I. N. Watt, M. G. Montgomery, M. J. Runswick, A. G. W. Leslie, and J. E. Walker, "Bioenergetic cost of making an adenosine triphosphate molecule in animal mitochondria.," *Proc. Natl. Acad. Sci. U. S. A.*, vol. 107, no. 39, pp. 16823–7, Sep. 2010.

[24] D. Pogoryelov, C. Reichen, A. L. Klyszejko, R. Brunisholz, D. J. Muller, P. Dimroth, and T. Meier, "The oligomeric state of c rings from cyanobacterial F-ATP synthases varies from 13 to 15.," *J. Bacteriol.*, vol. 189, no. 16, pp. 5895–902, Aug. 2007.

[25] W. Jiang, J. Hermolin, and R. H. Fillingame, "The preferred stoichiometry of c subunits in the rotary motor sector of Escherichia coli ATP synthase is 10.," *Proc. Natl. Acad. Sci. U. S. A.*, vol. 98, no. 9, pp. 4966–71, Apr. 2001.

[26] M. G. Duser, N. Zarrabi, D. J. Cipriano, S. Ernst, G. D. Glick, S. D. Dunn, and M. Borsch, "36° step size of proton-driven c-ring rotation in FoF1-ATP synthase," *EMBO J.*, vol. 28, no. 18, pp. 2689–2696, Jul. 2009.

[27] R. Ishmukhametov, T. Hornung, D. Spetzler, and W. D. Frasch, "Direct observation of stepped proteolipid ring rotation in E. coli FoF1-ATP synthase," *EMBO J.*, vol. 29, no. 23, pp. 3911–3923, Dec. 2010.

[28] "John E. Walker - Nobel Lecture: ATP Synthesis by Rotary Catalysis." [Online]. Available: http://www.nobelprize.org/nobel_prizes/chemistry/laureates/1997/walker-lecture.html. [Accessed: 22-Jul-2014].

[29] A. Wächter, Y. Bi, S. D. Dunn, B. D. Cain, H. Sielaff, F. Wintermann, S. Engelbrecht, and W. Junge, "Two rotary motors in F-ATP synthase are elastically coupled by a flexible rotor and a stiff stator stalk.," *Proc. Natl. Acad. Sci. U. S. A.*, vol. 108, no. 10, pp. 3924–9, Mar. 2011.

[30] H. Sielaff, H. Rennekamp, A. Wächter, H. Xie, F. Hilbers, K. Feldbauer, S. D. Dunn, S. Engelbrecht, and W. Junge, "Domain compliance and elastic power transmission in rotary F(O)F(1)-ATPase.," *Proc. Natl. Acad. Sci. U. S. A.*, vol. 105, no. 46, pp. 17760–17765, Nov. 2008.

[31] D. Okuno, R. Iino, and H. Noji, "Stiffness of γ subunit of F(1)-ATPase.," *Eur. Biophys. J.*, vol. 39, no. 12, pp. 1589–96, Nov. 2010.

[32] S. Ernst, M. G. Düser, N. Zarrabi, S. D. Dunn, and M. Börsch, "Elastic deformations of the rotary double motor of single F(o)F(1)-ATP synthases detected in real time by Förster resonance energy transfer.," *Biochim. Biophys. Acta*, vol. 1817, no. 10, pp. 1722–31, Oct. 2012.

[33] G. Oster and H. Wang, "Reverse engineering a protein: the mechanochemistry of ATP synthase," *Biochim. Biophys. Acta - Bioenerg.*, vol. 1458, no. 2–3, pp. 482–510, May 2000.

[34] R. Watanabe and H. Noji, “Timing of inorganic phosphate release modulates the catalytic activity of ATP-driven rotary motor protein,” *Nat. Commun.*, vol. 5, p. 3486, Apr. 2014.

[35] R. Watanabe, R. Iino, and H. Noji, “Phosphate release in F1-ATPase catalytic cycle follows ADP release.,” *Nat. Chem. Biol.*, vol. 6, no. 11, pp. 814–20, Nov. 2010.

[36] K. Adachi, K. Oiwa, T. Nishizaka, S. Furuike, H. Noji, H. Itoh, M. Yoshida, and K. Kinosita, “Coupling of rotation and catalysis in F(1)-ATPase revealed by single-molecule imaging and manipulation.,” *Cell*, vol. 130, no. 2, pp. 309–21, Jul. 2007.

[37] B. A. Feniouk, T. Suzuki, and M. Yoshida, “The role of subunit epsilon in the catalysis and regulation of FOF1-ATP synthase.,” *Biochim. Biophys. Acta*, vol. 1757, no. 5–6, pp. 326–38, Jan. 2006.

[38] T. Elston, H. Wang, and G. Oster, “Energy transduction in ATP synthase.,” *Nature*, vol. 391, no. 6666, pp. 510–3, Jan. 1998.

[39] A. Aksimentiev, I. A. Balabin, R. H. Fillingame, and K. Schulten, “Insights into the molecular mechanism of rotation in the Fo sector of ATP synthase.,” *Biophys. J.*, vol. 86, no. 3, pp. 1332–44, Mar. 2004.

[40] R. H. Fillingame, C. M. Angevine, and O. Y. Dmitriev, “Coupling proton movements to c-ring rotation in F1Fo ATP synthase: aqueous access channels and helix rotations at the a–c interface,” *Biochim. Biophys. Acta - Bioenerg.*, vol. 1555, no. 1–3, pp. 29–36, Sep. 2002.

[41] M. E. Pullman, H. S. Penefsky, A. Datta, and E. Racker, “Partial Resolution of the Enzymes Catalyzing Oxidative Phosphorylation. I. Purification and Properties of Soluble, Dinitrophenol-Stimulated Adenosine Triphosphate,” 1960.

[42] M. E. Pullman, H. S. Penefsky, A. Datta, E. Racker, C. Oxidative, and P. Ii, “Partial resolution of the enzymes catalyzing oxidative phosphorylation. II. Participation of a soluble adenosine tolphosphatase in oxidative phosphorylation.,” *J. Biol. Chem.*, vol. 235, pp. 3330–6, Nov. 1960.

[43] Y. Kagawa, E. Racker, and J. B. C. A. Sites, “Partial resolution of the enzymes catalyzing oxidative phosphorylation. 8. Properties of a factor conferring oligomycin sensitivity on mitochondrial adenosine triphosphatase.,” *J. Biol. Chem.*, vol. 241, no. 10, pp. 2461–6, May 1966.

[44] P. Mitchell, “Coupling of Phosphorylation to Electron and Hydrogen Transfer by a Chemi-Osmotic type of Mechanism,” *Nature*, vol. 191, no. 4784, pp. 144–148, Jul. 1961.

[45] Y. Kagawa and E. Racker, “Partial Resolution of the Enzymes Catalyzing Oxidative Phosphorylation. XXV. Reconstitution of Vesicles Catalyzing 32Pi;Adenosine Triphosphate Exchange,” *J. Biol. Chem.*, vol. 246, no. 17, pp. 5477–5487, Sep. 1971.

[46] A. T. Jagendorf and E. Uribe, “ATP formation caused by acid-base transition of spinach chloroplasts.,” *Proc. Natl. Acad. Sci. U. S. A.*, vol. 55, no. 1, pp. 170–7, Jan. 1966.

[47] N. Sone, M. Yoshida, H. Hirata, and Y. Kagawa, “Adenosine triphosphate synthesis by electrochemical proton gradient in vesicles reconstituted from purified adenosine triphosphatase and phospholipids of thermophilic bacterium.,” *J. Biol. Chem.*, vol. 252, no. 9, pp. 2956–60, May 1977.

[48] G. D. Winget, N. Kanner, and R. Efraim, “Formation of ATP by the adenosine triphosphatase complex from spinach chloroplasts reconstituted together with bacteriorhodopsin,” *Biochim. Biophys. Acta - Bioenerg.*, vol. 460, no. 3, pp. 490–499, Jun. 1977.

[49] C. Kayalar, J. Rosing, and P. D. Boyer, “An alternating site sequence for oxidative phosphorylation suggested by measurement of substrate binding patterns and exchange reaction inhibitions.,” *J. Biol. Chem.*, vol. 252, no. 8, pp. 2486–91, Apr. 1977.

[50] M. J. Gresser, J. A. Myers, and P. D. Boyer, “Catalytic site cooperativity of beef heart mitochondrial F1 adenosine triphosphatase. Correlations of initial velocity, bound intermediate, and oxygen exchange measurements with an alternating three-site model.,” *J. Biol. Chem.*, vol. 257, no. 20, pp. 12030–8, Oct. 1982.

[51] H. Noji, R. Yasuda, M. Yoshida, and K. Kinosita, “Direct observation of the rotation of F1-ATPase,” *Nature*, vol. 386, no. 6622, pp. 299–302, Mar. 1997.

[52] T. M. Duncan, V. V Bulygin, Y. Zhou, M. L. Hutcheon, and R. L. Cross, “Rotation of subunits during catalysis by Escherichia coli F1-ATPase.,” *Proc. Natl. Acad. Sci. U. S. A.*, vol. 92, no. 24, pp. 10964–8, Nov. 1995.

[53] D. Sabbert, S. Engelbrecht, and W. Junge, “Intersubunit rotation in active F-ATPase.,” *Nature*, vol. 381, no. 6583, pp. 623–5, Jun. 1996.

[54] H. Omote, N. Sambonmatsu, K. Saito, Y. Sambongi, a Iwamoto-Kihara, T. Yanagida, Y. Wada, and M. Futai, “The gamma-subunit rotation and torque generation in F1-ATPase from wild-type or uncoupled mutant Escherichia coli.,” *Proc. Natl. Acad. Sci. U. S. A.*, vol. 96, no. 14, pp. 7780–4, Jul. 1999.

[55] Y. Kato-Yamada, H. Noji, R. Yasuda, K. Kinosita, and M. Yoshida, “Direct Observation of the Rotation of ε Subunit in F1-ATPase,” *J. Biol. Chem.*, vol. 273, no. 31, pp. 19375–19377, Jul. 1998.

[56] Y. Sambongi, Y. Iko, M. Tanabe, H. Omote, A. Iwamoto-Kihara, I. Ueda, T. Yanagida, Y. Wada, and M. Futai, "Mechanical Rotation of the c Subunit Oligomer in ATP Synthase (F0F1): Direct Observation," *Science (80-.).*, vol. 286, no. 5445, pp. 1722–1724, Nov. 1999.

[57] O. Pänke, K. Gumbiowski, W. Junge, and S. Engelbrecht, "F-ATPase: specific observation of the rotating c subunit oligomer of EF(o)EF(1).," *FEBS Lett.*, vol. 472, no. 1, pp. 34–38, Apr. 2000.

[58] S. Kudo, Y. Magariyama, and S. Aizawa, "Abrupt changes in flagellar rotation observed by laser dark-field microscopy.," *Nature*, vol. 346, no. 6285, pp. 677–680, Aug. 1990.

[59] R. Yasuda, H. Noji, M. Yoshida, K. Kinosita, and H. Itoh, "Resolution of distinct rotational substeps by submillisecond kinetic analysis of F1-ATPase," *Nature*, vol. 410, no. 6831, pp. 898–904, Apr. 2001.

[60] R. Yasuda, H. Noji, K. Kinosita, and M. Yoshida, "F1-ATPase Is a Highly Efficient Molecular Motor that Rotates with Discrete 120° Steps," *Cell*, vol. 93, no. 7, pp. 1117–1124, Jun. 1998.

[61] K. Shimabukuro, R. Yasuda, E. Muneyuki, K. Y. Hara, K. Kinosita, and M. Yoshida, "Catalysis and rotation of F1 motor: cleavage of ATP at the catalytic site occurs in 1 ms before 40 degree substep rotation.," *Proc. Natl. Acad. Sci. U. S. A.*, vol. 100, no. 25, pp. 14731–6, Dec. 2003.

[62] T. Nishizaka, K. Oiwa, H. Noji, S. Kimura, E. Muneyuki, M. Yoshida, and K. Kinosita, "Chemomechanical coupling in F1-ATPase revealed by simultaneous observation of nucleotide kinetics and rotation.," *Nat. Struct. Mol. Biol.*, vol. 11, no. 2, pp. 142–8, Feb. 2004.

[63] H. Itoh, A. Takahashi, K. Adachi, H. Noji, R. Yasuda, M. Yoshida, and K. Kinosita, "Mechanically driven ATP synthesis by F1-ATPase," *Nature*, vol. 427, no. 6973, pp. 465–468, Jan. 2004.

[64] H. Ueno, T. Suzuki, K. Kinosita, and M. Yoshida, "ATP-driven stepwise rotation of FoF1-ATP synthase.," *Proc. Natl. Acad. Sci. U. S. A.*, vol. 102, no. 5, pp. 1333–8, Feb. 2005.

[65] M. Toei and H. Noji, "Single-molecule analysis of FoF1-ATP synthase inhibited by N,N-dicyclohexylcarbodiimide.," *J. Biol. Chem.*, vol. 288, no. 36, pp. 25717–26, Sep. 2013.

[66] K. Nishio, A. Iwamoto-Kihara, A. Yamamoto, Y. Wada, and M. Futai, "Subunit rotation of ATP synthase embedded in membranes: a or beta subunit rotation relative to the c subunit ring.," *Proc. Natl. Acad. Sci. U. S. A.*, vol. 99, no. 21, pp. 13448–52, Oct. 2002.

[67] M. Börsch, M. Diez, B. Zimmermann, R. Reuter, and P. Gräber, "Stepwise rotation of the γ-subunit of EFoF1-ATP synthase observed by intramolecular single-molecule fluorescence resonance energy transfer," *FEBS Lett.*, vol. 527, no. 1–3, pp. 147–152, Sep. 2002.

[68] S. Ernst, M. G. Düser, N. Zarrabi, and M. Börsch, "Three-color Förster resonance energy transfer within single F_0F_1-ATP synthases: monitoring elastic deformations of the rotary double motor in real time.," *J. Biomed. Opt.*, vol. 17, no. 1, p. 011004, Jan. 2012.

[69] M. Diez, B. Zimmermann, M. Börsch, M. König, E. Schweinberger, S. Steigmiller, R. Reuter, S. Felekyan, V. Kudryavtsev, C. A. M. Seidel, and P. Gräber, "Proton-powered subunit rotation in single membrane-bound FoF1-ATP synthase.," *Nat. Struct. Mol. Biol.*, vol. 11, no. 2, pp. 135–41, Feb. 2004.

[70] B. Zimmermann, M. Diez, M. Börsch, and P. Gräber, "Subunit movements in membrane-integrated EFoF1 during ATP synthesis detected by single-molecule spectroscopy.," *Biochim. Biophys. Acta*, vol. 1757, no. 5–6, pp. 311–9, Jan. 2006.

[71] M. Börsch and T. M. Duncan, "Spotlighting motors and controls of single FoF1-ATP synthase.," *Biochem. Soc. Trans.*, vol. 41, no. 5, pp. 1219–26, Oct. 2013.

[72] Y. Onoue, T. Suzuki, M. Davidson, M. Karlsson, O. Orwar, M. Yoshida, and K. Kinosita, "A giant liposome for single-molecule observation of conformational changes in membrane proteins.," *Biochim. Biophys. Acta*, vol. 1788, no. 6, pp. 1332–1340, Jun. 2009.

[73] R. Watanabe, K. V Tabata, R. Iino, H. Ueno, M. Iwamoto, S. Oiki, and H. Noji, "Biased Brownian stepping rotation of FoF1-ATP synthase driven by proton motive force.," *Nat. Commun.*, vol. 4, p. 1631, Jan. 2013.

[74] M. Nakanishi-Matsui, S. Kashiwagi, H. Hosokawa, D. J. Cipriano, S. D. Dunn, Y. Wada, and M. Futai, "Stochastic high-speed rotation of Escherichia coli ATP synthase F1 sector: the epsilon subunit-sensitive rotation.," *J. Biol. Chem.*, vol. 281, no. 7, pp. 4126–31, Feb. 2006.

[75] H. Ueno, T. Suzuki, K. Kinosita, and M. Yoshida, "ATP-driven stepwise rotation of FoF1-ATP synthase.," *Proc. Natl. Acad. Sci. U. S. A.*, vol. 102, no. 5, pp. 1333–8, Feb. 2005.

[76] R. Gibrat and C. Grignon, "Liposomes with multiple fluorophores for measurement of ionic fluxes, selectivity, and membrane potential.," *Methods Enzymol.*, vol. 372, pp. 166–86, Jan. 2003.

[77] P. Mueller, D. O. Rudin, H. Ti Tien, and W. C. Wescott, "Reconstitution of Cell Membrane Structure in vitro and its Transformation into an Excitable System," *Nature*, vol. 194, no. 4832, pp. 979–980, Jun. 1962.

[78] J. M. Tobias, "Phospholipid-Cholesterol Membrane Model: Control of resistance by ions or current flow," *J. Gen. Physiol.*, vol. 45, no. 5, pp. 989–1001, May 1962.

[79] A. D. Bangham and R. W. Horne, "Negative staining of phospholipids and their structural modification by surface-active agents as observed in the electron microscope," *J. Mol. Biol.*, vol. 8, no. 5, pp. 660–IN10, Jan. 1964.

[80] A. D. Bangham, M. M. Standish, and J. C. Watkins, "Diffusion of univalent ions across the lamellae of swollen phospholipids," *J. Mol. Biol.*, vol. 13, no. 1, pp. 238–IN27, Aug. 1965.

[81] L. M. Tsofina, E. A. Liberman, and A. V. Babokov, "Production of Bimolecular Protein-Lipid Membranes in Aqueous Solution," *Nature*, vol. 212, no. 5063, pp. 681–683, Nov. 1966.

[82] K. Funakoshi, H. Suzuki, and S. Takeuchi, "Lipid bilayer formation by contacting monolayers in a microfluidic device for membrane protein analysis.," *Anal. Chem.*, vol. 78, no. 24, pp. 8169–74, Dec. 2006.

[83] A. J. Heron, J. R. Thompson, A. E. Mason, and M. I. Wallace, "Direct detection of membrane channels from gels using water-in-oil droplet bilayers.," *J. Am. Chem. Soc.*, vol. 129, no. 51, pp. 16042–7, Dec. 2007.

[84] T. Kunitake, "Synthetic Bilayer Membranes: Molecular Design, Self-Organization, and Application," *Angew. Chemie Int. Ed. English*, vol. 31, no. 6, pp. 709–726, Jun. 1992.

[85] D. M. Vriezema, M. Comellas Aragonès, J. A. A. W. Elemans, J. J. L. M. Cornelissen, A. E. Rowan, and R. J. M. Nolte, "Self-assembled nanoreactors.," *Chem. Rev.*, vol. 105, no. 4, pp. 1445–89, Apr. 2005.

[86] V. P. Torchilin, "Recent advances with liposomes as pharmaceutical carriers.," *Nat. Rev. Drug Discov.*, vol. 4, no. 2, pp. 145–60, Feb. 2005.

[87] J. Wilschut and D. Hoekstra, "Membrane fusion: Lipid vesicles as a model system," *Chem. Phys. Lipids*, vol. 40, no. 2–4, pp. 145–166, Jun. 1986.

[88] D. van Swaay and A. deMello, "Microfluidic methods for forming liposomes," *Lab Chip*, vol. 13, no. 5, pp. 752–767, Mar. 2013.

[89] S. F. Fenz and K. Sengupta, "Giant vesicles as cell models.," *Integr. Biol. (Camb).*, vol. 4, no. 9, pp. 982–995, Sep. 2012.

[90] V. Noireaux and A. Libchaber, "A vesicle bioreactor as a step toward an artificial cell assembly," *Proc. Natl. Acad. Sci. U. S. A.*, vol. 101, no. 51, pp. 17669–17674, Dec. 2004.

[91] L. Song, M. R. Hobaugh, C. Shustak, S. Cheley, H. Bayley, and J. E. Gouaux, "Structure of staphylococcal alpha-hemolysin, a heptameric transmembrane pore.," *Science*, vol. 274, no. 5294, pp. 1859–66, Dec. 1996.

[92] J. R. Thompson, B. Cronin, H. Bayley, and M. I. Wallace, "Rapid assembly of a multimeric membrane protein pore.," *Biophys. J.*, vol. 101, no. 11, pp. 2679–83, Dec. 2011.

[93] S. M. Christensen, P.-Y. Bolinger, N. S. Hatzakis, M. W. Mortensen, and D. Stamou, "Mixing subattolitre volumes in a quantitative and highly parallel manner with soft matter nanofluidics," *Nat Nano*, vol. 7, no. 1, pp. 51–55, Jan. 2012.

[94] M. Dezi, A. Di Cicco, P. Bassereau, and D. Lévy, "Detergent-mediated incorporation of transmembrane proteins in giant unilamellar vesicles with controlled physiological contents," *Proc. Natl. Acad. Sci.*, Apr. 2013.

[95] M. Davidson, M. Karlsson, J. Sinclair, K. Sott, and O. Orwar, "Nanotube-vesicle networks with functionalized membranes and interiors.," *J. Am. Chem. Soc.*, vol. 125, no. 2, pp. 374–8, Jan. 2003.

[96] M. K. Doeven, J. H. A. Folgering, V. Krasnikov, E. R. Geertsma, G. van den Bogaart, and B. Poolman, "Distribution, lateral mobility and function of membrane proteins incorporated into giant unilamellar vesicles.," *Biophys. J.*, vol. 88, no. 2, pp. 1134–42, Feb. 2005.

[97] P. Girard, J. Pécréaux, G. Lenoir, P. Falson, J.-L. L. Rigaud, and P. Bassereau, "A new method for the reconstitution of membrane proteins into giant unilamellar vesicles.," *Biophys. J.*, vol. 87, no. 1, pp. 419–429, Jul. 2004.

[98] Y. Onoue, T. Suzuki, M. Davidson, M. Karlsson, O. Orwar, M. Yoshida, and K. Kinosita, "A giant liposome for single-molecule observation of conformational changes in membrane proteins.," *Biochim. Biophys. Acta*, vol. 1788, no. 6, pp. 1332–1340, Jun. 2009.

[99] N. Kahya, E.-I. I. Pécheur, W. P. de Boeij, D. A. Wiersma, and D. Hoekstra, "Reconstitution of Membrane Proteins into Giant Unilamellar Vesicles via Peptide-Induced Fusion," *Biophys. J.*, vol. 81, no. 3, pp. 1464–1474, Sep. 2001.

[100] J. S. Hansen, A. Vararattanavech, T. Vissing, J. Torres, J. Emnéus, and C. Hélix-Nielsen, "Formation of Giant Protein Vesicles by a Lipid Cosolvent Method," *ChemBioChem*, vol. 12, no. 18, pp. 2856–2862, Dec. 2011.

[101] A. Varnier, F. Kermarrec, I. Blesneac, C. Moreau, L. Liguori, J. Lenormand, and N. Picollet-D'hahan, "A Simple Method for the Reconstitution of Membrane Proteins into Giant Unilamellar Vesicles," *J. Membr. Biol.*, vol. 233, no. 1–3, pp. 85–92, Feb. 2010.

[102] Y.-H. M. Chan, B. van Lengerich, and S. G. Boxer, "Effects of linker sequences on vesicle fusion mediated by lipid-anchored DNA oligonucleotides.," *Proc. Natl. Acad. Sci. U. S. A.*, vol. 106, no. 4, pp. 979–84, Jan. 2009.

[103] C. Miller, P. Arvan, J. N. Telford, and E. Racker, "Ca++-induced fusion of proteoliposomes: Dependence on transmembrane osmotic gradient," *J. Membr. Biol.*, vol. 30, no. 1, pp. 271–282, Dec. 1976.

[104] C. Miller and E. Racker, "Ca++-induced fusion of fragmented sarcoplasmic reticulum with artificial planar bilayers," *J. Membr. Biol.*, vol. 30, no. 1, pp. 283–300, Dec. 1976.

[105] C. Miller, "Integral membrane channels: studies in model membranes," *Physiol Rev*, vol. 63, no. 4, pp. 1209–1242, Oct. 1983.

[106] C. Miller, *Ion Channel Reconstitution*. Boston, MA: Springer US, 1986.

[107] G. Nordlund, P. Brzezinski, and C. von Ballmoos, "SNARE-fusion mediated insertion of membrane proteins into native and artificial membranes.," *Nat. Commun.*, vol. 5, p. 4303, Jan. 2014.

[108] R. P. Rand and V. A. Parsegian, "Mimicry and mechanism in phospholipid models of membrane fusion.," *Annu. Rev. Physiol.*, vol. 48, pp. 201–12, Jan. 1986.

[109] D. Papahadjopoulos, S. Nir, and N. Duzgunes, "Molecular mechanisms of calcium-induced membrane fusion," *J. Bioenerg. Biomembr.*, vol. 22, no. 2, pp. 157–179, Apr. 1990.

[110] D. P. Pantazatos and R. C. MacDonald, "Directly Observed Membrane Fusion Between Oppositely Charged Phospholipid Bilayers," *J. Membr. Biol.*, vol. 170, no. 1, pp. 27–38, Jul. 1999.

[111] L. Stamatatos, R. Leventis, M. J. Zuckermann, and J. R. Silvius, "Interactions of cationic lipid vesicles with negatively charged phospholipid vesicles and biological membranes," *Biochemistry*, vol. 27, no. 11, pp. 3917–3925, May 1988.

[112] S. Chesnoy and L. Huang, "Structure and function of lipid-DNA complexes for gene delivery.," *Annu. Rev. Biophys. Biomol. Struct.*, vol. 29, pp. 27–47, Jan. 2000.

[113] G. Lei and R. C. MacDonald, “Lipid bilayer vesicle fusion: intermediates captured by high-speed microfluorescence spectroscopy.,” *Biophys. J.*, vol. 85, no. 3, pp. 1585–99, Sep. 2003.

[114] S. Fischer, P. Graber, and P. Turina, “The Activity of the ATP Synthase from Escherichia coli Is Regulated by the Transmembrane Proton Motive Force,” *J. Biol. Chem.*, vol. 275, no. 39, pp. 30157–30162, Sep. 2000.

[115] P. Turina, D. Samoray, and P. Gräber, “H+/ATP ratio of proton transport-coupled ATP synthesis and hydrolysis catalysed by CFoF1-liposomes.,” *EMBO J.*, vol. 22, no. 3, pp. 418–26, Feb. 2003.

[116] J. Solon, J. Pécréaux, P. Girard, M.-C. Fauré, J. Prost, and P. Bassereau, “Negative Tension Induced by Lipid Uptake,” *Phys. Rev. Lett.*, vol. 97, no. 9, p. 098103, Aug. 2006.

[117] Y. Sowa, B. C. Steel, and R. M. Berry, “A simple backscattering microscope for fast tracking of biological molecules,” *Rev. Sci. Instrum.*, vol. 81, no. 11, p. 113704+, Nov. 2010.

[118] H. Ueno, S. Nishikawa, R. Iino, K. V Tabata, S. Sakakihara, T. Yanagida, and H. Noji, “Simple dark-field microscopy with nanometer spatial precision and microsecond temporal resolution.,” *Biophys. J.*, vol. 98, no. 9, pp. 2014–23, May 2010.

[119] G. I. Mashanov, D. Tacon, A. E. Knight, M. Peckham, and J. E. Molloy, “Visualizing single molecules inside living cells using total internal reflection fluorescence microscopy.,” *Methods*, vol. 29, no. 2, pp. 142–52, Feb. 2003.

[120] R. R. Ishmukhametov, M. A. Galkin, and S. B. Vik, “Ultrafast purification and reconstitution of His-tagged cysteine-less Escherichia coli F1Fo ATP synthase.,” *Biochim. Biophys. Acta*, vol. 1706, no. 1–2, pp. 110–116, Jan. 2005.

[121] M. Tanabe, K. Nishio, Y. Iko, Y. Sambongi, A. Iwamoto-Kihara, Y. Wada, and M. Futai, “Rotation of a complex of the gamma subunit and c ring of Escherichia coli ATP synthase. The rotor and stator are interchangeable.,” *J. Biol. Chem.*, vol. 276, no. 18, pp. 15269–74, May 2001.

[122] S. Löbau, J. Weber, and A. E. Senior, “Catalytic site nucleotide binding and hydrolysis in F1Fo-ATP synthase.,” *Biochemistry*, vol. 37, no. 30, pp. 10846–53, Jul. 1998.

[123] R. Negrin, D. Foster, and R. Fillingame, “Energy-transducing H+-ATPase of Escherichia coli. Reconstitution of proton translocation activity of the intrinsic membrane sector,” *J. Biol. Chem.*, vol. 255, no. 12, pp. 5643–5648, Jun. 1980.

[124] R. Humbert, W. S. Brusilow, R. P. Gunsalus, D. J. Klionsky, and R. D. Simoni, "Escherichia coli mutants defective in the uncH gene.," *J. Bacteriol.*, vol. 153, no. 1, pp. 416–22, Jan. 1983.

[125] D. Spetzler, R. Ishmukhametov, T. Hornung, L. J. Day, J. Martin, and W. D. Frasch, "Single Molecule Measurements of F1-ATPase Reveal an Interdependence between the Power Stroke and the Dwell Duration," *Biochemistry*, vol. 48, no. 33, pp. 7979–7985, Jul. 2009.

[126] A. K. Mallia, M. D. Frovenzano, E. K. Fujimoto, B. J. Olson, D. C. Klenk, P. C. Company, P. K. Smith, R. I. Krohn, G. T. Hermanson, F. H. Gartner, M. D. Provenzano, and N. M. Goeke, "Measurement of protein using bicinchoninic acid.," *Anal. Biochem.*, vol. 150, no. 1, pp. 76–85, Oct. 1985.

[127] O. O. H. Lowry, N. J. N. Rosebrough, A. L. Farr, R. R. J. Randall, and L. Farr, "Protein Measurement With The Folin Phenol Reagent," *J. Biol. Chem.*, vol. 193, no. 1, pp. 265–75, Nov. 1951.

[128] H. Schägger, "Tricine-SDS-PAGE.," *Nat. Protoc.*, vol. 1, no. 1, pp. 16–22, Jan. 2006.

[129] S. Gatt and E. Racker, "Regulatory mechanisms in carbohydrate metabolism. I. Crabtree effect in reconstructed systems.," *J. Biol. Chem.*, vol. 234, no. 5, pp. 1015–23, May 1959.

[130] H. Towbin, T. Staehelin, and J. Gordon, "Electrophoretic transfer of proteins from polyacrylamide gels to nitrocellulose sheets: procedure and some applications.," *Proc. Natl. Acad. Sci.*, vol. 76, no. 9, pp. 4350–4354, Sep. 1979.

[131] G. E. Healthcare and L. Sciences, "Western Blotting."

[132] G. Kaim, M. Prummer, B. Sick, G. Zumofen, A. Renn, U. P. Wild, and P. Dimroth, "Coupled rotation within single FoF1 enzyme complexes during ATP synthesis or hydrolysis," *FEBS Lett.*, vol. 525, no. 1–3, pp. 156–163, Aug. 2002.

[133] T. J. Schuh, "An Introduction to Lipid Analysis in the Cell Biology Laboratory," *Am. Biol. Teach.*, vol. 64, no. 2, pp. 122–129, Feb. 2002.

[134] J. C. Touchstone, "Thin-layer chromatographic procedures for lipid separation.," *J. Chromatogr. B. Biomed. Appl.*, vol. 671, no. 1–2, pp. 169–95, Sep. 1995.

[135] B. Fuchs, R. Süss, K. Teuber, M. Eibisch, and J. Schiller, "Lipid analysis by thin-layer chromatography--a review of the current state.," *J. Chromatogr. A*, vol. 1218, no. 19, pp. 2754–74, May 2011.

[136] D. A. Kendall and R. C. MacDonald, "A fluorescence assay to monitor vesicle fusion and lysis.," *J. Biol. Chem.*, vol. 257, no. 23, pp. 13892–5, Dec. 1982.

[137] R. C. MacDonald, G. W. Ashley, M. M. Shida, V. A. Rakhmanova, Y. S. Tarahovsky, D. P. Pantazatos, M. T. Kennedy, E. V Pozharski, K. A. Baker, R. D. Jones, H. S. Rosenzweig, K. L. Choi, R. Qiu, and T. J. McIntosh, "Physical and biological properties of cationic triesters of phosphatidylcholine.," *Biophys. J.*, vol. 77, no. 5, pp. 2612–29, Nov. 1999.

[138] J. C. McIntyre and R. G. Sleight, "Fluorescence assay for phospholipid membrane asymmetry," *Biochemistry*, vol. 30, no. 51, pp. 11819–11827, Dec. 1991.

[139] S. Pautot, B. J. Frisken, and D. A. Weitz, "Production of Unilamellar Vesicles Using an Inverted Emulsion," *Langmuir*, vol. 19, no. 7, pp. 2870–2879, Apr. 2003.

[140] S. Pautot, B. J. Frisken, and D. A. Weitz, "Engineering asymmetric vesicles," *Proc. Natl. Acad. Sci.*, vol. 100, no. 19, pp. 10718–10721, Sep. 2003.

[141] G. Zhen, S. Zurcher, D. Falconnet, F. Xu, E. Kuennemann, and M. Textor, "NTA-Functionalized Poly(L-lysine)-g-Poly(Ethylene Glycol): A Polymeric Interface for Binding and Studying 6 His-tagged Proteins.," *Conf. Proc. IEEE Eng. Med. Biol. Soc.*, vol. 1, pp. 1036–8, Jan. 2005.

[142] M. V. Nesterenko, M. Tilley, S. J. Upton, and S. Note, "A simple modification of Blum's silver stain method allows for 30 minute detection of proteins in polyacrylamide gels," *J. Biochem. Biophys. Methods*, vol. 28, no. 3, pp. 239–242, Apr. 1994.

[143] U. K. Laemmli, "Cleavage of Structural Proteins during the Assembly of the Head of Bacteriophage T4," *Nature*, vol. 227, no. 5259, pp. 680–685, Aug. 1970.

[144] H. Schägger and G. von Jagow, "Tricine-sodium dodecyl sulfate-polyacrylamide gel electrophoresis for the separation of proteins in the range from 1 to 100 kDa.," *Anal. Biochem.*, vol. 166, no. 2, pp. 368–79, Nov. 1987.

[145] E. Schneider and K. Altendorf, "Bacterial adenosine 5'-triphosphate synthase (F1F0): purification and reconstitution of F0 complexes and biochemical and functional characterization of their subunits.," *Microbiol. Rev.*, vol. 51, no. 4, pp. 477–97, Dec. 1987.

[146] S. Grzesiek and N. A. Dencher, "The 'delta pH'-probe 9-aminoacridine: response time, binding behaviour and dimerization at the membrane.," *Biochim. Biophys. Acta*, vol. 938, no. 3, pp. 411–24, Mar. 1988.

[147] C.-S. Huang, S. J. Kopacz, and C.-P. Lee, "Mechanistic differences in the energy-linked fluorescence decreases of 9-aminoacridine dyes associated with bovine heart submitochondrial membranes," *Biochim. Biophys. Acta - Bioenerg.*, vol. 722, no. 1, pp. 107–115, Jan. 1983.

[148] S. Grzesiek, H. Otto, and N. A. Dencher, "delta pH-induced fluorescence quenching of 9-aminoacridine in lipid vesicles is due to excimer formation at the membrane.," *Biophys. J.*, vol. 55, no. 6, pp. 1101–9, Jun. 1989.

[149] J. Han and K. Burgess, "Fluorescent indicators for intracellular pH.," *Chem. Rev.*, vol. 110, no. 5, pp. 2709–28, May 2010.

[150] J. P. Dufour, A. Goffeau, and T. Y. Tsong, "Active proton uptake in lipid vesicles reconstituted with the purified yeast plasma membrane ATPase. Fluorescence quenching of 9-amino-6-chloro-2-methoxyacridine.," *J. Biol. Chem.*, vol. 257, no. 16, pp. 9365–71, Aug. 1982.

[151] J. W. T. Fiolet, E. P. Bakker, and K. van Dam, "The fluorescent properties of acridines in the presence of chloroplasts or liposomes. On the quantitative relationship between the fluorescence quenching and the transmembrane proton gradient," *Biochim. Biophys. Acta - Bioenerg.*, vol. 368, no. 3, pp. 432–445, Dec. 1974.

[152] E. Purification, D. L. Foster, R. H. Fillingame, J. B. Chem, and L. Foster, "Energy-transducing H + -ATPase of Energy-transducing of Escherichia coli," 1979.

[153] R. H. Fillingame, "Identification of the dicyclohexylcarbodiimide-reactive protein component of the adenosine 5'-triphosphate energy-transducing system of Escherichia coli.," *J. Bacteriol.*, vol. 124, no. 2, pp. 870–883, Nov. 1975.

[154] J. Hermolin and R. H. Fillingame, "H+-ATPase activity of Escherichia coli F1Fo is blocked after reaction of dicyclohexylcarbodiimide with a single proteolipid (subunit c) of the Fo complex.," *J. Biol. Chem.*, vol. 264, no. 7, pp. 3896–3903, Mar. 1989.

[155] W. Sebald, W. Machleidt, and E. Wachter, "N,N'-dicyclohexylcarbodiimide binds specifically to a single glutamyl residue of the proteolipid subunit of the mitochondrial adenosinetriphosphatases from Neurospora crassa and Saccharomyces cerevisiae.," *Proc. Natl. Acad. Sci.*, vol. 77, no. 2, pp. 785–789, Feb. 1980.

[156] M. Yoshida and W. S. Allison, "Modulation by ADP and Mg2+ of the inactivation of the F1-ATPase from the thermophilic bacterium, PS3, with dicyclohexylcarbodiimide.," *J. Biol. Chem.*, vol. 258, no. 23, pp. 14407–14412, Dec. 1983.

[157] R. E. Morton and T. A. Evans, "Modification of the bicinchoninic acid protein assay to eliminate lipid interference in determining lipoprotein protein content," *Anal. Biochem.*, vol. 204, no. 2, pp. 332–334, Aug. 1992.

[158] G. L. Peterson, "A simplification of the protein assay method of Lowry et al. which is more generally applicable.," *Anal. Biochem.*, vol. 83, no. 2, pp. 346–56, Dec. 1977.

[159] L. Paasonen, T. Laaksonen, C. Johans, M. Yliperttula, K. Kontturi, and A. Urtti, "Gold nanoparticles enable selective light-induced contents release from liposomes.," *J. Control. release*, vol. 122, no. 1, pp. 86–93, Sep. 2007.

[160] C. Kojima, Y. Hirano, E. Yuba, A. Harada, and K. Kono, "Preparation and characterization of complexes of liposomes with gold nanoparticles.," *Colloids Surf. B. Biointerfaces*, vol. 66, no. 2, pp. 246–52, Oct. 2008.

[161] W. T. Al-Jamal and K. Kostarelos, "Liposomes: from a clinically established drug delivery system to a nanoparticle platform for theranostic nanomedicine.," *Acc. Chem. Res.*, vol. 44, no. 10, pp. 1094–104, Oct. 2011.

[162] M. Abkarian, E. Loiseau, and G. Massiera, "Continuous droplet interface crossing encapsulation (cDICE) for high throughput monodisperse vesicle design," *Soft Matter*, vol. 7, no. 10, p. 4610, May 2011.

[163] H. C. Shum, D. Lee, I. Yoon, T. Kodger, and D. A. Weitz, "Double Emulsion Templated Monodisperse Phospholipid Vesicles," *Langmuir*, vol. 24, no. 15, pp. 7651–7653, Jul. 2008.

[164] S. Sugiura, T. Kuroiwa, T. Kagota, M. Nakajima, S. Sato, S. Mukataka, P. Walde, and S. Ichikawa, "Novel Method for Obtaining Homogeneous Giant Vesicles from a Monodisperse Water-in-Oil Emulsion Prepared with a Microfluidic Device," *Langmuir*, vol. 24, no. 9, pp. 4581–4588, Apr. 2008.

[165] K. Nishimura, H. Suzuki, T. Toyota, and T. Yomo, "Size control of giant unilamellar vesicles prepared from inverted emulsion droplets.," *J. Colloid Interface Sci.*, vol. 376, no. 1, pp. 119–125, Jun. 2012.

[166] D. L. Richmond, E. M. Schmid, S. Martens, J. C. Stachowiak, N. Liska, and D. A. Fletcher, "Forming giant vesicles with controlled membrane composition, asymmetry, and contents.," *Proc. Natl. Acad. Sci. U. S. A.*, vol. 108, no. 23, pp. 9431–6, Jun. 2011.

[167] J. C. Stachowiak, D. L. Richmond, T. H. Li, F. Brochard-Wyart, and D. A. Fletcher, "Inkjet formation of unilamellar lipid vesicles for cell-like encapsulation," *Lab Chip*, vol. 9, no. 14, pp. 2003–2009, 2009.

[168] Y. Elani, R. V Law, and O. Ces, "Vesicle-based artificial cells as chemical microreactors with spatially segregated reaction pathways.," *Nat. Commun.*, vol. 5, p. 5305, Jan. 2014.

[169] M. Chiba, M. Miyazaki, and S. Ishiwata, "Quantitative analysis of the lamellarity of giant liposomes prepared by the inverted emulsion method.," *Biophys. J.*, vol. 107, no. 2, pp. 346–54, Jul. 2014.

[170] S. Pautot, B. J. Frisken, and D. A. Weitz, "Production of Unilamellar Vesicles Using an Inverted Emulsion," no. 10, pp. 2870–2879, 2003.

[171] X. Chen and H. C. Berg, "Torque-speed relationship of the flagellar rotary motor of Escherichia coli.," *Biophys. J.*, vol. 78, no. 2, pp. 1036–41, Feb. 2000.

[172] S. W. Reid, M. C. Leake, J. H. Chandler, C.-J. Lo, J. P. Armitage, and R. M. Berry, "The maximum number of torque-generating units in the flagellar motor of Escherichia coli is at least 11.," *Proc. Natl. Acad. Sci. U. S. A.*, vol. 103, no. 21, pp. 8066–71, May 2006.

[173] Y. Natsume and T. Toyota, "Giant Vesicles Containing Microspheres with High Volume Fraction Prepared by Water-in-oil Emulsion Centrifugation," *Chem. Lett.*, vol. 42, no. 3, pp. 295–297, 2013.

[174] B. a, H. J. Gruber, and H. Schindler, "External surface and lamellarity of lipid vesicles: a practice-oriented set of assay methods," *Biochim. Biophys. Acta*, vol. 1189, no. 2, pp. 212–24, Jan. 1994.

[175] L. A. Bagatolli and D. Needham, "Quantitative optical microscopy and micromanipulation studies on the lipid bilayer membranes of giant unilamellar vesicles.," *Chem. Phys. Lipids*, vol. 181, pp. 99–120, Jul. 2014.

[176] K. Akashi, H. Miyata, H. Itoh, and K. Kinosita, "Preparation of giant liposomes in physiological conditions and their characterization under an optical microscope.," *Biophys. J.*, vol. 71, no. 6, pp. 3242–50, Dec. 1996.

[177] J. Wilschut, N. Düzgüne\cs, R. Fraley, D. Papahadjopoulos, and N. Düzgüneş, "Studies on the mechanism of membrane fusion: kinetics of calcium ion induced fusion of phosphatidylserine vesicles followed by a new assay for mixing of aqueous vesicle contents.," *Biochemistry*, vol. 19, no. 26, pp. 6011–6021, Dec. 1980.

[178] H. Ellens, J. Bentz, and F. C. Szoka, "Proton- and calcium-induced fusion and destabilization of liposomes," *Biochemistry*, vol. 24, no. 13, pp. 3099–3106, Jun. 1985.

[179] R. W. Holz and C. A. Stratford, "Effects of divalent ions on vesicle-vesicle fusion studied by a new luminescence assay for fusion," *J. Membr. Biol.*, vol. 46, no. 4, pp. 331–358, Dec. 1979.

[180] K. Lymperopoulos, R. Crawford, J. P. Torella, M. Heilemann, L. C. Hwang, S. J. Holden, and A. N. Kapanidis, "Single-molecule DNA biosensors for protein and ligand detection.," *Angew. Chem. Int. Ed. Engl.*, vol. 49, no. 7, pp. 1316–20, Feb. 2010.

[181] "Single-Molecule Techniques: A Laboratory Manual," 2008.

[182] M. J. Tipping, N. J. Delalez, R. Lim, R. M. Berry, and J. P. Armitage, "Load-dependent assembly of the bacterial flagellar motor.," *MBio*, vol. 4, no. 4, pp. e00551–13–, Jan. 2013.

[183] R. E. Thompson, D. R. Larson, and W. W. Webb, "Precise nanometer localization analysis for individual fluorescent probes.," *Biophys. J.*, vol. 82, no. 5, pp. 2775–2783, May 2002.

[184] K. Okazaki and S. Takada, "Structural comparison of F1-ATPase: interplay among enzyme structures, catalysis, and rotations.," *Structure*, vol. 19, no. 4, pp. 588–98, Apr. 2011.

[185] R. M. Berry, L. Turner, and H. C. Berg, "Mechanical limits of bacterial flagellar motors probed by electrorotation.," *Biophys. J.*, vol. 69, no. 1, pp. 280–6, Jul. 1995.

[186] A. L. Hodgkin, "The Croonian Lecture: Ionic Movements and Electrical Activity in Giant Nerve Fibres," *Proc. R. Soc. B Biol. Sci.*, vol. 148, no. 930, pp. 1–37, Jan. 1958.

[187] S. H. White, "A study of lipid bilayer membrane stability using precise measurements of specific capacitance.," *Biophys. J.*, vol. 10, no. 12, pp. 1127–48, Dec. 1970.

[188] R. Fettiplace, D. M. Andrews, and D. A. Haydon, "The thickness, composition and structure of some lipid bilayers and natural membranes.," *J. Membr. Biol.*, vol. 5, no. 3, pp. 277–96, Sep. 1971.

[189] L. C. M. Gross, A. J. Heron, S. C. Baca, and M. I. Wallace, "Determining membrane capacitance by dynamic control of droplet interface bilayer area.," *Langmuir*, vol. 27, no. 23, pp. 14335–42, Dec. 2011.

[190] A. Holoubek, J. Vecer, and K. Sigler, "Monitoring of the proton electrochemical gradient in reconstituted vesicles: quantitative measurements of both transmembrane potential and intravesicular pH by ratiometric fluorescent probes.," *J. Fluoresc.*, vol. 17, no. 2, pp. 201–13, Mar. 2007.

[191] K. Venema, R. Gibrat, J.-P. Grouzis, and C. Grignon, "Quantitative measurement of cationic fluxes, selectivity and membrane potential using

liposomes multilabelled with fluorescent probes," *Biochim. Biophys. Acta - Biomembr.*, vol. 1146, no. 1, pp. 87–96, Feb. 1993.

[192] T. Kubori, M. Okumura, N. Kobayashi, D. Nakamura, M. Iwakura, and S. I. Aizawa, "Purification and characterization of the flagellar hook–basal body complex of Bacillus subtilis," *Mol. Microbiol.*, vol. 24, no. 2, pp. 399–410, 1997.

[193] C. von Ballmoos, A. Wiedenmann, and P. Dimroth, "Essentials for ATP synthesis by F1Fo ATP synthases.," *Annu. Rev. Biochem.*, vol. 78, pp. 649–72, Jan. 2009.

[194] J. DeLeon-Rangel, R. R. Ishmukhametov, W. Jiang, R. H. Fillingame, and S. B. Vik, "Interactions between subunits a and b in the rotary ATP synthase as determined by cross-linking.," *FEBS Lett.*, vol. 587, no. 7, pp. 892–7, Apr. 2013.

[195] K. Brandt, S. Maiwald, B. Herkenhoff-Hesselmann, K. Gnirß, J.-C. Greie, S. D. Dunn, and G. Deckers-Hebestreit, "Individual interactions of the b subunits within the stator of the Escherichia coli ATP synthase.," *J. Biol. Chem.*, vol. 288, no. 34, pp. 24465–79, Aug. 2013.

[196] C. S. Gajadeera and J. Weber, "Escherichia coli F1Fo-ATP synthase with a b/δ fusion protein allows analysis of the function of the individual b subunits.," *J. Biol. Chem.*, vol. 288, no. 37, pp. 26441–7, Sep. 2013.

[197] D. Okuno, R. Iino, and H. Noji, "Rotation and structure of FoF1-ATP synthase.," *J. Biochem.*, vol. 149, no. 6, pp. 655–64, Jun. 2011.